



HAL
open science

Denudation history and palaeogeography of the Pyrenees and their peripheral basins: an 84-million-year geomorphological perspective

Marc Calvet, Yanni Gunnell, Bernard Laumonier

► **To cite this version:**

Marc Calvet, Yanni Gunnell, Bernard Laumonier. Denudation history and palaeogeography of the Pyrenees and their peripheral basins: an 84-million-year geomorphological perspective. *Earth Science Reviews*, 2021, 215, pp.103436. 10.1016/j.earscirev.2020.103436 . insu-03665935

HAL Id: insu-03665935

<https://insu.hal.science/insu-03665935v1>

Submitted on 10 Mar 2023

HAL is a multi-disciplinary open access archive for the deposit and dissemination of scientific research documents, whether they are published or not. The documents may come from teaching and research institutions in France or abroad, or from public or private research centers.

L'archive ouverte pluridisciplinaire **HAL**, est destinée au dépôt et à la diffusion de documents scientifiques de niveau recherche, publiés ou non, émanant des établissements d'enseignement et de recherche français ou étrangers, des laboratoires publics ou privés.



Distributed under a Creative Commons Attribution - NonCommercial 4.0 International License

1 Denudation history and palaeogeography of the 2 Pyrenees and their peripheral basins: an 84-million- 3 year geomorphological perspective

4
5 Marc Calvet^a

6 Yann Gonnell^b

7 Bernard Laumonier^c

8 ^a Université de Perpignan—Via Domitia, CNRS UMR 7194 Histoire Naturelle de l'Homme Préhistorique, 52 avenue Paul
9 Alduy, F-66860 Perpignan, France

10 ^b Université de Lyon—Lumière Lyon 2, CNRS UMR 5600 Environnement-Ville-Société, 5 Avenue P. Mendès-France, F-69676
11 Bron, France

12 ^c École des Mines de Nancy, GeoRessources, UMR 7359, Université de Lorraine, Campus ARTEM, CS14234, F-54042 Nancy,
13 France

14

15

16

17 **Abstract**

18 This review provides a synthesis of the evolution of the Pyrenees since ~84 Ma and is
19 uniquely focused on analysing jointly and comparatively its peripheral pro-foreland, retro-
20 foreland and Mediterranean basins. The reconstructions adopt a geomorphological
21 perspective focused on the waxing and waning of palaeorelief, and is underpinned by (i) the
22 denudation history of the mountain belt encoded in the sedimentary record of its basins, (ii)
23 rock-cooling histories inferred from low-temperature thermochronology, and (iii) the age
24 and spatial distribution of tectonic and erosional landforms. Existing geological
25 reconstructions of the Pyrenees commonly terminate at the end of the syntectonic collision
26 period (early Miocene). Here, the no-less eventful post-shortening period of the last 25–30
27 m.y. is also addressed. Accordingly, emphasis is given to the record provided by nonmarine
28 clastic sequences, and to the often understated depositional biochronology documented by
29 the continental fossils they contain. Sedimentological and provenance analysis of coarse
30 clastic deposits further documents the fine-scale palaeogeography of sources and sinks, and
31 is correlated with different generations of eustatic, tectonic, and volcanic features, as well as
32 extant populations of land surfaces such as rock pediments, palaeovalleys, and other

33 landforms indicative of palaeoelevation and palaeotopography. These interconnected and
34 age-bracketed diagnostic features are correlated with independent evidence concerning the
35 structural evolution of the orogenic belt at crustal and lithospheric scale. They show that the
36 Ancestral (i.e., Paleogene) Pyrenees were in many aspects dissimilar to the successor
37 mountain range we observe today. They also suggest that, despite its prima facie
38 topographic continuity from the Mediterranean to the Atlantic, the modern mountain range,
39 particularly in its eastern half, is in a transient topographic state. This would appear to have
40 been driven by large-scale asthenospheric flows contributing to regional uplift and erosion of
41 not just the mountain range but also its foreland basins during the last ~12 m.y.

42

43 **Contents**

44 **1 Introduction**

45 **2 An outline of Pyrenean tectonics**

46 **2.1. First-order structure of the orogenic wedge**

47 **2.2. The Pyrenees before the Pyrenees: pre-orogenic plate reconstructions**

48 ***2.2.1. Geological fabric of the Hercynian basement***

49 ***2.2.2. Mesozoic palaeogeography***

50 ***2.2.3. Geodynamic conditions in Cretaceous time***

51 **2.3. Tectonic legacies of plate convergence**

52 ***2.3.1. The North Pyrenean Fault (NPF), plate boundary between Iberia and Europe***

53 ***2.3.2. The late Cretaceous to Paleocene mountain range, or Proto-Pyrenees***

54 ***2.3.3. The Eocene–Oligocene mountain range, or Ancestral Pyrenees***

55 ***2.3.3.1. Crustal architecture of the European domain***

56 ***2.3.3.2. Crustal architecture of the Iberian domain***

57 ***2.3.3.2.1. Structure of the southeastern Pyrenees***

58 ***2.3.3.2.2. Structure of the south-central Pyrenees***

59 ***2.3.3.2.3. Structure of the southwestern Pyrenees***

60 ***2.3.4. Some unresolved issues***

61 **2.4. From the Ancestral to the Modern Pyrenees: insights from geophysics and geodynamics**

62 ***2.4.1. Western and central Pyrenees***

63 ***2.4.2. Eastern Pyrenees***

64 ***2.4.3. Crustal roots and their implications for geomorphology***

65 **2.5. Synthesis of Pyrenean tectonics**

66 **3. A view from the basins: a proxy record of mountain uplift and erosion**

67 **3.1. Chronology of clastic supply to the Aquitaine retro-foreland**

68 ***3.1.1. State of the art and data sources***

69	3.1.2. Synorogenic conglomerate beds: the Paleogene Palassou Series
70	3.1.3. Western analogues of the Palassou beds: the Jurançon sequence
71	3.1.4. The early and middle Miocene molasse
72	3.1.5. Sharp regime change during the late Miocene
73	3.1.5.1. Stratigraphic aspects
74	3.1.5.2. Growth of range-front megafans
75	3.2. Chronology of clastic supply to the Iberian pro-foreland
76	3.2.1. State of the art and data sources
77	3.2.2. Paleogene deposits of the Southeast Pyrenean Foreland Basin
78	3.2.2.1. From the Empordà Basin to the Ripoll syncline
79	3.2.2.2. From the Llobregat to west of the Segre River
80	3.2.3. Paleogene deposits of the South Pyrenean Foreland Basin
81	3.2.4. Two geological enigmas in the Graus–Trempt Basin
82	3.2.4.1. Unexplained offsets between the Southeast and South foreland sequences
83	3.2.4.2. The Noguères conglomerates anomaly
84	3.2.5. Early to middle Miocene sedimentation
85	3.2.5.1. General chronostratigraphy of the Miocene clastic deposits
86	3.2.5.2. Range-front conglomerate sequences south of the Sierras Exteriores
87	3.2.6. Sharp regime change during the late Miocene
88	3.3. The sedimentary record of extensional basins in the eastern Pyrenees
89	3.3.1. Oligocene to Miocene basin fills: proxies of surface dynamics in the Ancestral Pyrenees
90	3.3.2. Miocene to Pliocene basin fills: proxies of surface dynamics in the Modern Pyrenees
91	4. A view from the mountains: tracking relief evolution from landform assemblages and the rock cooling
92	record
93	4.1. Diagnostic landforms: the Pyrenean erosion surfaces
94	4.1.1. Mapping low-gradient montane surfaces: a note of caution
95	4.1.2. Geographical distribution of the erosion surfaces
96	4.1.2.1. Principal occurrences (Axial Zone and adjacent structures)
97	4.1.2.2. Occurrences in the outer fold-and-thrust belts
98	4.1.3. Age and origin of the erosion surfaces
99	4.1.3.1. Transient legacies of a low-energy environment: evidence from thermochronology
100	4.1.3.2. Refined age constraints on the two generations of erosion surface
101	4.1.3.2.1. The range-top paleoplain (S)
102	4.1.3.2.2. The range-flank pediments (P1)
103	4.1.3.3. Base-level controls on erosion surface completion
104	4.2. Late Neogene regrowth of the mountain range: chronology and evidence from landforms
105	4.2.1. Evidence of late Neogene uplift throughout the Pyrenees
106	4.2.1.1. Thermal relaxation and lithospheric thinning since 10 Ma

107	<i>4.2.1.2. Sedimentological signatures of growing relief amplitude</i>
108	<i>4.2.1.3. Late Neogene and Quaternary tectonic deformation</i>
109	4.2.2. Geomorphological indicators of episodic surface uplift
110	<i>4.2.2.1. A late Neogene generation of rock pediments (P2)</i>
111	<i>4.2.2.2. Dry valleys and drainage piracy</i>
112	<i>4.2.2.3. Staircases of alluvial terraces</i>
113	<i>4.2.2.4. The groundwater karst record</i>
114	5. Quaternary geomorphological evolution
115	5.1. Alluvial deposits
116	<i>5.1.1. Stratigraphic features</i>
117	<i>5.1.2. Components of an alluvial chronology</i>
118	5.2. The impacts of glaciation
119	6. Synthesis and discussion: issues resolved and unresolved
120	6.1. The Proto-Pyrenees
121	6.2. The Ancestral Pyrenees
122	<i>6.2.1. Growth of the mountain range from east to west</i>
123	<i>6.2.2. Correlation between conglomerate sequences of the pro- and retro-forelands</i>
124	<i>6.2.3. Topographic decline of the Ancestral Pyrenees</i>
125	<i>6.2.4. The summit erosion surfaces of the Ancestral Pyrenees</i>
126	6.3. Shaping of the Modern Pyrenees
127	7. Conclusion

128

129 **1 Introduction**

130 This review offers a fully integrated analysis of the Pyrenees from a geomorphological
131 perspective, i.e., understanding the cycles and chronology of mountain growth and decay
132 through the record of landforms as well as rocks. The emphasis, therefore, is on
133 reconstructing the successive states of the Pyrenees as a mountain range, thus deviating
134 from the more conventional approach which consists in presenting the Pyrenees as a belt of
135 crustal deformation with limited concern for its topographic features and transformations.
136 Like the mythical six blind men of Hindustan whose task was to characterise the complete
137 features of an elephant by each exploring one part of its anatomy, geoscience reviews of the
138 Pyrenees have tended recurrently to be delivered in spatially, conceptually, or
139 chronologically limited bundles. Because the mountains extend across several nations,
140 divisions have often fallen not just along linguistic (e.g., French, Spanish, Catalan, English)
141 and disciplinary lines (e.g., structural geology, solid-earth geophysics, stratigraphy,

142 sedimentology, palaeontology, geochronology, geomorphology, surface process modelling)
143 but also along scientific divides within identical disciplines (e.g., in terms of understanding
144 the metamorphic geology, displacement distances between Europe and Iberia, magnitudes
145 of crustal shortening, sequence stratigraphy, glacial geomorphology, alluvial sequence
146 analysis, karst evolution, etc.). As a result, our understanding of the palaeogeography and
147 topographic evolution of the Pyrenees has remained stubbornly piecemeal. The most robust
148 portrayals are often inferred from basin analysis but are equally often restricted to selected
149 subregions or geological epochs, and thus fall short of producing a narrative that spans the
150 late Mesozoic to the Present, extends from the highest peaks in Hercynian basement to the
151 most distal Neogene molasse deposits of the Ebro and Aquitaine basins, and deals with
152 Cenozoic and Quaternary landform assemblages from the Mediterranean to the Bay of
153 Biscay.

154 Some of the cutoff lines in this fragmented narrative have been of a spatial nature:

- 155 (i) Relative overemphasis on the Ebro Basin and the pro-wedge compared to the retro-
156 wedge and the Aquitaine Basin;
- 157 (ii) emphasis on the Mesozoic basin architecture of the Aquitaine foreland — in line with the
158 goals of petroleum exploration — with only a subsidiary focus on the record provided by
159 the overlying Cenozoic sequences;
- 160 (iii) emphasis on the central Pyrenees, where (since 1985) the ECORS-Pyrenees deep seismic
161 profile has spawned a model of crustal architecture which, however, does not
162 adequately describe the orogen's architecture further to the west (some data available
163 from the 1989 ECORS-Azacq profile) or to the east (no data of a similar nature);
- 164 (iv) emphasis on the ECORS-inspired subsurface crustal architecture of the Axial Zone in the
165 central Pyrenees rather than on the subaerial geometry of the orogen, which for 30 years
166 has been invariably portrayed as a thick and tight-folded anticlinal stack of basement
167 nappes despite growing evidence that other geometric reconstructions involving a lesser
168 magnitude of vertical crustal thickening, and possibly of horizontal shortening, can be
169 accommodated;
- 170 (v) emphasis on basin analysis in discrete, strike-perpendicular foreland segments or swaths,
171 fostering a potential for information offsets and apparent along-strike discrepancies —
172 e.g., between the Eocene foredeeps of Catalonia and Aragón, and among the fossil-poor
173 continental depositional records; and for similar inconsistencies in mapping criteria for

174 various Cenozoic deposits among different generations of geological maps in the French
175 Pyrenees.

176 (vi) emphasis on summit erosion surfaces, but without descending to the outer sierras and
177 foothills below elevations of 1000 m, where important geomorphological clues of a
178 similar nature also occur.

179 Other recurring cutoff lines are of a chronological nature:

180 (i) emphasis on the Alpine structures without sufficient consideration for Hercynian
181 tectonic inheritance; or, conversely, emphasis on Hercynian inheritance with insufficient
182 recognition of Alpine overprints. This has entailed major delays in the publication of
183 certain geological maps and impacted the publication agenda of synthetic and integrated
184 monographs about the Pyrenees (Barnolas and Chiron, 1996, 2018);

185 (ii) emphasis on the synorogenic (syntectonic) Pyrenees, i.e., on the late Cretaceous and
186 Paleogene epochs until the cessation of fold-and-thrust deformation, as if the post-
187 orogenic period (interchangeably also termed post-shortening period in this review),
188 which spans the Neogene and Quaternary, had remained uniquely uneventful and could
189 satisfy the expedient assumption of a topographic steady state;

190 (iii) emphasis on the orogen as if it were a closed plate-boundary system driven exclusively
191 by crustal thickening, erosion, and peripheral sedimentation — when actually the orogen
192 is also influenced by an independent chronology of Cenozoic intraplate and
193 asthenospheric processes affecting large tracts of Iberia, the French Massif Central, the
194 Western Mediterranean, and impacting on base-level changes within the mountain
195 range as well as its peripheral lowlands.

196 This matrix of spatial and chronological cutoff lines arises from a fragmentation of the
197 scientific cultures involved in documenting the Pyrenees. In 1789, geologist Louis Ramond de
198 Carbonnières wrote:

199 *“I doubt that there exists a mountain range better suited than the Pyrenees*
200 *to the observation by a naturalist of its structure and rock disposition.*
201 *Because it is simple and regular throughout most of its extent, the order*
202 *which presided over the formation of its peaks and the laws which govern*
203 *their degradation will soon become apparent. The relief will eventually be*
204 *reduced to shapeless accumulations of debris, and its pattern to a strange*

205 *labyrinth. Through the location, proportion and elevation of its different*
206 *parts, the naturalist will readily understand the constants and laws over*
207 *which he had stumbled in other settings”* (translation into English: this
208 study).

209 Despite these early hopes for a unified understanding of the mountain range, over 200 years
210 later we find that the investigation of the Pyrenees has suffered from the usual disconnect
211 between geological and geomorphological approaches, between orogen-scale desktop
212 modelling and local-scale field observations, between a focus on Alpine tectonics and a
213 neglect of Quaternary neotectonics, with many of its consequences listed above.

214 Restricting research to the confines of the time or spatial bundles listed above has generated
215 persistent blind spots with an entrenched risk of confirmation bias. This review attempts to
216 transcend some of those conventional boundaries of inquiry by operating from two key
217 angles: (i) we address the metabolism of the orogen as a mountain range rather than just as
218 a crustal wedge or mosaic of geological structures, and thus focus on its erosional history,
219 topographic evolution, and landform assemblages; (ii) we articulate the geodynamic history
220 of the Pyrenees with the palaeogeography of its Ebro, Aquitaine and Mediterranean
221 sedimentary basins simultaneously, spanning the earliest plate convergence episodes of the
222 latest Mesozoic to glaciation in the Pleistocene. As a result, rather than a small,
223 asymmetrically bi-vergent orogen captured over simplifyingly short intervals of geological
224 time, it portrays instead a mountain range evolving continuously by lateral and longitudinal
225 growth or destruction through a succession of three quite distinct avatars defined hereafter
226 as the Proto-Pyrenees, the Ancestral Pyrenees, and the Modern Pyrenees — respectively
227 and schematically during the late Cretaceous, Paleogene and Neogene–Quaternary. Each of
228 these Pyrenean ranges has displayed transient periods of crustal and topographic symmetry
229 and asymmetry, successions of range-parallel and range-transverse drainages, the
230 construction and unequal preservation of range-front megafans, uneven intensities of
231 crustal uplift and depths of rock denudation, unequal depths of fluvial incision and patterns
232 of alluvial deposition, and unequal intensities of glacial imprint in more recent time. Many
233 place names (massifs, peaks, towns, etc.) mentioned in the text are located in the figures,
234 but for precision and completeness it is recommended to use an Earth navigation browser.

235

236 **2. An outline of Pyrenean tectonics**

237

238 The natural landscapes of the Pyrenees became the focus of scientific investigation (e.g.,
239 Palassou, 1781–1823; Ramond de Carbonnières, 1789; Pasumot, 1797) somewhat before
240 gaining appeal as a cultural, aesthetic and touristic attraction in the 19th century (overviews
241 by Briffaud, 1994; Besson, 2000). Like the European Alps, the Pyrenees were approached
242 from the early days of geology as a reference model that would help geologists to
243 understand mountain building processes more generally. The mountain range has
244 accordingly attracted a vast effort of international research into its Hercynian basement
245 fabric, its Meso-Cenozoic cover rocks, and into the many thrusts and folds that shaped it
246 from the Cretaceous to the early Neogene. Among the earlier books, “Études pyrénéennes”
247 (de Margerie, 1946) constitutes a good starting point. More recent overviews include books
248 by Canerot (2008), Barnolas and Chiron (1996), Barnolas and Chiron (2018; but is 20 years
249 out of date despite its publication in 2018), and review papers: e.g., Mattauer (1968),
250 Mattauer and Henry (1974), Souquet et al. (1977), Choukroune (1992), Roure and
251 Choukroune (1998), Damotte (1998), Vergés et al. (2002), Teixell et al. (2018), and Muñoz
252 (2002, 2019).

253 Work on the geomorphology of the Pyrenees has been less abundant than in the case of
254 hard-rock geology, lithostratigraphy, tectonics and solid-earth geophysics, but it began
255 almost at the same time as the early geological work. The landscape of the Pyrenees has
256 been attracting geomorphologists since the late 19th century and has involved scholars from
257 Germany (Penck, 1886, 1894; Ashauer, 1934; Panzer, 1926, 1933), the Netherlands
258 (Pannekoek, 1935; Boissevain, 1934; de Sitter, 1952, 1954, 1961; Kleinsmiede, 1960;
259 Zandvliet, 1960; Hartevelt, 1970), Switzerland (Nussbaum, 1930, 1931, 1943), Spain (García
260 Sainz, 1940; Solé Sabaris, 1951) and France (de Martonne, 1910; Blanchard, 1914; Sorre,
261 1913; Birot, 1937; Goron, 1941a, b; Sermet, 1950; Taillefer, 1951; Viers, 1960, 1961; Barrère,
262 1963). For more detailed reference lists covering work before 1990, see Birot (1937) and
263 Calvet (1996).

264

265 **2.1. First-order structure of the orogenic wedge**

266

267 An Alpine orogenic belt roughly striking E–W and nearly 1700 km long extends from the
268 Galicia Bank in NW Spain to the western Alps in Provence. The Pyrenean orogen (Fig. 1)

269 forms the median segment of this orogenic belt over a length of 450 km between the Bay of
270 Biscay (Atlantic Ocean) and the Gulf of Lion (Mediterranean Sea), but crustal deformation
271 extends westward, uninterrupted, to the Cantabrian Mountains, and northeastward beyond
272 the Corbières virgation into coastal belt of Languedoc. The Cantabrian Mountains to the
273 west, which are topographically continuous with the Pyrenees, had until recently been
274 treated as a distinct morphotectonic system. Initially interpreted as resulting from
275 southward subduction of the Bay of Biscay's oceanic crust (e.g., Boillot and Capdevila, 1977),
276 the Cantabrian mountain belt is now viewed as a westward continuation of Pyrenean
277 structures because it also involves northward underthrusting of the Iberian crust (Pedreira et
278 al., 2003, 2007, 2015; Carballo et al., 2015; Teixell et al., 2018). A component of southward
279 oceanic underthrusting, of limited magnitude in the east but which amplifies westward
280 towards Galicia (Teixell et al., 2018), is nonetheless also involved.

281 The Pyrenees result overall from the protracted and complex evolution of the mobile crustal
282 belt situated between Eurasia and Iberia during the Triassic, then from the late Jurassic to
283 the late Cretaceous, with collisional tectonics from the late Cretaceous to the early Miocene.
284 As an Alpine mountain range, the Pyrenees thus defined are relatively small and extend for
285 370 km between Pic d'Orhy in the west and Cap de Creus in the east (the Basque Country,
286 which differs substantially from the rest of the orogen: e.g., Razin, 1989, is not analysed in
287 detail in this structural presentation). The mountain belt strikes N110°E, varies in width from
288 75 to 150 km, and between the Aquitaine Basin in the north and the Ebro Basin in the south
289 is structurally divided into a classic succession of five tectonostratigraphic belts. These are
290 known as the Sub-Pyrenean Zone, North-Pyrenean Zone (NPZ), Axial Zone (AZ), Noguères
291 Zone, and South-Pyrenean Zone (SPZ). From a more strictly tectonic viewpoint, the orogen
292 presents two major domains (Fig. 2):

- 293 • the European domain, where Alpine structures are north-vergent. It consists of most
294 of the NPZ, which overrides the Aquitaine retro-foreland basin along the North-
295 Pyrenean Frontal Thrust (NPFT). The southern edge of the Aquitaine Basin south of
296 the North-Pyrenean Front (Fig. 2) is also substantially crumpled over a blind thrust
297 (the so-called Sub-Pyrenean Thrust), which connects at depth with the NPFT and
298 marks the outermost limit of the crustal wedge. This outer tectonic belt is the Sub-

299 Pyrenean Zone and coincides with a fold-and-thrust belt geographically known as the
300 Petites Pyrénées.

- 301 • the Iberian domain, where Alpine structures are south-vergent. From north to south,
302 it consists of the southwestern part of the NPZ, the Axial Zone, the Nogueres Zone (a
303 small and controversial unit), and the SPZ; the SPZ overrides the Ebro Basin and
304 terminates at the South-Pyrenean Frontal Thrust (SPFT); between the Axial Zone and
305 the SPZ lies the Nogueres Zone — to which we return in Section 2.3.3.2.2. The rock
306 sequences of the Ebro Basin itself are variously deformed, thus displaying an element
307 of symmetry with the situation in the Sub-Pyrenean Zone of the Aquitaine Basin (Fig.
308 3).

309 In the central and eastern Pyrenees, cover-rock outcrops in the narrow southern fringe of
310 the NPZ are intensely deformed and underwent low-pressure–high-temperature (LP–HT)
311 metamorphism during the Alpine orogeny. Known as the Internal Metamorphic Zone (IMZ),
312 this belt of metamorphic outcrops can be considered as a sixth structural unit (Fig. 3), not
313 recognised as such in earlier literature. It defines the structural centreline of the orogen. It
314 derives directly from a hyperextended mid-Cretaceous rift, on the floor of which the
315 lithospheric mantle (today exposed as small outcrops of lherzolite) became exhumed
316 (Jammes et al., 2009; Lagabrielle et al., 2010). The Axial Zone and IMZ are abruptly separated
317 by the North-Pyrenean Fault (NPF), which has long been considered as the locus of the
318 Europe–Iberia plate boundary (e.g., Le Pichon et al., 1970; Choukroune et al., 1973). As
319 discussed in Section 2.3.1, however, matters are somewhat more complex.

320 The synorogenic Cretaceous and Cenozoic sequences are remarkably well preserved, and
321 this has made the Pyrenean orogen a very attractive area for studying thin- and thick-
322 skinned synsedimentary tectonics. Another outstanding feature of the Pyrenees, however, is
323 also its extensive outcrop of Paleozoic rocks. The crystalline rocks of the Paleozoic basement
324 make up most of the Axial Zone, for this reason also known as the ‘Haute Chaîne Primaire’
325 (Paleozoic High Range), and are also exposed in several North-Pyrenean massifs (part of the
326 North-Pyrenean Zone) and in the Mouthoumet massif (part of the Sub-Pyrenean Zone). The
327 Mesozoic and Cenozoic cover sequences of the Axial Zone were removed by nappe
328 displacement and/or by erosion during the Alpine tectonic cycle.

329

330 **2.2. The Pyrenees before the Pyrenees: pre-orogenic plate reconstructions**

331 **2.2.1. Geological fabric of the Hercynian basement**

332 The Pyrenees contain a segment of the southern outer zones of the vast Hercynian mountain
333 belt (Barnolas and Chiron, 1996). The Hercynian orogeny (~330–290 Ma, possibly 360–290
334 Ma according to Casas et al., 2019) resulted in the deformation of sedimentary and volcanic
335 rock sequences of Ediacaran to early Carboniferous age (~580–325 Ma) and of (mainly)
336 Ordovician intrusive rocks (~475–445 Ma). LP–HT regional metamorphism was widespread,
337 intensifying with depth to anatexis and represented by micaschists, marble, paragneisses,
338 metagranitic orthogneisses, and even migmatites. Large granitic plutons cross-cutting the
339 metamorphic country rock were emplaced mainly between 310 and 295 Ma. Inherited rock
340 textures, thrusts, large upright and recumbent folds, detachment faults, mylonitic zones, and
341 large dome structures such as the Canigou–Carançà in the eastern Pyrenees have been well
342 studied (e.g., Carreras and Capella, 1994; Laumonier et al., 2014).

343 Magnitudes of orogenic denudation were greater in the eastern and central Axial Zone than
344 in the west. As a result, the western Axial Zone is dominated by carbonate-rich, low-grade
345 Devonian and Carboniferous series, whereas crustal rocks exposed in the eastern half of the
346 Axial Zone are on average older and display deeper facies such as the Ediacaran Canaveilles
347 Group (schists and carbonates), the Cambrian Jujols Group (schists), and the Ordovician
348 Canigou metagranite. In the east, younger Hercynian rocks are rare and confined to narrow
349 synclines (e.g., Silurian, Devonian and Carboniferous at Villefranche-de-Conflent). The
350 Hercynian plutons (Saint-Laurent-de-Cerdans, Quérigut, Mont-Louis, Maladeta, Néouvielle,
351 etc.) cross-cut all of these series at all crustal levels. The Hercynian cycle ended in Permian
352 time with an abundant production of late-orogenic molasse and volcanic deposits under an
353 extensional to right-lateral tectonic regime; today these are mostly preserved along the
354 southern edge of the Axial Zone.

355 At least in the eastern half of the Axial Zone, the Hercynian structures and fabrics are
356 generally easy to distinguish from the more recent Alpine structures. The only exceptions
357 concern the reverse to dextral strike-slip mylonite belts along the Mérens Fault, the Têt
358 valley, and from the Col du Perthus to the eastern part of the Axial Zone. It is likely that they
359 are of Hercynian age but were reactivated during the Alpine orogeny. Among some locally
360 exposed Paleozoic granulite outcrops of the NPZ, major low-angle detachment fault planes

361 have been detected and attributed to extension during the Cretaceous followed by Alpine
362 tectonic inversion rather than to Hercynian inheritance (Laumonier, 2015; Cochelin et al.,
363 2018).

364

365 **2.2.2. Mesozoic palaeogeography**

366

367 Outcrops of the pre-orogenic sedimentary sequences are diversely distributed throughout
368 the orogen as a result of nondeposition, postdepositional erosion or tectonics, or because of
369 burial beneath Cenozoic sequences in the pro- and retro-foreland basins (for a synthesis, see
370 Puigdefàbregas and Souquet, 1986; Canérot, 2008). Like its Germanic counterpart, the
371 Triassic sequence (250–200 Ma) records a major transgression–regression cycle within the
372 widespread context of rifting prevalent throughout western Europe at the time (rapid
373 subsidence in the Aquitaine Basin): red fluvial Buntsandstein, covered by lagoonal and
374 marine Muschelkalk carbonates and terminating with Keuper evaporites and ophites
375 (hypovolcanic tholeiitic dolerites) (López-Gómez, 2019).

376 The Jurassic (200–145 Ma) records another major transgression–regression cycle, succeeded
377 by the lowermost Cretaceous transgression (145–125 Ma). The Jurassic carbonate shelf
378 sequence occupies the western confines of the Alpine Tethys and consists entirely of marl
379 and carbonate. Although the early and middle Jurassic were tectonically stable epochs, a
380 new rifting episode started during the late Jurassic and continued into the early Cretaceous,
381 depositing carbonate rocks (e.g., Urgonian limestone facies during Barremian time) in the
382 context of an extensive marine transgression — but this time clearly related to the opening
383 of the southern North Atlantic in the west.

384 In the future North-Pyrenean Zone, rifting intensified during Aptian and Albian times (125–
385 110 Ma), peaking during the Albian and Cenomanian (110–95 Ma). Mantle lherzolites
386 became exposed as a result of extreme crustal thinning in rapidly subsiding grabens (e.g.,
387 Jammes et al., 2009; Lagabrielle et al., 2010; Tugend et al., 2014; Clerc and Lagabrielle, 2014;
388 Lagabrielle et al., 2019), and syn-rift sedimentation reached thicknesses of 4–6 km in some
389 depocentres. Sediment fill was lithologically quite varied, ranging from fine-textured clastic
390 deposits (Aptian ‘Black marls’, and Middle Albian to Lower Cenomanian ‘Black flysch’
391 turbidites) to coarse breccia around the basin margins (e.g., ‘Poudingues de Mendibelza’)

392 (Souquet et al., 1985; Debroas and Azambre, 2012). Alkaline mafic magmatism also erupted
393 in the area of the (future) North-Pyrenean Zone.

394 During the early Cretaceous, the region corresponding to the future Axial Zone was largely a
395 land area, though not a mountain range. From middle Cenomanian time, rifting slackened
396 rapidly, and within a regional context of sea-level rise the North Pyrenean foredeep widened
397 northward (Cenomanian and Turonian 'Grey flysch': ~95–90 Ma, displaying a turbidite facies
398 with breccia; followed by Coniacian 'Furoid flysch': ~90–85 Ma). Meanwhile, to the south,
399 i.e., over the future western end of the Axial Zone, the former land area became submerged
400 and the new environment favoured the establishment of a carbonate platform ('Calcaires
401 des canyons', today forming the Arres d'Anie massif, for example). These are post-rift
402 deposits, well documented as such by the sharp Cenomanian angular unconformity which
403 used to be erroneously interpreted as the termination of a pre-Cenomanian orogenic event.
404 Metamorphic transformation of the Black flysch in the Internal Metamorphic Zone occurred
405 around this time (~100–90 Ma) in a yet poorly understood tectonic context. After 85 Ma, the
406 retro-foreland area evolved into a strike-parallel marine foredeep, which performed as a
407 receptacle for north-prograding clastic sequences. The foredeep filled sequentially from east
408 to west during the Campanian–Maastrichtian, in step with the Axial Zone in the east
409 progressively rising above sea level in response to early Pyrenean compressional
410 deformation. The foredeep sequences and part of the Axial Zone were soon covered by
411 continental red beds known regionally as the Garumnian series (e.g., Rosell et al., 2001).
412 Meanwhile, the west of the Pyrenees remained below sea level (see palaeogeographic map
413 sequence in Plate I). The end of the Cretaceous is thus the transitional period during which
414 syn-orogenic sedimentation took over from the pre-orogenic episodes and gave rise to the
415 Proto-Pyrenees.

416

417 ***2.2.3. Geodynamic conditions in Cretaceous time***

418

419 The kinematics of the Iberian Plate from the late Jurassic to the late Cretaceous (~160–84
420 Ma) remain difficult to reconstruct in terms of its strike-slip motion, angular distance of
421 anticlockwise rotation, and separation distance with the European Plate. Left-lateral strike-
422 slip motion of Iberia, for example, has been judged negligible by some authors — often

423 geologists on the basis of land-based criteria; but substantial by others — usually marine
424 geophysicists who focus on the kinematics of Atlantic sea-floor spreading between Iberia
425 and Newfoundland. In contrast, the $\sim 35^\circ$ anticlockwise rotation of Iberia associated with the
426 opening of the Bay of Biscay remains fairly uncontested, but its precise age (i.e., entirely, or
427 only partly, Aptian) remains debated (e.g., Gong et al., 2008; Vissers and Meijer, 2012a;
428 Tavani et al., 2018). The width of the rift zone between Iberia and Europe and the causes for
429 lherzolite exhumation are also controversial: whereas strike-slip motion would
430 accommodate small pull-apart basins but seems incompatible with transverse crustal
431 thinning, orthogonal plate extension (NNE–SSW) would be more compatible with the
432 exposure of mantle rocks. The existence of oceanic crust in this rift zone, though currently
433 undocumented, remains unlikely. A triangle of partly compatible end-member models is thus
434 still under scrutiny, with one model inferring > 500 km of transcurrent motion along an
435 ancient transform fault which has been conflated with the NPF (Le Pichon et al., 1970);
436 another advocating minimal motion in the Pyrenean region (particularly the strike-slip
437 component: 100 km at most), thus implying that Iberia never was a truly independent
438 microplate (Souquet et al., 1977; Canérot, 2016); and a third envisaging throughout the
439 Cretaceous the opening and subsequent subduction of a true oceanic domain, which could
440 have attained a width of 500 km in the east (Vissers et al., 2012). Some recent studies,
441 among them Olivet (1996) as a precursor, have attempted to reconcile the geological and
442 geophysical evidence. Nirrengarten et al. (2018), for example, estimate that the Pyrenean
443 rift was ~ 100 km wide and separated southern France from an Ebro microplate rather than
444 from all of Iberia. The Ebro microplate itself was separated from the rest of Iberia on its
445 south side by another Cretaceous rift, now inverted and forming the Iberian Range. Opening
446 of the Pyrenean rift and exposure of a lherzolite outcrop a few tens of kilometres wide
447 occurred during Albian to Cenomanian time, i.e., after left-lateral transcurrent motion of the
448 Ebro microplate and most of Iberia’s rotation during the early Cretaceous had ended (in this
449 model, its cumulative lateral throw is 300–400 km); it was also coeval with the opening of
450 the Bay of Biscay and associated ocean-floor spreading (rotation of Iberia was still ongoing).
451 All of these events occurred during the early Late Cretaceous.

452 The continuation eastward of the (future) Pyrenees depends on how the orogen connected
453 before the late Cretaceous to what lies further east. One scenario suggests that the future

454 Pyrenees simply continued between Provence and the Sardinia–Corsica bloc (which in this
455 case would be part of the Iberian Plate: this is the classic model); another scenario suggests
456 instead that the eastern extension of the future Pyrenees connected with expanses of the
457 Alpine Tethys to the southeast via a transform fault zone passing somewhere between the
458 Pyrenees and Sardinia prior to Sardinia’s rotation in the Miocene (discussion in Tavani et al.,
459 2018). In that case, the Sardinia–Corsica bloc would be part of the European Plate, but what
460 filled the palaeogeographic space east of Iberia and south of France (continental or oceanic
461 crust?) is unknown. It could have been an arm of the Tethys Ocean in Jurassic time.

462

463 **2.3. Tectonic legacies of plate convergence**

464

465 The Pyrenean crustal wedge began to form in mid Santonian time (~84 Ma). Convergence
466 was relatively rapid during two successive episodes, namely from the Santonian to the
467 Maastrichtian (~84–68 Ma) and subsequently from the early Eocene to the Aquitanian (~55–
468 20 Ma). Convergence rates slackened during the Paleocene sensu lato (~68–55 Ma) and have
469 done so once again since the Burdigalian. The mountain range thus grew in two pulses, first
470 during latest Cretaceous time (previously referred to as the Laramide phase at least in
471 French literature because of its coincidence with mountain building in the Laramide Rockies)
472 and producing the Proto-Pyrenees, then from the Eocene to the Oligocene (including the
473 classic late Eocene Pyreneo-Provençal phase) and producing the Ancestral (or Paleogene)
474 Pyrenees. The earlier period of crustal convergence caused tectonic inversion of the mid-
475 Cretaceous rift zone, whereas the second period corresponds to the collision itself. Note that
476 this chronology was established in, and is thus valid for, the central Pyrenees, but cannot
477 substitute for other, less well documented parts of the mountain range. Tectonic collision in
478 the Basque Country (westernmost Pyrenees), for example, had barely begun in mid-Eocene
479 time, whereas in the eastern Pyrenees collision had all but ended by early Oligocene time
480 and was being overprinted by a new deformation cycle impinging as a consequence of north-
481 west Mediterranean extensional dynamics.

482 Despite fairly good agreement over the broad geodynamic sketch presented above, much
483 disagreement still persists around some of its key aspects, some of which were highlighted in
484 the 1970s but with no ensuing consensus. Below we outline those persistent uncertainties.

485

486 **2.3.1. The North-Pyrenean Fault (NPF): plate boundary between Iberia and Europe?**

487

488 The NPF is a conspicuous crustal discontinuity separating the Axial Zone from the Internal
489 Metamorphic Zone of the NPZ, and is at least 250 km long. The NPF was originally
490 interpreted as a Hercynian fault reactivated during Pyrenean collision by a modest
491 component of vertical displacement (Mattauer, 1968), but after the advent of plate tectonics
492 theory it was reinterpreted as a major continental transform fault that had undergone
493 several hundreds of kilometres of left-lateral motion — despite being undetectable in the
494 western Pyrenees (Le Pichon et al., 1970; Choukroune et al., 1973; Boillot et al., 1973).
495 Others still have emphasized instead a case of asymmetry in the Cretaceous rift, with most
496 of the crustal thinning occurring on the European margin (i.e., the present-day NPZ) while
497 the Iberian Plate conserved its original thickness (the asymmetry could, of course,
498 potentially also result from long-distance left-lateral slip bringing together two plate edges
499 with different crustal thicknesses). Despite the ECORS profiles, understanding the depth and
500 angle of the NPF has also proved challenging: the NPF may reach the mantle and offset the
501 Moho (e.g., Choukroune, 1992), but the prevailing view is that it is cross-cut by the NPFT —
502 which is the major south-dipping thrust that has transported the NPZ and part of the Axial
503 Zone northward over the retro-foreland (Fig. 3). Currently, the NPF is considered to be just
504 one among other north-facing Cretaceous normal faults belonging to the Iberian side of the
505 rift and later inverted, the true plate boundary being concealed beneath the Internal
506 Metamorphic Zone. In the western part of the Axial Zone, the NPF could also be the root
507 zone of the south-verging Cotiella-Peña Montañesa system, which was thrust southward
508 over the Axial Zone (e.g., Espurt et al., 2019). At least in the eastern Pyrenees, reactivation of
509 the NPF in late Eocene time could be the main cause for raising the Axial Zone relative to the
510 NPZ. Consistent with this view is the fact that the NPF terminates with the Axial Zone in the
511 west.

512

513 **2.3.2. The late Cretaceous to Paleocene mountain range, or Proto-Pyrenees**

514 The Proto-Pyrenean mountain range rose above sea level only in the eastern part of where
515 the current range now stands, and is not well documented. The south-vergent Campanian

516 thrust of Bóixols in the central SPZ developed during this period. It results from an inversion
517 of the Cretaceous Organyà graben's southern boundary fault and has generated a fault-bend
518 fold (Sant Corneli ramp anticline) (Berástegui et al., 1990; Bond and McClay, 1995; Mencos
519 et al., 2015). The Bóixols thrust is covered by the unfaulted Garumnian series. Other thrusts
520 probably formed during Campanian–Maastrichtian time in the (future) NPZ, i.e., in and
521 around the highly thinned crust of the Cretaceous rift. The thrusts in the NPZ were either
522 north-vergent: i.e., the (still poorly-documented) Internal Metamorphic Zone overriding the
523 non- or weakly metamorphic segment of the NPZ and the incipient NPFT; or south-vergent:
524 i.e., the incipient Lakora Thrust and the probable root zone of the incipient Supra-Axial
525 Thrust (or SAT; Figs. 2, 3; see further specifications Section 2.3.3). At greater depths, most of
526 the lithospheric mantle disappeared as a result of either northward or southward
527 underthrusting (e.g., Teixell et al., 2016; Espurt et al., 2019; Ternois et al., 2019). By
528 Paleocene time, these convergent plate motions (several tens of kilometres of crustal
529 shortening) had resulted in (i) cancelling out the crustal extension generated by Cretaceous
530 rifting, (ii) restoring an almost normal-thickness crust beneath the NPZ, and (iii) accelerating
531 subsidence in the North Pyrenean foredeep.

532

533 ***2.3.3. The Eocene–Oligocene mountain range, or Ancestral Pyrenees***

534

535 A number of gently dipping tectonic boundaries (thrusts, reverse faults) carve up the
536 Hercynian basement and its cover sequence. Three categories of tectonic unit can be
537 distinguished at currently exposed erosional depths. Some units are cover-rock nappes,
538 consisting exclusively of pre- to syn-orogenic sedimentary sequences. For these cover
539 nappes, the Keuper beds (where present) have usually played a major role as a lubricant on
540 thrust planes or in diapiric fold evolution. Other tectonic units, often among the thickest, are
541 mixed: they consist of Hercynian basement and cover-rock packages (pre- to synorogenic
542 strata), concerning both the Axial Zone and the SPZ (Gavarnie nappe at the centre of the
543 range; Canigou–Vallespir and Cadí nappe in the east). Lastly, some units are basement
544 nappes and are confined to the Axial Zone (they may continue unexposed beneath cover
545 sequences in portions of the SPZ). Those three categories of tectonic unit may be termed
546 upper, middle, and lower, respectively, but scholars have stumbled on the difficulty of

547 correlating the basement units of the Axial Zone with the cover units of the SPZ (for the
548 eastern Pyrenees: e.g., Muñoz et al., 1986; Fontboté et al., 1986; Laumonier, 1987, 2015;
549 Laumonier et al., 2015; for the central Pyrenees: Vergés and Muñoz, 1990; Muñoz, 1992;
550 Muñoz et al., 2018; for the western Pyrenees: Labaume et al., 2016a; Labaume and Teixell,
551 2018).

552 A major consequence of the middle-late Eocene to early Oligocene tectonic movements has
553 been the uplift of the Axial Zone relative to the NPZ and SPZ, especially in the eastern part of
554 the mountain belt (see Section 2.3.1 above). As a result, the Axial Zone presents itself as a
555 vast basement window while also hosting the root zones of the middle and lower tectonic
556 units. Unlike the NPF, the limit between the Axial Zone and the SPZ presents itself as a large
557 range-front flexure, interpreted schematically as the frontal ramp fold affecting the
558 basement of the Ancestral Pyrenees. This tectonic structure of the Axial Zone was associated
559 with the emplacement of part of the middle units, and lastly of the lower units. Another
560 consequence of the late uplift of the Axial Zone is that the upper units of the SPZ are klippen
561 preserved in the frontal-ramp syncline and ‘floating’ on the Paleogene of the middle units
562 (Fig. 3D). The position of their root zones, perhaps within but, equally possibly, north of the
563 Axial Zone, is uncertain because the connection with the southern klippen has been removed
564 by denudation (Section 2.3.3.2).

565

566 *2.3.3.1. Crustal architecture of the European domain*

567

568 North of the Axial Zone, the Pyrenean retro-wedge consists of masses of Hercynian
569 basement (the North-Pyrenean massifs: Barousse; Arize; Saint-Barthélemy, also named
570 Montagne de Tabe; Trois-Seigneurs; Agly), and Mesozoic cover sequences (within the NPZ
571 and the Sub-Pyrenean Zone). The NPZ is narrow (10–15 km) and highly deformed in the east;
572 it widens (15–30 km) and has been well studied in the central Pyrenees along the ECORS-
573 Pyrenees profile (Baby, 1988; Ford et al., 2016; Rougier et al., 2016). The NPZ is the result of
574 tectonic basin inversion during the late Cretaceous (Proto-Pyrenees: ~80–66 Ma), and most
575 of all during the Eocene (~56–35 Ma). In the west, the NPZ corresponds with the moderately
576 deformed and inverted Cretaceous basins that today form the south-vergent ‘Chaînons
577 béarnais’ (Béarn Ranges) and north-vergent Mauléon Ranges (Teixell et al., 2016; Canérot,

578 2017; Saspiturry et al., 2019). Here outcrops of the Axial Zone and NPF pinch out, and the
579 NPZ and SPZ find themselves in direct contact with one another, the former being thrust over
580 the latter.

581 The North-Pyrenean Frontal Thrust (conspicuously exposed, e.g., at Pic de Bugarach) was
582 instrumental, mainly during end-Cretaceous and Eocene time, in displacing the NPZ, the NPF,
583 and part of the Axial Zone northward by 25–30 km. The narrow Sub-Pyrenean Zone consists
584 of folded synorogenic late Cretaceous and Eocene sedimentary series. Deformation of the
585 Sub-Pyrenean Zone was partly controlled by the Sub-Pyrenean Thrust — a blind thrust which
586 connects at depth with the NPFT (Fig. 3). In the western Pyrenees, the Sub-Pyrenean Zone
587 corresponds to the Arzacq Basin. North of the Sub-Pyrenean Zone, the synorogenic
588 sequences of the Aquitaine Basin remain weakly deformed or undeformed. In the European
589 Pyrenees, salt tectonics appear to play a major role (Canérot et al., 2005; Labaume and
590 Teixell, 2020; Ford and Vergés, 2020).

591 In the far east, the retro-wedge configuration changes abruptly: (i) the southern part of the
592 NPZ (i.e., the Internal Metamorphic Zone, Fig. 2) disappears in the Gulf of Lion as result of
593 the extensional tectonics prevalent since Oligocene time in this region; the eastward
594 continuation of the IMZ has nonetheless been detected offshore (Guennoc et al., 2000). (ii)
595 The northern part of the NPZ bends around and strikes in a NNE–SSW direction, forming the
596 large orocline known as the eastern Corbières nappe, and some Mesozoic thrust packages at
597 the southern tip of Provence (Cap Sicié) have been interpreted as a distant eastward
598 continuation of the NPZ (Jolivet et al., 2020). (iii) The Sub-Pyrenean Zone widens
599 considerably and also displays a basement outcrop (the Mouthoumet massif). E–W-striking
600 Pyrenean structures also impinge on the southern edge of the Massif Central, the most
601 obvious consequence of thrust tectonics being the Mazamet–Tantajo reverse fault, which
602 forms the boundary of the Montagne Noire (Fig. 1).

603

604 *2.3.3.2. Crustal architecture of the Iberian domain*

605

606 The Iberian pro-wedge is chiefly a south-vergent thrust sequence consisting of upper, middle
607 and lower tectonic units. The South-Pyrenean Frontal Thrust schematically represents the
608 leading edge of the middle and/or lower thrusts. This configuration is very clear in the

609 southeastern Iberian domain, where the orogenic pro-wedge ceased to grow outward during
610 the early Oligocene; but less so in the southern and southwestern domains, where collisional
611 deformation continued until the early Miocene. Here, deformed pro-foreland sedimentary
612 sequences became incorporated into the SPZ tectonic unit (South Jaca Basin, also known as
613 Guarga Syncline) by dint of the deepest, most recent and most southerly thrusts such as the
614 Upper Guarga thrust (surfacing at the Sierras Exteriores) and the Lower Guarga blind thrust
615 propagating southward into the Ebro Basin (Labaume and Teixell, 2018). Considerable lateral
616 variation along the strike of the orogen gains from a segmented examination of the main
617 structures from east to west.

618

619 *2.3.3.2.1. Structure of the southeastern Pyrenees*

620

621 From top to bottom, the eastern Pyrenees display the following tectonic units, mapped in
622 Figures 2 and 3:

- 623 (i) the Aspres upper unit, which is an Axial Zone upper basement nappe;
- 624 (ii) the upper SPZ units (Pedraforca nappe; klippen of Coustouges, Bac Grillera, Biure,
625 and the Empordà, further east), which are preserved within the Ripoll fault-bend
626 syncline (i.e., the frontal-ramp of the Ancestral Pyrenees);
- 627 (iii) the Canigou nappe: a thick and extensive middle unit, which incorporates a large
628 component of Axial-Zone basement rocks (as well as the Mesozoic sequence of the
629 so-called Amélie-les-Bains Basin, which is the only remaining evidence of pre-
630 orogenic cover rocks in the eastern Axial Zone) and most of the SPZ (Cadí units). The
631 thin and discontinuous Vallespir unit is the basal portion of the Canigou nappe in the
632 Axial Zone;
- 633 (iv) some lower units displaying outcrops of their basal thrust planes (Albères and Roc de
634 France units; Freser duplex structure);
- 635 (v) components of the lowermost unit (mainly the Saint-Laurent-de-Cerdans unit),
636 whose floor thrust (but no known outcrops of it) forms the base of the pro-wedge
637 and functions as the lowermost imbricate for the overlying frontal ramps;
- 638 (vi) the small and lowermost Serrat unit, concealed under the Cadí units.

639

640 In the Axial Zone, the lower units are visible beneath the Canigou nappe in the vast Albères
641 and smaller Freser windows (Laumonier, 2015). The eastern segment of the SPFT is known
642 by its local name as the Vallfogona Thrust, where the lower and middle thrusts join up. The
643 Pedraforca nappe and upper Bac Grillera klippe have no established root zones within the
644 Axial Zone (Figs. 2, 3). As in the case of the Bóixols unit (see below), it makes good sense
645 nonetheless (i) to situate their pre-tectonic home area in the northern part of the Axial Zone,
646 north of the Soldeu–L'Hospitalet fault in the case of the Upper Pedraforca unit (Fig. 2); and
647 (ii) to envisage that they were transported southward by means of a major thrust, named
648 here Supra-Axial Thrust (SAT), which forms the base of a Supra-Axial nappe overspanning the
649 Axial Zone (noted Supra-Axial Thrust Sheet in Fig. 3). The SAT was rooted north of the Axial
650 Zone in an area perhaps corresponding to the IMZ but today obscured by the FNP, which in
651 the eastern Pyrenees displays the attributes of a post-SAT reverse fault despite having the
652 geometric appearance of a backthrust (Fig. 3D), as discussed above (Section 2.3.1.). The
653 Coustouges, lower Bac Grillera and Biure klippen were originally connected to the Aspres
654 unit in the Axial Zone, but also perhaps to the SAT. The Empordà composite nappe (Bilotte et
655 al., 1979), which mirrors the northern Corbières nappe, is also linked to the SAT.

656 The orogen in the southeastern Ancestral Pyrenees began to acquire its characteristic
657 architecture (i) in early Ypresian time (Ilerdian) with the formation of the narrow Ripoll
658 foredeep. This continued (ii) through the middle Eocene (late Ypresian–early Lutetian) with
659 the leading edges of the upper units advancing as far as the foredeep (e.g., Muñoz et al.,
660 1986; Vergés and Martínez, 1988; Pujadas et al., 1989; Vergés and Muñoz, 1990; Martínez et
661 al., 1997). Crustal deformation continued (iii) through the middle Lutetian to Bartonian, a
662 time when the Canigou–Vallespir–Cadí nappe advanced southward and the Ripoll foredeep
663 itself became a piggyback basin. The lower thrust units were emplaced (iv) mainly during
664 Bartonian and Priabonian time (late Eocene), contributing to form the Ripoll fault-bend
665 flexure (soon to become the Ripoll syncline) and to raise the Axial Zone topographically. The
666 Vallfogona Thrust remained active until the early Oligocene.

667

668 *2.3.3.2.2. Structure of the south-central Pyrenees*

669

670 The central Pyrenees present a classic sequence of thrust units from north to south (review
671 in Oliva-Urcia, 2018): (i) within the Axial Zone, the Gavarnie Thrust shears the Paleozoic
672 basement internally but also overrides the Mesozoic sequences to the south, along the
673 border between the Axial Zone and the SPZ. The thrust plane separates the Gavarnie nappe
674 from the underlying Benasque–Orri nappe (includes here the Bielsa, Ribagorçana and Bono
675 units), which itself overrides the Rialp nappe (Fig. 3); (ii) just south of the Axial Zone, along
676 the fault-bend flexure, the Nogueres Zone is the leading edge of a nappe and consists of
677 basement units with a thin tegument of Permo-Triassic sediments; (iii) the central SPZ is a
678 vast, lobate allochthonous thrust sheet known as the South-Pyrenean Central Unit
679 (SPCU; actually a lateral continuation of the Pedraforca unit; Fig. 2), and its Serres Marginals
680 unit is effectively the western continuation into the central Pyrenees of the lowermost
681 Pedraforca nappe (Fig. 2). The SPCU mainly consists of the Montsec unit, which also
682 incorporated the Upper Cretaceous Bóixols unit.

683 After the pioneering work of Séguret (1972), interpretations of the SPCU were strongly
684 influenced by results from the deep seismic ECORS-Pyrenees profile produced in 1985–1986.
685 From this major work emerged a ‘standard model’ of the central Pyrenean crust (Fig. 3B;
686 Muñoz, 1992; Beaumont et al., 2000), which advocates the following geometry: (i) the
687 Gavarnie nappe extends southward via the Nogueres Zone, which is why the Gavarnie Thrust
688 has been renamed Nogueres Thrust in that area; (ii) the Axial Zone is interpreted as a thick
689 and vigorously compressed anticlinal nappe stack in which syn-orogenic thrust planes, such
690 as the eastern end of the Gavarnie (Nogueres) Thrust, have been tilted almost vertically; (iii)
691 the putative home area of the SPZ allochthonous units (particularly the Cretaceous Organyà
692 Basin) was given to be the Rialp basement unit, i.e., south of the present-day Axial Zone. A
693 partly similar model has been proposed for the Pedraforca nappe further east (Vergés et al.,
694 1995).

695 Despite having gained wide currency, this crustal model is vulnerable to a number of caveats
696 (Soler et al., 1998; Laumonier, 2015), particularly features such as the tight anticlinal stack of
697 the Axial Zone, and the series of major upturned Alpine thrusts both in the Axial Zone and
698 within the allochthonous South-Pyrenean units (whether above the Axial Zone basement or in
699 areas south of it). The revision of the ‘standard model’ shown in Fig. 3B, first elaborated by
700 Laumonier (2015) and illustrated in Fig. 3C, emphasizes instead:

- 701 (i) the absence in the east-central part of the Axial Zone, i.e., between the Gavarnie and
702 Aspres thrusts, of a major Alpine thrust, whether upturned or not;
- 703 (ii) the need for the basal thrust plane of the SPCU–Pedraforca units to be rooted north
704 of the Axial Zone, implying the existence of a major overspanning nappe — the
705 Supra-Axial Thrust unit (SAT) — overriding an Axial Central Unit (ACU, newly coined
706 for the occasion; Figs. 2, 3), i.e., from the NPZ to the SPZ. Here, the ACU lumps
707 together the eastern parts of the Gavarnie and Benasque–Orri units and the
708 basement of the Canigou nappe;
- 709 (iii) the need for the Nogueres units to form a basal duplex structure linked to the Supra-
710 Axial Thrust unit. This redefines the overspanning SAT unit as the true ‘Nogueres
711 Thrust’ sensu Teixell et al. (2018), which further south becomes the basal thrust of
712 the SPCU (Fig. 3C). For future reference it seems preferable, however, to avoid the
713 term ‘Nogueres Thrust’, which has been employed to mean too many different things
714 in the past.

715 From these reconsiderations it follows that crustal shortening within the Axial Zone was
716 more limited in the new than in the ‘standard’ model, and the home area of the SPCU–
717 Pedraforca nappe system was not situated south of the current Axial Zone but rather above
718 and overspanning it (Fig. 2). The home area of the Bóixols–Upper Pedraforca units (vertical
719 green and pink hatching in Fig. 2) lay north of the Gavarnie–Lladorre–Soldeu–l’Hospitalet
720 line, whereas the home area of the Montsec–Lower Pedraforca units lay south of this fault
721 line (southward displacement during Eocene time noted by white arrows in Fig. 2). In this
722 model, the (future) Bóixols Thrust represents the upper portion of the Lladorre Fault, i.e. the
723 mid-Cretaceous normal fault that became inverted at the end of the Cretaceous and was
724 initially instrumental in forming the Bóixols Anticline. Subsequently during Eocene time, the
725 SAT, which was rooted north of the Axial Zone (Fig. 3D), transported the entire Axial Zone’s
726 cover sequence southward over a distance of 40–50 km to its present-day position (i.e., the
727 SPCU and Pedraforca klippen). Meanwhile, crustal shortening within the underlying
728 basement itself (or Axial Central Unit: ACU, Figs. 2, 3D) was negligible. In its broad
729 principle, this model is analogous to the scenario advocated by Teixell et al. (2018, Fig. 20
730 therein) for the west-central Pyrenees. The Gavarnie–L’Hospitalet fault zone would thus be
731 the deeper portion of the Bóixols / Lladore Fault, first inverted at the end of the Cretaceous

732 and with the Bóixols unit subsequently transported southward by the Supra-Axial Thrust; the
733 home areas of the Montsec and Lower Pedraforca units were located south of the Gavarnie–
734 L'Hospitalet fault zone. Furthermore, unlike the standard model of Muñoz (1992), the nappe
735 stack does not form a thick anticlinal hump and is, instead, flatter and thinner (compare
736 cross-sections B and C, Fig. 3). Independent work compatible with the revised model is
737 currently emerging (Angrand, 2017; Cochelin et al., 2018, Figs. 9d and 9e therein; Teixell et
738 al., 2018; Espurt et al., 2019; Ternois et al., 2019). This has potential implications in terms of
739 estimating the total depths of denudation required to exhume the crystalline Paleozoic rocks
740 of the Axial Zone, and also bears on establishing when debris from the exposed Axial Zone
741 began to feed into the conglomerate sequences of the pro- and retro-foreland. These
742 corollary aspects would require further investigation, but Cochelin et al. (2018, their Fig. 10)
743 have already shown from independently published thermochronological data (Fitzgerald et
744 al., 1999; Sinclair et al., 2005) that the putative 'Nogueres' and Orri units shared similar
745 exhumation histories (rapid exhumation between 35 and 30 Ma), thus accrediting the view
746 that the central Pyrenees form a single tectonic unit (the ACU, Fig. 3C) delimited by the NPF
747 in the north, rather than the duplex structure of the 'standard' model shown in Figure 3B.
748 Because of its décollement seated in the Keuper evaporites, the SPCU has propagated much
749 further southward (and in a somewhat unclear manner) than its lateral SPZ extensions in the
750 east (Pedraforca, via the Segre ramp) and west (via the Ainsa Oblique Zone) (Fig. 2) (Muñoz
751 et al., 2013).

752

753 *2.3.3.2.3. Structure of the southwestern Pyrenees*

754

755 The western Pyrenees of today stand where the Axial Zone plunges beneath its envelope of
756 Cretaceous cover rocks. The Béarn Ranges ('Chaînons béarnais': Canérot et al., 1978; Teixell,
757 1990; Teixell et al., 2016), long held to belong to the southern part of the NPZ where
758 structural vergence is directed southward, directly override the SPZ (Lakora nappe, which
759 involves the basement and the cover sequence). This occurred before uplift of the Axial
760 Zone. The Lakora Thrust is thus the exact equivalent of the Supra-Axial Thrust (*sensu hic*) in
761 the central and eastern Pyrenees (i.e., the 'Nogueres Thrust' *sensu* Teixell et al., 2018).
762 Despite their position within the NPZ, the Béarn Ranges therefore really belong to the

763 Iberian side of the Cretaceous rift (southern NPZ) and not to its European side (northern
764 NPZ). The succession of small thrust slivers ('Écailles bordières') along the northern edge of
765 the Axial Zone also belongs to the Iberian domain (these can be interpreted as basal horses
766 beneath the Supra-Axial Thrust).

767 The Gavarnie nappe (Axial Zone and northern half of the SPZ to the Oturia Thrust)
768 propagated southward during the late Eocene and early Oligocene. It incorporates the
769 Larra–Sierras Interiores–Ordesa–Monte Perdido system, which is the westward extension of
770 the Serres Marginals thrust unit via the Ainsa Oblique Zone (Fig. 2), and has been dated to
771 the middle Eocene (Labaume et al., 2016a; Labaume and Teixell, 2018). This entire crustal
772 mass was subsequently transported on the back of the Guarga–Sierras Exteriores Thrust
773 during the Oligocene and earliest Miocene. The southern Jaca Basin has been transported
774 piggyback on the Guarga thrust unit (see also section 3.2.3).

775

776 **2.3.4. Some unresolved issues**

777 As revealed by the geological research presented above, the structure of the Proto-Pyrenees
778 and Ancestral Pyrenees is complex and still imperfectly understood. Three areas of
779 uncertainty are highlighted below, all dependent on tectonic models and their prior
780 assumptions.

781 (i) The successive stages of crustal wedge construction during the late Cretaceous (Proto-
782 Pyrenees) and Paleogene (Ancestral Pyrenees), and thus their respective legacies in the
783 mountain architecture, are still debated, particularly on the European side of the orogen.
784 The NPFT may have been at its most active during the late Cretaceous, contributing
785 substantially to mid-Cretaceous rift inversion and to the production of a pop-up
786 structure; whereas displacement along it, as likewise along the Sub-Pyrenean Thrust,
787 slackened during the Paleogene. Establishing the magnitude and chronology of the
788 vertical movements which were associated with these thrust displacements, and
789 whether they occurred above or below sea level, is important for interpreting the north-
790 Pyrenean conglomerate sequences (see Section 3.1 and Fig. 5), but constraints are still
791 imprecise.

792 (ii) Structural interpretations of the Iberian side of the Ancestral Pyrenees continue to
793 stumble on the links between the Axial Zone and SPZ thrust units (Fig. 2). Establishing the
794 geometries of the various units has bearing on the age of displacement on those thrusts
795 and on the true magnitude of Alpine shortening. For example, according to current
796 stratigraphic and structural evidence, the eastern middle thrusts of Canigou–Vallespir
797 and Cadí were mostly active during middle Lutetian and Bartonian times (~45–38 Ma),
798 whereas maximum displacement on the Gavarnie and Oturia thrusts farther west (Fig. 2)
799 occurred during the Bartonian and Rupelian (~40–30 Ma). Such lags in the evolution of
800 the crustal wedge emphasize an east-to-west polarity in the construction of the orogen.
801 A similar lag is recorded in the progressive shaping of the orogen’s southern boundary
802 flexure, and thus in the uplift and erosion of the Axial Zone and the out-of-step discharge
803 of foreland conglomerate sequences. Crustal shortening terminated overall much earlier
804 in the east (middle Oligocene, ~28 Ma) than in the west (base of the Middle Miocene,
805 ~16 Ma). These diachronous events are not clearly recorded by thermochronological
806 datasets (see Section 4.1.3), which mainly document a N–S age progression during those
807 periods of the Paleogene. The thermochronological record does likewise not clearly
808 reflect the east-to-west polarity in range-front conglomerate sequence ages, particularly
809 along the retro-wedge (evidence is somewhat clearer along the pro-wedge; Whitchurch
810 et al., 2011) (see sections 3.1 and 3.2 and Fig. 5). It would thus be spurious to establish
811 direct causal links between crustal shortening magnitudes and the production of
812 continental clastic sequences, and thus to calibrate them too systematically, on fission-
813 track-derived denudation patterns in the mountain range.

814 (iii) Whether based on balanced cross-sections or on magnetic anomalies in the Atlantic,
815 estimates of maximum synorogenic crustal shortening remain highly variable
816 (Choukroune, 1992; Muñoz, 1992; Roure and Choukroune, 1998; Vergés et al., 1995,
817 2002; Beaumont et al., 2000; Sinclair et al., 2005; Vissers and Meijer, 2012b; Mouthereau
818 et al., 2014; Teixell et al., 2016, 2018; Grool et al., 2018). Values adduced for the central
819 Pyrenees vary by a factor of almost 2 (90 to 165 km), and depend for example on
820 whether the band of exhumed mantle rocks flooring the pre-orogenic rift is considered
821 to be narrow (15–20 km) or much wider. Depending on the tectonic model of crustal
822 convergence, total shortening is also considered to have been greatest either in the
823 eastern or in the central Pyrenees. As a result, crustal shortening rates also vary widely

824 (0.5 to 5 mm/yr) depending on the time interval of interest. A consensus nonetheless
825 exists around low convergence rates (<1 mm/yr) during the Paleocene, and on peak rates
826 (3–5 mm/yr) during the middle and late Eocene and (at least in the west-central
827 Pyrenees) during the Oligocene. This scenario concurs with the convergence rates
828 between Africa, Iberia and Europe reconstructed from magnetic anomalies in the
829 Atlantic (e.g., Rosenbaum et al., 2002; Schettino and Turco, 2011; Vissers and Meijer,
830 2012b; Macchiavelli et al., 2017). Other authors, basing their inferences on
831 thermochronological data, have advocated a different chronology (e.g., Mouthereau et
832 al., 2014), but converting rock exhumation ages and rates to crustal shortening rates
833 remains a complex, assumption-laden exercise. For a wide-ranging discussion of these
834 issues, see Teixell et al. (2018) and Grool et al. (2018).

835

836 **2.4. From the Ancestral to the Modern Pyrenees: insights from geophysics and** 837 **geodynamics**

838 The Pyrenees have benefited from a number of geophysical studies aimed at (i) detecting
839 the subsurface continuation of surface structures (e.g., folds and faults in the Aquitaine
840 Basin, of importance for fossil hydrocarbon exploration); (ii) understanding the crustal- and
841 lithospheric-scale structure of the orogenic wedge; (iii) untwining the pre- and synorogenic
842 components of the detected structures; and (iv) reconstructing the more recent, post-
843 orogenic evolution of the crustal wedge, most of all in its atypical eastern region.

844

845 **2.4.1. Western and central Pyrenees**

846

847 Important data were acquired in the 1970s. Gravity surveys revealed a strong negative
848 Bouguer anomaly striking E–W beneath the high range, suggesting the existence of a crustal
849 root perhaps 50 km thick. Positive anomalies detected along the north side of the range
850 from the Labourd to Saint-Gaudens also suggested the presence of shallow dense crustal
851 bodies, at the time believed to be Mesozoic alkaline volcanics. Seismic surveys (synthesis in
852 Daignières et al., 1980–81) also revealed greater Moho depths beneath the Axial Zone than
853 beneath the NPZ. In the eastern half of the orogen, the vertical dip of the NPF was promptly

854 interpreted as resulting from an abrupt juxtaposition between a thicker Iberian crust (45–50
855 km) and a thinner European crust (~30 km).

856 A historic milestone in 1985–86 was the ECORS-Pyrenees deep seismic profile, the first of its
857 kind through a mountain range (ECORS Pyrenean Team, 1988). Crustal thickening beneath
858 the Axial Zone showed up for the first time as a north-dipping underthrust of the Iberian
859 lower crust beneath the European lithosphere, later confirmed by complementary surveys in
860 1988 (Anguy et al., 1991). The European lithosphere, with thinner crust than in the Axial
861 Zone, acted as a rigid backstop in the collision with Iberia. Despite being thinner, the
862 European crust acted as a rigid backstop in the collision with its Iberian counterpart. The NPF
863 was detected to depths of only 10 km, thus mitigating its importance as a primary plate
864 boundary. The ECORS-Arzacq profile was generated in 1988 but only on the French side, and
865 yielded somewhat disappointing results (Daignières et al., 1994).

866 Although the ECORS-Pyrenees schema became the cornerstone for interpreting the
867 architecture of the entire Pyrenean edifice, the implementation of other geophysical
868 methods also spawned new questions and opened new perspectives. For example, a dense
869 eclogitic root at the base of the Iberian Plate's leading edge has been inferred (e.g., Vacher
870 and Souriau, 2001; Dufrechou et al., 2018). Magnetotelluric surveys along the ECORS profile
871 have signalled the likely occurrence of partial melting of the lithospheric root (Pous et al.,
872 1995a, b). Campanyà et al. (2012, 2018) likewise detected a low-resistivity zone between 20
873 and 70 km beneath the central Pyrenees, also interpreting it as a region of partial melting.
874 Whether the melting recorded in the central Pyrenees is endemic to the orogenic
875 subduction itself, or whether it results from externally driven asthenospheric processes
876 impinging, without volcanism, on the base of the lithosphere in the central area as it does,
877 with volcanic activity, in the eastern Pyrenees and Languedoc, is unclear (Gunnell et al.,
878 2008; Jolivet et al., 2020). Either way, the evidence is an indication of transience in the
879 orogen's post-orogenic metabolism, which is further discussed in sections 4 to 6.

880 Tomographic imaging has recently generated higher-resolution, lithospheric-scale
881 interpretations of the orogen's deep structure (Chevrot et al., 2015, 2018; Teixell et al.,
882 2018) (Fig. 4). Through the central Pyrenees, the Iberian Moho is detected at 32 km beneath
883 the Ebro Basin, and plunges beneath the SPZ (37 km), the Axial Zone (40–50 km), the NPZ
884 (50–60 km), reaching 60–70 km below the Sub-Pyrenean Zone (Fig. 4D, panels A, B, C). The

885 European Moho, in contrast, is irregular in detail but occurs at average depths of 30–35 km.
886 The subduction plane lies at a depth of 30 km beneath the northern Axial Zone, and 50–70
887 km beneath the Sub-Pyrenean Zone, thus dipping north by at least 25–30°. It links up very
888 clearly with the basal thrust of the South-Pyrenean crustal taper. Many aspects of the
889 orogen's deep architecture nonetheless still remain debated, such as (i) the mode of slip
890 propagation (and partitioning) from the subduction plane to the shallower crustal thrusts;
891 and (ii) the dip and total length of the Iberian slab (e.g., Souriau and Granet, 1995; Souriau et
892 al., 2008): is it exclusively shallow-angle, or does it become vertical at greater depths, and if
893 so how deep does it go? Lengths of 100 km, and even > 200 km in numerical models, have
894 been proposed for a dense and unstable lithospheric root beneath the Pyrenees (e.g.,
895 Vanderhaeghe and Grabkowiak, 2014), dragging down the orogenic wedge until its
896 gravitational detachment caused vertical relaxation of the mountain range. A deep, vertical
897 Iberian slab does not, however, appear on recent seismic tomographies, and the Pyrenean
898 asthenospheric underworld is conspicuously absent from the global inventory of slab
899 graveyards detected in the Earth's mantle (van der Meer et al., 2018). A 'lost' slab has
900 nonetheless been detected beneath the Reggane anomaly in Saharan Africa and tentatively
901 deemed compatible with this scenario given the northward migration of both the African
902 and European plates since early Cretaceous time (Visser et al., 2016).

903

904 **2.4.2. Eastern Pyrenees**

905

906 From the time of the earliest studies in the east (Gallart et al., 1980, 1982; Daignières et al.,
907 1980–1981), it became apparent that the eastern Pyrenees were different. For example, the
908 gravity anomaly beneath the Axial Zone of the central Pyrenees pinches out in the east, and
909 at the longitude of Mt. Canigou the Moho beneath the Axial Zone and the NPZ rises to
910 depths of 30 km or less. At the Mediterranean coast, 50 km farther east, gravity and seismic
911 signatures (Moho at 20–22 km) already share more characteristics with those of the Gulf of
912 Lion than with those of an orogen wedge. Some faults, such as the North Mouthoumet and
913 Tech faults, additionally display offsets in the Moho. These strong indications of crustal
914 thinning are also clear at lithospheric scale, with a lithosphere–asthenosphere boundary
915 (LAB) at depths of 180 km beneath the central Pyrenees thinning to ~120 km in the eastern

916 Pyrenees (Gunnell et al., 2008; Fig. 4B, C). Unfortunately, the eastern Pyrenees have never
917 benefited from an ECORS transect. Recent tomographic imaging (Diaz et al., 2018; Chevrot et
918 al., 2018) nonetheless fully confirms those earlier studies (Fig. 4D), dispelling any notion that
919 the orogen is cylindrical or in any way a homothetic transformation of the ECORS-Pyrenees
920 model. The crustal root beneath the Axial Zone, which reaches depths of <45 km beneath
921 Andorra (itself situated 40 km to the east of the ECORS-Pyrenees profile), disappears entirely
922 100 km to the east of the ECORS traverse, i.e., below Mt. Canigou where the Moho is <35 km
923 deep (Fig. 4D, panels D and E). At this longitude, the flexural bend of the plunging Iberian
924 Moho has flattened out and the subduction plane is undetectable. A 5–7 km vertical offset in
925 the Moho beneath the Axial Zone could be the indication of a south-vergent thrust (Fig. 4D,
926 panel E), although it could also be the locus of the Têt Fault, also a major discontinuity in the
927 fabric of the orogen (Figs. 1, 2).

928 The causes and detailed breakup kinematics of the orogen in the Western Mediterranean
929 during the Neogene are also a matter of debate. Breakup was a result of southward trench
930 rollback of the Apennine subduction slab, and was guided by the Catalan Transfer Zone
931 (Rehault et al., 1984; Mauffret et al., 2001; also previously named accident Paul Fallot
932 (Durand-Delga and Fontboté, 1980) and, more recently, North Balearic Transform Zone
933 (Advocaat et al., 2014; see palaeogeographic maps presented in Plate I). This transfer zone is
934 a deep crustal fault striking NW–SE and along which the Corsica–Sardinia block sheared itself
935 away from the remainder of the Pyrenees. The resulting Gulf of Lion is a back-arc basin in
936 which a NW to SE gradient of intensifying crustal extension has been inferred. The Pyrenean
937 crust thus thins rapidly just 20 km east of the current Roussillon coastline, then yields
938 progressively offshore to necking in the lower crust, then to exhumed lower crust and/or
939 serpentinised upper mantle in the Provençal Basin (the presence of an aborted oceanic ridge
940 between Provence and Corsica is currently speculative; Granado et al., 2016; Canva et al.,
941 2020; Jolivet et al., 2020). As a result of crustal extension giving birth to the Western
942 Mediterranean, a dozen extensional basins were also generated on the continental seaboard
943 and in the eastern Pyrenees (Fig. 1), fragmenting the topography and progressively tearing
944 open the orogen from east to west along its Axial Zone. The first stage of extension affected
945 the Mediterranean back-arc during the late Oligocene–early Miocene (resulting onshore
946 basins: Roussillon, Conflent, Vallès-Penedès, Narbonne-Sigean and several other smaller

947 basins in the Corbières). The second episode extended into the core of the Axial Zone during
948 the late Miocene (resulting intermontane basins: Cerdagne, Capcir, Seu d'Urgell, Val d'Aran-
949 Pruëdo), but also impacted the Mediterranean onshore area of Catalonia (Selva, Empordà),
950 where the older basins closest to the coast (Vallès, Roussillon) were also reactivated during
951 the late Miocene and Pliocene (see Section 3.3).

952

953 **2.4.3. Crustal roots and their implications for geomorphology**

954

955 The history of the orogen's deep structures and their differences from east to west and
956 north to south are important for understanding (i) crustal behaviour during the orogenic
957 period, and (ii) vertical movements during the post-orogenic period. Implications for the
958 geomorphological evolution of the Pyrenees as a mountain range are essential and will be
959 examined more specifically from that angle in Section 4.

960 On a N-S cross-section through the west-central Pyrenees, it now remains fairly
961 straightforward to associate the deep crustal structures (underthrusting of the Iberian lower
962 crust beneath the European lithospheric mantle, etc.) with the structures in the mid- and
963 upper crust (i.e., the Pyrenean orogenic wedge), even though estimates of total crustal
964 shortening at depth and at the surface (at least ~100 km, see above) are highly variable.
965 Should it be inferred from the more recent crustal tomographies that plate convergence in
966 the eastern Pyrenees was very limited, thus failing to produce a crustal root? Such a
967 conclusion would violate the evidence from the nappe structures, which indicates
968 magnitudes of crustal shortening comparable to the central Pyrenees (e.g., Laumonier, 2015;
969 Grool et al., 2018). The major lateral architectural changes in the crustal wedge, which
970 (among other features) involves lateral heterogeneities in the European Moho (Chevrot et
971 al., 2015; Wang et al., 2016), require some other explanation, and these have been
972 addressed by a few publications (e.g., Gunnell et al., 2008; Chevrot et al., 2018; Jolivet et al.,
973 2020).

974 The most commonly proposed scenario is that the crustal root beneath the eastern Pyrenees
975 was initially no different to that detected farther west, but that it was destroyed by the
976 impinging extensional tectonics (e.g., Séranne, 1999; Lacombe and Jolivet, 2005). Gunnell et

977 al. (2008) speculated that the root was delaminated or thermally eroded by an influx of hot
978 asthenosphere channelled southward from the Massif Central (see Barruol et al., 2004).
979 Jolivet et al. (2020) proposed instead that the processes responsible for lithospheric thinning
980 beneath the eastern Pyrenees and for the hyperextended crust in the Gulf of Lion were
981 linked, and occurred on a mode reminiscent of metamorphic core complexes but also
982 involving asthenospheric processes at the lithosphere–asthenosphere boundary.

983 It still remains surprising that the basic orogenic structure, and particularly the superposition
984 of the respective Mohos, should have been so completely erased by these processes.

985 According to Chevrot et al. (2014, 2018), important differences in the pre-orogenic
986 Cretaceous rift structure (see also Tugend et al., 2014; Wehr et al., 2018) could explain why
987 compressional deformation might have been less focused and spatially more distributed in
988 the east of the orogen, particularly east of the Toulouse Fault — thus not forming a single,
989 massive crustal root. This scenario provides an alternative to the option advocating post-
990 orogenic eradication of a previously formed crustal root, but its authors do not adduce more
991 specific structural correlations or constraints with the surface geology.

992 A third scenario, until now never discussed, is also possible. Its premise, advocated by Teixell
993 et al. (2016) in the west-central Pyrenees, is that the formation of the Pyrenean crustal root
994 occurred after (i) restoration of normal crustal thickness in the Cretaceous rift zone, (ii)
995 subduction of the formerly exhumed mantle of the rift floor, and (iii) lower-crust
996 underthrusting (proto-collision) of the Iberian leading edge. Root-forming collision thus
997 occurred broadly after mid-Eocene time, but this third scenario emphasizes that collision in
998 the eastern Pyrenees was mostly associated with the lower thrust units, active during the
999 Priabonian and Rupelian; whereas farther west thrust displacement continued until the early
1000 Miocene, i.e., for a further 10 m.y. This alone could explain why the crustal root was smaller
1001 in the east than anywhere else documented until now.

1002 Clearly, the hypothesis of a smaller initial root in the eastern Pyrenees does not rule out the
1003 additional prospect of its full eradication during the Neogene, whether by purely brittle,
1004 more ductile, or melt-related processes. Both scenarios are thus compatible with one
1005 another. Previous work in the central Pyrenees had argued that the mountain range was
1006 isostatically overcompensated, i.e., mean elevation was less than predicted by Airy's model,
1007 perhaps because of a dense eclogitic root dragging it downward in that region (Vacher and

1008 Souriau, 2001). With a crust just ~30–35 km thick, evidence suggests instead that
1009 topography in the eastern Pyrenees is not supported by a crustal root of sufficient thickness
1010 for isostatic compensation of the mountain range to be occurring at the Moho. The notion
1011 that elevations in the eastern Pyrenees are anomalously high (Gunnell et al., 2008) is of
1012 special interest from a geomorphological perspective because it implies that this segment of
1013 the mountain range, where the lithosphere–asthenosphere boundary is relatively shallow
1014 (Fig. 4), is dynamically supported and is thus likely in a transient rather than in an equilibrium
1015 topographic state (Calvet and Gunnell, 2008; see point 3.3. for further discussion).

1016

1017 **2.5. Synthesis of Pyrenean tectonics**

1018

1019 The Pyrenees constitute a good example of a mountain range affected by multiple orogenic
1020 overprints. The long Variscan history of the region (Barnolas and Chiron, 1996) ended in the
1021 complete destruction of the Hercynian mountain belt and the burial of its residual
1022 topography under a mass of clastic debris (initially purple-coloured Permo-Triassic claystone
1023 and sandstone). A new chapter then began with the Alpine orogenic cycle (Barnolas and
1024 Chiron, 2018). This started with a long period of marine shelf sedimentation extending from
1025 the Trias (~240 Ma) to the Barremian (~125 Ma). A period of rifting then transformed the
1026 Europe–Iberia mobile belt, but convergence, collision and underthrusting of the Iberian Plate
1027 beneath the European Plate followed in a succession of stages between the late Cretaceous
1028 and at least the late Oligocene. A subsequent phase of crustal extension during the Neogene
1029 is recorded, impinging on the eastern half of the orogen (Barnolas and Chiron, 2018; Jolivet
1030 et al., 2020).

1031 We now possess a fairly satisfactory understanding of the orogenic growth and decay
1032 patterns of the Pyrenees through geological time (Teixell et al., 2018). The crustal wedge
1033 widened and thickened in three distinct stages, before partially undergoing hyperextensional
1034 collapse in a fourth (Jolivet et al., 2020):

1035 (i) late Cretaceous: burial of lithospheric mantle rocks initially exposed as a result of
1036 overstretched crust, and inversion of the earlier Cretaceous rifts structures;

1037 (ii) early to middle Eocene in the east, middle Eocene to early Oligocene in the west: tectonic
1038 convergence under a distinctly tangential regime (low dip angles of most thrusts), with
1039 formation of complex nappes structures (Canigou, Gavarnie, etc.);

1040 (iii) late Eocene and early Oligocene in the east, late Oligocene to early Miocene in the west:
1041 development, particularly in the Iberian domain, of more strongly dipping thrusts, giving the
1042 mountain range its final geometry of a collisional orogenic wedge. This process involved
1043 vertical uplift of the Axial Zone relative to the NPZ and SPZ, but also of the NPZ relative to
1044 the Sub-Pyrenean Zone, with development of a crustal root produced by underthrusting and
1045 subduction of the Iberian lower crust beneath the overriding European Plate.

1046 (iv) Oligocene to Neogene: post-orogenic hyperextension in the east as a consequence of
1047 Mediterranean trench rollback and slab tear along the Paul Fallot–North Balearic Transform
1048 Zone (Jolivet et al., 2020). This transformed the segment of the Pyrenees currently collapsed
1049 in the Gulf of Lion but also the entire eastern onshore part of the modern orogen, even as
1050 compression was continuing in its western part. The eastern Pyrenees are thermally the
1051 hottest part of the orogen, impacted by asthenospheric flow and volcanic activity. The cooler
1052 Pyrenees further west currently appear less directly impacted by these processes.

1053

1054 **3. A view from the basins: a proxy record of mountain uplift and erosion**

1055

1056 The denudation history of a mountain belt is recorded in the depositional history and
1057 stratigraphic architecture of its adjacent and intermontane sedimentary basins (e.g., García-
1058 Castellanos and Cloetingh, 2012). Constraints on the chronostratigraphy of the foreland
1059 sequences are usually provided by the marine and continental fossil record, and various
1060 methods of basin analysis help to reconstruct the tectonic regime and depositional systems
1061 through time (Allen and Allen, 2013). These clues yield indirect evidence about the
1062 topographic energy of the mountain range in the past. The facies characteristics of the
1063 sedimentary rocks also document the succession of palaeoclimatic conditions that presided
1064 over the erosional decay of the orogen.

1065 In the case of the Pyrenees, however, the post-shortening (i.e., late Cenozoic) environmental
1066 conditions are paradoxically less well documented than the earlier periods of Mesozoic
1067 rifting and Paleogene collision. Focus on the older geological periods has arisen from the

1068 priorities set by petroleum exploration. In a compilation which tries to make sense of several
1069 hundred local studies published in French, Spanish, Catalan and English but never previously
1070 linked up into a coherent narrative (recent partial exceptions: Garcés et al., 2020; Ortiz et al.,
1071 2020), we provide here a synthesis of the evolution of the Pyrenees captured through (i) the
1072 clastic record of denudation of the orogenic wedge in all of its peripheral and intermontane
1073 basins (this Section 3), (ii) the rock-cooling record of its Hercynian basement core (Section 4),
1074 and (iii) the denudation of the foreland basins themselves in relation to base-level changes
1075 affecting them. Whereas most reviews of the Pyrenean foreland basins focus on information
1076 provided by marine deposits and magnetostratigraphy, in this review we also highlight the
1077 rich biochronological evidence provided by continental fossil assemblages. Marine
1078 deposition ceased after the Priabonian on the Iberian side of the range, after the Ypresian in
1079 eastern Aquitaine, and occurred only intermittently in western Aquitaine during the
1080 Oligocene and Miocene. The reason for granting continental biostratigraphy pride of place in
1081 this review is that palaeontological data from nonmarine sequences are available from all
1082 three basin environments of the Pyrenees, i.e., the Ebro, Aquitaine, and Mediterranean. This
1083 allow consistent short- as well as long-distance correlations within a coherent and accredited
1084 reference frame. Furthermore, issues of endemism are not recognised as a potential barrier
1085 to robust comparisons because components of Iberian endemism among mammalian taxa
1086 only concern the Atlantic west and the Meseta. The literature has long established that the
1087 faunas in the southern Pyrenees were very similar to those of France and other parts of
1088 Europe, whether during the Eocene (Badiola et al., 2009) or the Oligocene and Burdigalian
1089 (Alvarez Sierra et al., 1990).

1090 The stratigraphic ages for clastic sedimentary sequences will follow the European Land
1091 Mammal Age (ELMA) scales of Vandenberghe et al. (2012) for the Paleogene, and Hilgen et
1092 al. (2012) for the Neogene, while also considering local updates or recalibrations from more
1093 recent magnetostratigraphic research in the Ebro Basin. The excellent documentation of the
1094 Ebro foreland by magnetostratigraphic research is unmatched everywhere else, mostly
1095 because of comparatively unsuitable open-air exposures and sampling conditions north and
1096 east of the mountain range.

1097

1098 **3.1. Chronology of clastic supply to the Aquitaine retro-foreland**

1099

1100 **3.1.1. State of the art and data sources**

1101

1102 After 1950, the Aquitaine Basin became the focus of a large number of studies based on
1103 seismic surveys and drilling in the context of oil and gas exploration (see Biteau et al., 2006).
1104 Given that oil plays tend to occur in the deeper stratigraphy, the Cenozoic molasse deposits
1105 were often ignored as overburden of little key interest (Cenozoic cover rocks are
1106 nonetheless addressed, for example, in Winnock et al., 1973; Kieken, 1973; Schoeffler, 1971,
1107 1973; Cavelier et al., 1997; Gély and Sztrakos, 2000; Serrano et al., 2001; Rougier et al.,
1108 2016; Barnolas and Chiron, 2018; Ortiz et al., 2020). The study of the clastic Cenozoic
1109 sequences by other means, however, is hampered by the dense vegetation, and by the
1110 widespread and often thick blanket of Quaternary regolith. The chronostratigraphy of the
1111 continental deposits in the Aquitaine retro-foreland is nonetheless suitably constrained at
1112 some localities by the frequent occurrence of interlayers of marine beds (Fig. 5), which recur
1113 between ~56 (Ypresian) and ~12 Ma (middle Miocene). Accommodation space and the
1114 wavelength of lithospheric flexural response to sedimentary loads seem to have varied along
1115 strike as a function of heterogeneities in pre-orogenic rift inheritance, and particularly
1116 magnitudes of Cretaceous crustal extension. Overall, flexural rigidity is found to decrease
1117 southwestward from the eastern Aquitaine Basin to the Arzacq subbasin (Angrand et al.,
1118 2018).

1119 The body of work devoted to the Eocene marine record is the largest (e.g., Plaziat, 1984;
1120 Sztrakos et al., 1998), but a few overviews also exist for the Oligocene and the Miocene
1121 (Cahuzac et al., 1995, 1996, 1999, 2010; Sztrakos and Steurbaut, 2017). Note that the
1122 Aquitaine Basin is the locus of two type sections of the International Stratigraphic Scale,
1123 namely the Aquitanian (defined in 1858 by K. Mayer Eymar) and the Burdigalian (defined in
1124 1892 by Depéret) (for recent reviews on this topic, see Parize et al., 2008, and Londeix,
1125 2014). The Aquitaine Basin also turns out to be an extremely rich repository of continental
1126 fossils, with an inventory of several hundred sites — whether in fluvio-lacustrine stratified
1127 context or in a karst setting. Some of these are benchmark sites used in the indexation of
1128 Paleogene (MP) and Neogene (MN) biozones of the ELMA scale (Richard, 1948; Crouzel,
1129 1957; Bergounioux and Crouzel, 1960; Sudre et al., 1992; Duranthon, 1991, 1993; Muratet et
1130 al., 1992; Muratet and Cavelier, 1992; Antoine et al., 1997, 2011; Legendre et al., 1997;
1131 Duranthon and Cahuzac, 1997; Astruc et al., 2003; etc.). The most significant among these

1132 reference sites, however, are situated in the distal, often lacustrine molasse deposits of the
1133 basin. This potentially weakens the quality of some chronostratigraphic correlation with the
1134 more proximal conglomerate sequences of the Pyrenean retro-foreland, but opportunities
1135 for multiple constraints are nonetheless plentiful, and Ortiz et al. (2020) have provided an
1136 areally extensive, integrated basin analysis of the onshore western Aquitaine–offshore Bay
1137 of Biscay continuum.

1138

1139 **3.1.2. Synorogenic conglomerate beds: the Paleogene Palassou Series**

1140

1141 The Palassou conglomerate sequence (Fig. 5) has been well studied in the eastern foothills
1142 area (Crochet, 1991), particularly the narrow band of almost vertically upturned beds
1143 between the Arize and Ariège rivers (here in the Sub-Pyrenean Zone). The outcrop broadens
1144 substantially to the east of the Ariège and into the Aude river catchment, where the
1145 sequence also underwent Alpine folding. The Palassou Series is > 2 km thick and has been
1146 subdivided into three units interpreted as three successive intervals of tectonic activity, each
1147 separated by syn-sedimentary unconformities that display fanning dip angles and grade into
1148 sharper angular unconformities nearer the mountain front. The conglomerate beds display
1149 point-bar facies typical of meandering or wandering streams on large range-front alluvial
1150 fans. In the Ariège, clast abrasion criteria imply a minimum transport distance of 6 to 7 km
1151 for limestone pebbles, and 30 km in the case of quartz (Crochet, 1991). The pebbles are large
1152 ($D_{99} = 164$ mm), with a marked up-sequence increase in size (D_{99} in youngest beds: 403 mm)
1153 and the largest debris in excess of 600 mm. Petrographic composition indicates that the
1154 alluvium has sampled the entire lithological assortment of the Ancestral Pyrenees in varying
1155 proportions. Inputs from the Axial Zone are in a minority (< 10%) in the older Palassou Unit 1
1156 and at the base of middle Unit 2, but become dominant (and at places exclusively so) in the
1157 remainder of Unit 2 (90%, including granite and metamorphic rocks). Debris from the Axial
1158 Zone are very scarce in uppermost Unit 3.

1159 The age of the Palassou sequence has been established on the basis of (i) its stratigraphic
1160 continuity with the marine and coastal Lower Ypresian (i.e., Ilerdian) beds, (ii) a series of
1161 mammalian fossil deposits (particularly in the Aude syncline and in the distal molasse
1162 deposits between Castelnaudary and Castres), and (iii) a selection of freshwater and
1163 terrestrial *Mollusca*. Unit 1 lies conformably over the Ilerdian (Lower Ypresian) and contains

1164 in its basal beds some mammalian assemblages ascribable to MP 7 and MP 8–MP 9
1165 (Marandat, 1991; Marandat et al., 2012), i.e., 54–52 Ma (Legendre and Lévêque, 1997;
1166 Escarguel et al., 1997; Vandenberghe et al., 2012). Unit 1 continues into the early Lutetian.
1167 The middle Palassou (Unit 2) spans the late Lutetian and Bartonian. The top of upper unit 3
1168 contains the mammalian fossil deposits of Mas-Saintes-Puelles (MP 19, ~35 Ma) and
1169 Villeneuve-la-Comtal (MP 20, ~34 Ma), and is thus compatible with a Priabonian age. The
1170 Bartonian and Priabonian sequences extend as far north as the Castres Basin, where they
1171 consist of finer Pyrenean molasse known as ‘Molasse de Blan’ and ‘Molasse de Saix’
1172 (Mouline, 1978, 1989). These formations contain about 60 mammalian fossil sites (3
1173 Lutetian, 39 Bartonian, and 16 Priabonian).

1174 The Palassou Series continues into the early Oligocene (Rupelian). This Unit 4 was not
1175 described by Crochet (1991) and is barely reported in the literature apart from a brief
1176 mention by Astre (1933). Its outcrops occur between the Hers valley and the Lauragais
1177 (‘Poudingues de Vals’), and continue towards the Castres Basin (‘Poudingues de Puylaurens’
1178 and ‘Molasses de Briatexte’; Mouline, 1967). The Rupelian beds around Castres contain 41
1179 mammalian sites. The ‘Poudingues de Vals’ are at least 200 m thick (though a lot less at
1180 Puylaurens) and exhibit very low dips. At Vals, pebble provenance is predominantly
1181 limestone from the outermost Pyrenean fold belts, with very little input from the Axial Zone.
1182 Palaeochannels containing small pebbles of weathered gneiss and granite are nonetheless
1183 frequent in the Lauragais and Puylaurens areas, with no proven provenance from the
1184 Montagne Noire. This pulse of clastic debris from the Pyrenees overlies distal lacustrine
1185 limestone beds than contain biozones MP 19 and MP 20 (34–33 Ma) at the seuil de
1186 Naurouze; and the top of the conglomerate unit itself contains biozones MP 24–25 at
1187 Puylaurens (~30–28 Ma). Palassou 4 is the outermost occurrence of conglomerates supplied
1188 by the Paleogene Pyrenean orogeny (Mouline, 1978). The clastic wedge may have reached
1189 these distal areas because of a decline in subsidence rate and accommodation space, forcing
1190 the rivers from Rupelian time to prograde northwards across the overfilled retro-foreland. A
1191 further age bracket is provided by the continuous sequence of the Bélesta and Briatexte
1192 lacustrine limestone beds capping Unit 4. This limestone formation can be traced southward
1193 to Belpech (at the Aude–Ariège border). The outcrop is probably time transgressive but
1194 includes biozones MP 24–25 and 26 (28–27 Ma) at the northern site of St-Martin-de-
1195 Casselvi, where two fossil exposures occur one above the other (Astruc et al., 2003). This

1196 lacustrine environment could be an indication of diminished clastic output from the
1197 Pyrenees, where topography may have therefore attained a state of subdued relief and
1198 moderate energy.

1199 The Chattian molasse overlying the Bélesta limestone is fine-textured and extremely
1200 monotonous in the Lauragais and Toulouse areas. The stratigraphic position of the distal
1201 facies above the Puylaurens conglomerate clearly indicates a decline in river-load clast sizes
1202 and, by inference, in catchment steepness in the Pyrenees. The thickness of this late
1203 Oligocene molasse has been overestimated by Astre (1959, 1964), who conflated this
1204 formation with the younger Aquitanian molasse (which admittedly displays an identical
1205 facies but whose age has been revised based on a reinterpretation of its fossil assemblage;
1206 Baudelot and Olivier, 1978; Duranthon, 1991, 1993). The base of the Aquitanian stage has
1207 now been recorded in a borehole sunk for the Toulouse underground train network at
1208 depths corresponding to 114–122 m a.s.l. (Antoine et al., 2006). The underlying Chattian
1209 beds attain estimated thicknesses of 180 to 380 m according to Astre (1959), i.e., 180 m if
1210 we assume that their dips decrease westward (a fact recently confirmed by excavations for
1211 the Toulouse underground metro network). The Chattian facies was described by Astre
1212 (1959) as that of silty to sandy shale floodplain deposits containing a few limestone beds,
1213 sporadically associated with broad, well-defined shoestring sand channels occasionally
1214 containing coarser sand and gravel. The presence of muscovite, biotite and tourmaline in the
1215 sand fraction imply some provenance from the Hercynian outcrops.

1216 The Oligocene molasse deposits of Pyrenean origin thus extend far into the Aquitaine Basin.
1217 In the lower plains of the Tarn and Aveyron rivers, four depositional units separated by
1218 disconformities have been described (Muratet and Cavelier, 1992; Muratet et al., 1992), and
1219 the most conspicuous erosional lacuna has been attributed to the late Rupelian eustatic fall.
1220 Northwest of the Tarn–Garonne river junction, the Pyrenean molasse outcrops disappear
1221 beneath the ‘Calcaires blancs’ (Aquitanian lacustrine beds of white limestone) of the Agen
1222 region, and eventually reappear and connect laterally with the fossil-rich marine (highstand:
1223 ca. 30 Ma) Rupelian limestone (Asteries Limestone) of the Bordeaux region (Sztrakos and
1224 Steurbaut, 2017).

1225

1226 ***3.1.3. Western analogues of the Palassou beds: the Jurançon sequence***

1227

1228 Outcrops of proximal Paleogene conglomerates, which are otherwise mostly obscured by
1229 Neogene overburden west of the Ariège River, occur around the city of Pau, where they are
1230 known as ‘Poudingues de Jurançon’. Jurançon is the type locality described in 1819 by
1231 Palassou himself, whose surname was used after 1862 by Leymerie, as a tribute to Palassou,
1232 to describe occurrences of this geological formation in the east (i.e., the outcrops examined
1233 in Section 3.1.2). The outcrops reported in the Garonne, Ariège and Aude catchments were
1234 considered to be Eocene by Noulet in 1858 (see Crochet, 1991). The western outcrops of this
1235 conglomerate formation, however, were renamed ‘Jurançon’ by Douvillé (1924), thereby not
1236 only dissociating it from the Palassou sequences but also ascribing it a Miocene age without
1237 any clear justification. A Tortonian age was even prescribed based on the notion that it was a
1238 proximal facies of the Neogene molasse (Crouzel, 1957). The Neogene age of the Jurançon
1239 Formation was then (spuriously) extended to the more distal, 1200 m-thick molasse
1240 sequences that fill the Arzacq Basin between the Gave de Pau and the Adour River.
1241 More recent investigations, however, have worked towards correlating the ‘Poudingues de
1242 Jurançon’ and ‘Molasses d’Arzacq’ formations with the synorogenic Paleogene units of the
1243 Palassou Series described in Section 3.1.2. Its westernmost outcrops near Lahontan extend
1244 laterally to (and are thus broadly coeval with) a facies of palaeontologically-dated Upper
1245 Eocene marine molasse and limestone (Boulangier and Poignant, 1970). Seismic profiles and
1246 borehole logs also evidence the lateral facies changes from the conglomerates to the
1247 Paleogene molasse beds in the Arzacq syncline. Age brackets are provided in the west by
1248 marine Oligocene beds (Schoeffler, 1969, 1971, 1973) and by the overlying Lower Rupelian
1249 ‘Faluns de Gaas’ (shelly sand) (Sztrakos and Steurbaut, 2017). In the east, the top of the 400-
1250 m-thick continental molasse beds of Arzacq has been dated by mammalian fossil indicators
1251 at Nassiet/Le Bourgadot (Rupelian, MP 23: Sudre et al., 1992; Viret, 1938; Glangeaud, 1938;
1252 Schoeffler, 1969); and its base likewise dated at Horsarieux/Pédelail (Eocene–Oligocene
1253 boundary: Stehlin, 1910, in Capdeville, 1997), just above the marine Bartonian beds.
1254 Like the Palassou Series units 1 to 3, the Jurançon conglomerates fall into three units, and a
1255 Paleogene age has been confirmed by two fossil invertebrate assemblages — one from the
1256 basal unit, which rests conformably on Upper Ypresian marine sandstone and Lutetian shale,
1257 and the other from the middle unit (Bartonian; Hourdebaigt et al., 1986; Hourdebaigt, 1988).
1258 As with the Palassou, lower and upper Jurançon units contain an assemblage of pebbles
1259 almost exclusively of outer-Pyrenean fold-belt provenance. Contributions from the Axial

1260 Zone, particularly from granite outcrops, are substantial in the middle sequence. This
1261 suggests that there has not been a simple or progressive pattern of denudation of the Axial
1262 Zone, whether in the east or the west of the orogen. With a D_{99} of 500 mm, the beds also
1263 include metre-sized boulders. Clast roundedness is less than among the Ariège Palassou
1264 sequences.

1265 Given that at Ossun and Pau the marine-to-continental transition occurred during the late
1266 Ypresian, it can be inferred that, from the Corbières in the east across to the Béarn in the
1267 west, the westward marine regression was fast along the strike of the orogen (see
1268 palaeogeographic maps in Plate I). West of Pau, the Paleogene piedmont of the Ancestral
1269 Pyrenees was a deep furrow undergoing a slower rate of sedimentation, mainly in the form
1270 of west-prograding deltaic sequences (Cavelier et al., 1997, Fig. 4 therein; Serrano et al.,
1271 2001). At Peyrehorade, continental upper Palassou beds display intercalations with
1272 Priabonian marine beds. In the lower Adour valley and on the Basque coast at Biarritz, the
1273 Paleogene marine sequence is continuous from the Eocene to the Oligocene. It contains at
1274 best a few sandstone and conglomerate beds, and olistoliths of middle Eocene age (Kieken,
1275 1973). In this area, the mountain belt undergoing crustal deformation at the time descended
1276 directly into the sea in a way reminiscent of the modern Cantabrian Ranges. Debris conveyed
1277 out of the rising Ancestral Pyrenees were thus delivered directly to the Bay of Biscay, which
1278 at the time formed a gulf extending much further east into the Aquitaine Basin than today
1279 (see palaeogeographic maps in Plate I). By the end of the Oligocene, these Pyrenean debris
1280 were evacuated directly via a submarine canyon (Bélus–Saubrigues canyon), ancestor to the
1281 present-day Gouf de Capbreton (Cirac et al., 2001). This canyon was cut during Oligocene
1282 time into the Saubrigues anticline up to 35 km east of the modern coastline, but soon
1283 became filled with sediment by late Chattian to Aquitanian time (Kieken, 1973; Cahuzac et
1284 al., 1995; Sztrakos and Steurbaut, 2017).

1285

1286 **3.1.4. The early and middle Miocene molasse**

1287

1288 By comparison with the Paleogene foreland deposits, their Neogene successors are thin and
1289 exhibit shallow dips. On seismic profiles, the Neogene cover sequence never exceeds
1290 thicknesses of a few hundred metres (Schoeffler, 1971, 1973) — on average 200–300 m,
1291 with localised depocentres attaining 600 m at the Landes coastline or beneath the middle

1292 Adour valley, 500 m north of Tarbes, 540 m north of Auch, and 560 m at Lézat (i.e., 15 to 30
1293 km north of the NPF).

1294 During the early and middle Miocene, marine sedimentation prevailed in the west and
1295 produced interlayers with the ongoing continental deposit accumulations farther east. Three
1296 marine transgressions have been recorded, each forming a wide triangular gulf advancing up
1297 to 150 km into the interior of the Aquitaine Basin, with its depocentres situated between
1298 100 and 75 km north of the Pyrenean mountain front. This configuration suggests that
1299 Pyrenean tectonics were no longer directly influencing the pattern and chronology of sea-
1300 level changes. The most extensive transgression occurred in Aquitanian time (Londeix,
1301 2014), its easternmost vertex reaching the city of Agen and depositing a bed of paralic,
1302 oyster-rich marls sandwiched between white lacustrine limestones ('Calcaires blancs') at
1303 their base and grey limestones ('Calcaires gris') at their top. This 'trilogie agenaise' is a
1304 distinctive geological feature of the region, totalling a thickness of 30 to 60 m and containing
1305 two mammalian sites (Paulhiac and Laugnac) emblematic of biozones MN 1 and MN 2 (Fig. 5,
1306 Ariège transect).

1307 The palaeogeography of the Burdigalian transgression was comparable, although slightly less
1308 extensive (Cahuzac and Poignant, 2004). The middle Miocene transgression invaded land
1309 somewhat farther to the south and reached Lectoure, also forming a narrow gulf along the
1310 base of the western Pyrenees around Orthez and Salies-de-Béarn. This shallow sea, also
1311 known as 'Mer des Sables fauves' (Tawny Sands in Figure 5), has fallen foul of contradictory
1312 interpretations. Although initially assumed to be a Tortonian feature (Crouzel, 1957), its
1313 Langhian to Serravallian age (~16–11 Ma) is now well established despite persistent
1314 uncertainty concerning the palaeogeography of its two successive highstands. According to
1315 some authors, the gulf of Lectoure was a Serravallian feature (Cahuzac et al., 1995; Cahuzac
1316 and Poignant, 1996), whereas for others this marine highstand occurred in Langhian time,
1317 the Serravallian ingress being the lesser of the two eustatic rises. Because of local flexural
1318 deformations in the Aquitaine Basin itself ('Celtaquitania flexure'), the Serravallian deposits
1319 occur as a series of drowned valley fills cut into the northern edge of the marine Langhian
1320 series and its underlying Aquitanian molasse (i.e., the 'trilogie agenaise') (Magné et al., 1985;
1321 Rey et al., 1997; Gardère, 2002, 2005; Gardère et al., 2002; Gardère and Pais, 2007). The
1322 southward migration of the marine depocentre as a result of this tectonic downwarp, which
1323 influenced the positions of two successive palaeoshoreline highstands, could be the

1324 manifestation of a slight reactivation of Pyrenean retro-wedge crustal loading during the
1325 middle Miocene.

1326 The carbonate-rich continental molasse sequences of the Miocene continue the trends
1327 previously observed in their marine counterparts. Geologists have reported 17 levels of
1328 younger deposits overlying the Aquitanian 'trilogie agenaise', 13 of them made conspicuous
1329 by the recurrence of a distinctive variety of lacustrine limestone and attaining a total
1330 thickness of 328 m (Crouzel, 1957). As the depozone narrowed progressively towards the
1331 south during the Miocene, the resulting furrow collected the most recent components of the
1332 foreland fill sequence. These can be observed at Saint-Gaudens and Montréjeau, and occur
1333 at the base of the Pyrenean mountain range, directly against the NPF. This southward
1334 rollover of the continental molasse depocentre could be the result of renewed subsidence of
1335 the Pyrenean foredeep, and thus of a brief revival of tectonic convergence in the central and
1336 western Pyrenees. All of these clastic levels contain mammalian fossils, for which revised
1337 biozone nomenclatures broadly confirms the stratigraphy originally established by Crouzel
1338 (1957). The site ages range from early Burdigalian (MN 3, at Estrepouy) to late Serravallian /
1339 early Tortonian (MN 8, at St-Gaudens and Montréjeau, where the faunal assemblages are
1340 precursors to the Vallesian but do not contain *Hipparion*). No site ascribable to MN 9 has yet
1341 been established (Antoine et al., 1997). The stratigraphic datum containing *Hipparion*
1342 (*Hippotherium primigenius*) has been debated (Sen, 1990), but the first known record of this
1343 indicator fossil at the Vallesian type locality in Catalonia set its age at 11.1 Ma (Garcés et al.,
1344 1997; Agustí et al., 2001). Based on this indirect criterion, the Neogene molasse sequence of
1345 the Aquitaine Basin is older than 11 Ma.

1346 Crucially, stratigraphic facies characteristics throughout the entire Neogene sequence all
1347 exhibit fine-textured debris (molasse) transported to low-energy depositional environments,
1348 indicative of substantially subdued relief in the Pyrenees and its piedmont in Neogene time.

1349 Deposit lithology ranges from siltstone to fine sand and greywacke, cross-cut by mica-rich
1350 sand-filled palaeochannels. The latter occasionally contain coarser sand and gravel, with very
1351 rare pebble beds (pebble size: 2–5 cm) barely 1 m thick, particularly in the Montréjeau–St
1352 Gaudens molasse. Unlike earlier periods of the Paleogene, when fine-textured debris
1353 accumulated mostly in the more distal, northern parts of the Aquitaine Basin, lacustrine marl
1354 and limestone formations were now being deposited in a proximal position, in direct,
1355 nonconformable contact with the Sub-Pyrenean fold structures buried beneath them. This

1356 configuration, for example, occurs in the case to the Aquitanian to early Burdigalian cover
1357 rocks at La Lèze ('Saint-Ybars Limestone', see Fig. 5: Aude and Ariège transects), or of the
1358 Serravallian–Tortonian basal beds at Montréjeau and Saint-Gaudens.

1359 The only coarser-textured facies in a proximal position to the mountain range occur at the
1360 base of the Neogene sequence near Pamiers. Here, the conglomerate outcrop forms a
1361 homoclinal scarp, and exposures on the scarp face exhibit an upward-fining fluvial sequence
1362 in which palaeochannels at the base of the unit contain large pebbles (long axis: 10–40 cm),
1363 whereas palaeochannels at the top contain 5–10-cm-sized pebbles (maximum) amid thick
1364 reddish clay beds. Mammalian fossil assemblages within the beds correlate these strata with
1365 the late Oligocene (MP 29) and Aquitanian (MN 1 and MN 2; Addé-Lacomme, 1935;
1366 Bergounioux and Crouzel, 1971; Duranthon, 1991, 1992). The pebbles are almost exclusively
1367 quartz-rich (granite, gneiss, micaschist), and their identifiable provenance links them to large
1368 swaths of the Axial Zone. Such a wide distribution of quartz-rich debris from the interior of
1369 the Pyrenean mountain belt provides strong evidence that the Sub-Pyrenean outer fold
1370 belts, by this time, no longer acted as barriers to the conveyance of debris from the eroding
1371 mountain range.

1372 As the overfilled synclines of the Petite Pyrénées were undergoing burial by the mass of
1373 incoming debris (thereby raising local base levels) the intervening anticline ridges rising
1374 slightly above the fill sequence underwent erosional thinning and truncation. The entire
1375 assemblage thus formed a composite area of low relief, perhaps at places a continuous
1376 topographic ramp between the mountain range and the Aquitaine Basin.

1377 Miocene deposition did not extend eastward much beyond the Ariège valley, and the
1378 stratigraphy exhibits a number of lacunae. For example, all of biozone MN 3, and perhaps
1379 the base of MN 4, are missing, i.e., 3 million years of Burdigalian biostratigraphy (Duranthon,
1380 1991). The geodynamic cause of this stratigraphic lacuna has never been discussed, but a
1381 eustatic fall is ruled out because a Burdigalian transgression was occurring at the same time
1382 farther west in the Aquitaine Basin. A tectonic influence thus seems more likely, the lacunae
1383 in that case being erosional: with east-facing faults of the Mediterranean rift system
1384 transforming the eastern Pyrenees exactly at that time and the west-facing Toulouse Fault
1385 array also undergoing reactivation (Astre, 1959), the land in between from Carcassonne to
1386 Castelnaudary stood as a horst exposed to denudation. This possibility is supported by the
1387 discovery at Bourg-Saint-Bernard (Astre, 1953, 1959), 22 km east of Toulouse, of a mastodon

1388 tooth (*Turicius turicensis simorreensis* Osborn), i.e., a genus whose arrival in Europe from
1389 Africa occurred ~18 Ma (Tassy, 1990; van der Made and Mazo, 2003), trapped in a fissure of
1390 exposed Chattian molasse (i.e., >23 Ma). This stratigraphically anomalous occurrence of a
1391 younger fossil in an older geological bed suggests erosion and redeposition of younger rocks
1392 across the land surface, here in a context of extensional crustal strain.

1393

1394 ***3.1.5. Sharp regime change during the late Miocene***

1395

1396 *3.1.5.1. Stratigraphic aspects*

1397

1398 Compared to the earlier Neogene molasse, the late Neogene stratigraphic sequence (Fig. 5)
1399 is radically different from anything that preceded it in at least two respects. Firstly, the
1400 sedimentology is characterised by an abrupt influx of almost pure siliciclastic debris, which
1401 furthermore always lack a carbonate matrix in their depositional settings. Secondly, the base
1402 of the sequence usually displays evidence of a sharp disconformity involving networks of
1403 channels vertically incised into the underlying molasse depositional sequences. This
1404 ravinement surface has been well described by Crouzel (1957, Fig. 38 therein), who
1405 nonetheless erroneously extended this observation to the base of the marine 'Sables fauves'
1406 farther out into the Aquitaine Basin. This highly irregular boundary has sporadically been
1407 refuted and interpreted instead as a Pliocene or early Pleistocene weathering front (Icole,
1408 1973). However, the erosional stratigraphic boundary is well documented throughout the
1409 foreland basin where decalcified, pebble-bearing clay deposits form a disconformable
1410 blanket across every existing geological structure from the Neogene molasse sequences
1411 (whether marine or continental) to the Paleogene Palassou conglomerate beds and the
1412 Cretaceous fold structures of the Sub- and North-Pyrenean zones.

1413

1414 *3.1.5.2. Growth of range-front megafans*

1415

1416 The late Neogene cover sequence (Fig. 5, Ariège and Béarn transects) extends as far out
1417 from the Pyrenees as the Landes plateau and the Entre-deux-Mers (between Dordogne and
1418 Garonne) near Bordeaux. Closer to the Pyrenean mountain front, it formed large alluvial fans

1419 at the mouths of the main Pyrenean valleys. Among these: the Lannemezan megafan (Neste
1420 River) (Boule, 1894; Patin, 1967; Icole, 1968, 1969), the Ger megafan (Gave de Pau) (Fig. 1,
1421 Fig. 5 Béarn transect), and lesser fans such as the Cieutat–Orignac (Adour River), the Gave
1422 d’Ossau, the Lasserre-Lahitère (Salat River), and residual strips of formerly much larger fans
1423 coaxial with the Arbas, Arize and Ariège rivers. The Ariège and Garonne rivers, however,
1424 have comparatively large watersheds and were relatively more efficient at exporting most of
1425 the bedload to the outer piedmont. In the Basque Country, the extensive limestone
1426 catchment lithology has limited the abundance of clastic supply. Fan debris accumulations
1427 attain 60–80 m in the Ger and Orignac–Cieutat, 90–110 m in the central and eastern
1428 Lannemezan, and 170 m in the western Lannemezan. The cumulative thickness of the Ger
1429 megafan attains 100–120 m.

1430 Four sedimentary units have been identified in some of those clastic sequence, with
1431 evidence of internal disconformities. The three uppermost units, clearly defined within the
1432 Ger megafan (Karnay et al., 1998; Capdeville et al., 1998), belong to the Pliocene. The basal
1433 unit of the late Neogene cover sequence is varyingly named ‘Clay-with-pebbles’ or
1434 ‘Variegated clays’ depending on the 1:50,000 scale map sheet concerned and on its proximal
1435 or distal position, respectively. The reported thickness of this unit ranges from 20 to 60 m. Its
1436 base is well dated at Orignac, where a lignite bed has yielded a rich assemblage of
1437 mammalian fossils (known since 1865) containing *Hipparion* (Astre, 1932; Richard, 1948;
1438 Crouzel, 1957). It can thus be assigned a Vallesian age (MN 10; Antoine et al., 1997), i.e., ~9.9
1439 Ma. The botanical fossils in the lignite (Sauvage, 1969) are similar to those at Capvern
1440 (Bugnicourt et al., 1988) as well as near Pau and Mont-de-Marsan, i.e., rich in warmth-loving
1441 plants such as palms. The stratigraphically equivalent beds at Arjuzanx, on the southern
1442 Landes plateau, have also yielded an Upper Miocene mammalian fossil (*Dorcatherium*)
1443 amidst similar floral assemblages which include the cinnamon tree (*Cinnamomum*
1444 *polymorphum*; Huart and Lavocat, 1963). The systematic presence of marine phytoplankton
1445 in the same formation near Mont-de-Marsan suggests a close proximity to the Tortonian
1446 shoreline at the time (Capdeville, 1990). The three upper units of the Ger alluvial fan each
1447 contain 2 to 4 upward-fining depositional sequences, but mean pebble size increases from
1448 Unit 1 (2–5 cm) to Unit 3 (15 cm; maximum: 25–30 cm). The age of the megafan top is
1449 currently unknown, but its surface itself is cut and filled by shallow alluvial channel deposits
1450 containing even coarser debris than Unit 3.

1451 The stratigraphy beneath the Landes area (Dubreuilh et al., 1995; Corbier et al., 2010; Bosq
1452 et al., 2019), where four fluvial sequences have cut and filled the underlying ‘Variegated
1453 clays’ of late Miocene age, attain a total thickness of 130 m. These formations, known
1454 respectively as Arengosse, Onesse–Beliet, Belin, and Castet, all contain lignite beds which
1455 document the decline in abundance, and ultimate extinction, of the warmth-loving plants
1456 still present in the slightly older strata elsewhere.

- 1457 • The Arengosse unit cuts deep into the underlying sequence and is consistent with a
1458 Pliocene age. Warmth-loving species record a sharp decline in the topmost beds. The
1459 Arengosse Formation is typical of a deltaic environment and includes marine sand
1460 containing assemblages of foraminifera. Borehole cores indicate a marine gulf in the
1461 south of the Landes extending ~10 km east of the current coastline during the Pliocene
1462 (Kieken et al., 1975).
- 1463 • The Onesse–Beliet unit, which was previously assigned chronostratigraphically to the
1464 Gelasian–Calabrian boundary (~1.8 Ma; Dubreuilh et al., 1995) but now considered older
1465 (i.e., closer to the Gelasian–Piacenzian boundary: 2.5–2.6 Ma; Corbier et al., 2010),
1466 includes only rare non-temperate taxa.
- 1467 • The Belin unit outlines an early floodway of the Garonne River, already established in its
1468 northern position at the time, thus suggesting an onset of fluvial incision of the
1469 Lannemezan clastic sequence.
- 1470 • The topmost Castet unit consists of reworked sediment from the older units. Despite
1471 having been formerly interpreted as an early Pleistocene fluvial unit (Corbier et al.,
1472 2010), it has recently been reinterpreted as an aeolian formation (a mid-latitude erg) and
1473 consists of a range of dated middle Pleistocene deposits (Marine Isotope Stages 10, 8
1474 and 6; Sitzia, 2014; Sitzia et al., 2015).

1475 Based on the coarse calibre of the debris forming the late Neogene megafan deposits, these
1476 landforms have been ascribed by most authors to a tectonic pulse in the Pyrenees. Taillefer
1477 (1951) took exception to this doctrine and ascribed them to a climatic cause. The current
1478 position of the top of the marine Langhian beds in Armagnac, which lie at 230 m (former gulf
1479 of Lectoure), nevertheless implies a magnitude of 200 m of post-Langhian uplift
1480 (conveniently, the Langhian was also the Miocene eustatic maximum, so the tectonic cause
1481 of this relative base-level rise is beyond doubt; see also Miller et al., 2011). Based on this

1482 criterion, projecting the gradient of the Langhian baseline up the Adour River from Aire-sur-
1483 l'Adour obtains a 0.4% post-Langhian tilt of the (originally horizontal) marine beds and
1484 projects the southward continuation of this line to an elevation of 400 m in the foothills of
1485 the Pyrenees. This altitude grades to the base of retro-foreland's megafan accumulations,
1486 and thus documents a post-Langhian tilt of the Pyrenean piedmont and a minimum uplift
1487 value of the Pyrenean retro-wedge since that time.

1488 The Neogene clastic wedge on the inner continental shelf of the Bay of Biscay (Landes)
1489 thickens offshore (Pujos-Lamy, 1984) and its aggradation rate appears to have increased
1490 through time. A 500-m-thick Miocene sequence and a 1000-m-thick Pliocene and
1491 Quaternary sequence were detected at the Ibis borehole (Kieken, 1973). Seismic profiles and
1492 more recent borehole data compiled by Ortiz et al. (2020), which provide a clear 3D
1493 reconstruction of the margin, now reveal that the post-Miocene wedge offshore is, on
1494 average, similar in thickness and volume to its Miocene predecessor (volume not quantified
1495 precisely by Ortiz et al.). Given that it was emplaced in just ~5 Ma (i.e., 3 to 4 times faster
1496 than its underlying Miocene sequence), with bypass to the abyssal domain by this time
1497 already substantial; and given, moreover, that it occurred prior to the acceleration of global
1498 cooling in the Pleistocene, the overall evidence is compatible with some form of tectonic
1499 reactivation in the Pyrenees and Massif Central starting in the late Neogene, with
1500 contributions from each of their river systems in currently unspecified proportions. The
1501 Pyrenees thus undoubtedly contributed to rapid Miocene, Pliocene and Quaternary
1502 sequence progradation in the south of the Aquitaine continental shelf zone (Bellec, 2003;
1503 Bellec et al., 2009).

1504

1505 **3.2. Chronology of clastic supply to the Iberian foreland**

1506

1507 **3.2.1. State of the art and data sources**

1508 In contrast to the Aquitaine Basin, exceptionally good outcrop exposures permitted by the
1509 much drier climate in the Iberian foreland have promoted many opportunities for extensive
1510 and detailed stratigraphic and sedimentological studies of the fill sequences. This has also
1511 spawned the description and naming of a multitude of lithostratigraphic units of local extent,
1512 resulting in a complicated inventory of place-based terminologies. Appearances of regional
1513 uniformity have been inferred on the basis of long-distance lithostratigraphic correlations,

1514 but unforeseen complications have arisen because many of those locally-defined units have
1515 turned out to be diachronous.

1516 The record of Paleogene clastic sequences in the pro-foreland setting can broadly be divided
1517 into two palaeogeographic segments from east to west (Barnolas et al., 2019): (i) the
1518 Southeast Pyrenean Foreland Basin, which is confined to eastern and central Catalonia and
1519 includes the large Ripoll piggyback basin (Fig. 5, Catalunya transect), cradled by the Canigou–
1520 Vallespir–Cadí nappe unit (Figs. 2, 3); and (ii) the South Pyrenean Foreland Basin in western
1521 Catalonia and onward into Aragón, which as far west as Pamplona is also a collection of
1522 piggyback basins — large (Ainsa, Jaca) and small (Pobla, Tremp, Ager), cradled by the SPZ
1523 thrust systems (Figs. 3, 5).

1524 As with the Aquitaine Basin, we emphasize clast provenance and the diachronous patterns
1525 of basin fill generated by the rising Pyrenees. Progress in clarifying the basic
1526 lithostratigraphic correlations has been gained from sequence stratigraphy,
1527 magnetostratigraphy, U–Pb and fission-track ages of detrital zircon crystals (Whitchurch et
1528 al., 2011; Thomson et al., 2017; Roigé et al., 2019), and from the correlation of various
1529 continental fossil assemblages to ELMA biozones. For example, 8 tectono-sedimentary units
1530 (TSUs) have been identified in the Iberian foreland (3 for the Paleogene, and 5 for the
1531 Neogene: Villena et al., 1992; Pérez-Rivaréz et al., 2018). The inventory, however, is confined
1532 to the Ebro basin itself and does not include the folded Eocene sequences that were being
1533 cannibalised and incorporated into the orogen by outward growth of the pro-wedge. In the
1534 Southeast Pyrenean Foreland Basin, 8 sequences were inventoried just within the Eocene
1535 series (Puigdefábregas et al., 1986). The pioneering work of Reille (1971) was updated by a
1536 more recent synthesis (Barnolas and Gil-Peña, 2001), which defines only 4 sequences within
1537 the Eocene series. Friend et al. (1996) have provided a comprehensive analysis of the
1538 continental deposits spanning the Priabonian to the Lower Miocene.

1539 Obtaining age constraints for these various depositional systems and their lithofacies
1540 assemblages has proven difficult chiefly for two reasons. Firstly, marine environments on the
1541 Iberian side of the orogen only endured until the Eocene. After ~36 Ma, the Ebro Basin
1542 became internally drained. Accordingly, the sedimentary sequences acquired thereafter a
1543 continental character, thus ruling out all prospect of chronostratigraphic constraints from
1544 marine indicator fossil evidence (reliable and independent constraints for the Neogene are
1545 even more tenuous than for the Paleogene, with only one radiometric age in the form of a

1546 19.7±0.3 Ma cinerite bed; Pérez-Rivaréz et al., 2018). Secondly, mammalian faunal
1547 assemblage sites have turned out to be (i) much less abundant than in the Aquitaine Basin
1548 despite a growing inventory through the years, (ii) comparatively poorer in species diversity,
1549 and (iii) very unevenly distributed through basin space and stratigraphic time. A synthesis
1550 produced by Cuenca et al. (1992) listed at the time a total of 123 fossil sites, mostly situated
1551 in the south and southeast of the Ebro Basin. They were much scarcer in the outer pro-
1552 wedge, and even more so within the tectonically deformed clastic sequences of the inner
1553 pro-wedge (for the Paleogene, see also: Crusafont and Golpe-Posse, 1973; Golpe-Posse,
1554 1981a; Sudre et al., 1992; Antunes et al., 1997; Cuesta et al., 2006; Badiola et al., 2009;
1555 Bonilla-Salomon et al., 2016; and for the Neogene: Crusafont et al., 1966; Crusafont and
1556 Pons, 1969; Cuenca et al., 1989; Alvarez-Sierra et al., 1990; Agustí et al., 1994, 2011).
1557 As a result of these key differences with the Aquitaine Basin, palaeogeographic
1558 reconstructions of the Ebro Basin have relied on magnetostratigraphy as the core method
1559 for tuning the record of continental deposits to index fossils in existing marine sequences
1560 (Garcés et al., 2020). Divergences of interpretation from one local study to another are
1561 understandably numerous (e.g., Burbank et al., 1992a, b; Costa et al., 2010, 2011; Hogan and
1562 Burbank, 1996; Arenas et al., 2001; Oliva-Urcia et al., 2016, 2019; Roigé et al., 2019), and the
1563 most robust chronological constraints in the case of continental deposits are obtained when
1564 magnetostratigraphic results are combined with ELMA-based evidence (Barberà et al., 2001;
1565 Larrasoaña et al., 2006). Resulting palaeogeographic interpretations and palaeogeographic
1566 maps for the Ebro foreland using either approach usually concur remarkably well. The most
1567 recent synthesis by Garcés et al. (2020) favours magnetostratigraphic evidence and
1568 prioritises correlations with the Geomagnetic Polarity Time Scale (GPTS). Within that
1569 particular reference frame, some offsets or mismatches with existing ELMA-based
1570 chronostratigraphic data, particularly at the fossil-rich sites of Sossis and Sant Jaume de
1571 Frontanyà, are not considered or discussed, and thus remain currently unresolved.

1572

1573 **3.2.2. Paleogene deposits of the Southeast Pyrenean Foreland Basin**

1574

1575 Unlike the Aquitaine foreland, where the sea withdrew rapidly from the Corbières westward
1576 to the Béarn in Ypresian time (~46 Ma), the Iberian foreland remained a marine environment
1577 until the early Priabonian (~36 Ma) (Sanjuan et al., 2012; Costa et al., 2013). Below we

1578 present the palaeogeography of the Southeast Pyrenean Foreland Basin in two longitudinal
1579 segments from east to west, with emphasis on the clastic output generated by the rising
1580 Pyrenees, on evidence of clast provenance, and on the diachronous chronostratigraphy of
1581 the basin fill.

1582

1583 *3.2.2.1. From the Empordà Basin to the Ripoll syncline*

1584

1585 The southward displacement of the Eocene foredeep has been well constrained from a
1586 sequence stratigraphy perspective from the Empordà Basin to the Ripoll syncline
1587 (Puigdefàbregas et al., 1986; Burbank et al., 1992b; Vergés and Burbank, 1996; Costa et al.,
1588 1996; Tosquella and Samsó, 1996; Barnolas and Gil Peña, 2001; Serra-Kiel et al., 2003;
1589 Barnolas et al., 2019). Nine depositional sequences (I to IX) were initially identified in this
1590 eastern segment of the foredeep: eight within the Eocene and one defining the base of the
1591 Oligocene. Their names are directly adopted from the regional lithostratigraphic unit names,
1592 hence some ambiguity in the literature between the two schemes — particularly in the case
1593 of Bellmunt (unit VI) and Milany (unit VII) and the respective boundaries of these units in
1594 each scenario. Units I–III (Ypresian) to IV (Lutetian) testify to thrust sheet emplacement
1595 below sea level, with olistoliths, turbidites, and deltaic facies. However, vestigial outcrops of
1596 proximal conglomerate beds of Ypresian and Lutetian age occur at several locations in the
1597 far east (mapped on the geological sheet of Figueres: Fleta et al., 1994; Pujadas et al., 1989),
1598 and occur likewise in the South Pyrenean Foreland Basin (see next Section). The younger
1599 depositional units (VI, VII, IX) exhibit thick conglomerate units, including the fan-deltas of the
1600 Lutetian Bellmunt (46–41 Ma) and Bartonian Milany (41–37 Ma) formations, which are
1601 themselves overlain by the Berga conglomerate sequence (Priabonian–Rupelian boundary,
1602 i.e., ~34 Ma). Units V (Beuda: gypsum) and VIII (Cardona: salt beds) consist of evaporites and
1603 document the growing confinement of the Ebro Basin and the definitive termination of the
1604 marine environment, respectively. Guided by a new calibration of Lower Lutetian biozone
1605 SBZ 13 (large foraminifera of the shallow benthic zone) Garcés et al. (2020; compare Figures
1606 2 and 6 therein) have offered a divergent interpretation of the Ripoll syncline based on a
1607 revision of the middle (clastic) sequences. In this new framework, the Bellmunt and Milany
1608 units are fully reallocated to the Lutetian and the Beuda unit to the Ypresian–Lutetian

1609 boundary — thus suggesting that these formations are substantially older than previously
1610 established (e.g., Berástegui et al., 2002).

1611 In the Empordà Basin, the Bellmunt Formation is 2 to 3 km thick and devoid of fossil
1612 remains. The top of the conglomerate sequence is covered by the Figueres nappe and in
1613 some publications attributed to the Priabonian (Fleta et al., 1994). The base of the Bellmunt
1614 Formation in the SW rests conformably on Lower Lutetian marine beds (48–45 Ma), but
1615 towards the NE the 1:50,000 scale geological map of Figueres (Fleta et al., 1994) indicates
1616 progradation of the conglomerates over Upper Ilerdian–Cuisian marine beds, beneath the
1617 Biure nappe (Pujadas et al., 1989). The Bellmunt conglomerates near Figueres are alluvial fan
1618 deposits containing a majority of limestone and sandstone pebbles from the Mesozoic and
1619 early Cenozoic cover sequences of the Pyrenees, but also containing some debris supplied by
1620 basement outcrops. The latter are initially uncommon (5–10%), but their abundance
1621 increases in the middle and upper units of the sequence, where they display schist (including
1622 a facies reminiscent of the Paleozoic Jujols Series), quartz, quartzite, black chert, various
1623 granites (sometimes exclusive in certain beds, with some cobbles up to 40 cm in diameter).
1624 However, the total absence of gneiss (particularly augengneiss), which forms substantial
1625 outcrops in the Roc de France and Albères massifs today, suggests that this eastern segment
1626 of the Axial Zone was not sufficiently deeply eroded at the time to expose this gneiss core.

1627 In the Ripoll syncline, the Milany Formation laps onto the edge of the Pedraforca nappe and
1628 is reported to contain granite clasts (Burbank et al., 1992b), but has (confusingly) been
1629 named Bellmunt instead of Milany by other authors (Busquets et al., 1992). No gneiss clasts
1630 are reported, suggesting that the Carançà gneiss outcrops in the Axial Zone were not yet
1631 exposed at the time. The fine-textured fluvial and palustrine basal beds contain the rich
1632 mammalian assemblages of Sant Jaume de Frontanyà (SJF) 1 (MP 15: ~40.5 Ma, Lower
1633 Bartonian) and (200–270 m lower down the sequence) SJF 2 and SJF 3 (MP14: ~42 Ma,
1634 Upper Lutetian) (Busquets et al., 1992; Badiola et al., 2009; Bonilla-Salomon et al., 2016).

1635 The outcrops of marine and deltaic facies occur 500 m further down in the stratigraphy
1636 (Coubet/Can Bernat Fm., Busquets et al., 1992); they are attributed to marine biozone SBZ13
1637 (Garcés et al., 2020) and are thus clearly Lower Lutetian.

1638 The ELMA-based chronological framework defined by the mammalian fossil sites has been
1639 challenged by recent reinterpretations of previous magnetostratigraphic data (Garcés et al.,
1640 2020). The three studies available in the literature for this area (Burbank et al., 1992b;

1641 Vergés et al., 1998; Garcés et al., 2020) differ nonetheless substantially; the most detailed
1642 (Burbank et al., 1992b, Figs. 9, 15 and 16 therein) spans chrons 21 to 18 or 17, and clearly
1643 exposes correlation uncertainties and options. The most recent (Garcés et al., 2020, Fig. 6
1644 therein) restricts the entire lithostratigraphic interval to Chron 21, but without explaining
1645 why the other options have been ruled out. Existing geological maps, and particularly the
1646 IGME sheet for La Pobla de Lillet (Vergés et al., 1994) and the IGC 1:25,000 scale sheet
1647 bearing the same name (Martínez et al., 2013), each also indicate divergent ages for the top
1648 of the conglomerate sequence, i.e., Priabonian and Bartonian, respectively. Birot (1937) had
1649 previously reported among these upper beds the presence of huge boulders of granite (in
1650 the upper levels, granite clasts dominate almost exclusively and the largest boulders are 3 m
1651 in diameter), probably supplied by the Mont-Louis batholith, whose nearest outcrops
1652 currently lie 30 km to the north, i.e., beyond the currently elevated massifs in Devonian
1653 limestone (Tossa d'Alp massif, at the southern edge of the Cerdagne Basin). This evidence
1654 suggests a presence at the time of small, steep catchments with high-energy streams
1655 capable of delivering large debris — and thus a granitic mountain front nearby (~30 km to
1656 the closest modern granite outcrop) and very different from the current landscape.
1657 Overall, given the 1400-m-thick sediment pile that separates the Sant Jaume de Frontanya
1658 fossil deposit from the top of the series, and given further the sedimentation rates that can
1659 be inferred between the two palaeontological sites SJF 1 and SJF 2–3 (separated by 270 m of
1660 sediment accumulation), it cannot be ruled out that the top of the depositional sequence is
1661 Priabonian. More data are needed from that region to reach a robust conclusion.

1662

1663 *3.2.2.2. From the Llobregat to west of the Segre River*

1664

1665 In this western part of the Southeast Pyrenean Foreland Basin, the Bellmunt and Milany
1666 sequences have been deformed by Pyrenean tectonics and partly incorporated into the
1667 Pedraforca nappe (Figs. 2, 3). South of this tectonic unit lie the well-documented Berga and
1668 Oliana conglomerate sequences, which are 2500 m thick and have been subdivided into
1669 three units based on conspicuous boundaries within the fanning dip structure (Riba, 1973,
1670 1976). The clast compositions are lithologically fairly uniform, with debris from the Axial
1671 Zone (granites included) rather unevenly distributed through the sequence. Axial Zone
1672 lithologies are thus sporadically abundant, such as in the lower Cardener conglomerate beds

1673 or at the top of the sequence near the town of Oliana, but are also at times rare or absent.
1674 Granite cobbles may attain diameters of 40–50 cm, with upward coarsening through the
1675 stratigraphy (limestone boulders ~1 m in diameter). The base of the Berga sequence lies
1676 conformably over the Lower Priabonian marine shales and is thus most likely also of
1677 Priabonian and Rupelian age (~36 to ~31 Ma; Carrigan et al., 2016), but the top of the
1678 sequence is undated. A revised magnetostratigraphy by Costa et al. (2010) of the results
1679 published by Burbank et al. (1992a) and Vergés and Burbank (1996) has confirmed the
1680 Priabonian age of the basal marine beds, and it additionally shows that the base of Oliana
1681 Unit 4 is part of the Rupelian (~30.5 Ma). This marker horizon, however, is still overlain by at
1682 least 500–700 m of conglomerate and sandstone beds, which — by linear extrapolation of
1683 the earlier sedimentation rates — should place the top of the Oliana–Berga conglomerate
1684 sequence in the late Oligocene (Chattian: 27–28 Ma). Farther out into the Ebro Basin, the
1685 conglomerate formations change to more distal molasse facies such as the yellow Solsona
1686 and red Artés sandstone sequences, and further still to shale and lacustrine limestones.
1687 These distal sequences contain a dozen mammalian fossil sites spanning Priabonian biozones
1688 MP 19–20 (or perhaps MP 18) at Cardona, Sant Cugat de Gavadons, and Roquefort de
1689 Queralt; upward to to MP 21 (Santpedor), MP 22 (Calaf), MP 23 (Tàrrega), and MP 23/24
1690 (Vinaixa) which, at ~30 Ma, all document the Rupelian Stage (Barberá et al., 2001; Costa et
1691 al., 2011).
1692 West of the Segre River, near Artesa de Segre, a magnetostratigraphic study covering an
1693 1800-m-thick molasse sequence consisting predominantly of clay and sandstone has yielded
1694 a Priabonian base (35 Ma) and a Chattian top (25 Ma) (Meigs et al., 1996). This molasse
1695 sequence transitions northward to a much coarser sequence of conglomerate beds
1696 consisting almost exclusively of Mesozoic limestone pebbles. These have buried portions of
1697 the SPCU thrust-front scarps between the Montsec and Oliana, for example around the Col
1698 de Comiols near Benavent. Five depositional sequences have been identified and correlated
1699 with those reported around Oliana (Maestro-Maideu and Serra-Roig, 1996). The chronology
1700 provided by Meigs et al. (1996), however, remains uncertain given the occurrence of
1701 interruptions in the stratigraphy and the absence (thus far) of independently corroborating
1702 geochronological evidence in this area.

1703

1704 **3.2.3. Paleogene deposits of the South Pyrenean Foreland Basin**

1705
1706 Still farther west along the strike of the orogen, roughly between the town of Tremp and the
1707 city of Pamplona, the Paleogene clastic sequences accumulated in a continuous depositional
1708 zone known as the South Pyrenean Foreland Basin (Barnolas et al., 2019), also commonly
1709 dubbed Jaca–Tremp Basin. This depositional area, however, is not easy to reconstruct, (i)
1710 partly because the Paleogene deposits have been concealed by younger Neogene sequences
1711 at the margins of the Ebro Basin, but also (ii) because the Montsec Thrust and the South
1712 Pyrenean Frontal Thrust (Fig. 2) detached and carried the Jaca–Tremp Basin piggyback
1713 southward in several stages during the middle and late Eocene to early Miocene — thus
1714 imparting tectonic deformations to all of the fill sequences. As a result, despite the fact that
1715 structural geologists consider the SPFT as the limit between the Pyrenean crustal wedge and
1716 the Ebro Basin, in terms of stratigraphy this limit is not adequate because parts of the South
1717 Pyrenean Foreland Basin were situated in the thrust-displaced, and others in the
1718 undisplaced, foreland area during the same period of the past. It is thus useful to bear in
1719 mind that synorogenic sedimentation in the south-Pyrenean foreland occurred in two
1720 contrasting environments separated by the Sierras Exteriores: the elongated piggyback Jaca–
1721 Tremp Basin situated north of the Sierras Exteriores, and the less intensely deformed outer
1722 Ebro foreland basin located south of them (Fig. 2).

1723 In the Sierras Exteriores west of the Noguera Ribagorçana River, the Peralta de la Sal Basin
1724 displays a very similar chronostratigraphic model to that of the Artesa area mentioned above
1725 (Meigs, 1997). In the Ebro foreland, the history of denudation in the orogen is recorded by
1726 the mudstone and sandstone sequences that overlie the Priabonian evaporites (Balaguer
1727 and Barbastro gypsum deposits, Fig. 5, E-Aragón transect), and that have been deformed
1728 into a fairly continuous frontal anticline. Extensive outcrops of the 1000-m-thick Peraltilla
1729 Formation (Fig. 5, E-Aragón transect), which consists of red mudstone floodbasin deposits
1730 interbedded with shoestring sandstones, can be observed west of the Cinca River. The
1731 bottom of the sequence (marl and lacustrine limestones) has been ascribed to the early
1732 Oligocene based on a flora of charophytes (Reille, 1967, 1971) and on a micromammalian
1733 fossil assemblage (locality: Peraltilla) assigned to MP 23, i.e., ~31 Ma (Alvarez-Sierra et al.,
1734 1990; Cuenca et al., 1992). The sequence has been folded and is unconformably covered by
1735 an Aquitanian terrigenous sequence. The fine-textured sedimentological features of the
1736 Peraltilla sequence (Fig. 5), with just a few gravel-bearing beds containing predominantly

1737 small quartz clasts, would suggest a relatively low-energy environment at the front of the
1738 outer sierras at the time, even though clast provenance analysis also documents some
1739 sediment transfer from the Axial Zone (Yuste et al., 2004). Overall, the age of the
1740 conglomerate beds in the region around Barbastro and Graus remains unclear, with some
1741 authors postulating continuous aggradation of the Huesca megafan from the early Oligocene
1742 to the Miocene (Hirst and Nichols, 1986; Luzon, 2005).

1743 The repository for the coarser, high-energy Paleogene clastic output from the Pyrenean
1744 orogen was the Jaca–Tresp Basin (Fig. 5, Aragón transects) situated to the north of the
1745 Sierras Exteriores, confirming that high relief was present in at least parts of the hinterland
1746 at the time. The Jaca–Tresp Basin began to form and accumulate deposits quite early in the
1747 Iberia–Europe convergence history. In the east, it received a 1000 m-thick discharge of the
1748 Garumnian series, which lies conformably over the late-Cretaceous marine and
1749 Maastrichtian littoral sandstone beds (Aren Formation). The leading edge of the upper
1750 Pedraforca–Bóixols upper nappe unit terminates in this sequence. An extensive Ilerdian
1751 carbonate platform documents a distinctive but brief respite in the tempo of clastic output
1752 from the rising orogen. Accordingly, these well-defined marine episodes (the Ilerdian Stage,
1753 i.e., Lower Ypresian, received its credentials as an international stratotype in the Tresp
1754 Basin: see Pujalte et al., 2009) were soon overprinted by an Upper Ypresian to Lutetian
1755 depositional system of piedmont, alluvial plain, deltaic and shelf-sea lithofacies. This
1756 succession of thick sandstone and conglomerate beds progrades from east to west (Nijman,
1757 1998), parallel to the strike of the orogen.

1758 The conglomerate units of the Tresp Basin were being supplied by topography situated to
1759 the northeast of the depositional area, i.e., where the Proto-Pyrenees had formed and were
1760 presently expanding westward to form the Ancestral Pyrenees. The source rocks were
1761 mainly sedimentary cover sequences, with nonetheless arkose deposits and a minority
1762 presence of basement clasts from the Axial Zone. The pebbles are well rounded, with
1763 median sizes ranging from 10–20 cm to 40–50 cm in the more massive Campanue Formation
1764 (500–1000 m thick), the top of which could be of early Lutetian age (~45 Ma; Fig. 5, E-Aragón
1765 transect). The fluvial facies exposures contain a large number of mammalian fossil sites, all
1766 rather limited in taxonomic diversity (Crusafont et al., 1956; Crusafont et al., 1973; Antunes
1767 et al., 1997; Badiola et al., 2009). In the Ager sub-basin (16 sites), the clastic sequence
1768 appears quite old (3 sites: MP 8–MP 9, i.e., ~52 Ma), with the remainder labelled as MP 10

1769 (~50 Ma). In the larger Graus–Trempe sub-basin (Montllobar: 6 sites; Pont de Montanyana: 10
1770 sites; Isabena: 11 sites), all of the fossil assemblages are now ascribed to biozone MP 10, i.e.,
1771 to the Upper Ypresian (Antunes et al., 1997; Badiola et al., 2009) instead of the Lutetian
1772 (Crusafont et al., 1956; Sudre et al., 1992).

1773 The Capella Formation (Fig. 5, E-Aragón transect), which is 600 m thick and of fluvial origin,
1774 records the tipping moment when its sedimentary sequences (which are exposed in the
1775 Isábena River valley) became lastingly cut off from marine influence. The Capella Formation
1776 is reported to connect laterally to the upper section of the Campanue Formation, but its age
1777 is poorly constrained: its base contains an MP 10 assemblage (at Torrelabad); and two sites
1778 from the middle part of the stratigraphy (Barranc de Estaran, Casa Ramon) are labelled as
1779 MP 11–MP 12, i.e., ~46–48 Ma (Antunes et al., 1997; Badiola et al., 2009). However, the
1780 Barranc site has been revised as MP 13, i.e., ~44 Ma, by Teixell et al. (2016), whereas the
1781 Graus occurrence (MP 14, i.e., Upper Lutetian) has not been precisely located in consulted
1782 publications although it appears to lie within the Capella Formation.

1783 The continental character of the basin environment was accentuated at the time of the
1784 Escanilla Formation (Fig. 5, E-Aragón transect), which on geological maps displays a slight
1785 unconformity over the underlying Capella and Campanue formations in the south and
1786 southwest, but forms a much more accentuated angular unconformity over the Triassic and
1787 Cretaceous outcrops of the Mediano anticline. The Escanilla Formation consists of 500 to
1788 1000 m of red- and ochre-coloured mudstone, and of grey conglomerates containing some
1789 pebbles from the Axial Zone. This formation also displays two levels of limestone and lignite
1790 containing the two taxonomically diverse fossil sites of Capella (MP 14, ~42 Ma, not to be
1791 confused with the name of the underlying formation) and Laguarres (200 m further up-
1792 sequence: MP 15, i.e., ~40.5 Ma according to Sudre et al., 1992; but MP 16, i.e., ~39 Ma
1793 according to Antunes et al., 1997 and Badiola et al., 2009). The age of the Escanilla sequence
1794 thus spans the Upper Lutetian and entire Bartonian. The top of the sequence, which has not
1795 been preserved, could thus potentially be extrapolated into the Priabonian, and perhaps
1796 even the early Oligocene. This biochronology is corroborated by magnetostratigraphic data
1797 from the same area (Bentham and Burbank, 1996; Vinyoles et al., 2020).

1798 West of the Graus meridian, the siliciclastic sequence of the Jaca–Trempe Basin forms a
1799 transition with the Ypresian and Lutetian flysch-filled Ainsa foredeep and the Hecho
1800 submarine fan system (4400 m thick; Labaume et al., 1985). It contains limestone

1801 olistostromes initially considered to have been supplied from a northern source area
1802 (Labaume et al., 1985), but more probably related to a destabilisation of the Guara
1803 carbonate platform located at the southern border of the flysch basin (Barnolas and Teixell,
1804 1994; Barnolas and Gil-Peña, 2001). To the north, the flysch sequence covered the region
1805 corresponding to the high Pyrenean range of today (Teixell, 1998), connecting with the
1806 Aquitaine foredeep in the vicinity of the modern Pic d’Anie. The meridian line passing
1807 through the Pic d’Anie consequently locates the point where the Ancestral Pyrenees
1808 terminated as an emerged mountain range during middle Eocene time.

1809 No Lutetian deltas or alluvial fans are documented west of the Campanue palaeofan. The
1810 default hypothesis is that none ever formed given the absence of a mountain range at these
1811 longitudes at that time. In Bartonian time, the pro-wedge foredeep rolled southward under
1812 the effect of increased crustal loading, and became until the early Priabonian a depocentre
1813 for 1700 m of marine shale (Pamplona Series). Compared to the earlier flysch episode, the
1814 depositional environments were shallower and included deltaic and continental facies
1815 indicative of rising uplands to the north and an active tectonic front probably located at the
1816 Oturia thrust front (Fig. 2). From base to top, and prograding to the SW over marine shales,
1817 the clastic sequence (Fig. 5, W-Aragón transect) consists of the Sabiñanigo Formation
1818 (Bartonian sandstone), the deltaic sandstone facies of Belsue–Atarés, and lastly the massive
1819 conglomerate and red mudstone beds of Santa Orosia, commonly tied to the Priabonian
1820 (Puigdefàbregas, 1975; Roigé et al., 2016, 2017; Garcés, 2020, Fig. 3 therein) but recently
1821 reassigned to the Upper Bartonian (Vinyoles et al., 2020). The clastic influx continues up-
1822 sequences with the Cancias conglomerates, which are Priabonian to Rupelian and transition
1823 laterally to the fluvial beds of the Campodarbe Fm. The extensive outcrops of Santa Orosia–
1824 Cancias conglomerates (500–900 m thick) between the modern Cinca and Gállego rivers
1825 contain boulders up to 60 cm in diameter consisting mainly of sandstone from Eocene flysch
1826 and (in lesser proportions) of limestone, with nonetheless rare evidence of debris
1827 transported from the Axial Zone (which was already exposed farther east: Roigé et al., 2016)
1828 and perhaps from the North-Pyrenean Zone (Roigé et al., 2017). This strongly suggests that
1829 the basement had not yet been exposed by denudation in this (nonetheless emergent)
1830 western segment of the Pyrenean orogen.

1831 The continental Campodarbe Formation, a western equivalent of the Escanilla Formation
1832 (Fig. 5, W-Aragón transect), conformably overlies the last deltaic and evaporitic deposits of

1833 Priabonian age and is ubiquitous from the Jaca syncline westwards to the Pamplona syncline
1834 and southwards to the south of the Sierras Exteriores, where the Peraltilla Formation is its
1835 stratigraphic equivalent (Fig. 5, E-Aragón transect). The Campodarbe Formation was studied
1836 in detail by Puigdefábregas (1975) and shown to attain maximum thicknesses of 3000 m at
1837 Guarga (east of the Gállego River), 4000 to 5000 m at Onsella (50 km to the west), and
1838 perhaps 7000 m near the border with the modern province of Navarra (i.e., another 50 km
1839 farther west; note that this maximum thickness includes the Miocene cover sequence). The
1840 Campodarbe Formation consists of fluvial sandstone and shale deposited by rivers flowing
1841 WNW, i.e., parallel to the strike of the orogen. The palaeochannels contain quartz pebbles.
1842 On its northern and northeastern edge, the formation is overtopped by thick, prograding
1843 synorogenic alluvial deposits produced by the eroding Ancestral Pyrenees, such as the Santa
1844 Orosia–Cancias palaeofans, which possibly continued to aggrade during the lower Oligocene,
1845 and the Peña de Oroel and San Juan de la Peña palaeofans near the city of Jaca.
1846 Stratigraphically, these two conglomerate sequences belong to the top of the Campodarbe
1847 Formation and exhibit overlapping syndepositional unconformities. Their clast content
1848 predominantly consists of Eocene sandstone and limestone from the aforementioned
1849 olistostromes of the flysch-filled Ainsa–Jaca trough, implying once again that the basement
1850 rocks of the Axial Zone were not yet exposed at that time.
1851 The age of the Campodarbe Formation is imprecise (Priabonian to late Oligocene) and based
1852 on charophyte remains. Magnetostratigraphic evidence (Hogan and Burbank, 1996) has
1853 provided a Priabonian age for the lower 1500 m (base at Chron 16rn, ~36 Ma, Costa et al.,
1854 2010) and a Rupelian age for the overlying 2300 m at the Salinas section, terminating at
1855 Chron 10r (~29 Ma). However, the Salinas section lacks the syntectonic upper conglomerate
1856 beds of the Peña de Oroel and San Juan palaeofans, which were ascribed to the late Chattian
1857 and even to the earliest Miocene by Reille (1971) and Puigdefábregas (1975). More recently,
1858 Oliva-Urcia et al. (2016) found that the top of the fluvial Campodarbe Formation in the
1859 foreland zone of the Sierras Exteriores coincided with Chron 7r (i.e., 24.5 Ma, latest
1860 Chattian); in the Jaca syncline, which at that time was still undergoing tectonic deformation,
1861 the top of the fluvial units of the Campodarbe Fm. (i.e., beneath the Peña de Oroel and San
1862 Juan conglomerates) is reported as no younger than 31 Ma. In this subregion, the Rupelian–
1863 Chattian deposits are thus understood to have been folded and eroded, thereby
1864 cannibalizing the Campodarbe Fm. and younger conglomerates of the deforming Jaca

1865 syncline, and supplying from this source-material the late Oligocene and Aquitanian Sariñena
1866 and Uncastillo formations (which make up the Luna Fan situated south of the Sierras
1867 Exteriores; Oliva-Urcia et al., 2019; Fig. 5, W-Aragón transect) (see Section 3.2.5 on Neogene
1868 deposits). Still more recent dating of volcanic zircon crystals contained in the San Juan de la
1869 Peña and Peña de Oroel conglomerate beds, however, has challenged this
1870 chronostratigraphic model and indicates instead that these conglomerate deposits of the
1871 Jaca Basin are as young as 24–22 Ma (i.e., Aquitanian) (Roigé et al., 2019). This would imply
1872 that sequences in the Luna Fan’s source area are the same age as the Luna Fan itself, in
1873 which case the Sariñena and Uncastillo conglomerate sequences cannot be merely re-
1874 eroded derivatives of the folded Jaca Basin conglomerates. Note that these very young ages
1875 remain unreported in the most recent synthesis on the region (Garcés et al., 2020, Fig. 3),
1876 according to which no conglomerate units are younger than Chattian, and which assigns
1877 Peña de Oroel to the Priabonian–Rupelian boundary and San Juan de la Peña fully to the
1878 Rupelian. In this region, where sequences suitable for magnetostratigraphy are scarce and
1879 where no terrestrial fossils have so far been reported from the San Juan and Peña
1880 conglomerate units, further field research is probably necessary as such occurrences may
1881 exist.

1882

1883 **3.2.4. Two geological enigmas in the Graus–Trempe Basin**

1884

1885 *1.2.4.1. Unexplained offsets between the Southeast and South foreland sequences*

1886

1887 Roughly between the towns of Graus and Trempe, the South-Pyrenean Central Unit (SPCU)
1888 consists of thrust units and a series of piggyback basins (Fig. 2), with the larger basin
1889 (Trempe–Graus) situated on the back of the Montsec Thrust Sheet, and the smaller (Ager)
1890 basin (south of the Montsec thrust front) riding on the Montroig Thrust Sheet which comes
1891 out at the base of the Serres Marginals (see Fig. 2; Turner, 1990; Teixell and Muñoz, 2000;
1892 Muñoz et al., 2018). This part of the SPCU is also known to geographers as the Conca de
1893 Graus–Trempe.

1894 The geometry and palaeogeography of the SPCU have raised a number of unresolved issues,
1895 summarised here. The clastic sequences of the piggyback basin were predominantly supplied
1896 by the high ranges of the Pyrenees, but secondarily also by the SPCU fold systems and by the

1897 Ebro massif to the south (which until at least the Paleocene was still above sea level:
1898 Puigdefábregas, 1975; Gómez-Gras et al., 2016; Thomson et al., 2017). Throughout the
1899 South Pyrenean Foreland Basin, the fill sequence gets younger from east to west and
1900 sedimentation was continuous from 66 to 28 Ma according to Garcés et al. (2020), and even
1901 until 25–23 Ma according to Roigé et al. (2019). It thus forms an uninterrupted, time-
1902 transgressive lateral progression along the Iberian foreland as far as the Jaca–Pamplona
1903 marine foredeep, which received a thick flysch sequence of early and middle Eocene age
1904 almost identical to the eastern sequence in the Ripoll Basin. The outstanding paradox of this
1905 regional succession is that the Catalonian flysch deposits of the Southeast Pyrenean Foreland
1906 Basin are mapped as overridden by the Pedraforca nappe on the east side of the SPCU,
1907 whereas the Aragonian flysch deposits appear to lie over the SPCU and the westward
1908 continuation of the South Pyrenean Zone in the Ainsa area (Fig. 2), riding piggyback on the
1909 SPCU and displaying their own endemic thrust sequence (e.g., Chanvry et al., 2018).
1910 Confusingly, therefore, what appears (at least in terms of lithostratigraphy and facies) to be
1911 the same Paleogene sequence either overlies or underlies the SPCU thrust units. This
1912 anomaly in the apparent architecture of the pro-wedge basins has often been sidestepped,
1913 but Nijman (1989) addressed it and offered three plausible explanations for this
1914 configuration. They are all underpinned by the logical inference that the Iberian foreland
1915 was made up in the early Paleogene of two marine foredeeps, one beneath the SPCU and
1916 overridden by it, and the other above it, with the two depositional sequences eventually
1917 merging in the west.

1918 Maps and reconstructions by Payros et al. (2009), Martinius (2012) and Thomson et al.
1919 (2017; Fig. 11 therein) suggest that a marine connection between the Ripoll and Ainsa basins
1920 could have occurred as a narrow corridor in the region of the Ager Basin at the time of
1921 deposition of the Ager Group, ~55–51 Ma, but that it is now either concealed beneath the
1922 advancing Montsec thrust, or lay over it but has since then been eroded (Muñoz et al.,
1923 2013). The very rapid southward advance of the SPCU by at least 40–45 km in just 4 Ma
1924 during the late Lutetian (44–41 Ma) emphasizes the importance of the Triassic evaporites as
1925 a lubricant on the thrust sole and is probably key to understanding the elusive
1926 palaeogeography of that period. Subsequent to the rapid thrust propagation, Thomson et al.
1927 (2017) suggest the South Pyrenean Foreland Basin became separated from the Southeast
1928 Pyrenean Foreland Basin as a result of topographic damming along the Segre oblique ramp

1929 fault zone (Fig. 2). No definitive solution has been put forward until now to adjudicate
1930 between these alternative palaeogeographic scenarios (Barnolas et al., 2019). A possible
1931 solution to the enigma would nonetheless be the coexistence of two distinct, strike-parallel
1932 marine foredeeps. The eastern foredeep, initially offset to the south of the western
1933 foredeep, opened out on the Tethys (see palaeogeographic maps in Plate I); it perhaps also,
1934 at least initially, communicated with its western counterpart through shallow straits not yet
1935 identified (discussion in Garcés et al., 2020).

1936

1937 3.2.4.2. *The 'Nogueres conglomerates' anomaly*

1938

1939 The unconformable 'Nogueres conglomerate units' (named collectively thus in this review,
1940 but more commonly named from just one of their four outcrops: the conglomerates of La
1941 Pobla de Segur) have long been singled out as unique and enigmatic within the Pyrenean
1942 orogenic environment (Ashauer, 1934; Birot, 1937; Crusafont et al., 1956; De Sitter, 1961;
1943 Rosell and Riba, 1966; Rosell, 1967; Reille, 1971; Mellere and Marzo, 1992; Coney et al.,
1944 1996; Vincent and Elliot, 1996; Vincent, 2001; Beamud et al., 2003, 2011). They occur in the
1945 Jaca–Trempe Basin between the modern Isábena and Segre rivers, and are mostly coaxial
1946 with the modern Noguera Ribagorçana and Noguera Pallaresa rivers — hence the 'Nogueres'
1947 appellation proposed here. Compared to other conglomerate sequences further east or
1948 west, their main characteristic is that they are recessed in a more northern position of the
1949 pro-wedge. A few residual outliers have also been mapped on the Pedraforca tectonic unit
1950 east of the Segre, but this Nogueres sequence mainly occurs as four geographically distinct
1951 outcrops, from west to east: Serra de Sis, Sierra de Gulp, La Pobla de Segur; and, offset to
1952 the north: the Senterada outcrop. Cumulative thicknesses attain 3500 m, subdivided into 5
1953 allostratigraphic units altogether forming a stack of 20 alluvial fans as well as an onlapping
1954 backfill sequence all the way up to the Axial Zone (Mellere and Marzo, 1992; Beamud et al.,
1955 2003, 2011). The size of the time gap recorded by the basal unconformity decreases from
1956 north to south, with the conglomerate beds resting successively on the Hercynian basement,
1957 on the folded Cretaceous cover sequence of the SPCU (Figs. 1, 3, 5), and on the Paleocene
1958 and Lower Eocene deposits of the Jaca–Trempe Basin (e.g., the upper Ypresian in the Sierra
1959 de Sis; MP 10 biozone near Cajigar, Isábena area, Badiola et al., 2009). Then, just a few

1960 kilometres to the SW, they connect to the Escanilla Formation, which itself rests
1961 disconformably on the underlying Lower Lutetian units (Beamud et al., 2003).
1962 The Nogueres conglomerate sequence can thus be considered to represent the proximal
1963 eastern tracts of the fluvial systems that supplied the Campodarbe Formation to the Jaca
1964 Basin (Michael et al., 2014). Their age at La Pobla de Segur has been constrained by 3
1965 mammalian fossil sites (Sosis, Roc de Santa, Claverol), which rank taxonomically among the
1966 most diverse of the Pyrenean Eocene. They are situated within the lacustrine facies of
1967 allostratigraphic Unit 2, to which may be added the slightly more elevated site of Casa
1968 Gramuntil at the base of allostratigraphic Unit 3 (López-Martínez, 1998). All of these
1969 assemblages are attributed to the base of the Priabonian, i.e., MP 17a (Crusafont et al.,
1970 1963; Crusafont and Golpe, 1973; Sudre et al., 1992; Antunes et al., 1997; Sigé, 1997; López-
1971 Martínez et al., 1998; Badiola et al., 2009). The lower allostratigraphic unit of La Pessonada
1972 (~1000 m thick) is then plausibly of Bartonian age. Magnetostratigraphic data place the top
1973 of allostratigraphic Unit 5 within the Chattian, i.e., 27 Ma (Beamud et al., 2011). Such an age
1974 is plausible, but in that case the magnetostratigraphy requires MP 17a to be pushed down
1975 the chronostratigraphic scale (by ~5 Ma) to the Upper Lutetian (Beamud et al., 2003). The
1976 proposition to recalibrate substantial portions of the ELMA scale on the basis of one local
1977 magnetostratigraphic study (see Fig. 6 in Beamud et al., 2003, which assigns biozones MP14
1978 to MP17a to the time bracket initially restricted to MP14) has so far not, however, been
1979 endorsed by more recent updates of the ELMA scale, which still appear to maintain MP 17a
1980 within the Priabonian (Badiola et al., 2009; Vandenberghe et al., 2012). The local
1981 magnetostratigraphic study of the Nogueres conglomerate beds thus lacks solid
1982 geochronological moorings, with currently little more than a long-distance correlation with
1983 the marine beds of the Ainsa foredeep. Moreover, biozone MP 17a was very short-lived
1984 (~0.4 Ma) and unfortunately falls entirely within a single, normal magnetic chron (C17n). In
1985 contrast, the > 200-m-thick Nogueres fossil-bearing sequence, despite mostly displaying a
1986 reverse polarity signal, is reported as spanning three polarity inversions, with some erratic
1987 results at the top of the sequence. The main fossil-bearing sites (Sosis, Claverol, Roc de
1988 Santa), which all occur within the same lacustrine carbonate unit (30–35 m thick; López
1989 Martínez, 1998), nonetheless all appear to correlate with a well-defined normal polarity
1990 interval (Beamud et al., 2003, Fig. 3 therein).

1991 The Nogueres conglomerates episode raises several questions in terms of orogen dynamics
1992 during the Paleogene. Firstly, the unconformable Nogueres clastic sequence has drowned a
1993 mountainous palaeolandscape in which continental erosion had produced a diverse gallery
1994 of high-amplitude structural landforms such as hogbacks, razorbacks and anticlinal or
1995 monoclinal valleys out of the folded Mesozoic cover sequence (Biro, 1937; Reille, 1971).
1996 Crustal deformation and differential erosion thus occurred simultaneously, but this first
1997 episode was followed, during and after Bartonian time (~37 Ma), by subsidence and burial.
1998 The subsidence migrated northward towards the orogen's axis, which is the reverse of what
1999 was happening at the same time in the Jaca–Tresp furrow (southward rollover of the
2000 depocentre). Clast provenance analysis of the Nogueres sequence indicates exclusive input
2001 from the local Mesozoic limestone outcrops near the base of the sequence, but with an
2002 increasingly high proportion of Hercynian basement lithologies towards the top. The source
2003 rocks, however, are fairly near-field outcrops belonging to the leading edge of the Nogueres
2004 basement nappe, and involve abundant Devonian limestone, Carboniferous sandstone,
2005 Silurian rocks, ophiolites, and Permo-Triassic sandstone and conglomerate. These features are
2006 equally true for the Pobla de Segur and Senterada outcrops. In the latter case, an increase in
2007 granite cobble frequency is only substantial in the uppermost beds, where metre-sized
2008 granite boulders associated with Devonian and Permo-Triassic boulders several metres in
2009 diameter suggest a proximal facies supplied by steep catchments on a steep mountain front
2010 (see Section 4.1.3.3 for links with the geomorphological evolution of this area). The granite
2011 outcrops geographically nearest to the Senterada sequence lie 12 to 15 km to the north of
2012 the current edge of the Axial Zone, where the highest summits today are made up of
2013 Paleozoic sedimentary rocks. It can be inferred from this evidence that the proximal facies of
2014 the upper Senterada sequence testifies to a topographic configuration of the Pyrenees in the
2015 late Paleogene very different from the Pyrenean mountain landscape of today — evidence
2016 already emphasized farther east in the Pedraforca–Ripoll area (late Priabonian beds of
2017 Catllaras–Serrat Negre). Vincent (2001) had reached a similar conclusion in the context of
2018 the Sierra de Sis. He noted, after Reille (1971), that the tourmaline-bearing petrographic
2019 fingerprint of certain granite clasts indicated a far-field provenance, potentially from
2020 outcrops in the massifs of Tramesaygues and Aiguestortes, which are situated in the upper
2021 valley of the Neste de Louron — i.e., 40 km to the NNW and 5 km to the north of the
2022 modern-day boundary between France and Spain (Reille, 1971; Michael et al., 2014). From

2023 this we can infer that, during the late Paleogene, the Ancestral Pyrenean mountain range
2024 was even more asymmetrical than its modern successor, with a continental drainage divide
2025 situated just 20 km to the south of the North Pyrenean Fault, and perhaps even (based on
2026 clast provenance studies) within the North-Pyrenean Zone at locations farther west (Roigé et
2027 al., 2017).

2028

2029 **3.2.5. Early to middle Miocene sedimentation**

2030

2031 *3.2.5.1. General chronostratigraphy of the Miocene clastic deposits*

2032

2033 Like their Oligocene predecessors (Campodarbe Fm., etc.), the Neogene sediments of the
2034 Ebro Basin (Figs. 1, 5) were initially entirely contained within an enclosed, internally drained
2035 basin, and as a result are much thicker than in the Aquitaine Basin, which remained
2036 connected to the Atlantic Ocean. The five tectono-sedimentary units (TSU 4 to TSU 8)
2037 reported in Iberian literature reach a total thickness of ~1000 m, and TSU 4 straddles the
2038 Oligocene and the Miocene. Between the Alcanadre River and the summit of the Sierra
2039 d'Alcubierre, the series spans an age band from 23 to 13.5 Ma and is 636 m thick.

2040 Magnetostratigraphy and mammalian fossil sites have provided constraints on the fill-
2041 sequence chronology, with TSU 5 falling between 21.5 and ~16 Ma (MN 2, MN 3, MN 4), TSU
2042 6 between ~16 and 14.4 Ma (MN 5), and TSU 7 between 14 and 12 Ma (top of MN 5, MN 6,
2043 MN 7–MN 8). The age of TSU 8, which is preserved only on the southern edge of the Ebro
2044 Basin, is uncertain (Pérez-Rivarés et al., 2002, 2004, 2018; Larrasoña et al., 2006; Agustí et
2045 al., 2011; Vázquez-Urbez et al., 2016). The Neogene outcrops of the Iberian foreland are
2046 organised in concentric belts with, starting from the centre and moving north towards the
2047 mountains, gypsum-rich evaporites (Zaragoza Fm.), then lacustrine carbonates (Alcubierre
2048 Fm.), followed by distal fluvial systems (ochre mudstone with shoestring sandstone channel
2049 fills), and lastly a discontinuous belt of proximal syntectonic conglomerates. The latter two
2050 sequences have been named Uncastillo Formation in the NW, and Sariñena Formation in the
2051 NE (Quirantes and Riba, 1973; Arenas, 1993; Arenas and Pardo, 1999; Arenas et al., 2001;
2052 Luzón, 2005) (Fig. 5, E- and W-Aragón transects).

2053 Clastic output from the Pyrenees during the Neogene was conveyed by two major river
2054 systems which were now perpendicular to the earlier Paleogene sediment routing systems

2055 of the Campodarbe Formation: one with its mountain hinterland in the central Pyrenees
2056 (which produced the Huesca megafan/Sariñena Formation) and coaxial with the Cinca
2057 palaeostream; the other with its hinterland in the western Pyrenees (Luna
2058 megafan/Uncastillo Formation) and coaxial with the Gállego catchment (Hirst and Nichols,
2059 1986; Jones, 2004; Nichols, 2005, 2018). These Ebro Basin megafans, with their apices
2060 situated along the front of the Sierras Exteriores, are associations of channel and overbank
2061 deposits tens of kilometres in radius. The Miocene outcrops do not extend eastward beyond
2062 the Cinca–Segre drainage divide. This interruption is most likely an erosional boundary, but
2063 whether a megafan the size of the Huesca fan ever existed to the east of the Segre River
2064 remains a matter of speculation. It is intriguing to note that the eastern limit of Neogene
2065 outcrops in the Ebro Basin occurs almost exactly at the same distance from the
2066 Mediterranean coastline (~100–120 km) as its counterpart in the Aquitaine Basin (Fig. 1) —
2067 thus reflecting perhaps a response to Mediterranean rifting farther east and to the ensuing
2068 regional uplift, which most likely resulted in displacing both the foreland and retro-foreland
2069 depocentres towards the west (Gaspar-Escribano et al., 2001).

2070 Denudation of the Ebro Basin during the late Neogene, after its connection with the
2071 Mediterranean base level, has resulted in a preservation of the harder lithologies such as the
2072 central carbonate and peripheral conglomerate masses, but has stripped a large proportion
2073 of the softer marl outcrops that formed the distal alluvial facies of the depositional fan
2074 systems. Added to the relative scarcity of continental fossil remains among the Cenozoic
2075 rocks along the southern fringe of the pro-wedge, stratigraphic correlations between (i)
2076 distal and proximal alluvial deposits as well as between (ii) proximal deposits along the strike
2077 of the orogen have been difficult to establish and thus require caution. As a result, variations
2078 through time in the intensity of sediment delivery by the Ancestral Pyrenees remain difficult
2079 to reconstruct regionally, but an attempt is made below to unravel these issues based on a
2080 critical review of the literature.

2081

2082 *3.2.5.2. Range-front conglomerate sequences south of the Sierras Exteriores*

2083

2084 The thickness of Neogene mountain-front conglomerate sequences in the Ebro Basin is
2085 usually several hundreds of metres, but along the base of the western Sierras Exteriores,
2086 e.g., near Luesia, the Miocene accumulation is reported to attain a thickness of 1600 m

2087 (Arenas et al., 2001). Its age has been difficult to establish directly, and mostly relies on far-
2088 field correlations with dated deposits lying at the centre of the Ebro Basin. The most
2089 significant fossil assemblage is from within the Sariñena Formation at Santa Cilia, and was
2090 obtained from a stratified fluvial sequence within the conglomerate beds situated at foot of
2091 the Sierra de Guara. The sequence has been tectonically deformed and rests unconformably
2092 on the Oligocene Peraltilla Formation. Taking account of dip angles, the fossil site seems to
2093 occur ca. 500 m above the unconformity, with an additional ~400 m thickness of the
2094 conglomerate sequence is stacked above it. The Santa Cilia age is earliest Aquitanian,
2095 biozone MN 1 (local zone X; Crusafont et al., 1966; Alvarez-Sierra et al., 1990; Cuenca et al.,
2096 1992). A second mammalian fossil site at Ayerbe has been deemed coeval with Santa Cilia
2097 because of its fossil mammalian contents, which are indicative of Aquitanian taxa at two
2098 separate locations (Crusafont and Pons, 1969). In a more distal position, the sites of San Juan
2099 and La Galocha were sampled over a vertical stratigraphic thickness of ~80 m. The base of
2100 San Juan is ascribed to biozone MN 2b, i.e., late Aquitanian or early Burdigalian (local zone
2101 Y2), whereas La Galocha 5, at the top of the section, corresponds to the base of MN 3, i.e.,
2102 early to middle Burdigalian (zone Z; Alvarez-Sierra et al., 1990). The magnetostratigraphic
2103 research has produced results of increasing quality and accuracy through time. The earlier
2104 work (Hogan and Burbank, 1996), which focused on the Priabonian marine beds and on the
2105 Ayerbe fossil site, reports from Campodarbe four pulses of syntectonic conglomerates
2106 separated by syndimentary unconformities. The first three pulses occurred between 29.5
2107 and 24 Ma (i.e., Oligocene), with only the fourth established as Aquitanian. Focusing on
2108 existing sequences around Huesca, other workers (Arenas, 1993; Arenas et al., 2001; Oliva-
2109 Urcia et al., 2016) identified three stratigraphic units (named U1 to U3), in which U3
2110 correlates with TSU 5 in the central part of the Ebro basin (21.5–16 Ma). These same authors
2111 have cast doubt on the significance of the Ayerbe assemblages, emphasizing instead the
2112 importance of erosion-related intraformational lacunae in the section studied by Hogan and
2113 Burbank (1996). The new magnetostratigraphic record at Luesia, which is reportedly more
2114 continuous, places the top of the Campodarbe Formation at 24.5 Ma. The age of the three
2115 youngest conglomerate sequences overlying the Campodarbe Fm. ranges between 24.5 and
2116 22.5 Ma (equivalent to units U1 and U2), and the fourth conglomerate sequence belongs to
2117 U3. Oliva-Urcia et al. (2019) have since proposed alternative magnetostratigraphic
2118 correlations for U3, which seems only the equivalent of the base of TSU 5. These authors now

2119 place the top of U3-2, which contains the entire Riglos conglomerate sequence (i.e., the
2120 fourth sequence) in the Aquitanian, ca. 21 Ma. No age is currently provided for U3-3. A fifth,
2121 quite thick and isolated conglomerate sequence known as Peña del Sol also occurs near
2122 Ayerbe (NW of Huesca). Its outcrop rises to ~1300 m and rests unconformably on the Sierras
2123 Exteriores. Although reported in the literature (Alastrué et al., 1957), its age is currently
2124 unknown but possibly Burdigalian.

2125 The Neogene chronostratigraphy is difficult to untwine because different authors have
2126 crafted different nomenclatures: Pérez-Rivarés et al. (2018), working on the Paleogene as
2127 well as the Neogene, have favoured the TSU idiom (which is calibrated on mammalian
2128 biozones and magnetostratigraphic criteria); but others (e.g., Arenas, 1993 and later), who
2129 focus chiefly on the Neogene and rely on the methods of sequence stratigraphy
2130 underpinned by magnetostratigraphy, have opted for the U (but also sometimes N) notation.
2131 It consists in subdividing the TSU units.

2132 In summary, based on the best quality fossil-bearing sites (chiefly Santa Cilia and La Galocha
2133 5), the Neogene conglomerate belt along the northern edge of the Ebro Basin south of the
2134 Sierras Exteriores contains debris supplied to it from the late Chattian to possibly the earliest
2135 Burdigalian. It cannot be ruled out that delivery by Pyrenean rivers of coarse gravel deposits
2136 continued into the middle Miocene given the occurrence, for example, of sandstone beds in
2137 TSU 7 at the centre of the Ebro Basin (i.e., in distal positions: San Caprasio, Sierra de
2138 Alcubierre). However, the great thickness (~500 m) of lacustrine limestone and evaporites in
2139 TSU 5 and TSU 6, which both appear to lap northward over the sandstone deposits of the
2140 Sariñena Formation (Pérez-Rivarés et al., 2002, 2018, see cross-sections therein), remains a
2141 robust indication that clastic output from the Pyrenean range had declined substantially
2142 after ~20 Ma. Further to the NW, the Bardenas Reales recorded a similar evolution, with a
2143 decline in clastic input from the Pyrenees (red sandstone and siltstone) giving way to
2144 lacustrine limestones near the boundary between TSU 5 and TSU 6, i.e., 16.1–16.05 Ma
2145 (Larena et al., 2020). A decline in tectonic activity is thus documented by the sedimentary
2146 petrology of the stratigraphic sequence from at least TSU 6 onwards, thereafter allowing a
2147 stronger expression of climatic signals in the region as recorded by fluctuations in palaeolake
2148 shoreline boundaries (Arenas, 1993; Larena et al., 2020). From this it can be inferred that
2149 topographic relief in the orogenic belt was becoming progressively more subdued during and
2150 after Burdigalian time.

2151 The Neogene conglomerate belt along the northern border of the Ebro Basin is clearly of
2152 syntectonic origin. This interpretation is supported by the thickness of the sequences, their
2153 synsedimentary intraformational unconformities, and their geographical and structural links
2154 with the outer Pyrenean frontal thrusts (Puigdefábregas and Soler, 1973; Puigdefábregas,
2155 1975; Hogan and Burbank, 1996; Arenas et al., 2001). The two earlier conglomerate pulses
2156 buried the Sierras Exteriores thrust front (e.g., west of the Gállego River: Ayerbe, Aguëro,
2157 San Felices areas). The Guarga thrust sheet was itself folded and sheared internally into finer
2158 thrust units, thereby giving rise, among the various structures, to the Santo Domingo
2159 anticline. This large, plunging anticline propagated westward at the time when the Uncastillo
2160 Formation was being deposited. In its eastern part, clastic pulses 4 and 5 (generating the
2161 conglomerate sequences observed at Riglos, and in the Linás palaeofan and the Peña del Sol)
2162 are only slightly folded in the vicinity of the thrust front (Nichols, 2018). As such, they record
2163 the last moments of tectonic deformation in the Sierras Exteriores (i.e., Aquitanian to early
2164 Burdigalian; Oliva-Urcia et al., 2019).

2165 In terms of size and clast provenance, two classes of early Neogene alluvial fan coexisted in
2166 the Ebro foreland. Numerous small alluvial fans form aprons along the fronts of the Sierras
2167 Exteriores. They contain boulders up to 3 m in diameter and consist of weakly rounded
2168 limestone pebbles. These sequences typically bury steep structural scarps and landforms
2169 (Reille, 1971). Much larger fans, chiefly the Huesca and Luna megafans but also the Peña del
2170 Sol, contain debris from much more distant sources. Palaeochannel fills in the Luna megafan
2171 display an abundance of pebbles of Eocene brown sandstone (70–95%) alongside greyish-
2172 blue limestone (5–30%) and very rarely quartz, quartzite and chert (Arenas, 1993). These
2173 debris assemblages may in some cases originate directly from the Eocene flysch outcrops of
2174 the west-central Pyrenees, but most of the time they are reworked debris from the Jaca
2175 syncline and its Campodarbe Formation (see Section 3.2.2), which at the time was
2176 undergoing intense folding and incorporation into the outward-growing pro-wedge (Hirst
2177 and Nichols, 1986; Arenas et al., 2001).

2178 The Huesca megafan contains biotite-rich arkose and sandstone suggestive of inputs from
2179 the Axial Zone (Hirst and Nichols, 1986), although proportions of these constituent
2180 lithologies are less than in the older Peraltilla Formation (Yuste et al., 2004). Provenance
2181 from the basement outcrops at places such as Alquezar and Bierge-Rodellar is nonetheless
2182 conspicuous, with an abundance of dark quartzite, quartz, Permo-Triassic conglomerate,

2183 some schist and granitoid pebbles. In the Cinca River saddle, between the Sierra de Guara
2184 and Sierra de Montsec, the Miocene Graus Formation (sandstone and conglomerate) laps
2185 extensively onto the Sierras Exteriores and fills up the Peralta de la Sal and Benabarre sub-
2186 basins. The Graus Formation also laps northward unconformably onto the Eocene Escanilla
2187 and Capella sequences. Its conglomeratic proximal and molassic distal facies are identical to
2188 those of the palaeontologically-dated Miocene deposits west of the Cinca valley.

2189 For the benefit of future investigations, it must be emphasized overall that geologists are
2190 undecided about where to locate the stratigraphic boundary between the Oligocene and
2191 Miocene conglomerate units east of the Cinca valley, i.e., along half the length of the
2192 mountain range. This is mostly ascribable to the scarcity of fossil-bearing sites. Depending on
2193 the publication date of the geological sheets, the gravel sequences covering the Paleogene
2194 fold structures (particularly the Graus Formation) are thus either labelled as Paleogene or
2195 Neogene. This also varies depending on whether focus is on Catalonia, where Paleogene
2196 conglomerate sequences are omnipresent, or on the west-central foreland zone around
2197 Huesca, where then Neogene age of the gravel beds is well constrained by their fossil
2198 content. For example in the Peralta Basin, a magnetostratigraphic sequence (Meigs, 1997)
2199 has revealed the existence of three syntectonic units, namely Priabonian–Rupelian, basal
2200 Chattian (Peraltilla Formation), and Upper Chattian. The latter unit appears to be an
2201 equivalent of the Sariñena–Graus units, which seal the youngest crustal-shortening-related
2202 fold structures and consist of clasts supplied by outcrops in the Axial Zone. It is likely that
2203 these unconformable conglomerate sequences have at times been bundled (or confused)
2204 with the unconformable Nogueres conglomerate units (described in Section 3.2.4.2), which,
2205 however, are of Paleogene age. Some authors have indeed suggested that the aggradation
2206 of the Nogueres sequence continued into the Miocene or at least the late Oligocene (Vincent
2207 and Elliott, 1996; Vincent, 2001; Jones, 2004), evidence for which is nonetheless debatable
2208 given the absence of direct, in situ biostratigraphic clues.

2209 In conclusion, establishing the age of conglomerate sequences is essential to the
2210 interpretation of mountain ranges, but dating conglomerate beds remains difficult. The
2211 interpretation advocated by Oliva-Urcia et al. (2019) for the Jaca Basin and the Luna Fan is
2212 currently the most coherent at the scale of the western Pyrenees, and more consistent with
2213 the Ayerbe and Santa Cilia ELMA ages than some previous palaeomagnetic studies. The
2214 endemic tectonic deformation recorded in the Jaca Basin also explains the absence of coeval

2215 conglomerate sequences of a similar nature to the Luna and Huesca fans in the Aquitaine
2216 Basin at those longitudes. On a more restricted scale, discrepancies between ages obtained
2217 for the fans of the Jaca Basin (San Juan de la Peña, and Oroel), which are early Neogene
2218 according to Roigé et al. (2019) on the basis of U–Pb and (U–Th)/He double dating, but 10 to
2219 12 m.y. older than that according to magnetostratigraphic reconstructions (Garcés et al.,
2220 2020), will require further clarification.

2221

2222 **3.2.6. Sharp regime change during the late Miocene**

2223

2224 The youngest generations of Cenozoic sedimentary deposits in the Ebro Basin are
2225 tectonically disturbed (gentle undulations illustrated by Pérez-Rivarés et al., 2018, Fig. 4
2226 therein) and imprecisely dated by palaeontological evidence. The most elevated
2227 palaeontological site of San Caprasio (812 m; Fig. 5, E-Aragón transect), which lies at the
2228 heart of the basin in the Sierra d’Alcubierre, had initially been dated to the Astaracian (i.e.,
2229 Aragonian–Vallesian boundary, biozones MN 7–MN 8; Agustí et al., 1994). However, this
2230 biochronological age was established from just three micromammalian taxa, and later
2231 magnetostratigraphic investigations within the carbonate rocks of TSU 7 reassigned the site
2232 to chron C5AC; this corresponds to the base of MN 6, i.e., 13.8 Ma (Pérez-Rivarés et al.,
2233 2002). This revised age has been validated by palaeontologists (Agustí et al., 2011). The most
2234 recent fossil-bearing sites are located in the SW part of the Ebro Basin near Tarrazona, but
2235 they occur in the topmost sections of TSU 7 (Villena et al., 1992; Cuenca et al., 1992;
2236 Murelaga et al., 2008) such as at El Buste (MN 7–MN 8, ~12.6 Ma) and La Ciesma (MN 7–MN
2237 8, ~12.1 Ma); the top of TSU 7 has not provided robust magnetostratigraphic constraints
2238 (Pérez-Rivarés et al., 2018; Fig. 7 therein). No fossil assemblages have been detected in TSU
2239 8, which corresponds to the tilted lacustrine limestone plateau of Muela de Borja (804–724
2240 m). In this area, the top of TSU 7 has been estimated as slightly younger than 12 Ma;
2241 accordingly, TSU 8, which is at most 60 m thick, should be younger still (Vasquez-Urbez et al.,
2242 2013). Early field geologists reported a site in that area known as Monteagudo ‘vallesiense’,
2243 which contained large mammalian fossils such as *Hipparion*, but it seems no archive has
2244 been kept of its precise location (mentioned in Cuenca et al., 1992).
2245 Despite these lacunae in the Miocene chronostratigraphy (i.e., TSU 8), it can be inferred that
2246 the termination of internal drainage in the Ebro Basin occurred at some time after 12–11

2247 Ma. Speculation over the exact timing of this major geodynamic change has nonetheless
2248 been intense, particularly in relation to the possible impact of the Messinian salinity crisis in
2249 reconnecting the Ebro Basin with the Mediterranean Sea (Coney et al., 1996). A late
2250 Cenozoic transition from internal to external drainage was actually a general feature across
2251 the Iberian Meseta, whether or not the rivers join up with the Mediterranean. Given that
2252 such was the case for the Tagus and the Duero, which connect to the Atlantic, there should
2253 thus be no reason for the short-lived Messinian base-level fall to have driven the process.
2254 Accordingly, some authors have ruled out the role of the Messinian sea-level fall and
2255 advocated instead a progressive rather than abrupt reconnection of the Ebro Basin,
2256 beginning only in the Pliocene. Babault et al. (2006) persuasively ruled out any major impact
2257 from the Messinian Salinity Crisis by showing that the Ebro Basin should in that case display
2258 a 300-km-long pre-Pliocene canyon, cut during the Messinian lowstand and similar to that of
2259 the Rhône River in France. This is clearly not the case.

2260 A consensus has progressively emerged in favour of a much earlier reconnection of the Ebro
2261 to the Mediterranean rather than an abrupt, short-lived event triggered by the Messinian
2262 salinity crisis (review in Garcés et al., 2020). Inferences in favour of this scenario are
2263 provided by numerical models rather than by field constraints, but consistently generate a
2264 best estimate falling between 13 and 8.5 Ma (García-Castellanos et al., 2003) or between 12
2265 and 7.5 Ma (García-Castellanos and Larrasoaña, 2015). This time window (late Serravalian–
2266 Tortonian) coincides with a strong influx of sediment into the Valencia Basin (Castellón
2267 Group) (Urgeles et al., 2011; Cameselle et al., 2014), and seems compatible with
2268 thermochronological data that have been produced for the Nogueres conglomerate beds,
2269 into which fluvial incision began ca. 9.5 Ma (Fillon and van der Beek, 2012; Fillon et al.,
2270 2013). Note that these studies postulate palaeoelevations of either ~1000 m (García-
2271 Castellanos et al., 2003; Babault et al., 2006) or 530–750 m (García-Castellanos and
2272 Larrasoaña, 2015) for the top of the Ebro Basin fill prior to marine base-level reconnection.
2273 In both cases these are substantial elevations above sea level, but they do not allow for the
2274 (highly likely) possibility that the Ebro Basin has itself undergone regional dynamic uplift in
2275 the last 12 m.y., with widespread evidence of elevation change and rock deformation (e.g.,
2276 Soto et al., 2016; Pérez-Rivarés et al., 2018; Conway-Jones et al., 2019).

2277 The onset of fluvial incision in the Ebro Basin coincided with (i) the major episode of incision
2278 also recorded in the Aquitaine Basin, i.e., the ravinement surface beneath the Vallesian (i.e.,

2279 middle Tortonian) ‘Clay-with-pebbles’ formation previously presented (Fig. 5, Ariège and
2280 Béarn transects); and with (ii) the growth of the Lannemezan megafan. Such symmetry and
2281 synchronicity in the response of the two foreland basins to fluvial incision strongly suggests a
2282 regional episode of crustal uplift occurring not just in the Pyrenees but also more widely in
2283 Iberia and the Massif Central (Boschi et al., 2010) — much rather than a contingent event
2284 such as drainage piracy restricted to the Ebro River. A regional, sub-crustal driving process
2285 among those examined in Section 2.4 would be a good candidate for explaining this
2286 situation. The hypothesis of mantle-supported dynamic topography (Casas-Sainz and de
2287 Vicente, 2009; Gunnell et al., 2008, 2009; Boschi et al., 2010; Calvet et al., 2015a)
2288 contributing to re-energise not just the Pyrenean mountain belt during the Neogene and
2289 Quaternary period, but also the pro- and retro-foreland basins themselves, substantially
2290 alters the conventional view that the Pyrenees arose purely out of crustal thickening at the
2291 plate margins during the late Cretaceous and Paleogene, and that its topographic mass has
2292 stood in dynamic steady state for 25 million years (Curry et al., 2019). Instead, the Pyrenees
2293 is a transient orogen which has undergone a complex history of topographic uplift, decay,
2294 and resurgence. This alternative scenario for the modern Pyrenees as a youthful Neogene
2295 mountain range successor to an older Paleogene ancestor is also better suited to explaining
2296 the 25 million years of internal drainage of the Ebro Basin. The Catalan Ranges that close the
2297 Ebro Basin to the east are merely a few tens of kilometres wide, and they have additionally
2298 been extensively fragmented since the early Miocene by coast-oblique extensional grabens
2299 through which streams would have easily made inroads to keep the Ebro Basin connected to
2300 sea-level.

2301 Contrary to the Aquitaine Basin, fluvial incision of the Ebro Basin after ~10 Ma was
2302 interrupted by only very few quiescent moments of alluvial aggradation and terrace
2303 formation, which explains why the Ebro Basin displays few late Neogene and Quaternary
2304 aggradational terraces compared to the Aquitaine Basin. The Ebro Basin likewise displays no
2305 analogues of the Lannemezan Formation and its multiple late Neogene megafans, which at
2306 one time buried considerable portions of the retro-wedge (see Section 3.1.5). This contrast is
2307 likely explained by regional dynamic (Conway-Jones et al., 2019), but also partly isostatic,
2308 uplift in excess of 800 m a.s.l. of the Ebro Basin itself during the last 10–12 m.y., following a
2309 different style and greater magnitude than the simple basinward tilt motion recorded in
2310 Aquitaine, where the piedmont grades much more progressively to its marine base level.

2311
2312
2313
2314
2315
2316
2317
2318
2319
2320
2321
2322
2323
2324
2325
2326
2327
2328
2329
2330
2331
2332
2333
2334
2335
2336
2337
2338
2339
2340
2341
2342

3.3. The sedimentary record of extensional basins in the eastern Pyrenees

The Gulf of Lion became established as a new marine base level for the Pyrenees towards the end of the Oligocene (Bache et al., 2010), i.e., at a time when the Ebro Basin was internally drained and the shores of the Aquitaine Basin lay far to the west. The first stages of crustal thinning occurred above sea level or in a very shallow sea. After ~23 Ma the entire system became rapidly submerged as a result of accelerated subsidence, resulting in today's hyperextended Gulf of Lion (Jolivet et al., 2020). The Mediterranean has controlled the geomorphological evolution of the eastern Pyrenees from Aquitanian time to the present in a context of increasing tectonic fragmentation of the Paleogene mountain range by Neogene extensional faulting.

3.3.1. Oligocene to Miocene basin fills: proxies of surface dynamics in the Ancestral Pyrenees

The extensional faulting has produced a population of half-grabens that strike NE–SW and NNE–SSW. The Oligocene basins onshore are relatively small, and their fill sequences were supplied by their eroding footwalls rather than by denudation occurring further afield in the Pyrenean hinterland. More information would be provided by the graben systems buried beneath the continental-shelf sediments, e.g., the Catalan, Cathare and Central grabens (the latter an extension of the onshore Roussillon Basin), but boreholes have until now barely reached those depths (Cravatte et al., 1974; Arthaud et al., 1981; Guennoc et al., 2000; Mauffret et al., 2001; Bache et al., 2010). The syn-rift sequence of these offshore basins contains conglomerate deposits made up of limestone and other Paleozoic clasts, anhydrite-rich red clay, and a cap of early Aquitanian marine limestone. The late Chattian marine beds have also been detected off- as well as onshore in western Provence, beneath the Aquitanian coastal parastratotype at Carry-le-Rouet (Oudet et al., 2010; Demory et al., 2011). The Catalan divergent margin and the Valencia Trough share a tectonic and sedimentary history similar to that of the Gulf of Lion. Extension in the south has even inverted some Oligocene piggyback basins that were previously linked to convergent tectonics in the Catalan Ranges (Roca, 1996; Roca et al., 1999).

2343 The Aquitanian sea-level rise approaching from the east did not initially reach past the
2344 longitude of Montpellier. The Narbonne–Sigean Basin at that time was receiving slope
2345 breccia, small matrix-supported (red clay) debris fans, well-rounded alluvial gravels
2346 comprising quartzite from as far away as the Mouthoumet Massif, but mostly shale and
2347 quite thick, white lacustrine limestone deposits — all suggesting low-energy topography in
2348 the Corbières hinterland (Calvet, 1996). The total thickness of the Narbonne fill sequence is
2349 ~1 km, and consists of two units (Aguilar, 1977; Aguilar and Michaux, 1977): the first is
2350 Oligocene (MP 28, ~26 Ma), and the other starts during the late Oligocene (MP 30, ~24 Ma)
2351 but consists mostly of an Aquitanian biozone (two MN 1 micromammalian assemblages
2352 among the lower beds). Aquitanian gypsum deposits are indicative of a paralic environment
2353 (Rosset, 1964), and thus of proximity to a coastline. Farther west on the mainland, the
2354 Tuchan–Paziols Basin only contains fluvial sequences (thickness: ~500 m) comprising
2355 quartzite-bearing basal conglomerate (Mouthoumet provenance), followed by a thick
2356 sequence of marl and pebbles of local limestone containing in its uppermost levels a late
2357 Oligocene faunal assemblage (perhaps MP 28; Calvet et al., 1991). To the south of the
2358 Ancestral Pyrenees, the small Campins Basin, in the Vallès, contains 700 m of clay, lignite,
2359 lacustrine limestone, arkose, and locally-sourced conglomerate containing basement clasts.
2360 The fossil faunal assemblages of Campins and Can Quarante both belong to biozone MP 25
2361 (~29 Ma) (Anadon and Villalta, 1975; Anadón, 1986; Aguilar et al., 1997).

2362 As most classic ‘steer’s head’ rift basins, these Oligocene to Aquitanian basins were
2363 eventually flooded and overtopped by a more widespread marine transgression. This
2364 occurred during the Miocene, promoting the deposition of a relatively thin mudstone and
2365 sandstone sequence (i.e., molasse) which rests unconformably over the tectonically
2366 deformed earlier sequences of, for example, the Narbonne–Sigean Basin. This Miocene
2367 sequence progressed landward onto the folded Mesozoic cover rocks of the Corbières and
2368 La Clape, and likewise farther east in Languedoc. The facies are characteristically littoral, but
2369 ages are poorly constrained. Bivalve fossils suggest Burdigalian (*Pecten tournali*) and
2370 Langhian to Serravallian ages (*Ostrea crassissima*); foraminifera have suggested biozone N 8,
2371 i.e., Langhian (Magné, 1978). Fossil rodent assemblages in the coastal facies deposits have
2372 yielded the most precise age brackets so far (Aguilar, 1979, 1980, 1981, 1982; see also
2373 revised biozones and updated tables in Aguilar et al., 2010 and Gunnell et al., 2009). Among
2374 these, Port-la-Nouvelle is a littoral karstic cavity in the Cretaceous limestone, buried by the

2375 molasse and also containing foraminifera and shark-like teeth. The corresponding biozone
2376 age (MN 4) captures the late Burdigalian sea-level rise (~16.4–17.2 Ma). Within the molasse,
2377 the assemblages of Luc-sur-Orbieu and ‘Leucate butte 1’ have yielded ages of ~13.4–14.2 Ma
2378 (MN 6), i.e., Langhian. Puisserguier (lower portion of biozones MN 7–MN 8), and La
2379 Grenatière (upper portion of biozones MN 7–MN 8) denote a Serravallian age (~11.2–13.4
2380 Ma). La Grenatière is situated in the uppermost levels of the marine component of the
2381 sequence, but aggradation continued uninterrupted in the form of some additional 100 m of
2382 shale and lacustrine limestone, which contain near the top the flagship biostratigraphic site
2383 of Montredon. This Vallesian site contains an extremely rich assortment of smaller and
2384 larger mammalian remains — including *Hipparion* — and has been placed within MN 10 (i.e.,
2385 8.9–9.9 Ma) (Aguilar et al., 1982; Michaux et al., 1988). These fine-textured lacustrine and
2386 palustrine deposits, totally devoid of coarser gravel clasts and situated at the landward tip of
2387 the Miocene gulf of Narbonne (today quite close to the mouth of the Aude River), again
2388 document a low-energy Pyrenean hinterland at this longitude.

2389 During the middle Miocene transgression, extensional fault activity slackened but did not
2390 cease. In the Lapalme Basin, for example, Miocene coastal beds containing mollusc-bored
2391 pebbles clearly show evidence of synsedimentary deformation in the immediate vicinity of
2392 the boundary fault planes (Calvet, 1996). The twin Thézan and Fabrezan basins record the
2393 most westerly ingress of the sea during the middle Miocene, but they also contain
2394 nonmarine marl interspersed with gravel-filled palaeochannels of uncertain stratigraphic
2395 age —probably early Miocene, and perhaps coeval with their laterally continuous marine
2396 beds (Ellenberger et al., 1987).

2397 At the more southerly latitude of the Axial Zone, but also further south in the Catalan
2398 Ranges, the extensional faults were active until the middle Miocene. The Roussillon Basin,
2399 and its westerly extension the Conflent Basin (for a synthesis: Calvet, 1996; Calvet and
2400 Gunnell, 2008), show this very clearly. The floor of the Roussillon Basin is plausibly floored by
2401 Oligocene deposits, but no outcrops exist. The only indirect indication of this possibility is
2402 provided by apatite fission-track cooling ages of 25–27 Ma (and zircon ages of 30 Ma)
2403 obtained from potential source rocks in the adjacent Canigou massif (Maurel et al., 2008).
2404 The Roussillon fill sequence is 2 km thick. Its lowest documented stratigraphic units are early
2405 Burdigalian (base of MN 3, ~19–19.5 Ma obtained in the Conflent Basin at the
2406 biostratigraphic site of Espira: Baudelot and Crouzel, 1974; Aguilar et al., 2003, Fig. 11

2407 therein). Its marine uppermost unit is Langhian (N 8–N 9, i.e., ~15 Ma, obtained from the
2408 Elne and Canet boreholes; Gottis, 1958; Clauzon and Cravatte, 1985; Berger et al., 1989). The
2409 marine molasse deposits are relatively thin (~200 m at Canet); they overlie some much
2410 thicker, variegated grey and reddish fluvial sand and clay deposits with lacustrine limestone
2411 at the base. This entire sequence becomes substantially coarser-textured along the SW
2412 border of the Roussillon and in the Conflent Basin, which in this proximal setting displays
2413 rounded boulders up to several metres in diameter.

2414 Such sedimentological features in the Roussillon–Conflent area clearly testify to a high-
2415 energy mountain environment with steep slope systems, ascribable to a period of rifting-
2416 related crustal uplift in the Axial Zone. This has been confirmed by apatite (U–Th)/He and
2417 fission-track rock-cooling ages (17–22 Ma) in the Canigou massif (Maurel et al., 2008), which
2418 record a continuation of the denudation that had already begun during the Oligocene. Clast
2419 provenance analysis of the fill sequence also documents — in inverse order — the successive
2420 stages of denudation of the stratified Canigou–Roc de France–Albères metamorphic dome,
2421 which at this time began to shed debris from the Canigou–Roc de France augengneiss
2422 envelope and from the Albères migmatites. The very coarse-textured sequences disappear
2423 beneath the outcrops of Langhian molasse and are correlated offshore with the thick
2424 Aquitanian and Burdigalian sequences documented from borehole evidence (Cravatte et al.,
2425 1974). Onshore, incision and denudation in the eastern reaches of the Roussillon Basin have
2426 stripped the top of the Neogene sequence down to its Langhian levels in response to the
2427 abrupt Messinian sea-level fall. Offshore, however, boreholes and seismic profiles reveal
2428 that thick Tortonian beds have been preserved on the continental shelf (almost 700 m of
2429 paralic and coastal facies documented by the Tramontane borehole), inclusive of early
2430 Messinian deposits emplaced prior to the salinity crisis.

2431 In Catalonia, the inner graben of the Vallés-Penedés Basin contains a sequence almost
2432 identical to that of the Roussillon (Magné, 1978; Agustí et al., 1990; Cabrera and Calvet,
2433 1996), with the difference that the Tortonian marine transgression in this area has long been
2434 recognised onshore in the coastal zone, e.g., at Barcelona, where rocks from at least the
2435 bottom half of this Stage has been reported (Magné, 1978).

2436

2437 ***3.3.2. Miocene to Pliocene basin fills: proxies of surface dynamics in the Modern Pyrenees***

2438

2439 A second stage of active rifting began during the late Miocene, simultaneously reactivating
2440 the older grabens near the coast but also opening entirely new intermontane grabens far
2441 into the west of the Axial Zone. Another novelty was the onset of protracted episodes of
2442 intraplate volcanism. Although eruptions did not occur in the mountain range itself, a trail of
2443 volcanic outcrops occurs from the Massif Central to the Languedoc coastline (Gillot, 1974),
2444 with a possible continuation on the continental shelf. The youngest alignment of volcanoes,
2445 from the Escandorgue to the coastal town of Agde, ranges from 2 to 0.5 Ma (Dautria et al.,
2446 2010). It is inferred to have been generated by lithospheric sources. Traces of volcanic
2447 activity reappear in the Iberian part of the Pyrenean crustal wedge, in the Selva and
2448 Empordà basins. Age data reach back to at least ~10 Ma and extend to the late Pleistocene
2449 (Donville, 1973a, b, c, d; Araña et al., 1983; López Ruiz and Rodríguez Badiola, 1985; Martí et
2450 al., 1992; Martí, 2004). The origin of this volcanic activity has been debated: it could be
2451 ascribed to partial melting of mantle rocks sourced at 50–60 km depths beneath the
2452 Valencia Trough (Martí et al., 1992); to lithospheric thinning beneath the Mediterranean
2453 margin of Iberia (Vergés and Fernàndez, 2006); to heating of the base of the crust as a result
2454 of lithospheric mantle delamination beneath the Pyrenees (Vanderhaeghe and Grabkowiak,
2455 2014; Chevrot et al., 2018; Dufrechou et al., 2018); to a southward deflection of the Massif
2456 Central ‘finger’ of rising hot asthenosphere (Barruol and Granet, 2002; Barruol et al., 2004;
2457 Gunnell et al., 2008); or even to an endemic ‘hot finger’ of asthenospheric mantle similar to
2458 others detected beneath continental Europe and the Mediterranean (Lustrino and Wilson,
2459 2007; Jolivet et al., 2020).

2460 Whereas, in Languedoc, Pliocene marine and continental sedimentation occupies drowned
2461 valleys that were cut at the time of the Messinian salinity crisis (Ambert, 1994; Clauzon et al.,
2462 1990), in Roussillon the Pliocene depocentre overlies its Miocene predecessor and the
2463 ravinement surface between the two sequences is largely concealed. The Pliocene sequence
2464 attains a thickness of 800 m at Canet (Clauzon and Cravatte, 1985; Clauzon et al., 1987;
2465 Duvail et al., 2000). The proximal facies consist of thick debris cones containing metre-sized
2466 boulders at the mouths of the Têt and Tech rivers, and likewise at the base of the south-
2467 facing Albères mountain front (Calvet, 1986, 1996; Calvet et al., 2015b; Donzeau-Wiazemski
2468 et al., 2010–2015: map and handbook). On the continental shelf, the Pliocene sequence
2469 consists of a series of prograding units topped by a distinctly more aggradational Gelasian to
2470 Pleistocene depositional wedge. This change of regime indicates a resumption of active

2471 tectonic subsidence of the margin after 2.6 Ma, thus increasing the accommodation
2472 space and permitting the aggradation (Lofi et al., 2003, 2005; Duvail et al., 2005). Each
2473 depositional sequence is roughly 1 km thick, but it remains difficult to distinguish the
2474 Pyrenean inputs from those from the Cévennes and from the Alps via the Rhône.
2475 In the Vallés Basin (Agustí et al., 1990; Cabrera and Calvet, 1996), the marine Langhian beds
2476 transition laterally to, but are also apparently conformably overlain by, a 1500 m-thick
2477 continental series of clastic beds rich in micromammalian assemblages. This series is very
2478 coarse-textured along the NW faulted boundary, and it filled the graben continuously during
2479 the late Miocene. The stratigraphy contains the eponymous continental stratotype known as
2480 the Vallesian (27 localities yielding assemblages ascribable to biozones MN 9 and MN 10)
2481 and ascends into the Turolian (only one locality, Piera: MN 11) (Villalta and Crusafont, 1943;
2482 Agustí et al., 1997; Casanovas-Villar et al., 2014). However, the drowned Llobregat valley,
2483 which contains a marine and continental Pliocene fill sequence, strikes orthogonally across
2484 the graben in a configuration similar to the pattern observed along the Languedoc coastal
2485 belt and in the lower reaches of the Ebro River in the Tortosa Basin. The continental shelf
2486 hosts a vast clastic sedimentary body known as the Pliocene and Quaternary Ebro Group,
2487 which rests disconformably on the older Castellon Group as a result of Messinian incision
2488 (Martínez del Olmo, 1996; Cameselle et al., 2014).

2489 New grabens formed along the Mediterranean seaboard in the transitional area between
2490 the Pyrenees and the Catalan Ranges, and they occur precisely in the main area that was
2491 impacted by late Neogene volcanism. These basins are the Empordà and the Selva grabens.
2492 Their boundary faults strike NW–SE, which is identical to the strike of the North Balearic
2493 Transfer Zone that controlled the opening of the western Mediterranean back-arc basin and
2494 separated it from the Valencia Basin. The Empordà Basin contains a number of internal
2495 compartments and secondary depocentres. It has been a receptacle for a series of highly
2496 contrasting clastic sequences (synthesis in Calvet, 1996; Saula et al., 1994). At the centre of
2497 the basin, around Figueres, a deep borehole has struck a Tortonian sequence comprising
2498 marine strata at its base, followed by paralic and coastal facies rocks at depths of 1000 m
2499 below the surface. These contain interlayered lava flows (Fleta et al., 1994). In the southern
2500 part of the Empordà Basin, the Vallesian (MN 9 at La Bisbal) is exclusively of detrital origin
2501 and grades westward to coarse-textured Turolian fluvial units (MN 11 to MN 13, i.e., ~8.9–
2502 5.3 Ma, at Olivas, Camallera and Bascara; Crusafont, 1961; Gibert et al., 1979, 1980; Agustí

2503 et al., 1990). The Turolian sequence is at least 350 m thick, and its content of limestone and
2504 sandstone pebbles records the denudation of the outer Pyrenean folds of La Garrotxa and of
2505 footwall blocks of the extensional Transverse Ranges (Saula et al., 1994). The sequence also
2506 contains a siliciclastic contribution from the southern basement outcrops, likely conveyed by
2507 an ancestral Ter River. The Pliocene sequence of Empordà is thinner than in the Roussillon
2508 Basin and is exclusively of Zanclean age. The Pliocene marine wedge occupies the position of
2509 a drowned valley on the Fluvia River, but nothing similar has been observed in the case of
2510 the Ter. The Pliocene continental wedge is quite extensive in the northern part of the
2511 Empordà Basin, where it was supplied with debris from the Axial Zone as well as from the
2512 outer Pyrenean fold belt.

2513 The Selva Basin is vast but its fill rather shallow (maximum 300 m; Pous et al., 1990), and
2514 contains late Miocene and Pliocene continental deposits (arkose, palustrine shale, and gravel
2515 fans along the western border of the basin). The stratigraphic architecture of these two
2516 sequences is poorly known, but their entire depositional history was punctuated by volcanic
2517 eruptions, for example at 7.7 and 5.1 Ma (Donville, 1973d, 1976). Pliocene mollusc
2518 assemblages are reported (Marcet Riba and Solé Sabaris, 1949; Marcet Riba, 1956), as well
2519 as some Miocene mammalian remains (Villalta and Palli, 1973). The lacustrine sediments
2520 contained in a maar near Caldes de Malavella (SE edge of the basin) contain a diverse
2521 assemblage of late Pliocene vertebrate fauna (MN 16–MN 17; Gomez de Soler et al., 2012).
2522 Simultaneously to the formation of the Empordà and Selva basins, other basins resulting
2523 from wrench-fault tectonics were breaking up the Axial Zone and forming as far as 200 km to
2524 the west of the Mediterranean shores. Among these, the Cerdagne and Seu d'Urgell half-
2525 grabens are aligned along a NE–SW tectonic lineament known as the Têt Fault. They contain
2526 up to 1 km of clastic fill, partly as coarse-textured alluvial fans and partly as fluvial and
2527 lacustrine beds (Chevalier, 1909; Pous et al., 1986; Cabrera et al., 1988; Roca, 1996).

2528 Biochronological constraints on the stratigraphy have been obtained from a large number of
2529 Vallesian mammalian assemblages (MN 9–MN 10)(Golpe Posse, 1981; Agustí et al., 1981;
2530 Agustí and Roca, 1987), with a Turolian age (MN 13: ~6.7–6 Ma) for the uppermost levels
2531 (Agustí et al., 2006). No Pliocene sequence has been detected. The clastic facies indicate
2532 growing relief in the surrounding basement-cored uplands, particularly in Turolian time
2533 when thick alluvial-fan deposits containing huge boulders suggest tectonic activity along the
2534 southern master fault of the Cerdagne Basin (Calvet, 1996; Calvet and Gunnell, 2008). The

2535 presence of warmth-loving plant remains in the sediment record (Menendez-Amor, 1955;
2536 Suc and Fauquette, 2012) and $\delta^{18}\text{O}$ measurements on fossil mammalian teeth (Huyghe et al.,
2537 2020) document a regional uplift of not just the mountain footwalls but also of the basins
2538 themselves since Messinian time. Estimated uplift of the Cerdagne Basin over the last 10
2539 m.y. is ~900 m (other estimates suggest this may have even been achieved just in the last 6.5
2540 Ma: Suc and Fauquette, 2012, Fig. 8 therein), or ~500 m over the last 6.5 Ma according to
2541 the $\delta^{18}\text{O}$ constraints. Unlike the Cerdagne and Seu d’Urgell basins, the Capcir Basin strikes
2542 N–S and is unique in that respect. It could be even younger than the other two, perhaps
2543 having formed in response to a new regional stress regime (N–S compression and E–W
2544 extension), but unfortunately its clastic fill has until now never been dated.

2545 Still further to the west, in the Val d’Aran, the Pruëdo Basin was noted by de Sitter (1954)
2546 and interpreted as a valley fill sequence of late Miocene age based on its pollen content. It
2547 was later mistaken for a Quaternary ice-marginal or interglacial aggradational deposit, but
2548 has more recently been dated as Vallesian based on a revision of its botanical remains
2549 (Ortuño et al., 2013). Its bounding master fault is the E–W Maladeta Fault. The Pruëdo Basin
2550 has been substantially disfigured by denudation and by Pliocene to Quaternary valley
2551 incision so that only very small, dispersed vestiges remain to be pieced together. It cannot
2552 be ruled out that other hard-to-find, late Neogene tectonic basins may exist in the Pyrenees.
2553 Possible candidates could be the topographic basin of Ossès in the Basque Country, which is
2554 aligned on a SW–NE fault (Viers, 1960); and likewise some small grabens across the Arres
2555 d’Anie, reported as neotectonic by Viers (1960) and Hervouët (1997). Extending the effects
2556 of Mediterranean rift and wrench tectonics to such westerly locations clearly calls for
2557 extreme caution, as they could more likely result from endemic gravitational forces being
2558 exerted on the west-Pyrenean crust since the relaxation of the compressive regime that
2559 endured until at least the middle Miocene, or from outer-arch extension in the crest of the
2560 Axial Zone antiform in the Anie–Larra context (e.g., Arlas graben).

2561

2562 **4. A view from the mountains: tracking relief evolution from landform** 2563 **assemblages and the rock cooling record**

2564

2565 The broad sketch of Pyrenean palaeogeography viewed from the basins gains further detail
2566 and finer resolution from (i) documentation by thermochronological methods of rock-
2567 cooling patterns within the mountains and valleys of the modern range; and (ii) the
2568 geomorphological information encoded in various suites of mountain and piedmont
2569 landforms.

2570 Orogens in numerical models have been described as dynamic systems that tend towards
2571 equilibrium. This state of equilibrium of the critical taper thus formed is expressed by a
2572 topographic steady state, in which the creation of topography by crustal thickening is
2573 balanced by its destruction by surface denudation (e.g., Willett and Brandon, 2002). Once
2574 the upward- and outward-growing orogen has attained the steady state, the orogen is said
2575 to be mature. In order to test this model, we should be able to distinguish the successive
2576 growth and steady-state phases in the geological record. In the case of the Ancestral
2577 Pyrenees, however, the record so far has revealed a permanent state of transience, in which
2578 rates of crustal deformation and crustal denudation during the Paleogene were neither
2579 steady through time at any given location nor spatially uniform. Signs of the orogen ever
2580 having attained a recognizable state of maturity are difficult to pin down (see also Rahl et al.,
2581 2011; Whitchurch et al., 2011; Parsons et al., 2012; Ford et al., 2016).

2582 Given these persistent signatures of transience in the sediment record, it is reasonable to
2583 expect that a record of unsteady or transient landscape evolution (Allen, 2008) should also
2584 be encoded in landform assemblages within the mountain range, whether in the Axial Zone
2585 or the outer fold belts. It is thus expected that slope systems, interfluvial summits, and
2586 perhaps valleys at times responded in characteristic ways to relative respites in the history of
2587 crustal deformation, and/or were at certain places buffered from base-level changes. A rapid
2588 overview of the mountain landscape would tend to confirm this working hypothesis, with its
2589 (i) mosaic of mountain-top, low-gradient surfaces of varying sizes and states of conservation,
2590 always in abrupt juxtaposition with (ii) a population of younger incisional landforms,
2591 themselves displaying evidence of successive stages of downcutting and drainage
2592 reorganisation such as dry valleys, wind gaps, mountain-flank pediments and rock benches,
2593 and all situated above (iii) the usual staircases of Quaternary alluvial terraces, fans and
2594 debris cones. In Section 4 we focus on the suites of older, pre-Quaternary erosional
2595 landforms, and address the Quaternary landforms in Section 5.

2596

2597 **4.1. Diagnostic landforms: the Pyrenean erosion surfaces**

2598

2599 An intriguing collection of elevated, low-gradient land surfaces populates a number of
2600 summit areas of the Pyrenees, whether in the elevated Axial Zone or the outer tectonic
2601 belts, and whether the massifs have undergone glaciation or not (Fig. 6). Most are invisible
2602 to road travellers, but hillwalking geomorphologists have been reporting them from various
2603 parts of the mountain range for over 100 years (de Martonne, 1910; Blanchard, 1914; Sorre,
2604 1913; Nussbaum, 1930, 1931; Boissevain, 1934; Pannekoek, 1935; Birot, 1937; Goron,
2605 1941a; Sermet, 1950; De Sitter, 1952; Zandvliet, 1960; Calvet, 1996). The presence of such
2606 low-energy geomorphological archives in a high-energy mountain landscape has never been
2607 fully explained, but generates at least five threads of inquiry:

2608

- 2609 • the spatial distribution of these low-gradient surfaces (are they ubiquitous or confined to
2610 certain areas? do they occur at uniform altitudes?);
- 2611 • the age of the erosion surfaces with respect to the Proto-, Ancestral and Modern
2612 Pyrenees, respectively;
- 2613 • the relative ages of the different surfaces (i.e., is there just one generation, which
2614 perhaps underwent subsequent tectonic offsets? or are there several distinguishable
2615 generations?);
- 2616 • the geodynamic conditions (pre-, syn-, or post-shortening evolution of the orogenic belt)
2617 under which the low-energy topographic end-state that they document could be
2618 attained;
- 2619 • the elevation at which the erosion surfaces were formed: did the Ancestral Pyrenees
2620 undergo some widespread form of summit levelling at high altitude (i.e., ‘altiplanation’)?
2621 Or did the transition from the synorogenic Ancestral to the postorogenic Modern
2622 Pyrenees involve some form of transient peneplanation prior to regional uplift and deep
2623 re-incision by rivers and glaciers?

2624 ***4.1.1. Mapping low-gradient montane surfaces: a note of caution***

2625

2626 Low-gradient summit surfaces require authentication by systematic field observation,
2627 particularly to make sure that the flat topography is erosional (e.g., truncates upturned

2628 geological strata, faults or rock fabrics) rather than depositional or structural. Given also that
2629 very small relics (0.1 to 1 km²), which may evade detection by digital elevation models, may
2630 provide crucial clues, field inspection is invaluable (Fig. 6).

2631 A number of DEM- and GIS-based automated mapping exercises have been attempted for
2632 various segments of the mountain range on the basis of user-defined topographic criteria.
2633 No single method is entirely unequivocal, thereby emphasizing the difficulty of producing a
2634 complete, unbiased database. For example, early work by Babault et al. (2005b) used a DEM
2635 with a ground resolution of 90 m, and inferred erosion surfaces from a comparison between
2636 local relief as defined within a 5 km moving window and mean relief as defined within a 30
2637 km window. The algorithm resulted in extracting a population of land surfaces displaying
2638 slope angles $\leq 11^\circ$ and local relief $\leq 750 \pm 250$ m, but this ended up including many of the
2639 Quaternary glacial cirque floors of the Axial Zone. Using the same DEM data source, Calvet
2640 and Gunnell (2008) produced instead a slope map. Retaining a mask with slope-angle values
2641 $\leq 8^\circ$, the authors then proceeded to manually eliminate all Quaternary landforms and
2642 structural and depositional surfaces based on independent knowledge. Bosch et al. (2016a)
2643 elaborated a strategy for eliminating glacial landforms by using a 25x25 m resolution DEM,
2644 and by retaining land surfaces that simultaneously obeyed a set of rules such as local relief \leq
2645 300 m and slope angle $\leq 20^\circ$. The claimed (and somewhat surprising) size detection
2646 threshold was 500 m². The resulting regional map is paradoxical in that it turns out to be
2647 very accurate in the light of independent field knowledge, but somehow misses the well
2648 documented population of erosion surfaces situated in the Sub-Pyrenean fold belts, as well
2649 as most surfaces that occur below 1000 m generally. Automatically excluding glacial
2650 landforms also runs the risk of under-representing the population of erosion surfaces
2651 because glaciers in the Pyrenees have often just barely retouched some of these erosional
2652 land surfaces, for example in the case of anomalously wide glacial cirque floors in granite
2653 outcrops of the eastern Pyrenees (Delmas et al., 2014, 2015; Crest et al., 2017). More
2654 recently still, Ortuño and Viaplana-Muzas (2018) used a 0.5x0.5 km moving window on a 60
2655 m ground-resolution DEM to produce a mask of land surfaces where slope angles were $\leq 20^\circ$
2656 and local relief ≤ 350 m, while also using independent knowledge as a control. Unlike
2657 previous outputs, the resulting map reveals a population of surfaces among the outermost
2658 Pyrenean fold belts, but occurrences at elevations below 1100 m remained undetected. In

2659 summary, despite the useful reconnaissance work achieved by these desktop methods, field
2660 inspection remains an essential tool in the chain of evidence.

2661

2662 **4.1.2. Geographical distribution of the erosion surfaces**

2663

2664 *4.1.2.1. Principal occurrences (Axial Zone and adjacent structures)*

2665

2666 The spatial pattern and morphology of erosion surfaces is well established in the east of the
2667 Modern Pyrenees (Fig. 7), where the total surface area of orogenic wedge concerned by the
2668 gentle topography is ~15% (Calvet, 1996; Calvet and Gunnell, 2008). Two distinct
2669 generations can be mapped in some massifs (e.g., eastern Corbières, Carlit), and this
2670 bimodal feature is extendable to southern Andorra, the Aston and the Madrès. The upper,
2671 mountain-top surface (noted S₀ in Calvet, 1996, and relabelled S in Calvet and Gunnell, 2008
2672 and in subsequent publications) initially was either an undulating peneplain or a true
2673 pediplain: there are no discriminating criteria other than the occasional presence of
2674 monadnocks such as the Pic Carlit itself (2921 m), rising like an inselberg above an almost
2675 perfectly smooth erosional platform (Fig. 7E, F). These residual summit surfaces have been
2676 embayed at lower elevations by a population of mountain-flank surfaces, or pediments,
2677 some of which are quite extensive (noted S1 in Calvet, 1996; but P1 in Calvet and Gunnell,
2678 2008 and publications thereafter). The elevation difference between S and P1 is typically 300
2679 to 500 m, regardless of whether they occur in the limestone thrust-and-fold belt of the
2680 eastern Corbières, or the plutonic Carlit or gneissic Aston massifs of the Axial Zone (Fig. 7E, F,
2681 G). In any given massif, S is always in a ridge-top position — whether at 600–900 m in the
2682 Corbières or at 2400 m in the Madrès, ~2800 m in the Carlit massif, and likewise around
2683 Andorra (Hartevelt, 1970).

2684 These widespread relics of low-gradient, low-energy topography are the legacy of some
2685 advanced state of orogenic downwearing of the Ancestral Pyrenees in at least the eastern
2686 third of the modern mountain range. Surface P1 occurs ca. 100–200 m a.s.l. at the
2687 Mediterranean seaboard, for example cross-cutting fold structures of the eastern Corbières
2688 orocline (Fig. 7A), of the Figueres-Montgri thrust sheet, and likewise basement structures in
2689 the Albères. From the Mediterranean seaboard, the elevation of P1 rises rapidly westward to
2690 400–600 m (Fig. 7D). Around the Madrès massif, low-gradient plateaus of P1 affinity occur

2691 between 1300 and 2000 m. Around the Carlit massif, a very extensive occurrence of P1
2692 (Plateau des Lacs) slopes from 2400 to 1600 m to the Cerdagne graben (Fig. 7E). In the Aston
2693 massif, P1 rises from 1400 to 2200 m (Fig. 7H) (see also Monod et al., 2016). The Canigou–
2694 Carançà–Puigmal horst appears to be the only massif of the eastern Pyrenees where P1 is
2695 not paired with a residual of S at some altitude above it. Here, P1 on the western flank of the
2696 Puigmal slopes gently westward from 2600 to 1800 m (Calvet, 1996); a more elevated, S-
2697 generation surface was either never completed or was destroyed by subsequent denudation
2698 — in either case because the Canigou–Puigmal was tectonically one of the most active
2699 massifs of the eastern Pyrenees during the late Oligocene and early Miocene (Calvet and
2700 Gunnell, 2008).

2701 West of Andorra and as far as the Pic du Balaitous, the Axial Zone lacks detectable remains
2702 of a summit surface. Early observers had reached the same conclusion (Biro, 1952), apart
2703 from the illusion of a possible *Gipfelflur* underpinned by the occasional blunt ridge top, or
2704 the few hectares of a steeply inclined topographic ramp here or there (e.g., the top of
2705 Montcalm: 3080 m, 3 ha; the Pic de Fonguera, on the eastern boundary of the Encantats
2706 massif: 2883–2764 m, 20 ha; Martí Bono and Puigdefábregas, 1968). In contrast to these
2707 tenuous vestiges of S, some lower surfaces corresponding to P1 are relatively widespread in
2708 the surroundings of the higher massifs. The most striking examples occur between the
2709 Noguera de Vallferrera and Noguera de Cardós rivers (Zandvliet, 1960), with the Pla de
2710 Boldís (150 ha, rising from 2450 to 2591 m) and the flat ridgetop of Roca Cigalera (35 ha,
2711 2542–2667 m). From the vantage point of these erosion surfaces, the Pica d’Estats–
2712 Montcalm (summit elevation: 3152 m) stand as large residual massif of the ancestral
2713 Pyrenees, perhaps never eroded for reasons of positional remoteness within the watershed
2714 systems rather than of intrinsic rock hardness. Zandvliet (1960) mapped at least two
2715 generations of paleoplains in that area, at 2600–2400 m and 2300–1800 m — the latter
2716 highly undulating. Similar low-gradient land surfaces of P1 affinity occur around 2000–2200
2717 m in the Val d’Aran, below the Encantats massif (Montanha de Porera, Pruëdo, Roquetes
2718 Blanques) (de Sitter, 1954; Kleinsmiede, 1960; Ortuño et al., 2008, 2013, 2018); and likewise
2719 between the Pique and Neste rivers in the Oueil massif, where flat-topped interfluvial strips
2720 (2000–1800 m) extend out from the residual summit of Mt. Né (2147 m). West of the Neste
2721 River, similar interfluvial strips occur around 2000 m and form a pattern of low-gradient
2722 chutes extending straight out of the vast, flat-floored granite cirques that ornate the

2723 northern front of the Néouvielle massif around 2200 m a.s.l. Barrère (1952) had previously
2724 emphasized the anomalously wide floors of these cirques and speculated that these prima
2725 facie glacial landforms were really preglacial etchbasins in the granite. Along the southern
2726 edge of the Axial Zone, a few conspicuous mountain-top surfaces occur between 2200 and
2727 2500 m to the south of the Aneto massif (Tuca Royero, 2548 m, 41 ha) and between the
2728 Cinca and Cinqueta rivers (e.g., the Tozal d'Escubillons: 2427 m, 20 ha).

2729 A gap appears to exist between the localities mentioned above and the westernmost
2730 Pyrenees of the Basque Country, where summit surfaces reappear (Viers, 1960). These
2731 summit surfaces belong to generation P1 rather than S because of the masses of residual
2732 relief that rise above them at many places. The land surfaces cut across folded Cretaceous
2733 limestones of the Axial Zone cover sequence, such as where the Lakora nappe (Devonian and
2734 Silurian rocks) overrides the Arres d'Anie (Fig. 8I). The Larra–Arres d'Anie is a vast karstic
2735 plateau sloping westward (2150–1600 m) away from the residual pyramidal peaks of Anie
2736 (2504 m), Soum Couy (2315 m), and Arlas (2044 m) (e.g., Uzel et al., 2020). At elevations
2737 below the upstanding residual Pic d'Orhy (2017 m), these erosion surfaces continue
2738 westward as the Pelluségagne (1600 m) and Okabe (1466 m) plateaus, which truncate the
2739 Devonian rocks of the Iraty massif as well as its folded Cretaceous and Eocene cover
2740 sequence further south (Fig. 8H). Lastly, all the ridge tops of the Pays des Nives are flat
2741 around 1400–1200 m, cutting across the Hercynian basement of the Aludes massif as well as
2742 across its envelope of overthrust cover rocks.

2743

2744 *4.1.2.2. Occurrences in the outer fold-and-thrust belts*

2745

2746 The previously mentioned erosion surfaces of the Corbières continue along much of the
2747 North- and Sub-Pyrenean zones. The S/P1 pair is mappable as far west as the Pays de Sault.
2748 Where it occurs on massive Jurassic and Lower Cretaceous limestone, surface S forms
2749 elevated plateaus which typically rise towards the SW and exhibit a rich gallery of mesoscale
2750 exo- and endokarstic features: Roc Paradet (900 m) (Fig. 7C), Fanges (1000 m), Bac d'Estable
2751 (1450 m), Forêt de la Serre (1330 m), etc. Erosional corridors ascribable to P1 present
2752 themselves more as wind gaps and dry valleys between these massifs, i.e., more as fluvial
2753 straths than as pediments. They are usually lined with quartz gravel trains and associated
2754 with horizontal endokarstic galleries and conduits, which are sometimes filled with deeply

2755 weathered allochthonous gravels supplied by the Axial Zone (e.g., Clat cave, in the Clat
2756 palaeovalley, 1130 m). From here westwards, however, any clear distinction between S and
2757 P1 becomes impossible. The only evidence is a generally bevelled appearance of massif
2758 summits, but at an apparently random range of mean elevations suggesting either the
2759 existence of several generations of surfaces, or differentiated magnitudes of neotectonic
2760 movements responsible for offsetting a single original surface (see Goron, 1931, 1937, 1941a
2761 for a descriptive inventory; chronological interpretations therein, however, are obsolete).
2762 Mountain-flank erosional benches are also noted in some basement massifs such as the
2763 Tabe, Arize (Le Planel, 1067 m; Plaine d'Uscla, 1274), and Bouirex. They are nonetheless best
2764 preserved on massive limestone such as, from east to west: La Frau (1650 m, which contains
2765 a very ancient network of horizontal endokarstic galleries at la Caunha de Montségur); the
2766 Pech de Foix (700–1000 m); the Sourroque (1200 m) and Paloumère massifs (1200–1600 m)
2767 in the Salat catchment; a sequence of very smooth ridgetop flats around 1200 m between
2768 the Garonne, Neste and Adour rivers; the Ourdinse plateau (1500 m) and the residual
2769 plateau of Mailh Massibé–Montagnon (1973 m), both situated between the Gave d'Ossau
2770 and Gave d'Aspe (Uzel et al., 2020); and lastly the Arbailles massif, deeply corroded by
2771 karstic processes but where upturned and folded geological structures appear truncated at
2772 an elevation of 1000–1200 m by an erosion surface ornamented by small erosional hills. The
2773 erosional nature of the plateau surface is further testified by a number of truncated karstic
2774 cavities now exposing speleothems to the open air (Viers, 1960; Vanara et al., 1997; Vanara,
2775 2000).

2776 On the Iberian side of the orogen, erosional bevels in the Pedraforca nappes have been
2777 documented (Calvet, 1996). East of the Segre valley, two generations of erosion surfaces
2778 have been identified on that basis: the summit surface, which has been tectonically
2779 deformed, cross-cuts the Odèn–Port de Comte fold structures (1800–2300 m) (Fig. 8A),
2780 bevels the top of El Verd (2282 m), probably also the Rasos de Peguera (2077 m) and Raso
2781 d'Ensija (2200–2298 m), and likewise the south-facing dip slope of the Serra del Cadí (2400–
2782 2600 m). Meanwhile, the lower surface, which is less conspicuous, forms a bench in the
2783 Pedraforca nappe around 1800 m (Roca de Santaló, Pla de Prat). West of the Segre (see
2784 detailed map by Peña, 1984), the vestiges of low-gradient topography descend from
2785 Boumort (2077 m) southward towards the Serra de Careu (1760 m); and also northward
2786 towards the Serra de Prada (1800–1600 m), where the surface cross-cuts not just the

2787 massive Upper and Lower Cretaceous limestones but also the unconformable cover of
2788 Paleogene conglomerates dipping NNW (Fig. 9B, C, G, H; Peña, 1984, with detailed maps).
2789 Farther north, the same generation of erosion surfaces can be observed at the top of the
2790 Serra de Tahús and as far as the Col de Cantó (1900–1750 m). They cut across the
2791 complicated geological structure at the leading edge of the Noguera thrust sheet.
2792 The fold belt of the Sierras Interiores, between the Noguera Ribagorçana and Noguera
2793 Pallaresa as well as towards the Isábena River, are likewise truncated by summit surfaces.
2794 The truncated beds include the unconformable and tectonically deformed conglomerate
2795 sequences such as at Sis, where the upper units of the Collegats Fm. form an anticline, then
2796 dip 15 to 30° to the NNE, and are finally upturned near Bonansa (dips of 42°S; Vincent, 2001,
2797 Figs. 2, 5 and 10a therein; see also geological sheet 'Pont de Suert' by García Senz et al.,
2798 2009). The low-gradient topographic surface of the Serra de Sis (1700–1780 m a.s.l.) cross-
2799 cuts all of these structures, indicating that the erosion surface is younger than the observed
2800 tectonic deformations of the conglomerate beds. Conspicuous vestiges of summit erosion
2801 surfaces affecting the folded Mesozoic structures of the area likewise occur at similar
2802 elevations at Cruz de Bonansa (1800 m), Sant Gervàs–Muntanya d'Adons (1850–1750 m, 60
2803 ha) and Serra de Comillini (1550 m), where the surface even slopes very slightly towards the
2804 Axial Zone and suggests a component of tectonic tilting in the opposite direction to their
2805 initial slope (Fig. 9F). Other conspicuous summit surfaces occur on the Sierra de Ballabriga
2806 (2000 m, 20 ha), the Turbón anticline (2370–2250 m, 82 ha, Fig. 8G), the Cotiella massif
2807 (where residual relief subsists above the floor of the erosion surface), Punta Llerga (2240 m,
2808 38 ha), and the Entremón plateau (2300 m, 250 ha). South of the Graus–Trempt Basin, the
2809 Montsec range clearly displays a pair of tiered surfaces: the upper level (Fig. 8C), which was
2810 mapped by Peña (1984), has been deformed but bevels the northern dip slope of the thrust
2811 sheet between 1650 and 1500 m; the second, more extensive surface is subhorizontal and
2812 extends at the lower elevation of 1150 m around the Col de Comiols (Fig. 8B, D). Peña (1984)
2813 had also reported this lower surface but interpreted it as an older surface partly exhumed
2814 from beneath the conglomerate beds. Reinspection of the Comiols area shows that the
2815 massive Cretaceous limestone and its unconformable cover of SE-dipping Paleogene
2816 conglomerate beds are both bevelled by the lower topographic surface, which can thus be
2817 subsumed under generation P1. P1 also displays benches cut into the southern flank of the
2818 Montsec, and locally at the NE termination of the sierra. Although some of these benches

2819 locally appear structural at some locations, their erosional nature is not in doubt. The
2820 surface is also observed at the NW edge of the Montsec range, where it grades to the top of
2821 the (unconformable) Graus conglomerate and finer molasse sequence — which is presumed
2822 of Miocene age. East (Peña, 1984) and west of the Noguera Ribagorçana, the Sierras
2823 Exteriores also bear erosion surfaces (Sant Mamet, 1300 m, Fig. 8B; Serra de Milla, 900–1000
2824 m; Sierra de Carrodilla, 900–1000 m, etc.).
2825 West of the Cinca River, in the Sierras Interiores, Monte Perdido displays structural summit
2826 surfaces coinciding with the top of recumbent folds (Biro, 1937). Likewise, the sierras of
2827 Tendeñera, Collarada and Visaurin exhibit an assemblage of structural and glacial landforms,
2828 but no erosion surfaces. An exception is noted at the border between Aragón and Navarra,
2829 where in the Sierra de Leire (1300 m; Barrère, 1981) the folded structures in limestone
2830 (Campanian, Paleocene and Ilerdian sequence) rising above the flysch have been bevelled by
2831 erosion. Plateau areas in soft flysch, such as the Llano de la Sierra (1100 m) and the Plana de
2832 Sassi (1000 m) in Navarra (Barrère, 1962), may represent partial planation landforms of a
2833 younger generation than P1. The Sierra de Guara displays up to 3 erosional bench levels
2834 (Barrère, 1952; Rodríguez-Vidal, 1986). The most conspicuous level is tilted from west to
2835 east, dipping from 1700 m near the centre (Fig. 8F) to ~1200 m at Sierra de Sevil (Fig. 8E).
2836 Throughout the area, a number of ~300 m-tall residual rock masses nonetheless rise above
2837 it. The surface truncates the tight folds in Upper Cretaceous to Lutetian limestone, but also
2838 (farther north) the succession of accordant homoclinal ridges in the Paleogene Campodarbe
2839 sandstone. This extensive erosional level possibly grades to the top of the Peña del Sol
2840 conglomerate beds, suggesting a chronostratigraphic link between the two. More recent
2841 partial planation benches form mountain-flank notches into the south and east sides of the
2842 Sierra de Guara, where they also appear to cut across the dipping conglomerate beds of the
2843 Sariñena and Uncastillo formations (e.g., at El Ciano, 1100 m, and at the Santa Cilia
2844 belvedere, 900–1000 m).

2845

2846 ***4.1.3. Age and origin of the erosion surfaces***

2847

2848 The major items of evidence arising from the inventory of erosion surfaces in the Pyrenean
2849 orogenic wedge are (i) the near-systematic occurrence of a pair of surfaces — a mountain-
2850 top and a mountain-flank surface — throughout the eastern third of the Pyrenees; (ii) the

2851 regional extent of the mountain-top surface within this eastern segment of the mountain
2852 range; (iii) the absence of a well-defined mountain-top surface in the elevated Axial Zone
2853 massifs of the central Pyrenees, i.e., over a distance of 160 km from the Encantats westward
2854 to the Pic d’Anie; and (iv) the occurrence, often very clear but sometimes more hypothetical,
2855 of erosion surfaces (sometimes several generations) throughout the fold-and-thrust belts of
2856 the pro- and retro-wedges, as well as in the ranges standing along the continental drainage
2857 divide in the western Pyrenees (Basque Country). Age constraints on all of these features
2858 have been provided.

2859

2860 *4.1.3.1. Transient legacies of a low-energy environment: evidence from thermochronology*

2861

2862 None of the erosion surfaces in the inventory above are pre-orogenic, i.e., none were
2863 formed before the Proto- or the Ancestral Pyrenees. Such a view was once held on the basis
2864 of a small vestige of marine Cretaceous caprock at the top of the Pic de Balaitous (García
2865 Sainz, 1940), i.e., precisely in the segment of the Pyrenees where no other vestigial summit
2866 surface occurs. It is now clear, however, that the isolated character of this outlier confirms
2867 on the contrary that all other potential vestiges of this sub-Cretaceous unconformity have
2868 been destroyed by vigorous syntectonic denudation (Upper Cretaceous beds occur farther
2869 east, but are buried beneath the Gavarnie Thrust; they can be followed for ~40 km but
2870 cannot be used as geomorphological markers). Abundant apatite fission-track (AFT) and
2871 apatite helium (U–Th/He, or AHe) data exist for the central and western Pyrenees (Yelland,
2872 1990, 1991; Fitzgerald et al., 1999; Morris et al., 1998; Sinclair et al., 2005; Gibson et al.,
2873 2007; Metcalf et al., 2009; Jolivet et al., 2007; Meresse, 2010; Filleaudeau et al., 2011;
2874 Beamud et al., 2011; Rahl et al., 2011; Fillon et al., 2013; Michael et al., 2014; Vacherat et al.,
2875 2014, 2016; Bosch et al., 2016; Labaume et al., 2016b; DeFelipe et al., 2019). Somewhat
2876 fewer have been produced for the eastern Pyrenees (Garwin, 1985; Yelland, 1990, 1991;
2877 Sère, 1993; Morris et al., 1998; Maurel, 2003; Maurel et al., 2002, 2008; Gunnell et al., 2009;
2878 Rushlow et al., 2013) and Catalan Ranges (Juez-Larré and Andriessen, 2006). These rock-
2879 cooling studies show that Paleogene denudation depths were much too large (at least 6–10
2880 km) for any pre-tectonic erosion surfaces to have survived the orogeny of the Ancestral
2881 Pyrenees. The data mostly document the pre- and synorogenic histories, particularly the
2882 Paleogene denudation maximum, and also reveal a north-to-south time lag in the timing of

2883 peak denudation. They subsidiarily detect some effects of Oligocene to Miocene crustal
2884 extension in the east, and locally pick up recent valley incision in the Central Pyrenees (out of
2885 250 AFT central ages, 11 lie between 10 and 20 Ma, with 2 ages at 11 and 12 Ma at Bielsa
2886 and in the Ossau massif; among 150 published AHe ages, 22 lie between 10 and 20 Ma, and
2887 8 are younger than 10 Ma).

2888 Gunnell et al. (2009; Fig. 10) produced a series of AFT and AHe data exclusively focused on
2889 samples collected from relict surfaces in the eastern Pyrenees. They show that denudation
2890 rates at those locations declined after the Paleogene tectonic paroxysm. By late Oligocene to
2891 early Miocene time, rock-cooling histories at each sampling site across the region had
2892 attained a low-temperature plateau indicative of a terminal decline in denudation intensity
2893 (Fig. 10C). Because of sensitivity limitations, the thermochronology cannot confidently
2894 discriminate between different generations of erosion surface such as S and P1, which in the
2895 landscape are nonetheless clearly distinct and typically offset by elevation differences of 0.5
2896 km or less. Regardless of this minor caveat, however, a plateau in the rock cooling curves of
2897 a low-relief landform in a high-energy mountain range is nonetheless a clear signal of post-
2898 shortening topography having reached a state of low erosional energy and, by reasonable
2899 inference, of low relief. As evident in the landscape, the low-gradient topography has
2900 endured from ~25 Ma to this day (Fig. 10C). Such patterns have been observed in many
2901 mountain ranges around the world (for a review: Calvet et al., 2015a), and in the Pyrenees
2902 they are fully consistent with the fact that the erosion surfaces cross-cut the many
2903 syntectonic structures of the orogenic wedge such as thrust sheets, nappes and folds —
2904 whether in the Axial Zone or among the crumple belts of the pro- and retro-wedge.

2905 Diagnostic but understated rock-cooling plateaus such as illustrated in Fig. 10 have been
2906 obtained independently in most other studies of Pyrenean thermochronology, whether
2907 based on the interpretation of vertical profile sampling or on single-sample modelling of
2908 fission-track lengths. For example, in the Maladeta massif three cooling models have
2909 detected a slackening of denudation rates (Gibson et al., 2007), with a succession of
2910 moderate denudation rates between 50 and 30 Ma (300 m/Ma), followed by a sharp but
2911 brief acceleration around 30 Ma (1.5 km/Ma), then followed by a comparatively quiescent
2912 and definitive phase of very slow cooling after 30 Ma (30 m/Ma) (Fig. 10D). Again in the
2913 Maladeta massif, an independent study using the vertical profile method has evidenced a
2914 long stagnation of the samples in the apatite fission-track Partial Annealing Zone between 30

2915 and 5–10 Ma subsequent to a period of very rapid denudation ca. 35–30 Ma (Fitzgerald et
2916 al., 1999). Along the southern edge of the Axial Zone, five samples from another study
2917 extending between the Noguera and the Ter watersheds have documented a sharp rock-
2918 cooling plateau after ~20 Ma (Rushlow et al., 2013). In the Arize and Trois Seigneurs massifs,
2919 three cooling models by Vacherat et al. (2016) likewise reveal a clear thermal plateau after
2920 50 or 35 Ma depending on location. AFT ages obtained from detrital apatite crystals
2921 extracted from unconformable Paleogene conglomerate sequences in the pro-foreland have
2922 also provided similar thermal signatures, with clear flatlining after either 50 Ma or 30 Ma
2923 (depending on the model and location), and thus suggesting a sharp and lasting decline in
2924 denudation intensity after Rupelian time at the latest. The exact timing probably depends on
2925 the provenance location (latitude, i.e., distance) of the granite pebbles collected for the
2926 study, and perhaps also on a moderate component of burial and exhumation of the samples
2927 from within the conglomerate (Beamud et al., 2011; Rahl et al., 2011).

2928 Attempts at remodelling the existing data for the central Pyrenean Axial Zone (31 AFT and 17
2929 AHe samples) have confirmed the rock-cooling plateau, which presents itself as a period of
2930 extremely low denudation (20m/Ma) between ~30 Ma and the Present and was preceded by
2931 an episode of extremely rapid denudation between 37 and 30 Ma (> 2.5 km/Ma) (Fillon and
2932 van der Beek, 2012). Thermochronological evidence from the western Pyrenees also shows a
2933 thermal plateau after 30 to 15 Ma depending on the location, but cooling models produce a
2934 post-Pliocene acceleration involving rapid denudation after ~5 Ma (Jolivet et al., 2007).

2935 Given that this acceleration also concerns the high summits of the Néouvielle massif, this
2936 could tentatively be an expression of the ‘Miocene acceleration’ artefact pointed out by
2937 Gunnell (2000) and Dempster and Persano (2006), which is related to parameter choices
2938 around the fission-track annealing algorithms used in the modelling. Still farther west, the
2939 outlines of a thermal plateau after 20–10 Ma are apparent in profile models of the Pic de
2940 Balaitous, as likewise in the Lakhoura profile after 30–20 Ma, on a longitudinal traverse close
2941 to the Pic d’Anie (Bosch et al., 2016).

2942

2943 *4.1.3.2. Refined age constraints on the two generations of erosion surface*

2944

2945 In the eastern Pyrenees, rifting during the early Miocene was largely responsible for the
2946 tectonic regime which generated the pairs of S–P1 surfaces. Rifting generated substantial

2947 local relief in certain areas such as Mt. Canigou, but this was an exception. Other
2948 morphotectonic units (Carlit, Campcardos, Aston, Madrès, Corbières...) were not affected by
2949 such large vertical fault offsets. Rifting initiated a cycle of topographic rejuvenation in
2950 response to the newly forming local marine (Mediterranean) base levels, with generation P1
2951 developing 200 to 500 m below summit surface S.

2952

2953 *4.1.3.2.1. The range-top paleoplain (S)*

2954

2955 The precise age of the summit surface, S, is poorly constrained but broadly fits into a time
2956 window between the late Oligocene and the Aquitanian. The sedimentological inflexion
2957 observed during Chattian time in the eastern Aquitaine Basin (see Section 3.1.2), when
2958 conglomerate influx was replaced in the stratigraphy by lacustrine limestone, provides a
2959 relatively robust palaeoenvironmental indication of declining topographic energy in the
2960 Ancestral Pyrenees at the time. Thick lacustrine limestone also occurs in the Upper
2961 Oligocene units of the Narbonne Basin and (with interlayers of lignite) in the eastern Ebro
2962 Basin at Calaf, Tàrrega (Rupelian), and Mequinenza (Chattian) (Cabrera and Saez, 1987;
2963 Gomis et al., 1997). Some climate-driven lake fluctuations relevant to ~1 m.y. cycles nested
2964 within this broader pattern have also been detected (Valero et al., 2014).

2965 It is often admitted that these low-energy deposits grade laterally to the Nogueres and
2966 Berga conglomerates, and that the latter are thus also of Chattian age (e.g., Vincent and
2967 Elliott, 1996; Vincent, 2001; Jones, 2004). No direct palaeontological evidence in the Solsona
2968 molasse or in the Berga conglomerates, however, currently supports a Chattian age for the
2969 conglomerates; the youngest magnetostratigraphic record is mid-Rupelian (i.e., ~30 Ma;
2970 Carrigan et al., 2016; see also discussion in Section 3.2.2.2). As recorded from all three
2971 piedmont basins to the north, east and south of the Ancestral Pyrenees, a period of
2972 decreasing clastic output from the eastern part of the mountain range thus cannot be ruled
2973 out during Chattian time. A low-energy environment is more difficult to infer from
2974 lithostratigraphic criteria for the subsequent Aquitanian stage, particularly in the eastern
2975 half of the Pyrenees, because the region east of the Segre River has been an area of either
2976 nondeposition or complete erosion of whatever Aquitanian record may have existed. An
2977 expansion of lacustrine limestone facies has nonetheless been described in the lower Cinca
2978 catchment around that time (Valero et al., 2020), thereby suggesting limited coarse-textured

2979 terrigenous influx from the Pyrenees in that area. Aquitanian siltstone and limestone
2980 deposits likewise overlie the Pyrenean molasse in the centre of the Aquitaine Basin ('trilogie
2981 agenaise') and exist in the eastern basins (Narbonne Basin, and base of the Roussillon Basin
2982 fill sequence at depths of –1200 to –1500 m in the Canet borehole; Berger et al., 1988).
2983 The absence of erosion surfaces in the central Pyrenees, i.e., the exclusive presence of
2984 mountains with spiky rather than flat tops (Adams, 1985; Calvet et al., 2015a), calls for three
2985 alternative scenarios (Fig. 11):

2986 (i) Scenario A: the paired S/P system was ubiquitous throughout the Pyrenees; surface S
2987 also existed in this portion of the Ancestral Pyrenees, but it was destroyed by more
2988 intense denudation (and, later, by glaciation) than in the eastern Ancestral Pyrenees, and
2989 by higher magnitudes of post-shortening uplift (confirmed by the high modern elevations
2990 of the central Pyrenean massifs).

2991 (ii) Scenario B (a variant of A): the paired S/P system only existed in the east of the orogen,
2992 in direct relation with Mediterranean extensional tectonics. Subdued relief was also
2993 generated in the western Pyrenees, but the two erosion surfaces conspicuous in the east
2994 here blur into a single phase of downwearing which terminated in the middle Miocene.
2995 This single surface was destroyed by subsequent morphotectonic events but is preserved
2996 among fold and thrust units on both flanks of the crustal wedge as well as on the
2997 continental dividing ranges of the Basque Country.

2998 (iii) Scenario C: surface S never developed in the higher massifs of central Pyrenees because
2999 of persistent tectonic activity in this segment of the orogen, where thrust displacement
3000 continued until the early Miocene and possibly as late as the middle Miocene (Jolivet et
3001 al., 2007; Huyghe et al., 2009). As a result, little more than pediments would have
3002 developed on the flanks of the high range, beveling folds in the pro- and retro-wedges
3003 and at the western termination of the orogen. These imperfect but mappable erosional
3004 landforms would have evolved iteratively from the end of the Paleogene to the middle
3005 Miocene, thereby granting them stronger membership ties to generation P1 than to
3006 generation S.

3007 *4.1.3.2.2. The range-flank pediments (P1)*

3008

3009 Age constraints on surface P1 are good in the eastern Pyrenees. Depending on location,
3010 different occurrences of pediment P1 (i) cross-cut uptilted Upper Oligocene and Aquitanian
3011 beds within the Narbonne and Tuchan–Paziols basins; (ii) grade to the top of the middle
3012 Miocene shoreline outcrops of the Mediterranean seaboard (Fig. 7A, B); and (iii) display
3013 across their treads a very large number of fossil micromammalian assemblages preserved in
3014 regolith-filled cracks of the limestone pavements, with ages ranging between 20 and 10 Ma.
3015 The preservation of these fossil assemblages suggests a low-energy geomorphological
3016 environment. In the Canigou massif, P1 formed after the intense period of rifting and deep
3017 unroofing of the Paleozoic gneiss dome, which (based on the inverse stratigraphy and age of
3018 correlated deposits in the adjacent intermontane basins such as the Conflent; see Section
3019 3.3.1) occurred during early Aquitanian to Burdigalian time. In the Corbières and Minervois,
3020 P1 continued to evolve in the late Miocene, coevally with the lacustrine limestone deposits
3021 of Montredon (biozone MN 10, 10–9 Ma) (Calvet, 1992, 1996; Calvet and Gunnell, 2008;
3022 Gunnell et al., 2009). In the Ariège, the upward-fining molasse sequence from the Aquitanian
3023 through to the late Burdigalian, as likewise the onlap of lacustrine limestone beds southward
3024 up to the outermost folds of the Petites Pyrénées, suggest a similar chronology valid for the
3025 planar surfaces of the Aston massif. Hillslope gradients probably reached their lowest energy
3026 state during the middle Miocene.

3027 Along the pro-wedge, the Sierras Interiores and their overlying (unconformable and often
3028 north-dipping) Noguères conglomerate sequences between the Segre and Esera valleys have
3029 been truncated by a single erosion surface. This population of occurrences is at least post-
3030 Chattian, and perhaps belongs to generation S. Along the margins of the Ebro Basin, the
3031 upper surface at Montsec probably also correlates with generation S. The lower surface,
3032 however, which truncates the conglomerate sequence reputedly of Chattian terminal age,
3033 would correlate with P1. This interpretation is supported by the apparent stratigraphic
3034 correlation between the surface and the conglomerate sequence at the western end of the
3035 Sierra del Montsec, the Sierra Carrodilla, and the Sierra de Guara, where occurrences of P1
3036 grade to the top of the Graus, Sariñena and Uncastillo formations, respectively (Fig. 8).
3037 Attenuation of relief steepness is also indirectly documented by the widespread
3038 progradation of carbonate platforms after 15–16 Ma (see Section 3.2.5.2).

3039

3040 *4.1.3.3. Base-level controls on erosion surface completion*

3041
3042 Compared to continental-scale peneplains, which are generated over time scales compatible
3043 with the Wilson cycle, the short geological time to completion of low-gradient surfaces S and
3044 P1 in the Pyrenees can be explained by three complementary causes, all of which are
3045 particularly relevant to the eastern Pyrenees.

- 3046 • The narrowness of the Ancestral Pyrenees at the end of the Paleogene is a first factor.
3047 Whether in the retro- or the pro-foreland, the Pyrenean fold-and-thrust belts were in
3048 large part buried beneath the molasse and conglomerate sequences described in
3049 previous sections, so that the Paleogene mountain range was effectively a narrow
3050 backbone consisting mainly of the Axial Zone and the NPZ. Whereas the compressionally
3051 deformed crust in the central Pyrenees (inclusive of the SPCU) is 160 km and the
3052 mountainous relief currently ca. 140 km wide, during the Paleogene the width of
3053 mountainous relief at that same longitude would not have exceeded 80 km.
- 3054 • The interruption of tectonic convergence during the Oligocene in the eastern Pyrenees,
3055 and the onset of Mediterranean extension responsible for fragmenting the mountain
3056 belt into a collection of basins and footwall uplands, is a second factor. The overall rate
3057 at which denudation occurs depends on the ratio of surface-area to volume of rock to be
3058 consumed by denudational processes — i.e., the greater the surface area of exposed
3059 mountain fronts (e.g., a mosaic of footwall uplands separated by local tectonic base
3060 levels, more vulnerable to erosional inroads made by river catchments than a monolithic,
3061 e.g. cylindrical, mountain range), the faster the volume as a whole can be consumed by
3062 backwearing river systems. Here, extensional fragmentation into discrete tectonic blocks
3063 multiplied the total length of mountain fronts vulnerable to erosion by steep
3064 catchments, reduced the size of relief units exposed to denudation, and thus conspired
3065 to promote conditions of rapid relief decay and erosion-surface completion.
- 3066 • Possibly also a dense lithospheric root (see Section 2.4) was pulling downward and
3067 delaying the full potential for isostatic rebound. Rebound is a function of the elasticity of
3068 the underthrust Iberian Plate and of orogen width (assumed to represent a line load). In
3069 the case of an orogen narrower and shorter than the Modern Pyrenees, isostatic
3070 rebound of the Ancestral Pyrenees was perhaps 15% of what Airy isostasy would
3071 otherwise predict (Montgomery, 1994).

3072 These considerations relax the need for assuming that the summit surfaces were formed at
3073 palaeoelevations of 2000 m or more, i.e., at their currently observed altitudes of occurrence,
3074 just by clipping off the tops of certain massifs of the Ancestral Pyrenees in Oligocene time.
3075 This is theoretically feasible under the assumption of substantially raised foreland base
3076 levels, for which there is, however, potential evidence only in the anomalous Nogueres area
3077 on the Iberian side and none whatsoever on the retro-wedge side. This view is an avatar of
3078 the hypothesis formulated ca. 30 years ago that climate rather than tectonics drive
3079 mountain building (Molnar and England, 1990), subsequently simulated in sandbox models
3080 inspired by the (striking, but atypical) Nogueres pro-foreland setting (Babault et al., 2005a,
3081 2007). Opposite conclusions have since been drawn from global data and levelled at the
3082 climate-driven doctrine (Willenbring and von Blackenburg, 2010). Note that in the Pyrenean
3083 context, the raised foreland scenario would also imply (i) that the narrow, Ancestral
3084 Pyrenees somehow remained altitudinally stationary and unaffected by fluvial dissection
3085 during the last ~25 m.y.; and (ii) that the externally drained Aquitaine Basin somehow was
3086 also (like parts of its Ebro counterpart) an overfilled basin, with clastic backfill rising up to the
3087 Axial Zone. No evidence in favour of such north–south symmetry, however, exists (see also
3088 Sinclair et al., 2009).

3089 The scenario of a raised base level caused by an overfilled Ebro basin would imply that the
3090 summit erosion surface graded to the top of the pro-foreland Nogueres conglomerate
3091 sequence, for which there is no direct evidence comparable with, for example, the clastic
3092 depositional ramps (so-called ‘gangplanks’) that today still connect the Colorado Front Range
3093 to the Ogallala Formation of the High Plains of Texas, Colorado or Wyoming (see Calvet et
3094 al., 2015a, and references therein, for an overview).

3095 Initially formulated by Coney et al. (1996), the scenario portraying the Nogueres
3096 conglomerates (sensu Section 3.2.4.2) as a backfill sequence lapping northward onto low-
3097 gradient erosion surfaces in the Axial Zone, with the erosion surfaces evolving concomitantly
3098 at elevations controlled by this raised clastic base level, has reverberated widely through
3099 Pyrenean literature and been simulated in sandbox experiments (Babault et al., 2005b,
3100 2007). This model, however, is unique to the south-central Pyrenees (no similar
3101 conformations occur in the eastern Pyrenees, or along the Aquitaine retroforeland, or in the
3102 context of the Berga–Serrat Negre conglomerates further east or the Santa Orosia–Cancias

3103 conglomerates further west), and is actually unsupported by field evidence in its own testing
3104 ground.

3105 Any notion that the topmost Nogueres conglomerate beds and extant summit erosion
3106 surfaces in the Axial Zone are coeval and cogenetic is challenged by a number of
3107 underpinning criteria (Fig. 9):

- 3108 (i) the huge boulder-bed facies of the proximal deposits, requiring a high-energy
3109 environment in the Axial Zone (Fig. 9A, B, D, E) rather than low-energy, low-gradient
3110 land surfaces (these typically generate finer-textured alluvium more akin to the
3111 Ogallala Fm. in the foreland of the Laramide Rockies);
- 3112 (ii) the attitude of the conglomerate beds, which, far from having conserved the
3113 depositional slope typical of clastic ramps between a mountain range and its
3114 foreland, are systematically folded and/or tilted northward towards the Axial Zone
3115 (Fig. 9F).
- 3116 (iii) the fact that the conglomerate sequences are themselves cross-cut by low-gradient
3117 erosional topography. These land surfaces are thus necessarily younger than the
3118 structures they have truncated, and thus younger than the clastic sequences
3119 themselves.

3120 To the west of the Nogueres conglomerate outcrops, the Santa Orosia conglomerates
3121 (Bartonian to Priabonian) have been warped into the shape of a syncline and offset by the
3122 Oturia Thrust. The erosion surfaces at Col de Comiols and Serra de Sis, which were analysed
3123 in Section 4.1.2.2 (Fig. 8B, D; Fig. 9), and in the Boumort massif (Fig. 9) call for similar
3124 conclusions: the conglomeratic fan deposits have all undergone tectonic deformation and
3125 tilting towards the Axial Zone, i.e., towards their source areas (Biro, 1937; Rosell and Riba,
3126 1966; Rosell, 1967; Reille, 1971; Muñoz et al., 2010). The intensity of deformation decreases
3127 upsequence but affects the entire stratigraphy, including the topmost 'allogroups'
3128 (Senterada and Antist, Fig. 9F), which are inexplicably illustrated as horizontal beds in some
3129 publications (Melleres and Marzo, 1992; Beamud et al., 2011, Fig. 2 therein). Overall, the
3130 summit surface on all of the structures from the Bóixols anticline to the Serra de Prada cross-
3131 cuts not just the homoclinal structures in massive Mesozoic limestone but also the entire
3132 Nogueres conglomerate sequence itself, from the Pessonada allogroup in the south to the
3133 Pallaresa allogroup in the north (Fig. 9C, G, H).

3134 In the Aquitaine foreland, the homologous Palassou conglomerates are likewise folded and,
3135 at many places, upturned vertically and cross-cut by low-gradient erosional surfaces — for
3136 example north of the Mouthoumet massif. As on the Iberian side of the orogen, there is thus
3137 no robust evidence to support the hypothesis that the Palassou conglomerates and the
3138 elevated erosion surfaces on massifs such as Aston, Arize and the Pays de Sault are coeval
3139 and cogenetic. As an additional caveat, connecting by imaginary lines vestiges of generation
3140 S or P1 at their current altitudes in the Axial Zone to the top units of conglomerate
3141 sequences in the Aquitaine or Roussillon basins would require gradients of 4% to account for
3142 these putative clastic ‘gangplanks’. Unless allowance is made for uplift-related
3143 postdepositional tilting, such steep gradients are unrealistically high compared to the natural
3144 depositional slopes commonly reported for alluvial megafans of the sizes typically observed
3145 along mountain range fronts (Calvet and Gunnell, 2008).

3146 By logical elimination, it thus appears highly likely that the summit surfaces are vestiges of a
3147 paleoplain that formed regionally across parts of the Ancestral Pyrenees at lower elevations
3148 than the current altitudes of its vestiges would suggest — and that they were later uplifted.
3149 A variety of geophysics- and geomorphology-based inferences calibrated against the
3150 anomalously high longitudinal gradients of Quaternary alluvial terraces (Delmas et al., 2018),
3151 and predicated on realistic depositional slopes observed in modern piedmont zones (i.e., the
3152 natural gradients of large piedmont fans: see Miall, 2016; Ventra and Clarke, 2018), have
3153 suggested that the initial altitude of this paleoplain — i.e., its mean altitude when the
3154 orogen had attained an all-time state of least topography, including in the Axial Zone —
3155 would have not exceeded 800 m (Gunnell et al., 2008, 2009). The topography of the eastern
3156 Pyrenees was thus neither a sea-level peneplain nor a high-elevation peneplain but a mid-
3157 elevation, irregular plateau region displaying a greater proportion of low-gradient erosion
3158 surfaces than of steep alpine peaks.

3159

3160 **4.2. Late Neogene regrowth of the mountain range: chronology and evidence from** 3161 **landforms**

3162

3163 Fundamentally, the altiplanation hypothesis for the Pyrenees postulates that the Modern
3164 Pyrenees are just a vertically incised but altitudinally unmodified version of the Ancestral
3165 Pyrenees (Curry et al., 2019). It thus downplays the magnitude of the step change required

3166 to explain the transformation of the Ancestral into the Modern Pyrenees, and essentially
3167 regards the distinction as unimportant. Much evidence is available, however, to show that
3168 the late Neogene, i.e., the last 10–12 million years, was the period of a second rising of the
3169 Pyrenees as a continuous and elevated mountain range between Iberia and Europe. The
3170 evidence in support of this phenomenon derives primarily from geomorphological clues,
3171 now widely recognised (Section 4.1) but commonly misreported (e.g., Curry et al., 2019). It is
3172 further corroborated by a number of tectonic and stratigraphic observations and backed up
3173 by indications concerning the processes at the lithosphere–asthenosphere boundary (see
3174 Section 2.4, and Jolivet et al., 2020).

3175

3176 **4.2.1. Evidence of late Neogene uplift throughout the Pyrenees**

3177

3178 *4.2.1.1. Thermal relaxation and lithospheric thinning since 10 Ma*

3179

3180 If we assume that the Pyrenean paleoplain formed at a mean palaeoelevation of less than 1
3181 km (mean or maximum is immaterial in the context of a low-relief erosional plain; Gunnell et
3182 al., 2008, 2009; Delmas et al., 2018), it follows that ~60% of the topographic relief we
3183 observe today (summits in the eastern Pyrenees: ~2.7 km) was produced during the late
3184 Neogene, and in several stages involving regional surface uplift. The inferred mean
3185 topographic uplift rate is 0.2 mm/yr, i.e., sufficiently slow to lie within the uncertainty
3186 envelope of present-day detection of vertical crustal motion by GPS (0.1 ± 0.2 mm/yr:
3187 Nguyen et al., 2016). In the west-central Pyrenees (Aspe valley), Uzel et al. (2020) inferred
3188 ca. 1 km of Neogene and Quaternary uplift-driven valley incision, with evidence of greater
3189 relative uplift in the Axial Zone than in the NPZ. Assemblages of late Miocene warmth-loving
3190 plant remains and $\delta^{18}\text{O}$ measurements in fossil teeth in the sedimentary deposits of the
3191 Cerdagne Basin (1200 m a.s.l.) confirm the notion of recent regional uplift (Suc and
3192 Fauquette, 2012; Huyghe et al., 2020), and even more so in the Val d’Aran (now at ~2000 m;
3193 Ortuño et al., 2013; see also section 3.3.2). As argued in Section 2.4, maintaining the
3194 buoyancy of the crust to the east of Andorra almost certainly implies a thermal contribution
3195 from the asthenospheric mantle, which in turn causes thermal or mechanical thinning of the
3196 mantle lithosphere (Gunnell et al., 2008, 2009). The resulting dynamic uplift supports the
3197 regional topography of the Modern Pyrenees at least in the east (Chevrot et al., 2018) — a

3198 process also consistent with the situation inferred for the neighbouring Catalan Ranges
3199 (Lewis et al., 2000) and with the incidence of late Neogene volcanism, and which has also
3200 been adduced to explain the geologically recent uplift of the Moroccan Atlas Mts. (Teixell et
3201 al., 2005). The most recent deep tomography based on teleseismic and gravity data has
3202 imaged a low-velocity anomaly located between the surface and a depth of 100 km. It
3203 coincides with a strong density anomaly interpreted as a mass of eclogite in the deep crust,
3204 also consistent with the depth-distribution of seismic activity in the crust (Dufréhou et al.,
3205 2018). The conjunction of these independent components of evidence supports the notion
3206 of a crustal drip or a delamination process currently occurring beneath the Modern Pyrenees
3207 west of Andorra. Meanwhile, the Ancestral Pyrenees to the east of Andorra had lost their
3208 crustal root much earlier, most likely during early Neogene (see also Jolivet et al., 2020), thus
3209 also explaining the unique geomorphological identity of the eastern Pyrenees.

3210

3211 *4.2.1.2. Sedimentological signatures of growing relief amplitude*

3212

3213 An increase in clastic output, both in terms of volume of debris and average clast size, since
3214 the late Miocene is recorded in piedmont deposits such as the Lannemezan megafan, among
3215 the eastern extensional basins such as the Roussillon, Empordà, Cerdagne, and in the
3216 Mediterranean and Atlantic offshore clastic wedges (Kieken, 1973; Lofi et al., 2003; Duvail et
3217 al., 2005; Bache et al., 2010; Cameselle et al., 2014; Granado et al., 2016; Ortiz et al., 2020;
3218 also see sections 3.1.5.2, 3.2.6 and 3.3.2). A climatic cause for accelerated denudation is
3219 theoretically possible, but the time period of regional uplift spans palaeoclimatic regimes as
3220 diverse as the warm subtropical conditions alternating between super-humid and semi-arid
3221 of the Tortonian, Messinian and Pliocene; and the cold, glaciated and temperate oscillations
3222 of the Quaternary. Tectonics-driven relief growth and steepening of hillslopes seems a more
3223 plausible explanation for terrigenous delivery by the mountain range, and is consistent with
3224 the lithospheric and mantle processes mentioned above. Another strong indication of
3225 neotectonic activity is the occurrence of well-preserved triangular-faceted spurs, for
3226 example along the southern boundary-fault scarp faces of the Roussillon and Cerdagne
3227 basins. These are in each case associated with debris-cone sequences several hundred
3228 metres thick, of Pliocene and Turolian age, respectively, containing giant boulders supplied
3229 by very steep range-front catchments (Calvet, 1996; Calvet and Gunnell, 2008).

3230

3231 *4.2.1.3. Late Neogene and Quaternary tectonic deformation*

3232

3233 Many Pyrenean deposits of Miocene to Quaternary age exhibit tectonic strain indicators,
3234 from tilting to fault-controlled offsets (synthesis in Philip, 2018). The known spatial
3235 distribution of these tectonic indicators, however, is quite uneven: in the Roussillon Basin,
3236 for example, faults in the Miocene fill sequences are widespread, but faults in the Pliocene
3237 wedge-top layers are more uncommon and restricted to a few documented sites. At the
3238 scale of the entire Pyrenees, the inventory of tectonically offset Quaternary deposits does
3239 not exceed ~20 sites (Fig. 12). The intensity of deformation is variable depending on the
3240 sequence: Upper Miocene units are steeply upturned in the Cerdagne, La Seu, and Empordà
3241 basins, and fault throws through the graben fills attain ~1 km. Strata in Pliocene sequences
3242 exhibit shallower dips, and fault throws do not exceed a few hundred metres. Tectonic
3243 offsets through Quaternary deposits are an order of magnitude less. Deformational style is
3244 also variable, and includes extensional (widespread in the Mediterranean domain and as far
3245 west as the Val d'Aran), strike-slip, and thrust faults (Viers, 1960, 1961a; Ellenberger and
3246 Gottis, 1967; Birot, 1969; Mouline et al., 1969; Ambert, 1977; Pous et al., 1986; Cabrera et
3247 al., 1988; Briaies et al., 1990; Philip et al., 1992; Massana, 1994; Saula et al., 1994; Carbon et
3248 al., 1995; Roca, 1996a; Genna et al., 1997; Goula et al., 1999; Calvet, 1996, 1999; Fleta et al.,
3249 2001; Baize et al., 2002; Alasset and Meghraoui, 2005; Dubos-Sallée et al., 2007; Ortuño et
3250 al., 2008, 2018; Lacan et al., 2012; Lacan and Ortuño, 2012; Philip, 2018). Inside limestone
3251 cave systems, endokarstic galleries offset by tectonic throws of up to 10 m have been
3252 reported at La Pierre Saint-Martin (Maire, 1990), in the Arbailles massif (Vanara et al., 1997),
3253 and in the Villefranche syncline (Coronat massif, Calvet et al., 2015b; Hez et al., 2015);
3254 however, the ages and slip directions of these tectonic fractures are difficult to establish. As
3255 a result, just as it is proving difficult to determine the fault-plane solutions of modern-day
3256 earthquakes in the Pyrenees (see below), the chronology of stress regimes during the late
3257 Neogene is difficult to reconstruct. It is likely that it was neither uniform across the orogen
3258 nor constant through time at any given site.

3259 During the latest Miocene and Quaternary, N–S convergence resumed but was apparently
3260 too weak or too short-lived to contribute measurably to mountain building. Evidence for this
3261 is provided by a reverse fault along the southern boundary of the Roussillon Basin, where

3262 the Miocene beds are overthrust but the unconformable Pliocene overburden appears
3263 undisturbed by additional tectonic strain (Calvet, 1996, 1999). The Quaternary deposits,
3264 however, are in turn reverse-faulted, with similar features also observed elsewhere —
3265 whether in the Axial Zone (Cerdagne, Estavar and Martinet reverse faults) or in the outer
3266 belts of the orogenic wedge. Most of the faulting occurrences affect middle and younger
3267 Pleistocene sequences. Characteristic occurrences in the retro-wedge/retro-foreland zone
3268 include reverse faults at Caramany (Agly River valley), in the Montagne Noire near Revel, and
3269 cutting through the Horsarrieu and Meilhan anticlines along the Adour River valley; an
3270 anticline warping the Würmian alluvial terrace along the Gave d'Aspe at Asasp-Arros; the
3271 small fracture swarms in early Pleistocene (or Pliocene?) deposits at Biarritz; and contrasting
3272 evidence in Holocene deposits along the Lourdes Fault of a reverse-fault geometry at
3273 Arcizac, but a Holocene normal-fault geometry at Capbis. Among occurrences in the pro-
3274 wedge, worth mentioning are the reverse faults at Isaba in the Roncal River valley, Canelles
3275 along the Noguera Ribagorçana, Balaguer along the Segre, and Serinyà along the Fluvià.
3276 Indices of extensional faulting in Quaternary deposits are comparatively scarce anywhere
3277 within the orogen: e.g., at Osséja (Cerdagne), at La Seu d'Urgell, and at Graffan–Ferrals
3278 (Corbières), where Pleistocene travertine on the Orbieu River exhibit tectonic offsets. Pure
3279 strike-slip motion is reported in the early Pleistocene lacustrine limestone beds of the Fluvià
3280 watershed. Extensional and strike-slip displacement of the entire Pliocene sequence have
3281 been well documented in the Roussillon Basin, with an additional offset of ~10 m (for
3282 example at the protected site of special geological interest near Ille-sur-Têt) also affecting
3283 the uppermost alluvial terrace deposit of the Têt River.

3284 Present-day tectonic activity is very weak throughout the Pyrenees. The rate of convergence
3285 measured by GPS between Africa and Europe is 3–4 mm/yr. The Pyrenees are undergoing
3286 extension, today principally in their western segment, at a rate of ~0.5 mm/yr — although
3287 only a few of the GPS measurements truly register above the background noise. From this it
3288 has been inferred that Iberia and Europe are now locked to one another, thus forming a
3289 single tectonic plate (Nocquet and Calais, 2003, 2004; Fernandes et al., 2007; de Vicente et
3290 al., 2008; Asensio et al., 2012). The main focus of continental deformation has jumped to the
3291 southern boundary of the Iberian Plate in the Betic Ranges. Seismicity in the Pyrenees is
3292 moderate (Fig. 13), with 35 events exceeding M_L 5 since 1950 (e.g., St-Paul-de-Fenouillet,
3293 1996, M_L 5.2; Arudy, 1980, M_L 5.1; Rigo and Cushing, 1999), and 12 of a higher intensity (i.e.,

3294 > VIII on the Modified Mercalli scale) since the Middle Ages (Souriau and Pauchet, 1998).
3295 Focal mechanisms, however, are poorly constrained: some studies have supported a
3296 compressional stress regime (Goula et al., 1999), which is in agreement with geological
3297 evidence of Quaternary reverse and strike-slip faulting (Philip et al., 1992; Calvet, 1996,
3298 1999; Carbon et al., 1995; Goula et al., 1999; Fleta et al., 2001; Baize et al., 2002; Alasset and
3299 Meghraoui, 2005; Lacan et al., 2012; Lacan and Ortuño, 2012); but recent revisions favour
3300 instead an extensional regime (Chevrot et al., 2011). The most recent synthesis (Rigo et al.,
3301 2015), however, suggests a more nuanced picture, with emphasis on variation in
3302 deformational style and intensity through time, and with a gradient from weak transtension
3303 in the west to weak transpression in the east.

3304 Vertical crustal motions have been documented by levelling methods, with debatable values
3305 of up to 1 mm/yr at Mt. Canigou and in the Têt valley (cited in Calvet, 1996, after Lenôtre
3306 and Fourniguet, unpublished BRGM report from 1987; see also Philip, 2018), and 1–4 mm/yr
3307 in NE Catalonia (Gimenez et al., 1996). With very low measured values of 0.1 ± 0.2 mm/yr,
3308 GPS measurements of vertical displacement currently remain within the noise of analytical
3309 error (Nguyen et al., 2016). This inventory excludes the occurrences of slope tectonics that
3310 have been mapped and analysed by Jarman et al. (2014) and Ortuño et al. (2017), and which
3311 tend to impact the upper portions of slopes in some massifs. On balance, field evidence
3312 weighs in favour of a compressive regime during Quaternary time, thus at odds with focal
3313 mechanism data as well as with short-span GPS measurements.

3314

3315 ***4.2.2. Geomorphological indicators of episodic surface uplift***

3316

3317 *4.2.2.1. A late Neogene generation of rock pediments (P2)*

3318

3319 Late Neogene uplift was not steady. Pauses or relative lulls allowed pediments (i.e., partial
3320 planation surfaces) to expand across the edges of the Neogene extensional basins in the
3321 east, but also into more interior areas of the Axial Zone in the form of flat-floored erosional
3322 corridors, bedrock straths or topographic basins, usually in soft or weatherable rock
3323 outcrops such as marl, flysch, deeply weathered granite; but also limestone basins (poljes),
3324 which today have become fossil landforms (Figs. 6, 14). The age of these landforms is often

3325 difficult to establish. The oldest occurrences grade to (and thus seem correlative of) the
3326 Vallesian deposits of Cerdagne and La Selva.

3327 The pediment generation most indicative of unsteady post-shortening uplift regime is a
3328 second generation of rock pediments and palaeovalleys, here labelled generation P2. Its
3329 residual occurrences grade to the tops of retro-wedge megafans such as the Lannemezan,
3330 and are thus roughly of late Pliocene or earliest Pleistocene estimated age (Goron, 1941a;
3331 Delmas et al., 2018). These partial pediments are several kilometres across. They form deep,
3332 flat-floored embayments into the mountain topography, typically hanging today 200–400 m
3333 above the modern valley floors. Smaller erosional benches of a younger generation (labelled
3334 here P3) grade laterally to the oldest Pleistocene alluvial terrace deposits (generation T5, see
3335 Section 4.2.2.3 and Section 5), and may thus qualify as bedrock straths. These successive
3336 cohorts of planar landforms are relatively ubiquitous and formed prior to the deep vertical
3337 valley incision and widespread slope steepening events of the Pleistocene. Quaternary
3338 glaciation has often failed to erase these late Neogene features from the landscape.

3339 Occurrences of these characteristically low-gradient landforms have been widely mapped in
3340 the central Pyrenees, e.g., in the Noguera Pallaresa, Ariège, and Salat watersheds, and even
3341 more conspicuously in the Agly and Tech watersheds and around the edges of the eastern
3342 Neogene basins such as the Roussillon, Cerdagne, and Empordà. These pediments
3343 are particularly extensive among granitic outcrops but also in schist (Goron, 1931, 1937,
3344 1941a; Zandvliet, 1960; Hartevelt, 1970; Lagasquie, 1969, 1984a, b, 1987; Calvet, 1996;
3345 Delmas et al., 2018). Around the edges of the Cerdagne Basin, a good example of P2 is the
3346 Plateau de la Perche (Fig. 14D), which bevels the basement along the edge of the basin as
3347 well as an upturned sequence of Vallesian and Turolian deposits within in. Other landforms
3348 belonging to this generation include the Plateau de Sault, the surface of which is smeared
3349 with siliciclastic lag deposits displaying identical facies to the constituent depositional units
3350 of the Lannemezan megafan. Occurrences of pediment P2 are also observed in the Neste
3351 watershed, in the weathered granite outcrops of Bordères (Monod et al., 2016). In the outer
3352 relief units of the orogenic wedge, e.g., in the Empordà Basin, the pediment surfaces grade
3353 to the top of the Pliocene gravel beds of the Llers–Figueres plateau. Similar configurations
3354 are reported on either side of the lower Aude valley, e.g., in the Corbières (at Les Vals) and in
3355 the Minervois (Montouliers–Montplo) (Biro, 1969; Ambert, 1994; Larue, 2008). Farther
3356 west, from the Ariège to the Gave rivers, the P2 piedmont ramp cuts across almost all of the

3357 Sub-Pyrenean fold sequences — particularly folds in the Cretaceous and Eocene flysch —
3358 and is even locally embayed into its regional P1 predecessor (Fig. 14A, B, C).

3359 The Lannemezan gravels and their analogues, which form a debris mantle widely distributed
3360 across the P2 topographic surface, are a constant diagnostic feature of P2 (Goron, 1941a;
3361 Taillefer, 1951; Lagasquie, 1969, 1984b). Save a few very rare exceptions, this generation of
3362 deposits seems absent from the Basque Country, where the watersheds are mostly in
3363 limestone and thus could not supply siliciclastic debris to the piedmont. P2 is nonetheless
3364 very extensive in the Basque region. Despite the scarcity of diagnostic gravels, the landform
3365 is topographically continuous with the Ossau megafan (Fig. 14B), which displays a debris
3366 accumulation of the same nature as the lag gravels encountered across, and basinward of,
3367 occurrences of P2 farther to the east. The spatial distribution of P2 between the Adour River
3368 and the Pyrenean mountain front overall forms a belt of pediments ~20 km wide at
3369 elevations ranging between 300 and 180 m (Fig. 14A). The erosional surface cuts mainly
3370 across flysch, but equally across vertically upturned beds of massive Cretaceous limestone as
3371 well as gneiss and schist. A few large, residual monadnocks in the Garralda quartzite, the
3372 Ursuya gneiss, and the Permo-Triassic sandstone of La Rhune have resisted denudation, and
3373 these topographic residuals themselves display hillflank benches that are legacies of an older
3374 generation of pediments. P2 often extends inward between those massifs, and for example
3375 joins up with the interior topographic basins of Ossès and Saint-Jean-Pied-de-Port (Viers,
3376 1960).

3377 On the pro-wedge, similar suites of planar landforms extend across outcrops of Eocene and
3378 Cretaceous flysch and shale. In francophone literature, these are known as the ‘mature
3379 hanging landforms’ of Navarre (Barrère, 1962) and (in the case of the oldest vestiges of soft-
3380 rock wash pediments in that region) have also been named ‘coronas’ (Barrère, 1952, 1975,
3381 1981; Peña, 1984; Stange et al., 2018). The most elevated generation of pediments is capped
3382 by very ancient breccia containing large boulders. Occurrences of this caprock are well
3383 preserved at the wide col below the village of Merli, 350 m above the Isabena River and 450
3384 m above the Esera River; and likewise at San Victorian–La Mula, at the base of the abrupt
3385 Peña Montañesa range (2300 m) — i.e., ~500 m above the Cinca River and 360 m above
3386 more local tributaries. The most elevated generations of wash pediments in the Conca de
3387 Tremp hang 200–250 m above the Noguera Pallaresa, and farther to the east the Pla de

3388 Lladurs hangs ~400 m above the Cardener River (Fig. 14E). All of these mantled pediments in
3389 soft rock belong to the same generation P2.

3390

3391 *4.2.2.2. Dry valleys and drainage piracy*

3392

3393 Dry valleys in the Pyrenean landscape consist mostly of broad, shallow furrows which
3394 document a time of progressive drainage reorganisation during the early rise of the Modern
3395 Pyrenees, when the intensity of fluvial incision into the low-relief landscape of the late
3396 Ancestral Pyrenees was still moderate. These ancient valleys sometimes display perfectly
3397 preserved entrenched meander belts (e.g., the dry valley at Col de Saint Louis, in the
3398 Fenouillèdes massif). Different generations of ancient valley floors have been identified.
3399 Occurrences at high altitudes are rare and, in that case, correlate with pediment surface P1.
3400 They often lie at elevations identical to the upper portion of the pediments. The largest
3401 population of dry valleys is coeval with pediment generation P2 and occurs systematically at
3402 elevations lower than P1. In the piedmont zones, some of the valleys are Quaternary.
3403 Whatever their exact age, they all document a diachronous process of river piracy and
3404 progressive drainage reorganisation during post-shortening time. This process and its
3405 intricate patterns, however, have never been studied comprehensively or systematically.
3406 The most spectacular dry valley is perhaps the Pla de Beret (1870 m), which occurs in the
3407 catchment headwaters of a strikingly underfit Noguera Pallaresa in the central Pyrenees (Fig.
3408 14G). This flat-bottomed hanging valley is 500 to 800 m wide and has been only lightly
3409 transformed by glacial erosion. Its gentle descent northwards eventually curves eastwards
3410 around the granitic Marimanya massif — an obvious adaptation to the local structural
3411 geology. Its natural watershed is the Encantats massif to the south, but the retro-foreland
3412 Garonne River, which in this area is much closer to its regional base level than the pro-
3413 foreland rivers, has beheaded the Noguera watershed. This process was probably assisted by
3414 late Neogene tectonic activity along the Maladeta Fault (Ortuño et al., 2008), and as a result
3415 of deep incision the Garonne now flows ~600 m below the Pla de Beret. Another major
3416 drainage capture along the main divide occurred at the Col de Puymorens in the eastern
3417 Pyrenees, also a broad palaeovalley. A river flowing through it used to join up with the Segre
3418 and the Mediterranean but now joins the current Ariège drainage network northwards to
3419 the Atlantic (Fig. 14F). In the eastern Pyrenees, the Têt River has also lost part of its left bank

3420 watershed to the Aude River as a consequence of tectonic downthrow in the Capcir graben;
3421 the shallow cradle of abandoned hanging valleys can still be observed along the skyline of
3422 the N–S boundary fault scarp to the east of the graben.

3423 Most of the other dry valleys have been preserved by dint of the drainage becoming
3424 subterranean through extensive belts of massive limestone. A series of dry valleys, for
3425 example, has been preserved in the retro-wedge Aptian/Barremian outcrops that extend
3426 from the Fenouillèdes to the Pays de Sault. The dry valleys document a redirection of
3427 drainage towards the Aude (a Mediterranean river), thereby beheading the Hers (an Atlantic
3428 river) and also leading to internal drainage reorganisations within the Agly catchment
3429 (another Mediterranean river). Similar ancient valleys correlate topographically with karstic
3430 landforms such as the large Pays-de-Sault polje, and stratigraphically with gravel deposits of
3431 Lannemezan affinity which occur as a well-preserved trail all the way into the youngest and
3432 best-preserved dry valley of the area at the Col du Chandelier. All of these ancient valleys
3433 currently hang 300–400 m above the modern active valley floors. Similar configurations have
3434 been well studied in the Arbailles massif (Vanara et al., 1997; Vanara, 2000), which is cut by
3435 the two large dry valleys of Ithé and Eltzarreordokia. The floors of these dry valleys lie more
3436 than 400 m above the active Bidouze and Saisons watersheds, and they are the legacy of
3437 ancient streams flowing northward through the Arbailles from the Mendibelza massif
3438 situated to its south. In the South-Pyrenean massifs of the pro-wedge, the Llinars–Pla de la
3439 Llacuna dry valley (see Fig. 8A), which must be very ancient given its relative elevation of 875
3440 m above the Segre River at Oliana, is an important landmark. The eastern termination of the
3441 Montsec thrust-front scarp is incised by three ramified dry valleys that have been cut to
3442 depths of 100–150 m beneath pediment P1 and currently hang 750 to 650 m above the
3443 Noguera Pallaresa river channel (Fig. 8B). These ancient streams used to drain the eastern
3444 half of the Conca de Tremp and joined either the Segre or the Noguera Pallaresa after having
3445 cut through the Montsec gorges. They were subsequently beheaded and became diverted
3446 towards the Noguera Pallaresa upstream of its gorge through the Montsec, thus abandoning
3447 their earlier courses.

3448 The retro-foreland basin retains a number of unexplained features deserving future
3449 investigation, such as the Aude valley and its watershed, for example. It has been speculated
3450 that parts of the Aude headwaters at one time joined up with the Garonne via the Plateau
3451 de Sault and the Hers Vif valley; or via Limoux, then the Seuil de Naurouze and the Hers Mort

3452 valley, which contains vestiges of a middle Pleistocene alluvial terrace at Castelnaudary
3453 (Gottis et al., 1972). Very little direct evidence supports these views, however, and heavy
3454 mineral provenance studies in the alluvial material have proved inconclusive (Larue, 2007). It
3455 appears that the Aude has primarily captured left-bank rivers flowing down from the
3456 Montagne Noire, such as the Fresquel, which were former tributaries of the Garonne.
3457 Several dry valleys in the lower region of the Aude watershed, which are associated with
3458 mappable middle Pleistocene alluvial deposits, have been cut into erosional benches
3459 consistent with generations P1 and/or P2, and suggest a progressive drift of the Aude
3460 drainage network towards the NE through its limestone fold belts until fairly recently.
3461 Whether this trend was driven by tectonic (Ellenberger and Gottis, 1967; Genna et al., 1997;
3462 Larue, 2001, 2007) or climatic (Ambert, 1976, 1994) causes remains debated.

3463

3464 *4.2.2.3. Staircases of alluvial terraces*

3465

3466 Vertical successions of alluvial terraces are commonly used as records of crustal uplift
3467 (Bridgland, 2000; Kiden and Törnqvist, 1998; Bridgland and Westaway, 2014; Demoulin et
3468 al., 2017), particularly when the elevation offset between two given generations of alluvial
3469 deposit increases upstream but tends to level off in the vicinity of the coastline and
3470 eventually become a stack of conformable stratigraphic units on the continental shelf. In the
3471 Pyrenean context, this configuration is valid in the case of the Roussillon Basin (see Section
3472 5), where five generations of Quaternary alluvial deposits fit this scenario (Delmas et al.,
3473 2018), and where the steep seaward tilt of the boundary between Pliocene marine and
3474 Pliocene continental deposits also confirms a rise of the east-Pyrenean Axial Zone during the
3475 last 4–5 Ma (the stratigraphic boundary is detected at –200 m at the coastline in the Canet
3476 borehole, and at +280 m in the intermontane Conflent Basin to the west). The hinge zone at
3477 the coast remained relatively stationary over that time period, which explains why the
3478 Corbières and Albères coastlines fail to display the abundance of uplifted Pleistocene marine
3479 terraces that might be expected in other active tectonic settings. The presumed Tyrrhenian
3480 Stage (i.e., highstand palaeoshoreline), which is the best preserved among potential
3481 candidates in the Roussillon-Languedoc region, occurs at an altitude of +7 m (Barrière,
3482 1966). Alluvial terrace sequences similar to those of the Têt are also recognised along the
3483 Orb (Larue, 2008) and Aude rivers in Languedoc, the Fluvià and Ter rivers in Catalonia, and

3484 equally the Garonne, the Gave rivers, and the lower Adour. Alluvial terraces have similarly
3485 been used in the Ebro Basin to document regional uplift, with patterns likewise suggesting
3486 increasing magnitudes of uplift towards the mountain belt and an acceleration of uplift
3487 during the late Neogene (Stange et al., 2013a, 2016; Lewis et al., 2017).

3488 The vertical successions of alluvial terraces also record a number of strike-perpendicular
3489 tectonic upwarps that have caused the rivers to migrate laterally across their foreland
3490 topography. In the Aquitaine Basin (Enjalbert, 1960; Barrère et al., 2009), the middle
3491 segment of the Garonne has steadily drifted eastward by at least 25 km, forming the
3492 extensive left-bank staircase of terraces in the Toulouse area and undercutting the upper
3493 terrace system of the Tarn River in the process. The lower Ariège River has undergone a
3494 similar evolution. The magnitude of retro-foreland tectonic deformation is appreciated by
3495 comparing the maximum altitude of the highest terrace of the Garonne in the Forêt de
3496 Bouconne (330 m), west of Toulouse, with the heights of interfluvial summits in the Lauragais
3497 area, which are capped by coeval alluvial gravels from the Montagne Noire and never exceed
3498 280 m between the Ariège and Hers Mort valleys. Likewise, the Comminges area, which is
3499 situated between Saint-Gaudens and Tarbes, was in late Serravallian time the last surviving
3500 fluvio-lacustrine depocentre of the Aquitaine Basin: as a consequence of uplift, its deposits
3501 now hold a commanding position over the piedmont at an altitude of ~450 m, and the
3502 lignite-bearing lacustrine Tortonian beds of Orignac lie at 500 m. Further west, a consistent
3503 pattern of downwarping is observed, with for example the successive positions of the alluvial
3504 belt of the Gave de Pau indicating a progressive westward drift during the middle
3505 Pleistocene. The alluvial belts of the lower Adour River between Soustons and Bayonne also
3506 tell a story of southward drift between the early Pleistocene and the present, probably
3507 driven by the pattern of coastal subsidence during that same period. This evidence does not
3508 appear to be included in existing numerical models that aim to simulate the evolution of the
3509 region, and which have emphasized instead the influence of autogenic processes instead of
3510 tectonic drivers on both the construction and subsequent incision of the Lannemezan
3511 megafan (Mouchéné et al., 2017a).

3512

3513 *4.2.2.4. The groundwater karst record*

3514

3515 During periods of crustal stability, the altitude of major drainage conduits in the karst is
3516 adjusted to the upper surface of water tables, the position of which is itself dictated by local
3517 topographic base levels. Vadose systems (which typically consist of vertical shafts and
3518 narrow meandering saw-cuts) develop instead at times of base-level fall, i.e., in response to
3519 crustal uplift and valley incision (Audra and Palmer, 2011, 2013). Discontinuous uplift has
3520 accordingly been recorded by the groundwater karst system of some Pyrenean limestone
3521 massifs, where several levels of horizontal endokarstic galleries have been mapped over
3522 vertical heights of 1 km (Maire and Vanara, 2008). As such, and in similar ways to the alluvial
3523 terrace systems but over much longer intervals of geological time, dating the alluvial fill
3524 contained in successive generations of endokarstic galleries should provide clues to the
3525 chronology of Pyrenean uplift. Thus far, occurrences in the Axial Zone and/or the retro-
3526 wedge tectonic belts include the Arbailles massif (5 major levels over a vertical distance of
3527 800 m; Vanara et al., 1997, Vanara, 2000), the Pierre St Martin–Arres d’Anie (8 levels
3528 between 1950 m and 450 m; Maire, 1990), the Arbas massif (6 major levels over a vertical
3529 distance of 900 m; Bakalowicz, 1988), the Tarascon syncline (middle Ariège valley, with 10
3530 levels over a vertical distance of 600 m; Sorriaux et al., 2016–2018), the upper Aude valley (9
3531 levels over a vertical distance of 600 m), and the Villefranche-de-Conflent syncline (10 to 12
3532 levels over a vertical distance of 1100 m; Calvet et al., 2015b; Hez et al., 2015; Calvet et al.,
3533 2019). Among the pro-wedge tectonic units, the Cotiella massif records at least 3 main levels
3534 (Belmonte, 2014), and probably 5 to 6 levels occurring at elevations between 2300 and 800
3535 m.

3536 When such karstic cavities are entered by allocthonous rivers transporting quartz-rich debris
3537 from Hercynian basement outcrops located upstream, the alluvium deposited in the caves
3538 can benefit from terrestrial cosmogenic nuclide (TCN) burial dating in order to establish its
3539 residence time under ground. The burial age calculation relies on the radioactive decay of
3540 the TCN because, once confined to the cave environment, the debris are shielded from
3541 exposure to cosmic rays and thus from further nuclide accumulation. This method usually
3542 relies on measuring the concentrations of two nuclides with different half-lives, most
3543 commonly ^{26}Al and ^{10}Be , and allows residence times typically between 0.2 and 5.5 Ma to be
3544 detected (Granger et al., 1997; Granger and Muzikar, 2001). This kind of work in the
3545 Pyrenees is still in its infancy, but data from the Villefranche karst have yielded a mean
3546 incision rate of 0.06 mm/yr since the beginning of the Pliocene and 0.11 mm/yr since 1 Ma

3547 (Calvet et al., 2015b). The Arbas massif has recorded 0.24 to 0.13 mm/yr of uplift-driven
3548 valley incision since 3.7 to 3 Ma; the Flamisell (Pallars province): 0.11 mm/yr since 1.12 Ma;
3549 and the Cotiella massif (Cinqueta canyon) a record 0.67 mm/yr since 1.24 Ma (Genti, 2015;
3550 Vernant, 2018) —in a part of the Pyrenees that has also yielded the youngest AFT rock-
3551 cooling ages of the orogen (11 Ma). An incision rate of 0.4 mm/yr during the last 400 ka
3552 through the Arbailles massif was inferred from the U–Th ages of speleothems (Vanara et al.,
3553 1997).

3554 Recent attempts at dating much larger numbers of cave-deposit clasts have nonetheless
3555 revealed situations of extreme intraformational age dispersal, with the risk of drawing
3556 spurious or arbitrary conclusions about valley incision rates on the basis of inconsistent
3557 results (Sartégou et al., 2018). The occurrence of large age dispersals within a seemingly
3558 horizontal and laterally continuous alluvial deposit emphasizes two potential sources of
3559 error: (i) either a situation of postdepositional sediment mixing within the cave system
3560 (possible cause: inputs of older deposits from higher cave levels polluting the deposit
3561 through vertical shafts); (ii) or an alluvial unit containing clasts with widely divergent and
3562 individually complex exposure histories acquired within the watershed prior to their burial in
3563 the cave. In such situations, based on the laws of stratigraphy (in the present case: Charles
3564 Lyell’s Law of Included Fragments, which governs the logic of relative dating in geology and
3565 states that rock fragments must be older than the rock formation containing them), the
3566 most likely burial age of an alluvial deposit in a cave must, by default, be the age of its
3567 youngest dated clast (Calvet et al., 2019).

3568

3569 **5. Quaternary geomorphological evolution**

3570 The modern landscapes of the Modern Pyrenees and their piedmonts are dominated by
3571 fluvial and glacial landforms. Aeolian, periglacial, and karstic environments have left a less
3572 impacting or more localised imprint and are not presented in this review.

3573

3574 **5.1. Alluvial deposits**

3575

3576 Alluvial terrace treads have been mapped in the pro-wedge valleys outward of the Sierras
3577 Interiores, and in some more interior areas near the southern edge of the Axial Zone.

3578 Occurrences are also widespread in the upper valleys of the Basque Country, where the

3579 Pyrenees are moderately elevated and were only lightly impacted by glaciation; and
3580 throughout the eastern Pyrenees, where the alluvial terrace systems of rivers such as the
3581 Têt, the Aude and the Segre have met with opportunities for wide floodplain development in
3582 the intermontane grabens of Cerdagne, Conflent and Capcir.

3583

3584 ***5.1.1. Stratigraphic features***

3585

3586 Stages of fluvial incision can be reconstructed from five main generations of alluvial terraces
3587 in the eastern basins (Cerdagne, Conflent, Roussillon, Aude) and Aquitaine foreland (Ariège,
3588 Garonne, Adour, various Gave rivers). This alluvial chronostratigraphy has benefited from
3589 several generations of geological studies underpinned by relative dating criteria such as
3590 terrace-tread altitude, palaeontological content, embedded archaeological artefacts (Boule,
3591 1894; Depéret, 1923; Chaput, 1927; Denizot, 1928, etc.), weathering indices, soil
3592 characteristics, and connections with frontal moraines (Alimen, 1964; Tricart et al., 1966;
3593 Icole, 1968, 1969, 1973; Hubschman, 1973, 1975a, b; Calvet, 1981, 1996; Debals, 2000).

3594 Relatively robust correlations have been established on that basis between most watersheds
3595 (Calvet et al., 2008; Barrère et al., 2009).

3596 Generations of alluvial deposits in the French geomorphological mapping system are
3597 numbered T0 to T5, upward from the modern floodplain to the oldest vestige; on 1:50,000
3598 geological sheets, the ranking is similar but with an alphabetical scheme, i.e., Fz (youngest)
3599 to Fu (most ancient). In some cases, a single chronostratigraphic generation of alluvial
3600 deposit will be distributed among a population of several terrace treads at slightly different
3601 altitudes — e.g., up to 4 treads in the case of T3 on the Têt River (Calvet, 1996; Delmas et al.,
3602 2018) and 3 on the Ariège (Delmas et al., 2015) — despite exhibiting identical soil profile and
3603 clast weathering characteristics. The opposite situation also occurs, e.g., on some of the
3604 Garonne alluvial terraces, when very wide terrace treads are considered diachronous despite
3605 being topographically continuous (Chaput, 1927).

3606 In Spain, the earlier systematic inventories tended to share the French approach of
3607 numbering generations of alluvial deposits from bottom to top (Mensua et al., 1977; Bomer,
3608 1979; Peña, 1984; Rodríguez-Vidal, 1986; Peña and Sancho, 1988), but Iberian studies have
3609 operated on strictly watershed-based inventories of terrace treads, and distinctions between
3610 terrace generations are restricted to altitudinal criteria and topographic continuity. The

3611 synthesis for the central part of the Ebro Basin, for example, records 6 terrace levels (from
3612 T1, i.e., the modern floodplain, to TVI) spread over an elevation range of 250 m (Mensua et
3613 al., 1977). The uppermost level was given a 'Pliocene to Quaternary' age. The overview
3614 produced for the Segre River basin by Peña and Sancho (1988) identified up to 11 terrace
3615 levels within a vertical elevation bracket of 200 m in the Cinca tributary watershed and,
3616 along similar lines: 8 in the Noguera Ribagorçana and 6 along the Segre itself (modern
3617 floodplain included). For the Aragón River, Bomer (1979) reported a minimum of 6 levels.
3618 More recent investigations have maintained the tradition of catchment-confined inventories
3619 but elected to invert the labelling scheme, thereafter numbering alluvial vestiges from the
3620 most elevated / oldest vestige down to the floodplain. This has not only upset the task of
3621 matching terrace systems among different valleys of the pro-foreland, but increased the
3622 difficulty of correlating the incision histories of watersheds on opposite sides of the
3623 mountain range. Under this new rationale, 12 levels were identified by Benito et al. (1998,
3624 2010) above the active floodplain of the lower Gállego River, but only 9 by Lewis et al. (2009,
3625 2017) — who also reported 10 in the Cinca watershed (as opposed to the 11 by Peña and
3626 Sancho, 1988). A study by Stange et al. (2013a) reports 8 levels for the Segre (noted TQ0
3627 down to TQ7), 8 for the Cinca (noted in that study Qt2 to Qt10), and 7 for the Noguera
3628 Ribagorçana (noted T8 to T2 — but numbering for this particular watershed, unlike the
3629 others, starts from the bottom). A correlation of the full sequence of terraces was attempted
3630 for the Segre catchment by Peña et al. (2011).

3631 Unlike the Aquitaine Basin, soil and alluvium weathering criteria have not been emphasized
3632 in Iberian research, except by Bomer (1979) and Lewis et al. (2009). Predicating correlations
3633 between the pro- and retro-foreland river systems on the basis of such criteria holds little
3634 promise (i) given the overwhelming prevalence of limestone debris in the Iberian Quaternary
3635 alluvium; and (ii) given further the aridity of the Ebro Basin, which has promoted the
3636 development of calcrete on all terrace levels (even though caprock indurations get
3637 substantially thicker and harder among the older generations of alluvial deposits), except in
3638 the upper catchment areas where soil eluviation prevails because of higher rainfall.
3639 Indurated facies of this kind are entirely absent from the more humid Aquitaine piedmont,
3640 and even from the more Mediterranean Roussillon Basin, where soil eluviation and
3641 carbonate dissolution are the rule except locally along limestone scarp-foot settings where
3642 hydrological conditions can favour the precipitation of calcium carbonate.

3643 The coarse, and often clast-supported gravel texture of all the Quaternary terrace levels
3644 indicates a prevalence of braided channel belts forming floodplains sometimes up to 10 km
3645 wide. The depositional sequences are relatively thin (mean thicknesses between 5 and 10
3646 m), and tend to thicken upstream towards the mountain front and near the terminal
3647 moraines of outlet glaciers. In the Iberian foreland and among the Mediterranean basins in
3648 the east, the alluvial deposits almost always grade laterally to wash pediments covered by a
3649 thin mantle of colluvium. These low-gradient and typically concave slope systems become
3650 laterally quite extensive in soft-rock outcrops such as shale and molasse, where different
3651 generations of these pediments form staircase topography and where the valleys become
3652 correspondingly very wide (Barrère, 1975, 1981; Bomer, 1979; Peña, 1984; Stange et al.,
3653 2018). Such landscapes are typical of the Iberian drylands and the Maghreb. Apart from the
3654 Aude valley, no such landscapes exist in the Aquitaine Basin, where hillslope profiles are
3655 more typically convexo-concave and where colluvial deposits are thicker and were emplaced
3656 by solifluction and cryogenic transfer rather than by hillwash processes. This sharp contrast
3657 emphasizes the profound climatic differences between the pro- and retro-foreland
3658 environments, as well as the enduring continuity of the climatic differences — still prevalent
3659 today — throughout the Quaternary.

3660

3661 **5.1.2. Components of an alluvial chronology**

3662

3663 Several of the terraces — mainly the lower levels — connect directly with glacial moraines.
3664 Terrace T1, whether along the Garonne or the Ariège, contains numerous Pleistocene faunal
3665 remains, typically *Mammuthus primigenius* (Pouech, 1873; Harlé, 1893; Astre, 1928; Clot and
3666 Duranthon, 1990), a species that became extinct after the Magdalenian period; but also
3667 *Mammuthus trogontherii*, which is understood to have become extinct in the early
3668 Weichselian (Astre, 1967).

3669 The first radiometric ages produced in the Pyrenees with the aim of obtaining indirect
3670 constraints on the glaciation chronology were ¹⁴C ages from peat and lake levels adjacent to
3671 some terminal moraines. Results delivered an early Würmian age for these landforms as well
3672 as for alluvial deposits from generation T1 (Andrieu et al., 1988; Jalut et al., 1992). In the
3673 Roussillon Basin, the continuation offshore of these alluvial units also yielded early or middle
3674 ($\geq 35,000$ yr BP) to late Würmian ($18,300 \pm 750$ yr BP) radiocarbon ages (obtained from

3675 intraformational shell specimens; Monaco et al., 1972). Newer studies have, however,
3676 provided ages by direct dating of the alluvial materials, whether by Optically Stimulated
3677 Luminescence (OSL) (Lewis et al., 2009, 2017; Benito et al., 2010; García-Ruiz et al., 2013), by
3678 TCN burial dating (Stange et al., 2013b, 2014; Delmas et al., 2015, 2018; Nivière et al., 2016;
3679 Mouchéné et al., 2017b) or by Electron Spin Resonance (ESR) (Duval et al., 2015; Sancho et
3680 al., 2016; Delmas et al., 2018). Radiocarbon (Lewis et al., 2009) and palaeomagnetic dating
3681 (Sancho et al., 2016; Lewis et al., 2017) have also been attempted, but multi-method dating
3682 of alluvial terrace systems is otherwise still an all too rare endeavour.

3683 A Pyrenean-scale synthesis of alluvial chronostratigraphy was produced by Delmas et al.
3684 (2018). In the Iberian foreland, only the two uppermost levels are older than the Brunhes–
3685 Matuyama boundary, i.e., > 780 ka. The topmost alluvial deposits have been dated by ESR in
3686 the Cinca and Têt watersheds as 1.27 Ma and 1.1 Ma, respectively. These depositional ages
3687 are consistent with indirect estimates given by palaeobotanical assemblages for
3688 stratigraphically coeval deposits such as the Belin and Sadirac formations in the Landes (see
3689 Section 3.1.5.2), likewise for the proto-Garonne floodway (Dubreuilh et al., 1995) — and
3690 thus also for the upper units of the Lannemezan Formation (noted ‘Fu’ on French geological
3691 maps), which are distinguished by the exceptionally large calibre of their boulder beds (Icole,
3692 1968, 1969, 1973). In the extensional basins of the Mediterranean seaboard, T5 is inset in
3693 the the continental Pliocene wedge-top alluvial sequence. The 2–3 Ma age for the top of
3694 that sequence was determined on the basis of micromammalian assemblages (MN 15 and
3695 MN 16) contained in coeval alluvium trapped in karstic cavities among the limestone
3696 plateaus situated at identical elevations along the edge of the Roussillon Basin (Delmas et
3697 al., 2018).

3698 For the Middle Pleistocene, an ESR age of 817 ± 68 ka was obtained for TQ2 in the Alcanadre
3699 River valley (Duval et al., 2015). Existing TCN profiles have mostly provided minimum ages
3700 for the alluvial terraces (Delmas et al., 2018). Combined TCN and ESR ages obtained for
3701 generation T3 point to an age range between MIS 16 (terminates at 621 ka) and MIS 8
3702 (terminates at 243 ka) for the Têt, Ariège, and Garonne rivers, which is consistent with the
3703 abundance of Pebble culture or Acheulian artefacts collected from these terrace treads
3704 (Collina-Girard, 1976, 1986; Capdeville et al., 1997; Bruxelles et al., 2003; Martzluff, 2006;
3705 Mourre and Collonge, 2007; Hernandez et al., 2012). With a dozen OSL ages, two TCN
3706 vertical profiles, and two ESR ages, the most intensively dated generation of terraces in the

3707 Pyrenees are Level 5 of the Iberian foreland and its equivalent T2 ('Fx') on the French side. It
3708 has consistently yielded ages compatible with MIS 6 (terminates at 130 ka).
3709 During the recent Pleistocene, terrace sequence geometries in the Ebro Basin contrasted
3710 quite strongly with those of the other piedmonts. In Aquitaine, TCN profiles indicate that
3711 glacial valley train T1 aggraded continuously until the Last Glacial Maximum (LGM, 26–
3712 19 ka), perhaps extending into the Lateglacial. In Iberia, the last glacial cycle generated a
3713 sequence of 4 terraces along the left-bank tributaries of the Ebro River, with just the
3714 lowermost tread correlating with the LGM. Fluvial incision rates thus appear to have
3715 accelerated everywhere during the Middle Pleistocene, but more so in the Iberian foreland
3716 than in Aquitaine, probably because of comparatively larger magnitudes of regional crustal
3717 uplift in the Iberian foreland and the rest of the Iberian Plate.

3718

3719 **5.2. The impacts of glaciation**

3720

3721 Despite their southerly position (43–42° N), the Pyrenees were glaciated at every stage of
3722 the Pleistocene, and are still residually glaciated today. Contrary to other Mediterranean
3723 mountain ranges, where Quaternary glaciation usually produced localised glaciated core
3724 areas, the Pyrenean icefield during glacial maxima typically extended uninterrupted for 250
3725 km from the Capcir Basin in the east to the Pic d'Orhy in the west (Fig. 12). The spatial
3726 distribution of Pleistocene glaciers is now well established and has been synthesised and
3727 updated repeatedly (Penck, 1883, 1894; Taillefer, 1957, 1967, 1969; Hérail et al., 1987; Martí
3728 Bono and García Ruiz, 1994; Calvet, 2004; Barrère et al., 2009; Calvet et al., 2011).

3729 The spatial distribution of Quaternary glaciers was dictated by a combination of E–W and N–
3730 S climatic gradients. The N–S asymmetry is the sharpest, with the northern mountain front
3731 open to Atlantic influence and concentrating 75% of the glaciated surface area. The
3732 Pleistocene mean Equilibrium Line Altitude (ELA) lay between 1200 and 1600 m along the
3733 outermost mountain front, rising a little into the core of the Axial Zone (reconstruction from
3734 cirque-floor elevations). The tips of the largest outlet glaciers reached lowland altitudes of
3735 350 m (Ariège) and 450 m (Garonne), with glacier lengths attaining 43 km along the Gave
3736 d'Ossau, 53 km along the Gave de Pau, 79 km for the Garonne, 65 km for the Ariège, with
3737 maximum ice thicknesses in each case 0.8–1 km. Limiting factors of ice extent have been the
3738 narrowness of the Pyrenees and the dominance of transverse drainage (limited

3739 opportunities for confluent iceways). Transfluence cols between parallel valleys are
3740 uncommon (col de Lhers, col du Portillon) because of fairly ubiquitous supraglacial relief
3741 channelling ice in underfilled pre-existing valleys. The large ice accumulation on the north
3742 side of the range nonetheless contributed to spill over onto the southern side via a number
3743 of divide breaches, each situated at increasingly lower elevations from east to west and
3744 some of them late Neogene palaeovalleys (see Section 4.2.2.2) (Col de Puymorens: 1917 m;
3745 Port de Bonaigua: 2072 m; Pla de Beret: 1870 m; Col du Pourtalet: 1795 m; Col du Somport:
3746 1631 m). The only documented example of a reverse situation occurs around the Pico de
3747 Aneto, the highest summit of the Pyrenees, where several glacial diffluences benefited the
3748 Garonne.

3749 The Iberian pro-wedge contained comparatively shorter and thinner (400–600 m) valley
3750 glaciers, with outlet-glacier ice fronts terminating at elevations between 750 m and 940 m.
3751 Glacier lengths rarely exceeded 30 km (Aragón Subordan: 25 km; Aragón: 23 km; Gállego: 42
3752 km; Ara: 32 km; Cinca: 26 km; Pallaresa: 48 km; Esera: 34 km; Ribagorçana: 24 km; Valira: 31
3753 km). The Pallaresa and Valira trunk glaciers may have attained maximum lengths of 58 and
3754 39 km, respectively, probably aided by inputs from tributary valley glaciers feeding into the
3755 trunk valley during periods of maximum ice advance (Serrat et al., 1994; Turu et al., 2007;
3756 Turu, 2011; Turu et al., 2011, 2017). On the Iberian side, the ELA rises rapidly southward to
3757 elevations above 2100–2200 m in the outermost massifs of the Axial Zone and Sierras
3758 Interiores, and to even higher altitudes in the case of south-facing slopes.

3759 The E–W climatic gradient along the range is gradual. The icefield was more fragmented in
3760 the east as a combined result of diminishing Atlantic moisture advection from the west, and
3761 of the increase in aggregate sunshine hours under Mediterranean influence. Among the
3762 outlet glaciers along the northern mountain front, only the Gave de Pau at Lourdes and Gave
3763 d'Ossau at Arudy formed piedmont glacier lobes. The ELA was particularly low in the Basque
3764 Country (1100–1200 m; Viers, 1960), a fact confirmed by small glacial cirques on east- and
3765 north-facing summits as low as 1300 and 1500 m (e.g., Autza, 1304 m), and even
3766 occasionally on south-facing slopes (e.g., Oranzurieta, 1570 m). From there, the ELA rose
3767 progressively towards the central Pyrenees (Barrère, 1954, 1963), where it maintained itself
3768 around 1300–1400 m among the outermost massifs as far east as the Ariège, whether on
3769 north-facing or on south-facing slopes (in the latter case by virtue of disproportionate
3770 supplies of windblown snow from the NW, as for example in the Arize massif). The ELA

3771 attains 1600 m in the upper catchments of the Hers, Aude and Boulzane (Dourmidou massif),
3772 i.e., ~60 km from the Mediterranean coast. In the eastern Pyrenees, (i) greater
3773 fragmentation of relief resulting from the Neogene extensional tectonics and (ii) relative
3774 aridity of the sheltered intermontane basins have conspired to a confinement of glaciation
3775 to the most elevated massifs of the Axial Zone. Here the ELA is situated between 2000 and
3776 2300 m, the valley glaciers were short (among the longest, the Têt: 18 km, and the Querol:
3777 25 km) and never extended below the 1000–1500 m elevation belt. At these easterly
3778 longitudes, the icefield was often little more than a population of cirque glaciers.
3779 Quaternary climatic contrasts in the palaeoglaciology of the Pyrenees were merely an
3780 exaggerated version of present-day climatic contrasts, also reflected in the pattern of the
3781 modern winter snowline. It can thus be safely inferred that average climatic conditions and
3782 average atmospheric circulation patterns in the region have remained similar throughout the
3783 Quaternary (Barrère, 1954; Taillefer, 1982; Calvet, 1996). These conditions include: (i)
3784 permanent air flow from the W to NW, bringing snow but also favouring its local
3785 redistribution over ridgetops and thereby supplying east- and even south-facing cirques
3786 (e.g., Crest et al., 2017); (ii) the interference of Mediterranean air flow from the southeast,
3787 which is also a source of abundant snowfall in present-day conditions in the eastern part of
3788 the range; and (iii) the considerably greater dryness and warmth of the southern and eastern
3789 Pyrenees — with negative consequences on the thermal budget of glaciers in those areas.
3790 It would be spurious to overstate the geomorphological legacy of Quaternary glaciation on
3791 Pyrenean landscapes and slope systems. The glacial imprint is strongest in the cirque belt
3792 (Crest et al., 2017), which in some massifs displays characteristic arêtes and a few pyramidal
3793 peaks. In the eastern Pyrenees, however, the limited erosive power of the Pleistocene
3794 glaciers has, for example, failed to eradicate the erosion surfaces, and indeed even the very
3795 deep mantles of saprolite which, at many places, cover these elevated residuals of Neogene
3796 topography (Delmas et al., 2009). Farther west, a number of valleys include areas that
3797 underwent between 230 and 400 m of glacial overdeepening (e.g., Gave de Pau and
3798 Garonne, based on gravimetric surveys; Perrouty et al., 2015), and up to 100 m in the Ariège
3799 valley at Ussat (borehole evidence from BRGM–Banque du Sous-Sol). On the pro-wedge,
3800 overdeepened valley sections likewise attain ~400 m at Estèrri d’Aneu (Noguera Pallaresa),
3801 300 m at Benasque (Ésera valley), 200 m at Bono and 160 m at Barruera (Noguera
3802 Ribagorçana; Bordonau, 1992), 80 m in Andorre (Valira valley), and 160 m at Biescas (Gállego

3803 valley; Turu et al., 2007). Overall, however, most of the larger valleys exhibit large bedrock
3804 steps, e.g., along the Ariège at Tarascon and Les Cabannes. None of the wider glacial troughs
3805 are calibrated to a characteristic U shape, and V-shaped gorge sections are frequent and
3806 even include entrenched fluvial meanders (such as between Ax-les-Thermes and Mérens on
3807 the Ariège). This relatively light erosional imprint of warm-based glaciers also explains the
3808 indecision among scholars as to the true terminal positions of valley glaciers in some V-
3809 shaped valleys such as the Noguera Pallaresa, Cinca, Valira, and Salat.

3810 Rare estimates of catchment-wide glacial denudation during the last glacial cycle have been
3811 obtained by calculating the density-corrected volume of glacial sediments contained in
3812 glacial accumulation zones. For the short Têt glacier (18 km), mean Würmian (Late
3813 Pleistocene) denudation depths did not exceed 5 m (mean denudation rate of 0.05 mm/yr)
3814 — a low value compatible with the good state of preservation of pre-glacial erosion surfaces
3815 and their regolith in that area (Delmas et al., 2009). Based on sediment volumes trapped in
3816 valley-floor rock basins along the Gave de Pau and the Garonne (Perrouy et al., 2015),
3817 bedrock denudation during the last 30 ka (i.e., since the onset of ice retreat from its terminal
3818 positions) can be calculated after density correction and produces rates of ~0.08 mm/yr and
3819 ~0.05 mm/yr, respectively. Based on TCN nuclide concentrations contained in glacially
3820 polished bedrock-step surfaces among the cirques of three massifs in the Axial Zone
3821 (Maladeta, Bassiès, Carlit), Crest et al. (2017) demonstrated that glacial denudation in the
3822 cirques was weaker under icefield conditions during the Würm (1–30 mm/kyr, because the
3823 ELA was situated much lower down in the valleys) than under residual (but steep and
3824 erosive) cirque-glacier conditions in the widely deglaciated environments of the Younger
3825 Dryas and the Holocene (tens to hundreds of mm/kyr). TCN data from supraglacial ridges,
3826 meanwhile, document erosion rates of 10–30 mm/kyr during the last 15 to 60 ka. Würm-
3827 averaged denudation ratios between cirque floors and ridgetops thus suggest that they
3828 underwent similar rates of downwearing, but that cirque glaciers during short time windows
3829 and under certain specific conditions are far from negligible geomorphic agencies.

3830

3831 **6. Synthesis and discussion: issues resolved and unresolved**

3832

3833 From the late Cretaceous to the present, the Pyrenees as a mountain range rising between
3834 Europe and Iberia went through three successive and definable states: the Proto-Pyrenees,
3835 the Ancestral Pyrenees, and the Modern Pyrenees. Throughout this 84 m.y. period, the
3836 mountain range changed in length, width, relief and elevation. Clearly, portrayals of those
3837 successive incarnations become more precise for recent geological time as a richer catalogue
3838 of indicators becomes available to direct field observation, including landforms and
3839 superficial deposits. The oldest landforms of value are the erosion surfaces preserved from
3840 the late stages of the Ancestral Pyrenees. Uncertainty nonetheless still hangs over a number
3841 of issues, which we present and discuss in this synoptic overview which can be followed by
3842 inspecting Plate I.

3843

3844 **6.1. The Proto-Pyrenees**

3845

3846 Folded structures detected as far west as the Basque Country began to develop after ~84
3847 Ma, but at the end of the Cretaceous the resulting mountain range, or Proto-Pyrenees,
3848 formed only in the eastern third of today's Pyrenean range and extended farther east into
3849 the area now occupied by the Gulf of Lion. The west-central and western Pyrenees did not
3850 exist as a mountain range at the time, i.e., rather only as a belt of crustal deformation (Plate
3851 I, panel A). The Garumnian continental sequence is a late- to post-tectonic molasse (only a
3852 few growth strata indicating mild deformation), and as such is the product of these eroding
3853 Proto-Pyrenees but also of eroding topography in the southeast (e.g., Montseny; Gómez-
3854 Gras et al., 2016) and potentially in Corsica and Sardinia (Odlum et al., 2019). Outcrops of
3855 Garumnian molasse have been preserved north of the Proto-Pyrenees in the Corbières, and
3856 south between Tremp and the Llobregat River valley (Plaziat, 1981, 1984; Rosell et al., 2001).
3857 High-energy denudation ca. 78 Ma, probably driven by high relief, has been inferred from
3858 fission-track evidence in U–Pb-dated detrital zircons in the Iberian foreland sequences
3859 (Whitchurch et al., 2011), and likewise between 80 and 68 Ma from AHe ages on detrital
3860 zircon crystals (Filleaudeau et al., 2011). This record of rapid denudation has been confirmed
3861 by late-Cretaceous to Paleocene zircon FT cooling ages in bedrock in the NE Axial Zone and
3862 North-Pyrenean Zone (Yelland, 1991) and ZHe cooling ages (Ternois et al., 2019). Denudation
3863 of the Proto-Pyrenees was sufficiently advanced by early Paleogene time that part of the
3864 orogen became drowned by sea-level rise and covered by an early Ypresian (i.e., Ilerdian:

3865 ~56–52 Ma) carbonate platform and by shale. A fission-track age of 81 Ma, however, was
3866 also obtained from the Ursuya Massif (Basque Country) (Yelland, 1991), and is associated
3867 with comparatively ancient AHe ages (Vacherat et al., 2014). This evidence could indicate
3868 higher topography farther west during the Garumnian episode than previously believed.
3869 Continuing research may provide new resolution to the Basque and Catabrian palaeorelief
3870 and denudation histories of that period (DeFelipe et al., 2019). The fate of the eastern Proto-
3871 Pyrenees remains largely speculative (Jolivet et al., 2020), but the extended period of
3872 tectonic quiescence reported in the literature between 68 and 56 Ma, the abundance of
3873 lacustrine limestone in the Garumnian molasse, and the Ilerdian marine transgression (Plate
3874 I, panel B) over much of the region suggest that the Proto-Pyrenees had by that time
3875 attained a residual state of relative low-elevation and low-relief topography.

3876

3877 **6.2. The Ancestral Pyrenees**

3878

3879 *6.2.1. Growth of the mountain range from east to west*

3880

3881 The Pyrenees grew westward during the Eocene as a consequence of continuing tectonic
3882 inversion from east to west of the Cretaceous and early Eocene flysch-filled pro- and retro-
3883 foredeeps (Plate I, panels B, C, D). Still by the end of Lutetian time, the emergent successor
3884 mountain range, i.e., the Ancestral Pyrenees, did not extend westward beyond the Pic d’Anie
3885 (0°43’ W). Denudation of the thickening crust supplied thick range-front megafans. The
3886 debris were delivered in a terrestrial environment to the retro-foreland (Palassou
3887 sequences) and in a deltaic environment to the pro-foreland (Plate I, panel C). Crustal
3888 denudation of the Axial Zone resulted in part from the north- and southward transport of its
3889 sedimentary cover nappes, but also from fluvial erosion. The Hercynian basement core of
3890 the orogen only gained widespread exposure during the Bartonian, after which time the
3891 delivery of granite and gneiss pebbles to the piedmonts occurred regularly, often in periodic
3892 pulses, from the basement window. The Ancestral Pyrenees appear to have peaked (peak
3893 energy, peak topography) from the Priabonian to the Oligocene, at a time when the Ebro
3894 Basin was also entering its ~25 million-year period of internally-drained confinement and
3895 when the mountain-front fan systems on both sides of the orogen became ubiquitous (Plate
3896 I, panels D, E). The western Basque termination of the orogen is unique in having remained

3897 marine to this day. Low-temperature thermochronology evidence from crystalline basement
3898 rocks in the Axial Zone, from its satellite massifs, as well as from the conglomerate
3899 sequences of the pro-foreland, provides a consistent picture of accelerated denudation
3900 beginning ca. 50 Ma and peaking around 35–30 Ma (e.g., cooling-inferred denudation rates
3901 of up to 1–3 km/Ma between ~35 and 30 Ma in the Maladeta massif; Fitzgerald et al., 1999;
3902 Sinclair et al., 2005; Gibson et al., 2007). Denudation also appears to have been spatially
3903 nonuniform, progressing from east to west but mostly from north to south (Whitchurch et
3904 al., 2011).

3905 The classic model of the central Pyrenees as a high-amplitude antiformal duplex structure
3906 (Muñoz, 1992; Vergés et al., 1995) — implying ~20 km of crustal denudation in the Axial
3907 Zone in order to attain the current outcrop pattern — has been substantially reconsidered
3908 here on the basis of new interpretations of Hercynian and Alpine structures and their tectonic
3909 geometries (Soler et al., 1998; Laumonier, 2015; Angrand, 2017; Cochelin et al., 2018; Teixell
3910 et al., 2018; Espurt et al., 2019; Ternois et al., 2019). The Hercynian structures of the Axial
3911 Zone are only weakly offset by the putative décollement of the ‘Nogueres’ Thrust (see Fig.
3912 3), and the magnitudes and timing of crustal denudation in the Axial Zone to the north
3913 (Marimanya–Artiès massif) and south (Maladeta massif) of that crustal discontinuity are
3914 identical (see Cochelin et al., 2018, after Fitzgerald et al., 1999, Sinclair et al., 2005, and
3915 Gibson et al., 2007). ZFT results also confirm that denudation depths were not as extreme as
3916 initially postulated, as shown for example by many zircon grains having retained the
3917 signature of Mesozoic extension in the North-Pyrenean (Vacherat et al., 2016) and Axial
3918 zones (Yelland, 1991; Sinclair et al., 2005). Detrital zircons from Paleogene molasse
3919 sequences in the Ebro Basin convey a similar message, with only 17% of the 842 grain ages
3920 reviewed by Whitchurch et al. (2011) recording a ZFT age compatible with the collisional
3921 stages of the Pyrenean orogeny. Erosional denudation did thus probably not exceed depths
3922 corresponding to the total resetting of the zircon FT clock, e.g., 7–10 km when assuming an
3923 average geothermal gradient of 25–30 °C/km (Whitchurch et al., 2011).

3924 The evidence for reconstructing the elevation, relief and morphology of the Ancestral
3925 Pyrenees is very limited. The Paleogene mountain range was narrower than its modern
3926 successor, and the fold belts of the retro-wedge were mostly buried beneath the debris of
3927 the Aquitaine piedmont. The pro-wedge was likewise drowned by unconformable
3928 conglomerate sequences, locally backfilling all the way up to the edge of the Axial Zone in

3929 one atypical region (Nogueres) of the south-central pro-wedge. Flexural modelling of the
3930 Ebro Basin has produced maximum palaeoaltitude estimates in middle Lutetian time of 2000
3931 \pm 460 m for the mountain range (Millán et al., 1995), with mean and maximum
3932 palaeotopographic values estimated as 1.5 and 3.5 km, respectively, during the Oligocene
3933 orogenic climax (Curry et al., 2019). Other work has used oxygen isotope ratios in Eocene
3934 oyster shells sampled from the Ebro Basin. By comparing the $\delta^{18}\text{O}$ ratios with those
3935 measured in a reference set of similar-aged mollusc shells from the Paris Basin, Huyghe et al.
3936 (2012) inferred a magnitude of Pyrenean uplift of 2000 ± 500 m between 50 and 41 Ma. The
3937 palaeoaltimetric calibration fails to be valid past the late Bartonian.

3938

3939 *6.2.2. Correlation between conglomerate sequences of the pro- and retro-forelands*

3940

3941 Beyond these first-order similarities between the pro- and retro-wedges in the Ancestral
3942 Pyrenees, some uncertainty remains over the finer detail of the foreland and retro-foreland
3943 geological records. For example, no correspondence has ever been established between the
3944 four generations of Palassou clastic pulses, which were given a uniform name by French
3945 geologists and are now correlated with their Jurançon analogues, and the conglomeratic
3946 sequences of the Iberian side, which have received a collection of local names in the
3947 literature (Fig. 5). From east to west along the strike of the Ebro Basin, we suggest the
3948 following chronostratigraphic correlations:

3949

- 3950 (i) Palassou 1 could be an equivalent of at least part of the Bellmunt formation in the east,
3951 the Queralt conglomerates at Berga, and of the Campanue Formation further west;
- 3952 (ii) Palassou 2 could match the Milany sequence and upper part of the Bellmunt formation
3953 in the east, the basal beds of the unconformable Nogueres sequence (Pessonada unit),
3954 the lower part of the Escanilla Formation, and still further west the Sabiñanigo deltaic
3955 sandstones, whose proximal conglomeratic facies has an unidentified provenance (its
3956 source area could be the Escanilla Fm. in the east; if correct, this would confirm that no
3957 mountainous relief shedding clastic debris yet existed at that longitude to the north);
- 3958 (iii) Palassou 3 could correspond to the lower levels of the Berga sequence in the east, to the
3959 Serrat Negre–Catllaras conglomerates and middle levels of the Nogueres sequence in the

3960 central pro-foreland, and to the lower part of the Campodarbe Formation further west
3961 (Escanilla and Santa Orosia conglomerate beds);
3962 (iv) Palassou 4 could correlate with all of the younger remaining Oligocene conglomerate
3963 beds of the pro-wedge mountain front.

3964
3965 These correlations are inevitably tentative because the tectonic regime of the Ancestral
3966 Pyrenees was unsteady, spatially nonuniform, and diachronous given the evident polarity of
3967 crustal deformation from east to west and asymmetrical vergence from north to south (Fig.
3968 2). The more striking asymmetry between the pro and retro basins lies in the cumulative
3969 thickness of the proximal conglomeratic sequences, which turn out to be considerably
3970 greater in the Iberian foreland. This imbalance, however, may be more apparent than real
3971 for several reasons: (i) the pro-wedge watersheds were larger than their retro-wedge
3972 counterparts, thus with more potential for sediment delivery; (ii) in the Aquitaine Basin, the
3973 Paleogene rivers were afforded uninterrupted opportunities to export at least their finer
3974 clastic loads to the Atlantic, whereas the Ebro Basin was denied opportunities of sediment
3975 bypass for 25 m.y. after the Priabonian; (iii) the outward growth of the orogenic wedge
3976 during the Paleogene was much more extensive on the south side of the orogen (e.g.,
3977 producing the SPCU and the Guarga Unit), with the resulting crustal thickening thus
3978 promoting greater opportunities for denudation and for peripheral lithospheric flexure to
3979 accommodate greater depositional thicknesses; (iv) the northern piedmont has undergone
3980 limited uplift and the Paleogene conglomerate sequences accordingly feature few good
3981 exposures, whereas the southern piedmont has risen to 1500–2000 m and been deeply
3982 incised, thereby affording an exceptionally rich display of outcrops and stratigraphic
3983 sections.

3984 Given that the Cenozoic conglomerate sequences are continental, resorting to the ELMA
3985 scale is both inevitable and necessary, but progress on the chronostratigraphy of Paleogene
3986 and Neogene clastic sequences would gain from continued efforts towards narrowing the
3987 gaps and discrepancies sporadically apparent between the ELMA scale (Vandenberghé et al.,
3988 2012; Hilgen et al., 2012) and the magnetostratigraphic scale, particularly when uncertainty
3989 envelopes surrounding age constraints are not systematically reported. Although not
3990 exceedingly large, discrepancies appear most acute in parts of the Ebro Basin, which overall

3991 nonetheless benefits from an unusually continuous magnetostratigraphic record (e.g.,
3992 Beamud et al., 2003, 2011; Garcés et al., 2020) compared to the other Pyrenean
3993 depocentres.

3994

3995 *6.2.3. Topographic decline of the Ancestral Pyrenees*

3996

3997 Crustal convergence, which intensified from east to west during the Eocene, ceased fairly
3998 abruptly in the east in Chattian time, after which back-arc extension began to open the
3999 Western Mediterranean (Plate I, panels E, F). AFT and ZFT data from the Canigou–Carançà
4000 and Albères massifs record the early Oligocene to Miocene rifting event quite clearly
4001 (Maurel, 2003; Maurel et al., 2002, 2008), but it remains difficult elsewhere in the eastern
4002 Pyrenees to attribute any of the Oligocene cooling ages unequivocally to rifting rather than
4003 to the final stages of collision.

4004 Meanwhile, compressional tectonics continued in the western half of the Ancestral Pyrenees
4005 at least until early Burdigalian time, and perhaps as late as Langhian time according to
4006 Huyghe et al. (2009). Thermochronological data in the western part of the Axial Zone
4007 document this episode of uplift and erosion, particularly on the south side with some AFT
4008 ages spanning the Aquitanian to the middle Miocene (Jolivet et al., 2007; Bosch et al.,
4009 2016b). The most salient paradox in this part of the orogen is the absence on its north side
4010 of an equivalent of the synorogenic, early Miocene Huesca and Luna megafans (Plate I, panel
4011 G), at least given that the age of the Jurançon conglomerates has now been revised and
4012 assigned to the Paleogene. The cause of the asymmetry lies perhaps in the southward
4013 vergence of tectonic deformation during these late stages of crustal convergence. Folding in
4014 the Sierras Exteriores, in particular, was promoted by the progression of the youngest and
4015 outermost thrust sheets, i.e., the Bielsa and (further south) the Guarga thrusts. Resulting
4016 folds in the poorly consolidated sediments of the Jaca Basin display a total structural
4017 amplitude of ~2 km (e.g., the Santo Domingo and the Yebra de Basa anticlines). Such high
4018 structural relief associated with lithologies that are quite susceptible to erosion is unique to
4019 the south side of the orogen, and the resulting erosion has generated a large proportion of
4020 the Huesca conglomerate sequences (i.e., the Aquitanian to Burdigalian Uncastillo and
4021 Sariñena formations) (Puigdefábregas and Soler, 1973; Teixell and Garcia-Sanseguendo, 1995;
4022 Jolivet et al., 2007; Huyghe et al., 2009; Bosch et al., 2016b). Meanwhile, clastic output to

4023 the retro-foreland, where tectonic activity was less intense, was comparatively finer-
4024 textured and thus more readily exported to the deep ocean through the Bélus–Saubrigues
4025 palaeocanyon, which was functional at that time.

4026

4027 *6.2.4. The summit erosion surfaces of the Ancestral Pyrenees: resolved and unresolved issues*

4028

4029 The summit erosion surfaces are the most ancient landforms of the present landscape and
4030 record a period of low energy that prevailed at the time of transition between the Ancestral
4031 and the Modern Pyrenees. When compared with a large number of other ranges around the
4032 world, these low-gradient land surfaces are far from unique features (Calvet et al., 2015a),
4033 and the list of arguments concerning their age and origin presented in Section 4.1.3 supports
4034 a parsimonious explanation emphasizing regional base-level controls. The view that these
4035 elevated erosion surfaces in the Axial Zone, and the former depositional surfaces of the
4036 Noguères or Palassou conglomerates in each of the piedmont zones, at one time formed a
4037 coeval and cogenetic low-gradient continuum is challenged by the fact that deformed
4038 structures in the conglomerate units are themselves cross-cut by low-gradient erosion
4039 surfaces. The erosion surfaces are thus younger than the youngest conglomerate deposits.
4040 The altiplanation theory inspired by sandbox models (Babault et al., 2005b, 2007; Bosch et
4041 al., 2016a) is therefore unsupported by primary field evidence.

4042 Unresolved issues include the multiplicity of erosion surfaces and their possible diachronous
4043 development across the orogen (Fig. 11). This is *prima facie* the logical consequence of
4044 diachronous tectonic deformation from east to west, with compressional tectonics still
4045 prevalent during the early Miocene in the west whereas rifting had started in mid Oligocene
4046 time in the east. The widespread mountain-top surface, S, was produced in the east
4047 between the late Oligocene and the Aquitanian (Plate I, panel F), a time frame also
4048 consistent with the approximately simultaneous aggradation of abundant carbonate facies
4049 across all three piedmont areas of the Pyrenees. This consistent pattern would suggest low
4050 turbidity levels because of diminished terrigenous influx from a tectonically active orogen
4051 rather than exclusively a palaeoclimatic signal. Partial planation surface P1 spared a number
4052 of large residual massifs and grades very clearly to middle Miocene marine strandlines in the
4053 Corbières and Languedoc (Plate I, panel H), suggesting a simultaneous relative lull in crustal
4054 deformation at the time of the Langhian highstand.

4055 Uncertainty over these scenarios increases farther west. Among the three conceptual
4056 models summarised in Fig. 11, scenario A is improbable given that the clastic record in the
4057 western pro- and retro-foreland basins contains no evidence of declining energy in the
4058 sedimentary systems: supply of coarse-textured synorogenic sequences was uninterrupted
4059 from Priabonian to Chattian time included, and even extended into the Aquitanian according
4060 to the new ages (22 Ma) obtained by Roigé et al. (2019) for the Campodarbe Group
4061 conglomerates of La Peña. Scenario B postulates diachronous peneplanation of the Pyrenees
4062 from east to west. Its main weakness is that it implies minimal mountainous relief at a peak
4063 time of evaporite accumulation in the Ebro Basin. Although it could explain the development
4064 of thick lacustrine limestone in the last stages of internal drainage in the Ebro Basin (see
4065 Section 3.2.6; Vázquez Urbez et al., 2013; Pérez Rivarés et al., 2018) and the return to
4066 externally-drained conditions after ~10 Ma, it fails to justify how such extreme aridity could
4067 prevail at < 100 km from the Atlantic Ocean without shelter from a mountain barrier. By
4068 reference, however, to the sharp contrast in mean annual precipitation observed today
4069 across the continental dividing ranges of the Basque Country, whose summits do not exceed
4070 1400–1500 m, it would seem nonetheless that an Ancestral Pyrenean mountain range
4071 attaining maximum elevations of ~1400 m among its residual massifs would have been
4072 sufficient to shelter the Ebro basin from Atlantic humidity — as advocated by scenario C in
4073 Figure 11.

4074 Scenario C admits the possibility that the Pyrenees were never substantially levelled other
4075 than in the east. Only partial planation surfaces (i.e., pediments) analogous to P1 formed
4076 around the edges of the pro- and retro-wedges, as well as as in the Basque Country
4077 (compare Plate I panels F, G and H). This scenario is tentatively the most realistic because in
4078 keeping with the chronology of tectonic deformation and the chronostratigraphy of the
4079 foreland conglomerate sequences. It concurs with the preservation of the crustal root west
4080 of Andorra, whose ongoing erosion / removal (by debated processes, see Section 2.4)
4081 appears to have only recently begun (Dufréhou et al., 2018). It is also consistent with the
4082 necessity for a sharp climatic contrast between the humid north and arid south sides of the
4083 mountain range to have been upheld from the Paleogene through to the middle Miocene.
4084 The absence of coarse clastic Miocene sequences in the Aquitaine foreland does not,
4085 however, militate in favour of a high-relief mountain range in the hinterland at the time.
4086 Likewise, although thermochronology is an insufficiently sensitive tool for discriminating

4087 between scenarios A, B and C given that (for example) cooling ages obtained from sampling
4088 sites on surfaces S and P1 are usually indistinguishable, the widespread documentation of a
4089 thermal plateau in Pyrenean rock cooling curves (Section 4.1.3.1, Fig. 10C) after 30 or 20 Ma
4090 does not militate in favour of intense denudation occurring in the Axial Zone during the
4091 Miocene. Limited relief still remains the best candidate for explaining this situation, with
4092 low-gradient erosion surfaces forming at elevations of ~800 m or less in connection with one
4093 or several among the three base levels of the orogen.

4094

4095 **6.3. Shaping of the Modern Pyrenees**

4096

4097 The multiple and abrupt breaks in the geological record around and after 10 Ma in all three
4098 piedmont environments of the orogenic wedge (Aquitaine, Mediterranean, Ebro) turned a
4099 definitive page in the history of the Paleogene mountain range, or Ancestral Pyrenees. The
4100 orogen thereafter entered the age of the modern mountain range as we observe it today.

4101 The characteristics of these successor Pyrenees (i.e., Modern, post-shortening) were
4102 heralded by major changes in the geodynamic regime, involving:

- 4103 (i) a relaxation of Cenozoic crustal convergence intensity;
- 4104 (ii) a return to external drainage in the Ebro Basin;
- 4105 (iii) the opening of new extensional basins far into the Axial Zone, i.e., in locations
4106 progressively more remote from the Mediterranean back-arc basin;
- 4107 (iv) the occurrence of volcanic activity in the eastern part of the mountain belt;
- 4108 (v) a symmetrical interruption in the depositional stratigraphy not just of the Ebro Basin
4109 (which became exorheic after ~10 Ma), but also of the Aquitaine Basin (major
4110 ravinement surface beneath the Lannemezan megafan and its coeval analogues
4111 along the strike of the mountain range: Ger, Salat, etc.);
- 4112 (vi) the conveyance of increasingly coarser clastic debris to actively subsiding basins
4113 (Turolian fill of the Cerdagne, Empordà and Vallés; Pliocene fill of the Roussillon and
4114 Empordà; Lannemezan megafan and its analogues); and lastly
- 4115 (vii) the construction of increasingly voluminous siliclastic wedges on the continental
4116 shelves of the Aquitaine, Valencia, and Gulf of Lion marine domains.

4117 The pull-apart tectonics prevalent during the Oligocene and Miocene in the eastern
4118 Pyrenees (Plate I, panels E, F, G, I) progressively gave way to regional uplift of the Pyrenees,
4119 elevating the surfaces S and P1 to maxima of 2900 m (e.g., in the Campcardos massif); and
4120 likewise raising their younger successor population P2, such as the Plateau de la Perche
4121 pediment (eastern Pyrenees) or the Pla de Beret palaeovalley (central Pyrenees), to altitudes
4122 exceeding 1500 m. This late regional uplift (Plate I, panels J, K) caused extremely rapid
4123 incision of V-shaped valleys during the latest Pliocene and Quaternary. At locations where
4124 glaciation has failed to alter valley longitudinal profiles, some large fluvial knickpoints have
4125 been preserved such as on the Têt River near Mont-Louis, on the Segre River at Martinet,
4126 and on the Aude at Escouloubre — thereby preserving some expanses of unrejuvenated,
4127 pre-Quaternary landscape upstream of these knickzones (Figs. 6, 14D).

4128 The geologically recent (and successive stages of) post-shortening surface uplift of the
4129 Pyrenees by perhaps up to 2 km is documented not just indirectly by the erosion surfaces,
4130 which considered on their own could give rise to circular arguments, but additionally by a
4131 range of independent clues:

- 4132 (i) the substantial increase in volume and clast size of terrigenous inputs to the
4133 piedmonts and offshore sequences (particularly the Zanclean of the Roussillon and the
4134 Turolian of Cerdagne), which occurred prior to the major climatic downturns of the
4135 Pleistocene and therefore cannot systematically be attributed to climatic drivers;
- 4136 (ii) the deformation, tilting, and normal, inverse or strike-slip faulting recorded in all
4137 sedimentary sequences of late Miocene to late Quaternary age, thus testifying to
4138 crustal instability caused by more than just an isostatic response to erosional
4139 unloading (Vernant et al., 2013; Genti, 2015) (given that extensional faulting can also
4140 result from gravitational slope tectonics, reverse and strike-slip faulting are deemed
4141 comparatively more robust indices of neotectonic activity, but of course do not rule
4142 out normal faulting);
- 4143 (iii) the geometry of successions of Quaternary alluvial terraces, whose relative vertical
4144 offsets increase upstream towards the mountain fronts and into the mountain range
4145 (Delmas et al., 2018) but converge and merge as they approach their regional base
4146 levels where subsidence has persisted;
- 4147 (iv) the vertical distribution of fossil cave levels on canyon walls and phreatic or
4148 epiphreatic galleries (and even water-table rivers) in limestone massifs, which

4149 provide a more robust record of uplift-driven valley incision than fluvial terraces
4150 because, under a solution-limited regime, equilibrium profiles in limestone are
4151 attained after a very short time and produce very low gradients (Calvet et al., 2015b);
4152 (v) the fossil warmth-loving plant assemblages in the Cerdagne and Pruëdo
4153 intermontane basin fills, which imply very low elevations in the Axial Zone during
4154 Vallesian and Turolian time and subsequent uplift of those basin floors by 1000 to
4155 1500 m, i.e., to modern elevations now incompatible with the environmental
4156 requirements of these taxa (Suc et al., 2012; Ortuño et al., 2013). Other
4157 palaeoaltimetric data for the Cerdagne Basin in the eastern Pyrenees also confirm at
4158 least 500 m of late Neogene uplift in the Axial Zone (Huyghe et al., 2020).

4159 Transpression or transtension relating to the Africa–Iberia–Europe convergence and to
4160 Mediterranean extension appear to have played a subsidiary and progressively declining role
4161 in the rise of the Modern Pyrenees. Uplift, which has impacted not just the mountain range
4162 but also its foreland basins and perhaps the entire Iberian Plate, and likewise the Massif
4163 Central (Macles et al., 2020) is now attributed to subcrustal and sublithospheric processes
4164 driven by boundary conditions that are only partly related to the intrinsic metabolism of an
4165 orogenic crustal wedge (see Section 2.4 and Section 4.2.1.1; Pous et al., 1995a, 1995b, Lewis
4166 et al., 2000; Barruol et al., 2002, 2004; Gunnell et al., 2008, 2009; Boschi et al., 2010; Casas-
4167 Sainz et al., 2009; Chevrot et al., 2014, 2015, 2018; Dufréchoux et al., 2018; Wehr et al.,
4168 2018; Conway-Jones et al., 2019; Ortiz et al., 2020; Jolivet et al., 2020). Still unexplained is
4169 the apparent acceleration of the uplift and its unsteady regime, illustrated for example by
4170 the contrast between generation P2 of wide pediments penetrating deep into parts of the
4171 orogen, and the abrupt vertical incision of these planar landforms by the deep, often V-
4172 shaped, younger valleys.

4173

4174 **7. Conclusion and outlook**

4175

4176 The Pyrenean orogen is commonly presented in cuts and slices of space or time. This beef-
4177 butcher-diagram approach to Earth science is inevitably part of the naming and classification
4178 process of naturalistic endeavour. Ramond de Carbonnières (see Introduction) had forecast
4179 the Pyrenees to be a fairly simple model of mountain range, and sure enough: in modern

4180 textbooks the Pyrenees have been erected as a reference model of how the subduction of
4181 the lower crust and lithospheric mantle of one plate beneath another produces an
4182 asymmetric, doubly vergent collisional orogen. Structural style in the Pyrenees was strongly
4183 controlled by architectural differences along strike in the early Cretaceous rift and in the
4184 Hercynian basement, but the most prominent signature of the orogen has been showcased
4185 in the geological literature as its south-vergent duplex structure composed of imbricate
4186 thrust sheets of Hercynian basement and forming an almost round-arched antiform (Fig. 3B).
4187 As shown in this review, such an interpretation of the south-vergent Pyrenean nappe
4188 structure leaves room for an alternative model involving a Supra-Axial Thrust overspanning
4189 the Axial Zone and displaying architecturally a much more elliptical intrados, thus rather
4190 resembling a three-centered or round-rampant arch (Fig. 3C).
4191 Other narratives have been nurtured in which local features have been extrapolated and
4192 held valid for the rest of the orogen: e.g., the implicit view that Ebro Basin overfilling can
4193 explain the erosional response of the entire mountain range in the Cenozoic regardless of
4194 features and events in the Aquitaine Basin or the Mediterranean; or consideration that the
4195 history of the Pyrenees ended with the end of compressional deformation, i.e., in the
4196 earliest Miocene, and that the following 25 Ma were essentially a footnote to the orogen's
4197 history — the main key event being the reconnection of the Ebro Basin to the
4198 Mediterranean and the ensuing downcutting of fluvial valleys in a orogenic edifice (the
4199 Ancestral Pyrenees) that was generated during the Paleogene and somehow succeeded in
4200 maintaining steady topographic characteristics thereafter. Conversely, other issues have been
4201 overlooked or sidestepped despite being essential to a full understanding of Pyrenean
4202 evolution: for example, what exactly are the architecture and history of the Eocene Iberian
4203 foredeep in relation to the SPCU? Why have Miocene continental deposits been abundantly
4204 mapped in Aragon but not in Catalonia? The most likely answer is that none were deposited
4205 in the Catalanian part of the Ebro Basin, but the eastern boundary of existing deposits of
4206 that age between the Cinca and Noguera rivers does not provide consistent information
4207 among existing geological maps. Why do the early Miocene conglomerate sequences of the
4208 Ebro foreland display no substantial equivalent in the Aquitaine retroforeland? The primary
4209 reason is the greater preservation potential of the internally-drained Ebro Basin, whereas a
4210 proportion of sediment was exported out of the Aquitaine Basin via the Saubrigues
4211 palaeocanyon; but this falls short of explaining the absence of coarse terrigenous deposits of

4212 Miocene age in the Aquitaine retroforeland. Why have chronostratigraphic correlations
4213 between the pro- and retroforeland conglomerate sequences never been attempted? Why
4214 have the widespread erosion surfaces, some of which were reported or mapped nearly 100
4215 years ago and provide diagnostic clues about mountain evolution and periods of relative
4216 base-level stability, been left out of geodynamic scenarios?

4217 This review has provided tentative answers by elimination of the least plausible, but few are
4218 currently definitive. It has presented for the first time a joined-up understanding of the
4219 Pyrenees, preferring to deal with the mountain range primarily as a topographic entity and
4220 using sedimentary rock facies, thermochronology as well as landforms to infer erosional
4221 depths, palaeorelief height or steepness, and the orogen's successive rise and decline
4222 through time on both sides of the Europe–Iberia boundary. Spanning ~84 Ma of topographic
4223 history as a mountain range, reconstructions show that topography was continuously
4224 transient, responding to the push of collisional tectonics, but equally to the drawdown of
4225 marine base-level changes; to the encroachment of post-shortening extensional tectonics; to
4226 the possible vertical pull by a dense crustal root (eclogite) or a lithospheric underthrust of
4227 uncertain angle and size; and likely to the buoyancy afforded by asthenospheric processes in
4228 a post-shortening context which, since Neogene time, had essentially become an intraplate
4229 rather than a plate-boundary setting. As a result, evidence shows that Pyrenean topography
4230 has been through a sequence of contrasted states and characteristics, some elevated and
4231 mountain-like: e.g., in late Cretaceous time (Proto-Pyrenees), then between the Eocene and
4232 late Oligocene (Ancestral Pyrenees), and finally since the late Neogene (Modern Pyrenees);
4233 but others less elevated and more plateau-like (including in the form of regional, base-level
4234 peneplains): particularly during the late Cretaceous stage of pre-collisional rift inversion west
4235 of the Proto-Pyrenees, likewise during the relatively quiescent Paleocene to Ilerdian interval,
4236 and most of all later between ~25 and ~9 Ma (Plate I, panels F, G, H, I). Regional uplift in the
4237 late Neogene not just rejuvenated the crustal wedge along much of the modern mountain
4238 belt, but it also affected the piedmonts, which, whether in the pro-, retro-, or Mediterranean
4239 foreland areas, are currently deeply incised by rivers as a result.

4240 Links between asthenospheric, lithospheric, and surface processes are perhaps best
4241 illuminated by the suite of diagnostic landforms examined in this review — a long-neglected
4242 component of the puzzle. More than 100 years ago, some geomorphologists interpreted
4243 certain mountain ranges as 'raised peneplains' (e.g., Davis, 1902), thereby implying recent

4244 uplift (and concomitant valley incision) of older, eroded orogenic structures. Although the
4245 driving mechanism was unknown, the Pyrenees were viewed as one of these mountain
4246 ranges (de Sitter, 1952); such a two-stage uplift scenario, however, requires attention to
4247 landforms and is likely to remain untested by lithospheric-scale numerical models with a low
4248 sensitivity to geomorphological constraints (Curry et al., 2019). The counter-intuitive view
4249 that elevated mountain ranges may not just be the result of a closed system involving crustal
4250 thickening and rock crumpling appears nonetheless to be gaining new relevance globally,
4251 partly through the growing awareness that a global intensification of lithospheric and
4252 sublithospheric processes with strong impacts on the Earth's surface relief has been
4253 occurring since the late Neogene (e.g., Potter and Szatmari, 2009; Baran et al., 2014; Calvet
4254 et al., 2015a; Leroux et al., 2017; Kästle et al., 2019). In the case of the Pyrenees, it is now
4255 being recognised that the mountain range stands above a large-scale flow of asthenosphere
4256 (Gunnell et al., 2008) that does not result from Pyrenean deformation and yet is strongly
4257 affecting the behaviour of the lithosphere and crust of the orogenic belt (Jolivet et al., 2020).
4258 It is also affecting the geomorphic response of topography within the mountain range as well
4259 as across its flanking sedimentary basins. As shown here, observation-based geomorphology
4260 can provide clues about the underlying crustal, lithospheric and sub-lithospheric factors that
4261 drive long-term landscape evolution, and can thus potentially be used as a calibration tool
4262 when tackling orogen-scale evolution as an inverse problem.

4263

4264 **Acknowledgements.** This review benefited from thorough and valuable comments by
4265 Antonio Teixell and Miguel Garcés. BL thanks Mary Ford and Pierre Labaume for fruitful
4266 discussions around the Alpine tectonics of the Pyrenees.

4267

4268 **References**

- 4269 Adams, J.E., 1985. Large-scale tectonic geomorphology of the Southern Alps, New Zealand. In: Morisawa, M.,
4270 Hack, J.T. (eds), *Tectonic geomorphology*. Allen & Unwin, Boston, pp. 105–128.
- 4271 Addé-Lacomme, J., 1935. Étude de l'Aceratherium de Bézac (Ariège). *Bull. Soc. Hist. Nat. Toulouse* 65, 76–10.
- 4272 Aguilar, J.P., 1977. Données nouvelles sur l'âge des formations lacustres des bassins de Narbonne-Sigean et de
4273 Leucate (Aude) à l'aide des micromammifères. *Geobios* 10, 643–645.
- 4274 Aguilar, J.P., Michaux, J., 1977. Remarques sur la stratigraphie des terrains tertiaires des bassins de Narbonne-
4275 Sigean et de Leucate (Aude). *Geobios* 10, 647–649.

- 4276 Aguilar, J.P., 1979. Principaux résultats biostratigraphiques de l'étude des rongeurs miocènes du Languedoc.
4277 C.R. Acad. Sci. Paris D 288, 473–476.
- 4278 Aguilar, J.P., 1980. Rongeurs du Miocène inférieur et moyen en Languedoc. Leur apport pour les corrélations
4279 marin–continental et la stratigraphie. *Palaeovertebrata* (Montpellier) 9, 155–203.
- 4280 Aguilar, J.P., 1981. Évolution des rongeurs miocènes et paléogéographie de la Méditerranée occidentale. Thèse
4281 doct. Etat Sci., USTL Montpellier, 203 p.
- 4282 Aguilar, J.P., 1982. Biozonation du Miocène d'Europe occidentale à l'aide des rongeurs et corrélations avec
4283 l'échelle stratigraphique marine. C. R. Acad. Sci. Paris sér. II 294, 49–54.
- 4284 Aguilar, J.P., 2002. Les Sciuridés des gisements karstiques du Miocène inférieur à moyen du sud de la France :
4285 nouvelles espèces, phylogénie, paléoenvironnement. *Geobios* 35, 375–394.
- 4286 Aguilar, J.P., Crochet, J.Y., Green, M., Sigé, B., 1982. Contributions à l'étude des micromammifères du gisement
4287 miocène supérieur de Montredon (Hérault). *Palaeovertebrata* (Montpellier) 12, 75–140.
- 4288 Aguilar, J.P., Calvet, M., Crochet, J.Y., Legendre, S., Michaux, J., Sigé, B., 1986a. Première occurrence d'un
4289 mégachiroptère pteropodidé dans le Miocène moyen d'Europe (gisement de Lo Fournas 2, Pyrénées
4290 orientales, France). *Palaeovertebrata* (Montpellier) 16, 173–184.
- 4291 Aguilar, J.P., Calvet, M., Michaux, J., 1986b. Découvertes de faunes de micromammifères dans les Pyrénées-
4292 Orientales (France) de l'Oligocène supérieur au Miocène supérieur ; espèces nouvelles et réflexions sur
4293 l'étalonnage des échelles continentales et marines. C. R. Acad. Sci. Paris sér. II 303, 755–760.
- 4294 Aguilar, J.P., Michaux, J., 1987. Essai d'estimation du pouvoir séparateur de la méthode biostratigraphique des
4295 lignées évolutives chez les rongeurs néogènes. *Bull. Soc. Géol. Fr.* 8, 1113–1124.
- 4296 Aguilar, J.P., Michaux, J., 1990. A paleoenvironmental and paleoclimatic interpretation of a Miocene rodent
4297 faunal succession in Southern France. Critical evaluation of the use of rodents in paleoecology.
4298 *Paléobiologie continentale* (Montpellier) 16, 311–327.
- 4299 Aguilar, J.P., Michaux, J., Bachelet, B., Calvet, M., Faillat, J.P., 1991. Les nouvelles faunes de rongeurs proches
4300 de la limite mio-pliocène en Roussillon. Implications biostratigraphiques et biogéographiques.
4301 *Palaeovertebrata* (Montpellier) 20, 147–174.
- 4302 Aguilar, J.P., Legendre, S., Michaux, J., 1997. Synthèses et tableaux de corrélations. In: Aguilar, J.P., Legendre,
4303 S., Michaux J. (eds.), Actes du Congrès BiochronM'97. *Mém. Trav. EPHE* (Montpellier) 21, pp. 769–805.
- 4304 Aguilar, J.P., Michaux, J., 1997. Les faunes karstiques néogènes du Sud de la France et la question de leur
4305 homogénéité chronologique. In: Aguilar, J.P., Legendre, S., Michaux J. (eds.), Actes du Congrès
4306 BiochronM'97. *Mém. Trav. EPHE* (Montpellier) 21, pp. 33–38.
- 4307 Aguilar, J.P., Escarguel, G., Michaux, J., 1999. A succession of Miocene rodent assemblages from fissure fillings
4308 in southern France: palaeoenvironmental interpretation and comparison with Spain. *Palaogeogr.*
4309 *Palaeoclim., Palaeocol.* 145, 215–230.
- 4310 Aguilar, J.P., Antoine, P.O., Crochet, J.Y., López-Martínez, N., Métais, G., Michaux, J., Welcomme, J.L., 2003. Les
4311 mammifères du Miocène inférieur de Beaulieu (Bouches-du-Rhône, France), comparaison avec Wintershof-
4312 West et le problème de la limite MN3/MN4. *Coloquios de Paleontología, Univ. Complutense de Madrid*, Vol.
4313 Ext. 1, 1–24.

- 4314 Aguilar, J.P., Lazzari, V., Michaux, J., Sabatier, M., Calvet, M., 2007. Lo Fournas 16-M (Miocène supérieur) et Lo
4315 Fournas 16-P (Pliocène moyen), nouvelles localités karstiques à Baixas, Sud de la France) : Partie I-
4316 Description et implications géodynamiques. *Géologie de la France* 1, 55–62.
- 4317 Aguilar, J.P., Michaux, J., Aunay, B., Calvet, M., Lazzari, V., (2010. Compléments à l'étude des rongeurs
4318 (Cricetidae, Eomyidae, Sciuridae) du gisement karstique de Blanquatère 1 (Miocène moyen, Sud de la
4319 France). *Geodiversitas* 32, 515–533.
- 4320 Agustí, J., Roca, E., 1987. Síntesis bioestratigráfica de la fosa de la Cerdanya (Pirineos orientales). *Estud. Geol.*
4321 (Madrid) 43, 521–529.
- 4322 Agustí, J., Gibert, J., Moya, S., Cabrera, L., 1981. Roedores insectívoros del Mioceno superior de La Seu d'Urgell.
4323 *Acta Geol. Hispanica* ("Homenatge a Lluís Solé Sabaris") 14, 36–369.
- 4324 Agustí, J., Domènech, R., Julià, R., Martinell, J., 1990. Evolution of the Neogene basin of Emporda (NE Spain),
4325 Field Guidebook. In: Agustí, J., Domènech, R., Julià, R., Martinell, J. (eds), *Iberian Neogene basins. Paleontol.*
4326 *Evol. (Sabadell)*, Spec. Publ. 2, pp. 251–267.
- 4327 Agustí, J., Cabrera, L., Domènech, R., Martinell, J., Moyà-Solà, S., Ortí, F., de Porta, J., 1990. Neogene of
4328 Penedes area (Prelittoral Catalan Depression, NE Spain), Field Guidebook. In: Agustí, J., Domènech, R., Julià,
4329 R., Martinell, J. (eds), *Iberian Neogene basins. Paleontol. Evol. (Sabadell)*, Spec. Publ. 2, pp. 187–207.
- 4330 Agustí, J., Arenas, C., Cabrera, L., Pardo, G., 1994. Characterisation of the latest Aragonian–Early Vallesian (Late
4331 Miocene) in the Central Ebro Basin (NE Spain). *Scripta Geol. (Leiden)* 106, 1–10.
- 4332 Agustí, J., Cabrera, L., Garcés, M., Parés, J.M., 1997. The Vallesian mammal succession in the Vallès-Penedès
4333 basin (northeast Spain): paleomagnetic calibration and correlation with global events. *Palaogeogr.*
4334 *Palaeoclim., Palaeocol.* 133, 149–180.
- 4335 Agustí, J., Oms, O., Furió, M., Pérez-Vila, M.J., Roca, E., 2006. The Messinian terrestrial record in the Pyrenees:
4336 the case of Can Vilella (Cerdanya Basin). *Palaogeogr. Palaeoclim., Palaeocol.* 238, 179–189.
- 4337 Agustí, J., Cabrera, L., Garcés, M., Krijgsman, W., Oms, O., Parés, J.M., 2001. A calibrated mammal scale for the
4338 Neogene of Western Europe. State of the art. *Earth-Sci. Rev.* 52, 247–260.
- 4339 Agustí, J., Pérez-Rivarés, F.J., Cabrera, L., Garcés, M., Pardo, G., Arenas, C., 2011. The Ramblian–Aragonian
4340 boundary and its significance for the European Neogene continental chronology. Contributions from the
4341 Ebro Basin record (NE Spain). *Geobios* 44, 121–134.
- 4342 Alasset, J.P., Meghraoui, M., 2005. Active faulting in the western Pyrenees (France): Paleoseismic evidence for
4343 late Holocene ruptures. *Tectonophysics* 409, 39–54.
- 4344 Alastrué, B., Almela, A., Ríos, J.M., 1957. Explicación al mapa geológico de la provincia de Huesca. Escala
4345 1:200.000. Inst. Geol. y Min. de España, Madrid, 253 p.
- 4346 Alimen, H., 1964. Le Quaternaire des Pyrénées de Bigorre. Mémoire du Service de la Carte Géologique, Paris,
4347 394 p.
- 4348 Allen, P.A., 2008. Time scales of tectonic landscapes and their sediment routing systems. In: Gallagher, K.,
4349 Jones, S.J., Wainwright, J. (eds), *Landscape evolution: denudation, climate and tectonics over different time*
4350 *and space scales. Geological Society, London, Spec. Publ.* 296, pp. 7–28.
- 4351 Allen, P.A., Allen, J.R. 2013. *Basin analysis* (3rd edn). Blackwell, London, 619 p.

- 4352 Alvarez-Sierra, M., Daams, R., Lacomba, J.I., López-Martínez, N., Meulen, A. van der, Sesé, C., de Visser, J.,
4353 1990. Paleontology and biostratigraphy (micromammals) of the continental Oligocene–Miocene deposits of
4354 the north-central Ebro Basin (Huesca, Spain). *Scripta Geol. (Leiden)* 94, 1–77.
- 4355 Ambert, P., 1976. Les pertuis de l'Aude Minervoise. *Rev. Géogr. Pyrén. Sud-Ouest* 47, 275–288.
- 4356 Ambert, P., 1977. Déformation tectonique d'une terrasse quaternaire de la Cesse à Bize (Aude). *Bull. Soc. Hist.*
4357 *Nat. Toulouse* 113, 147–151.
- 4358 Ambert, P., 1994. L'évolution géomorphologique du Languedoc central depuis le Néogène (Grands Causses
4359 méridionaux–Piémont languedocien). *Doc. BRGM* 231, Orléans, 210 p.
- 4360 Anadón, P., Villalta, J.F., 1975. Caracterización de terrenos de edad estampiense en Campins (Vallés oriental).
4361 *Acta Geol. Hispánica* 10, 6–9.
- 4362 Anadón, P., 1986. Las facies lacustres del Oligoceno de Campins (Valles Oriental, Provincia de Barcelona). *Cuad.*
4363 *Geol. Ibérica* 10, 271–294.
- 4364 Andeweg, V., 2002. Cenozoic tectonic evolution of the Iberian Peninsula, causes and effects of changing stress
4365 fields. PhD Thesis, Vrije Universiteit, Amsterdam, 178 p.
- 4366 Andrieu, V., Hubschman, J., Jalut, G., Hérail, G., 1988. Chronologie de la déglaciation des Pyrénées françaises.
4367 *Bulletin de l'Assoc. Fr. Étude Quat. (Paris)* 34–35, 55–67.
- 4368 Angrand P. 2017. Évolution 3D d'un rétro-bassin d'avant-pays : le Bassin d'Aquitaine, France. PhD thesis, Univ.
4369 de Lorraine, 170 p.
- 4370 Angrand, P., Ford, M., Watts, A.B., 2018. Lateral variations in foreland flexure of a rifted continental margin: the
4371 Aquitaine Basin (SW France). *Tectonics* 37, 430–449.
- 4372 Anguy, Y., Damotte, B., Roure, F. 1991. Tirs sismiques latéraux complémentaires au profil ECORS-Pyrénées:
4373 apports à la connaissance de l'architecture profonde de la chaîne. *C. R. Acad. Sci. Paris sér. II* 313, 677–684.
- 4374 Antoine, P.O., Duranthon, F., Tassy, P., 1997. L'apport des grands mammifères (Rhinocerotidés, Suoidés,
4375 Proboscidiens) à la connaissance des gisements du Miocène d'Aquitaine (France). In: Aguilar, J.P., Legendre,
4376 S., Michaux J. (eds.), *Actes du Congrès BiochronM'97. Mém. Trav. EPHE (Montpellier)* 21, pp. 581–590.
- 4377 Antoine, P.O., Duranthon, F., Hervet, S., Fleury, G., 2006. Vertébrés de l'Oligocène terminal (MP30) et du
4378 Miocène basal (MN1) du métró de Toulouse (Sud-Ouest de la France). *C. R. Palevol*, 5, 874–884.
- 4379 Antoine, P.O., Métais, G., Orliac, M.J., Peigné, S., Rafaÿ, S., Solé, F., Vianey-Liaud, M., 2011. A new late Early
4380 Oligocene vertebrate fauna from Moissac, South-West France. *C. R. Palevol* 10, 239–250.
- 4381 Antunes, M.T., Casanovas, M.L., Cuesta, M.A., Checa L., Santafé, J.V., Agustí, J., 1997. Eocene mammals from
4382 Iberian Peninsula. In: Aguilar, J.P., Legendre, S., Michaux, J. (eds.), *Actes du Congrès BiochroM'97. Mem.*
4383 *Trav. E.P.H.E. (Inst. Montpellier)* 21, 337–352.
- 4384 Araña, V., Aparicio, A., Martín-Escorza, C., García-Cacho, L., Ortiz, R., Vaquer, R., Barberi, F., Ferrara, G., Albert,
4385 J., Gassiot, X., 1983. El volcanismo neógeno-cuaternario de Catalunya: caracteres estructurales, petrológicos
4386 y geodinámicos. *Acta Geol. Hispanica* 18, 1–17.
- 4387 Arenas, C., 1993. Sedimentología y paleogeografía del Terciario del margen pirenaico y sector central de la
4388 cuenca del Ebro (zona aragonesa occidental). Tesis, Universidad de Zaragoza, 858 p.

- 4389 Arenas, C., Pardo, G., 1999. Latest Oligocene–late Miocene lacustrine systems of the north-central part of the
4390 Ebro Basin (Spain): sedimentary facies models and palaeogeographic synthesis. *Palaeogeogr. Palaeoclim.*
4391 *Palaeoecol.* 151, 127–148.
- 4392 Arenas, C., Millán, H., Pardo, G., Pocoví, A., 2001. Ebro Basin continental sedimentation associated with late
4393 compressional Pyrenean tectonics (north-eastern Iberia): controls on basin margin fans and fluvial systems.
4394 *Basin Res.* 13, 65–89.
- 4395 Arthaud, F., Ogier, M., Séguret, M., 1980–81. Géologie et géophysique du golfe du Lion et de sa bordure nord.
4396 *Bull. BRGM I*, 175–193.
- 4397 Asensio, E., Khazaradze, G., Echeverria, A., King, R.W., Vilajosana, I., 2012. GPS studies of active deformation in
4398 the Pyrenees, *Geophys. J. Int.* 190, 913–921.
- 4399 Ashauer, H., 1934. Die östliche Endigung der Pyrenäen. *Abh. Ges. Wiss. Göttingen, Math.-Phys. Kl.* 10, 2–115.
- 4400 Astre, G., 1926. Répartition stratigraphique des deux types de Mammouths. *Bulletin Soc. Hist. Nat. Toulouse*,
4401 183–188.
- 4402 Astre, G., 1932. Mammifères des lignites pontiens d’Orignac. *Bull. Soc. Hist. Nat. Toulouse* 64, 581–584.
- 4403 Astre, G., 1933. Sur quelques mammifères oligocènes de la vallée de l’Ariège. *Bull. Soc. Hist. Nat. Toulouse* 65,
4404 120–126.
- 4405 Astre, G., 1937. Nummulites remaniés dans le Pliocène de Néfiach en Roussillon. *C. R. Somm. Soc. Géol. Fr.*,
4406 347–351.
- 4407 Astre, G., 1953. Mastodonte de Bourg-Saint-Bernard et érosions miocènes dans le bassin sous-pyrénéen. *Bull.*
4408 *Soc. Géol. Fr.* 5, 253–259.
- 4409 Astre, G., 1959. Terrains stampiens du Lauragais et du Tolosan. *Bull. Soc. Hist. Nat. Toulouse* 94, 8–168.
- 4410 Astre, G., 1964. Le problème des aires d’affleurement du Stampien terminal au sommet des marno-molasses
4411 Tolosanes. *Bull. Soc. Hist. Nat. Toulouse* 99, 229–234.
- 4412 Astre, G., 1967. *Elephas trogontherii* dans des graviers de Palaminy. *Bull. Soc. Hist. Nat. Toulouse* 103, 19–29.
- 4413 Astruc, J.G., Huguene, M., Escarguel, G., Legendre, S., Rage, J.C., Simon-Coignon, R., Sudre, J., Sigé, B., 2003.
4414 Puycelci, nouveau site à vertébrés de la série molassique d’Aquitaine. Densité et continuité
4415 biochronologique dans la zone Quercy et bassins périphériques au Paléogène. *Geobios* 36, 629–648.
- 4416 Audra, P., Palmer, A.N., 2011. The pattern of caves: controls of epigenic speleogenesis. *Géomorphologie: Relief*
4417 *Process. Environ.* 4, 359–378.
- 4418 Audra, P., Palmer A.N., 2013. The vertical dimension of karst: controls of vertical cave pattern. In: Shroder, J.F.
4419 (Ed.-in-chief), Frumkin, A. (Volume Ed.), *Treatise on Geomorphology*, vol. 6, Karst Geomorphology.
4420 Academic Press, San Diego, pp. 186–206.
- 4421 Babault, J., Bonnet, S., Crave, A., van den Driessche, J., 2005a. Influence of piedmont sedimentation on erosion
4422 dynamics of an uplifting landscape: an experimental approach. *Geology*, 33, 301–304.
- 4423 Babault, J., Van den Driessche, J., Bonnet, S., Castelltort, S., Crave, A., 2005b. Origin of the highly elevated
4424 Pyrenean peneplain. *Tectonics*, 24, TC2010, doi: 10.1029 /2004TC001697.
- 4425 Babault, J., Loget, N., van den Driessche, J., Castelltort, S., Bonnet, S. and Davy, P., 2006. Did the Ebro Basin
4426 connect to the Mediterranean before the Messinian salinity crisis. *Geomorphology* 81, 155–165.

- 4427 Babault, J., Bonnet, S., van den Driessche, J., Crave, A., 2007. High elevation of low-relief surfaces in mountain
4428 belts: does it equate to post-orogenic surface uplift? *Terra Nova* 19, 272–277.
- 4429 Bache, F., 2008. Évolution Oligo-Miocène des marges du micro-océan Liguro-Provençal. PhD thesis, Univ. de
4430 Bretagne occidentale, 338 p.
- 4431 Bache, F., Olivet, J.L., Gorini, C., Aslanian, D., Labails, C., Rabineau, M., 2010. Evolution of rifted continental
4432 margins: the case of the Gulf of Lions (Western Mediterranean Basin). *Earth Planet. Sci. Lett.* 292, 345–356.
- 4433 Badiola, A., Checa, L., Cuesta, M.A., Quer, R., Hooker, J.J., Astibia, H., 2009. The role of new Iberian finds in
4434 understanding European Eocene mammalian paleobiogeography. *Geol. Acta* 7, 243–258.
- 4435 Bakalowicz, M., 1988. L'évolution paléohydrologique et morphologique des Pyrénées centrales : l'exemple du
4436 massif karstique d'Arbas (Pyrénées garonnaises). Actes des Journées F. Trombe, 8–10 mai 1987, Moulis,
4437 CNRS, pp. 43–57.
- 4438 Baize, S., Cushing, M., Lemeille, T., Granier, B., Grellet, B., Carbon, D., Combes, C., Hibsich, C., 2002. Inventaire
4439 des indices de rupture affectant le Quaternaire, en relation avec les grandes structures connues en France
4440 métropolitaine et dans les régions limitrophes. *Mém. Hors Série Soc. Géol. France* 175, 142 p.
- 4441 Bandet, Y., 1975. Les terrains néogènes du Conflent et du Roussillon nord-occidental. PhD Thesis, Univ. Paul-
4442 Sabatier, Toulouse.
- 4443 Baran, R., Friedrich, A.M., Schlunegger, F., 2014. The late Miocene to Holocene erosion pattern of the Alpine
4444 foreland basin reflects Eurasian slab unloading beneath the western Alps rather than global climate change.
4445 *Lithosphere* 6, 124–131.
- 4446 Barbera, X., Cabrera, L., Marzo, M., Parés, J.M., Agustí, J., 2001. A complete terrestrial Oligocene
4447 magnetobiostratigraphy from the Ebro Basin, Spain. *Earth Planet. Sci. Lett.* 187, 1–16.
- 4448 Barca, S., Costamagna, L.G., 2010. New stratigraphic and sedimentological investigations on the Middle
4449 Eocene–Early Miocene continental successions in southwestern Sardinia (Italy): paleogeographic and
4450 geodynamic implications. *C. R. Geoscience* 342, 116–125.
- 4451 Barnolas, A., Teixell, A., 1994. Platform sedimentation and collapse in a carbonate-dominated margin of a
4452 foreland basin (Jaca Basin, Eocene, southern Pyrenees). *Geology* 22, 1107–1110.
- 4453 Barnolas, A., Chiron, J.C. (eds), 1996. Synthèse géologique et géophysique des Pyrénées. Volume 1:
4454 introduction, géophysique, cycle hercynien. BRGM and ITGE, 729 p.
- 4455 Barnolas, A., Chiron, J.C. (eds), 2018 (2002). Synthèse géologique et géophysique des Pyrénées. Volumes 2 and
4456 3: Cycle alpin, stratigraphie et phénomènes alpins. AGSO and BRGM, 1353 p.
- 4457 Barnolas, A., Gil-Peña, I., 2001. Ejemplos de relleno sedimentario multiepisódico en una cuenca de antepaís
4458 fragmentada: la Cuenca Surpirenaica. *Bol. Geol. Min.* 112, 17–38.
- 4459 Barnolas, A., Larrasoña, J.C., Pujalte, V., Schmitz, B., Sierro, F.J., María P. Mata, M.P., van den Berg, B.C.J.,
4460 Pérez-Asensio, J.N., Salazar, Á., Salvany, J.M., Ledesma, S., García-Castellanos, D., Civis, J., Cunha, P.P., 2019.
4461 Alpine foreland basins. In: South Pyrenean Foreland and Basque–Cantabrian Paleogene Basins. In: Quesada
4462 C., Oliveira J.T. (eds), *The geology of Iberia: a geodynamic approach*, vol. 4: Cenozoic basins. Springer, pp. 7–
4463 59.

- 4464 Barrère, P., 1952a. Le relief des massifs granitiques de Néouvielle, de Cauterets et de Panticosa. *Rev. Géogr.*
4465 *Pyrén. Sud-Ouest* 23, 69–98.
- 4466 Barrère, P., 1952b. La morphologie des Sierras Oscences. *Actas del Primer Congreso de Estudios Pirenaicos, San*
4467 *Sebastian, 1950, V, Geografía, 51–79.*
- 4468 Barrère, P., 1954. Equilibre glaciaire actuel et quaternaire dans l'Ouest des Pyrénées centrales. *Rev. Géogr.*
4469 *Pyrén. Sud-Ouest* 24, 116–134.
- 4470 Barrère, P., 1962. Reliefs mûrs perchés de la Navarre orientale. *Rev. Géogr. Pyrén. Sud-Ouest* 33, 309–323.
- 4471 Barrère, P., 1963. La période glaciaire dans l'Ouest des Pyrénées centrales franco-espagnoles. *Bull. Soc. Géol.*
4472 *Fr. 7, 516–526.*
- 4473 Barrère, P., 1975. Terrasses et glacis d'érosion en roches tendres dans les montagnes du Haut-Aragon. In:
4474 *Etudes géographiques, Mélanges offerts à G. Viers. Presses Univ. de Toulouse-le-Mirail, 2 vols., pp. 29–43.*
- 4475 Barrère, P., 1981. Le bassin de Sanguesa, articulation majeure du versant sud des Pyrénées. In: *Estudios de*
4476 *Geografía, Homenaje a Alfredo Floristan, Instituto Principe de Viana, 31–39.*
- 4477 Barrère, P., Calvet, M., Courbouleix, S., Gil Peña, I., Martin Alfageme, S., 2009. In: Courbouleix, S., Barnolas, A.,
4478 eds), *Carte géologique du Quaternaire des Pyrénées, 1:400,000 scale. BRGM and ITGM.*
- 4479 Barrière, J., 1966. Le rivage tyrrhénien de l'étang de Bages et de Sigean (Aude). *Bull. Assoc. Fr. Etude Quat.* 3,
4480 251–283.
- 4481 Barruol, G., Granet, M., 2002. A Tertiary asthenospheric flow beneath the southern Massif Central indicated by
4482 upper mantle seismic anisotropy and related to the west Mediterranean extension. *Earth Planet. Sci. Lett.*
4483 202, 31–47.
- 4484 Barruol, G., Deschamps, A., Coutant, O., 2004. Mapping upper mantle anisotropy beneath SE France by SKS
4485 splitting indicates Neogene asthenospheric flow induced by Apenninic slab roll-back and deflected by the
4486 deep Alpine roots. *Tectonophysics* 394, 125–138.
- 4487 Baudelot, S., Cruzel, F., 1974 La faune burdigalienne des gisements d'Espira de Conflent. *Bull. Soc. Hist. Nat.*
4488 *Toulouse* 110, 311–326.
- 4489 Baudelot, S., Olivier, P., 1978. Les rongeurs (mammalia, Rodentia) de l'Oligocène terminal de Dieupentale, Sud-
4490 Ouest de la France : Tarn et Garonne). *Geobios* 11, 5–19.
- 4491 Baulig, H., 1928. Le Plateau Central de la France et sa bordure méditerranéenne – Etude morphologique. A.
4492 Colin, Paris, 591 p.
- 4493 Beamud, E., Garcés, M., Cabrera, L., Muñoz, J.A., Almar, Y., 2003. A new middle to late Eocene continental
4494 chronostratigraphy from NE Spain. *Earth Planet. Sci. Lett.* 216, 501–514.
- 4495 Beamud, E., Muñoz, J.A., Fitzgerald, P.J., Baldwin, S.L., Garcés, M., Cabrera, L., Metcalf, J.R., 2011.
4496 Magnetostratigraphy and detrital apatite fission track thermochronology in syntectonic conglomerates:
4497 constraints on the exhumation of the South-Central Pyrenees. *Basin Res.* 23, 309–331.
- 4498 Beaumont, C., Muñoz, J.A., Hamilton, J., Fullsack, P., 2000. Factors controlling the Alpine evolution of the
4499 central Pyrenees inferred from a comparison of observations and geodynamical models. *J. Geophys. Res.*
4500 105, 8121–8145.

- 4501 Bellec, V., 2003. Évolution morphostructurale et morphosédimentaire de la plate-forme aquitaine depuis le
4502 Néogène. PhD thesis (unpubl.), Univ. of Bordeaux, 268 p.
- 4503 Bellec, V., Cirac, P., Faugères, J.C., 2009. Formation and evolution of paleo-valleys linked to a subsiding canyon,
4504 North Aquitaine shelf (France). *C.R. Geosciences* 341, 36–48.
- 4505 Belmonte, A., 2014. Geomorfología del macizo de Cotiella (Pirineo oscense): cartografía, evolución
4506 paleoambiental y dinámica actual. PhD thesis, Universidad de Zaragoza, 581 p.
- 4507 Benito, G., Pérez-González, A., Gutiérrez, F., Machado, M.J., 1998. River response to Quaternary large-scale
4508 subsidence due to evaporite solution (Gállego River, Ebro Basin, Spain). *Geomorphology* 22, 243–263.
- 4509 Benito, G., Sancho, C., Peña, J.L., Machado, M.J., Rhodes, E.J., 2010. Large-scale karst subsidence and
4510 accelerated fluvial aggradation during MIS6 in NE Spain: climatic and paleohydrological implications. *Quat.*
4511 *Sci. Rev.* 29, 2694–2704.
- 4512 Bentham P., Burbank D.W., 1996. Chronology of Eocene foreland basin evolution along the western oblique
4513 margin of the South-Central Pyrenees. In: Friend, P.F. Dabrio, C.J. (eds), *Tertiary basins of Spain, the*
4514 *stratigraphic record of crustal kinematics*. Cambridge University Press, Cambridge, pp. 144–152.
- 4515 Berástegui, X., García-Senz, M., Losantos, M., 1990. Tecto-sedimentary evolution of the Organyà extensional
4516 basin (central south Pyrenean unit, Spain) during the Lower Cretaceous. *Bull. Soc. Géol. Fr.* 8, 251–264.
- 4517 Berástegui, X., Caus, E., Puig, C., Serra-Kiel, J., 2002. Le Paléogène du secteur oriental du bassin sud-pyrénéen,
4518 livret guide. IUGS–UNESCO–IGCP, AGSO, GEP, 77 p.
- 4519 Berger, G., Clauzon, G., Michaux, J., Suc, J.P., Aloïsi, J.C., Monaco, A., Got, H., Augris, C., Gadel, F., Buscail, R.,
4520 1988. Carte géologique de la France, 1:50,000 scale, sheet Perpignan (1091), Orléans, BRGM. Handbook by
4521 Clauzon, G., Berger, G., Aloïsi, J.C., Got, H., Monaco, A., Buscail, R., Gadel, F., Augris, C., Marchal, J.P.,
4522 Michaux, J., Suc, J.P. (1989), 40 p.
- 4523 Bergounioux, F.M., Crouzel, F., 1960. Mastodontes du Miocène du Bassin d'Aquitaine. *Bull Soc. Hist. Nat.*
4524 *Toulouse* 48, 232–286.
- 4525 Bergounioux, F.M., Crouzel, F., 1971. Un gisement fossilifère Oligocène à Saverdun (Ariège). *Bull Soc. Hist. Nat.*
4526 *Toulouse* 107, 89–92.
- 4527 Besson, F., 2000. Le paysage pyrénéen dans la littérature de voyage et l'iconographie britannique du dix-
4528 neuvième siècle. *L'Harmattan*, Paris 463 p.
- 4529 Bestani, L., Espurt, N., Lamarche, J., Bellier, O., Hollender, F., 2016. Reconstruction of the Provence Chain
4530 evolution, southeastern France. *Tectonics* 35, 1506–1525.
- 4531 Bilotte, M., Peybernès, B., Souquet, P., 1979. Les Pyrénées catalanes dans la région de l'Empordà. Relations
4532 entre zones isopiques crétacées et unités structurales. *Acta Geol. Hisp.*, 14, 280–288.
- 4533 Birot, P., 1937. Recherches sur la morphologie des Pyrénées orientales franco-espagnoles. *Baillièrè edit.*, Paris,
4534 318 p.
- 4535 Birot, P., 1952. Sur quelques contrastes fondamentaux dans la structure et la morphologie des Pyrénées. *Actas*
4536 *del Primer Congreso de Estudios Pirenaicos*, San Sebastian, 1950. *Geografia* 5, 17–21.
- 4537 Birot, P., 1969. Le Quaternaire de la basse vallée de l'Orbieu. Livret guide excursion A6, Pyrénées orientales et
4538 centrales, Roussillon, Languedoc occidental, VIIIe Congrès INQUA, Paris, 101–105.

- 4539 Blanchard, R., 1914. La morphologie des Pyrénées françaises. *Ann. Géogr.* 23, 303–324.
- 4540 Blockley, S.P.E., Lane, C.S., Hardiman, M., Rasmussen, S.O., Seierstad, I.K., Steffensen, J.P., Svensson, A., Lotter,
4541 A.F., Turney, C.S.M., Ramsey, C.B., 2012 Synchronisation of palaeoenvironmental records over the last
4542 60,000 years and an extended INTIMATE event stratigraphy to 48,000 b2k. *Quat. Sci. Rev.* 36, 2–10.
- 4543 Boillot, G., Capdevila, R., 1977. The Pyrenees: subduction and collision? *Earth Planet. Sci. Lett.* 35, 151–160.
- 4544 Boillot, G., Capdevila, R., Hennequin-Marchand, I., Lamboy, M., Leprêtre, J.-P., 1973. La zone nord-pyrénéenne,
4545 ses prolongements sur la marge continentale nord-espagnole et sa signification structurale. *C. R. Acad. Sci.*
4546 *Paris D* 277, 2629–2632.
- 4547 Boissevain, H., 1934. Étude géologique et géomorphologique d'une partie de la vallée de la haute Sègre
4548 (Pyrénées Catalanes). *Bull. Soc. Hist. Nat. Toulouse* 66, 33–170.
- 4549 Bomer, B., 1979. Les piedmonts du Bassin de l'Ebre (Espagne). *Méditerranée* 36, 19–25.
- 4550 Bond, R.M.G., McClay, K.R., 1995. Inversion of a Lower Cretaceous extensional basin, south central Pyrenees,
4551 Spain. In: Buchanan, J.G., Buchanan, P.G. (eds), *Basin Inversion*. Geological Society, London, Spec. Publ. 88,
4552 pp. 415–431.
- 4553 Bonilla-Salomon, I., Minwer-Barakat, R., Vianey-Liaud, M., Moya-Sola, S., 2016. Middle Eocene rodents from
4554 Sant Jaume de Frontanya (eastern Pyrenees, northern Spain) and biochronological implications. *J. Vertebr.*
4555 *Paleontol.* 36, e1121149-2.
- 4556 Bordonau, J., 1992. Els Complexos glacio-lacustres relacionats amb el darrer cicle glacial als Pirineus. *Geoforma*
4557 *edit.*, Logroño, 251 p.
- 4558 Bosch, G.V., van den Driessche, J., Babault, J., Robert, A., Carballo, A., Le Carlier, C., Loget, N., Prognon, C.,
4559 Wyns, R., Baudin, T., 2016a. Peneplanation and lithosphere dynamics in the Pyrenees. *C. R. Géoscience* 348,
4560 194–202.
- 4561 Bosch, G.V., Teixell, A., Jolivet, M., Labaume, P., Stockli, D., Doménech, M., Monié, P., 2016b. Timing of
4562 Eocene–Miocene thrust activity in the western Axial Zone and Chaînons Béarnais (west-central Pyrenees)
4563 revealed by multi-method thermochronology. *C. R. Geoscience* 348, 246–256.
- 4564 Boschi, L., Faccena, C., Becker, T.W., 2010. Mantle structure and dynamic topography in the Mediterranean.
4565 *Geophys. Res. Lett.*, 37, L20303, doi:10.1029/2010GL045001.
- 4566 Bosq, M., Bertran, P., Beauval, C., Kreutzer, S., Duval, M., Bartz, M., Mercier, N., Sitzia, L., Stéphan, P., 2019.
4567 Stratigraphy and chronology of Pleistocene coastal deposits in northern Aquitaine, France; a
4568 reinvestigation. *Quaternaire* 30, 5–20.
- 4569 Boulanger, D., Poignant, A., 1970. A propos de l'âge de la base des poudingues de Jurançon. *C.R. Somm. Soc.*
4570 *Géol. France*, 2, 35–36.
- 4571 Boule, M., 1894. Le plateau de Lannemezan et les alluvions anciennes des hautes vallées de la Garonne et de la
4572 Neste. *Bull. Serv. Carte Géol. France* 43, 447–469.
- 4573 Bourcart, J., 1947. Étude des sédiments pliocènes et quaternaires du Roussillon. *Bull. Serv. Carte Géol. France*
4574 218, 395–476.

- 4575 Briais, A., Armijo, R., Winter, T., Tapponnier, P., Herbecq, A., 1990. Morphological evidence for Quaternary
4576 normal faulting and seismic hazard in the Eastern Pyrenees. *Ann. Tectonicae* 4, 19–42.
- 4577 Bridgland, D.R., 2000. River terrace systems in north-west Europe: an archive of environmental change, uplift
4578 and early human occupation. *Quat. Sci. Rev.* 19, 1293–1303.
- 4579 Bridgland, D.R., Westaway, R., 2014. Quaternary fluvial archives and landscape evolution: a global synthesis.
4580 *Proc. Geol. Assoc.* 125, 600–629.
- 4581 Briffaut, S., 1994. Naissance d'un paysage. La montagne pyrénéenne à la croisée des regards, XVIe–XIXe siècle.
4582 Sources et Travaux d'Histoire Haut-Pyrénéenne (Association Guillaume Mauran), vol. 8, 622 p.
- 4583 Bruxelles, L., Berthet, A.L., Chalard, P., Colonge, D., Delfour, G., Jarry, M., Lelouvier, L.A., Arnoux, T., Onézime,
4584 O., 2003. Le paléolithique inférieur et moyen en Midi toulousain : nouvelles données et perspectives de
4585 l'archéologie préventive. *Paleo (Les Eyzies)* 15, 7–28.
- 4586 Bugnicourt, D., Claracq, P., Dupéron, J., Privé-Gil, C., Sauvage, J., 1988. Sédimentologie, bois fossils et
4587 palynology d'une couche à lignites de Capvern, plateau de Lannemezan (Hautes-Pyrénées). *Bull. Centre*
4588 *Rech. Explor. Prod. Elf Aquitaine (Pau)* 12, 739–757.
- 4589 Burbank, D.W., Verges, J., Muñoz, J.A., Bentham, P., 1992a. Coeval hindward- and forward-imbricating
4590 thrusting in the south-central Pyrenees, Spain: timing and rates of shortening and deposition. *Geol. Soc.*
4591 *Am. Bull.* 104, 3–17.
- 4592 Burbank, D.W., Puigdefabregas, C., Muñoz, J.A., 1992b. The chronology of the Eocene tectonic and stratigraphic
4593 development of the eastern Pyrenean foreland basin, northeast Spain. *Geol. Soc. Am. Bull.* 104, 1101–1120.
- 4594 Busquets, P., Ramos-Guerrero, E., Moyà-Solà, S., Agustí, J., Colombo, F., Checa, L., Khöler, M., 1992. La
4595 Formación de Bellmunt (Unidad del Cadí, Pirineo oriental): aportaciones bioestratigraficas de los sistemas
4596 lacustres y palustres asociados. *Acta Geol. Hisp.* 25, 109–116.
- 4597 Cabrera, L., Roca, E., Santanach, P., 1988. Basin formation at the end of a strike-slip fault: the Cerdanya basin
4598 (Eastern Pyrenees). *J. Geol. Soc. (London)* 145, 261–268.
- 4599 Cabrera, L., Saez, A., 1987. Coal deposition in carbonate-rich shallow lacustrine systems: the Calaf and
4600 Mequinenza sequences (Oligocene, eastern Ebro Basin, NE Spain). *J. Geol. Soc. (London)* 144, 451–461.
- 4601 Cabrera, L., Calvet, F., 1996. Onshore Neogene record in NE Spain: Vallés-Penedés and El Camp half-grabens
4602 (NW Mediterranean). In: Friend, P.F., Dabrio, C.J. (eds), *Tertiary basins of Spain, the stratigraphic record of*
4603 *crustal kinematics*. Cambridge University Press, Cambridge, pp. 97–105.
- 4604 Cahuzac, B., Janin, M.C., Steurbaut, E., 1995. Biostratigraphie de l'Oligo-Miocène du bassin d'Aquitaine fondée
4605 sur les nannofossiles calcaires. Implications paléogéographiques. *Géologie de la France* 2, 57–82.
- 4606 Cahuzac, B., Poignant, A., 1996. Foraminifères benthiques et Microproblematica du Serravallien d'Aquitaine.
4607 *Géologie de la France* 3, 35–55.
- 4608 Cahuzac, B., Turpin, L., 1999. Stratigraphie isotopique du Strontium dans le Miocène marin du Bassin
4609 d'Aquitaine (SW France). *Rev. Soc. Geol. Esp.* 12, 37–56.
- 4610 Cahuzac, B., Poignant, A., 2004. Les foraminifères du Burdigalien moyen à supérieur de la région sud-aquitaine,
4611 golfe de Saubrigues, SW France). *Rev. Micropaléontol.* 47, 153–192.

- 4612 Cahuzac, B., Janssen, A.W., 2010. Eocene to Miocene holoplanktonic Mollusca (Gastropoda) of the Aquitaine
4613 Basin, southwest France. *Scripta Geologica* 141, 1–193.
- 4614 Calvet, M., 1986. La stratigraphie du Néogène du Roussillon et le problème des séries détritiques de bordure.
4615 Essai de mise au point. *Géologie de la France* 2, 205–220.
- 4616 Calvet, M., 1981. Nappes alluviales et niveaux quaternaires du bas-Vallespir. Implications néotectoniques et
4617 paléoclimatiques. *Rev. Géogr. Pyrén. Sud-Ouest* 52, 125–159.
- 4618 Calvet, M., 1992. Aplanissements sur calcaire et gîtes fossilifères karstiques. L'exemple des Corbières
4619 orientales. *Tübinger Geogr. Stud.* 109, pp. 37–43.
- 4620 Calvet, M., 1996. Morphogenèse d'une montagne méditerranéenne : les Pyrénées orientales. Doc. BRGM 255,
4621 3 vols. BRGM, Orléans, 1177 p.
- 4622 Calvet, M., 1999. Régime des contraintes et volumes de relief dans l'Est des Pyrénées. *Géomorphologie : Rel.,*
4623 *Proc., Environ.* 3, 253–278.
- 4624 Calvet, M., Lemartinel B., 2002. Précipitations exceptionnelles et crues éclair dans l'aire pyrénéo-
4625 méditerranéenne. *Géomorphologie : Rel., Proc., Environ.* 1, 35–50.
- 4626 Calvet, M., 2004. The Quaternary glaciation of the Pyrenees. In: Ehlers, J., Gibbard, P. (eds), *Quaternary*
4627 *glaciations — extent and chronology; part I: Europe.* Elsevier, Amsterdam, pp. 119–128.
- 4628 Calvet, M., Aguilar, J.P., Crochet, J.Y., Dubar, M., Michaux, J., 1991. Première découverte de mammifères
4629 oligocènes et burdigaliens dans les bassins de Paziols–Tautavel–Estagel (Aude et Pyrénées-Orientales),
4630 implications géodynamiques. *Géologie de la France* 1, 33–44.
- 4631 Calvet, M., Gunnell, Y., Delmas, M., 2008. Géomorphogenèse des Pyrénées. In: Canérot, J., Colin, J.P., Platel,
4632 J.P., Bilotte, M. (eds), *Pyrénées d'hier et d'aujourd'hui.* Atlantica and BRGM, Biarritz–Orléans, pp. 129–143.
- 4633 Calvet, M., Gunnell, Y., 2008. Planar landforms as markers of denudation chronology: an inversion of East
4634 Pyrenean tectonics based on landscape and sedimentary basin analysis. In: Gallagher, K., Jones, S.J.,
4635 Wainwright, J. (eds), *Landscape Evolution: Denudation, Climate and Tectonics Over Different Time and*
4636 *Space Scales,* Geological Society, London, Spec. Publ. 296, pp. 147–166.
- 4637 Calvet, M., Delmas, M., Gunnell, Y., Braucher, R., Bourlès, D., 2011. Recent advances in research on Quaternary
4638 glaciations in the Pyrenees. In: J. Ehlers, Gibbard, P.L. (eds), *Quaternary glaciations, extent and chronology,*
4639 *a closer look; Part IV. Developments in Quaternary Science* 15, Elsevier, pp. 127–139.
- 4640 Calvet, M., Gunnell, Y., Farines, B., 2015a. Flat-topped mountain ranges: their global distribution and value for
4641 understanding the evolution of mountain topography. *Geomorphology*, 241, 255–291
- 4642 Calvet, M., Gunnell, Y., Braucher, R., Hez, G., Bourlès, D., Guillou, V., Delmas, M., Aster Team, 2015b. Cave
4643 levels as proxies for measuring post-orogenic uplift: evidence from cosmogenic dating of alluvium-filled-
4644 cave in the French Pyrenees. *Geomorphology* 246, 617–633.
- 4645 Calvet, M., Autran, A., Wiazemsky, M., Laumonier, B., Guitard, G., 2015. Carte géologique de la France,
4646 1:50,000 scale, sheet Argelès-sur-Mer / Cerbère (1097). BRGM, Orléans. Handbook by Laumonier, B., Calvet,
4647 M., Barbey, P., Guennoc, P., Lambert J., Lenoble, J.L., Wiazemsky, M., 149 p.
- 4648 Calvet, M., Hez, G., Gunnell, Y., Jaillet, S., 2019. Le karst du synclinal de Villefranche, enregistreur de l'incision
4649 de la vallée de la Têt. *Bol/ Soc. Esp. Speleo. Sci. Karst* 14, 15–32.

4650 Cameselle, A.L., Urgeles, R., de Mol, B., Camerlenghi, A., Canning, J.C., 2014. Late Miocene sedimentary
4651 architecture of the Ebro Continental Margin (Western Mediterranean): implications to the Messinian
4652 Salinity Crisis. *Int. J. Earth Sci.*, 103, 423–440.

4653 Campanyà, J., Ledo, J., Queralt, P., Marcuello, A., Liesa, M., Muñoz, J.A. 2012. New geoelectrical
4654 characterisation of a continental collision zone in the West-Central Pyrenees: Constraints from long period
4655 and broadband magnetotellurics. *Earth Planet. Sci. Lett.* 333–334, 112–121.

4656 Campanyà, J., Ledo, J., Queralt, P., Marcuello, A., Muñoz, J.A., Liesa, M., Jones, A.J., 2018. New geoelectrical
4657 characterization of a continental collision zone in the Central. Eastern Pyrenees: Constraints from 3-D joint
4658 inversion of electromagnetic data. *Tectonophysics*, 742–743, 168–179.

4659 Canérot, J., 2006. Réflexions sur la “révolution danienne” dans les Pyrénées. *C. R. Geoscience* 338, 658–665.

4660 Canérot, J., 2008. Les Pyrénées, vol. 1: Histoire géologique, vol. 2: Itinéraires de découverte. Atlantica and
4661 BRGM, Biarritz–Orléans, 516 and 127 p.

4662 Canérot, J., 2017. The pull apart-type Tardets-Mauléon basin, a key to understand the formation of the
4663 Pyrenees. *Bull. Soc. Géol. Fr.* 188, 35. <http://doi.org/10.1051/bsgf/2017198>

4664 Canérot, J., Hudec, M.R., Rockenbauch, K., 2005. Mesozoic diapirism in the Pyrenean orogen: salt tectonics on a
4665 transform plate boundary. *Am. Assoc. Petrol. Geol. Bull.* 89, 211–229.

4666 Capdeville, J.P., Dubreuilh, J., 1990. Carte géologique de la France, 1:50,000 scale, sheet Mont-de-Marsan
4667 (951). BRGM, Orléans. Handbook by Capdeville, J.P., 41 p.

4668 Capdeville, J.P., Gineste, M.C., Turq A., Vergain P., 1997. Handbook to the Carte géologique de la France,
4669 1:50,000 scale, sheet Hagetmau (978). BRGM, Orléans, 70 p. Map by Capdeville, J.P.

4670 Capdeville, J.P., Darboux, F., 1998. Carte géologique de la France, 1:50,000 scale, sheet Aire-sur-l'Adour (979).
4671 BRGM, Orléans. Handbook by Capdeville, J.P., D. Millet, D., F. Millet, F., 51 p.

4672 Capdeville, J.P., Chalard, P., Jarry, M., Millet, D., O'yl, W., 1997. Le gisement acheuléen d'En Jacca. La
4673 Sauvegarde à Colomiers (Haute-Garonne) : nouvelles données. *Paléo* 9, 69–99.

4674 Carballo, A., Fernandez, M., Jiménez-Munt, I., Torne, M., Vergés, J., Melchiorre, M., Pedreira, D., Afonso, J.C.,
4675 Garcia-Castellanos, D., Díaz, J., Villaseñor, A., Pulgar, J.A., Quintana, L., 2015. From the North-Iberian margin
4676 to the Alboran Basin: a lithosphere geo-transect across the Iberian Plate. *Tectonophysics* 663, 399–418.

4677 Carbon, D., Combes, P., Cushing, M., Granier, T., Grellet, B., 1995. Rupture de surface post-pléistocène moyen
4678 dans le bassin aquitain. *C. R. Acad. Sci. Paris sér. Ila* 320, 311–317.

4679 Carcenac, C., Coinçon, R., Taillefer, F., 1969. Carte géomorphologique du Mas d'Azil. *Rev. Géogr. Pyrén. Sud-*
4680 *Ouest* 40, 329–351.

4681 Carreras, J., Capella, I., 1994. Tectonic levels in the Paleozoic basement of the Pyrenees: a review and a new
4682 interpretation. *J. Struct. Geol.* 16, 1509–1524.

4683 Carrigan, J.H., Anastasio, D.J., Kodama, K.P., Par, J.M., 2016. Fault-related fold kinematics recorded by
4684 terrestrial growth strata, Sant Llorenç de Morunys, Pyrenees Mountains, NE Spain. *J. Struct. Geol.* 91, 161–
4685 176.

- 4686 Casanovas-Vilar, I., van den Hoek Ostende, L.W., Furió, M., Madern, P.A., 2014. The range and extent of the
4687 Vallesian Crisis (Late Miocene): new prospects based on the micromammal record from the Vallès-Penedès
4688 basin (Catalonia, Spain). *J. Iberian Geol.* 40, 29–48
- 4689 Casas, J.M., Clariana, J., García-Sansegundo, J., Margalef, A., 2019. The Pyrenees. In: Quesada, C., Oliveira, J.T.
4690 (eds.), *The geology of Iberia: a geodynamic approach*, vol. 2, The Variscan cycle. Springer, pp. 335–337.
- 4691 Casas-Sainz, A.M., de Vicente, G., 2009. On the tectonic origin of Iberian topography. *Tectonophysics* 474, 214–
4692 235.
- 4693 Cavelier, C., Fries, G., Lagarigue, J.L., Capdeville, J.P., 1997. Sédimentation progradante au Cénozoïque
4694 inférieur en Aquitaine méridionale : un modèle. *Géologie de la France* 4, 69–79.
- 4695 Chanvry, E., Deschamps, R., Joseph, P., Puigdefàbregas, C., Poyatos-Moré, M., Serra-Kiel, J., Garcia, D.,
4696 Teinturier, S., 2018. The influence of intrabasinal tectonics in the stratigraphic evolution of piggyback basin
4697 fills: Towards a model for the Tremp–Graus–Ainsa Basin (South-Pyrenean Zone, Spain). *Sed. Geol.* 377, 34–
4698 62.
- 4699 Chaput, E., 1927. Recherches sur l'évolution des terrasses de l'Aquitaine. *Bull. Soc. Hist. Nat. Toulouse* 56, 17–
4700 84.
- 4701 Chevalier, M., 1909. Note sur la « cuencita » de la Seo de Urgell (Province de Lerida, Espagne). *Bull. Soc. Géol.*
4702 *Fr.*, 158–178.
- 4703 Chevalier, M., 1954a. Le relief glaciaire des Pyrénées du Couserans. I. Les cirques. *Rev. Géogr. Pyrén. Sud-Ouest*
4704 25, 97–124.
- 4705 Chevalier, M., 1954b. Le relief glaciaire des Pyrénées du Couserans. II. Les vallées. *Rev. Géogr. Pyrén. Sud-Ouest*
4706 25, 189–220.
- 4707 Chevrot, S., Sylvander, M., Delouis, B., 2011. A preliminary catalog of moment tensors for the Pyrenees.
4708 *Tectonophysics* 510, 239–251.
- 4709 Chevrot, S., Villaseñor, A., Sylvander, M., Benahmed, S., Beucler, E., Cougoulat, G., Delmas, P., de Saint
4710 Blanquat, M., Diaz, J., Gallart, J., Grimaud, F., Lagabrielle, Y., Manatschal, G., Mocquet, A., Pauchet, H., Paul,
4711 A., Péquegnat, C., Quillard, O., Roussel, S., Ruiz, M., Wolyniec, D., 2014. High-resolution imaging of the
4712 Pyrenees and Massif Central from the data of the PYROPE and IBERARRAY portable array deployments. *J.*
4713 *Geophys. Res. (Solid Earth)* 119, 6399–6420.
- 4714 Chevrot, S., Sylvander, M., Diaz, J., Ruiz, M., Paul, A. and the PYROPE Working Group, 2015. The Pyrenean
4715 architecture as revealed by teleseismic P-to-S converted waves recorded along two dense transects.
4716 *Geophys. J. Int.* 200, 1096–1107.
- 4717 Chevrot, S., Sylvander, M., Diaz, J., Martin, R., Mouthereau, F., Manatschal, G., Masini, E., Calassou, S.,
4718 Grimaud, F., Pauchet, H. Ruiz, M., 2018. The non-cylindrical crustal architecture of the Pyrenees. *Sci. Rep.*,
4719 8:9591, DOI:10.1038/s41598-018-27889-x
- 4720 Choukroune, P., 1992. Tectonic evolution of the Pyrenees. *Annu. Rev. Earth Planet. Sci.* 20, 143–158.
- 4721 Choukroune, P., Le Pichon, X., Séguret, M., Sibuet, J.C., 1973. The Pyrenees: subduction and collision? *Earth*
4722 *Planet. Sci. Lett.* 18, 109–118.

- 4723 Cirac, P., Bourillet, J.F., Griboulard, R., Normand, A., Mulder, T., ITSAS' Team, 2001. Canyon of Capbreton: new
 4724 morphostructural and morphosedimentary approaches, First results of the ITSAS cruise, C. R. Acad. Sci.
 4725 Paris sér. IIa 332, 447–455.
- 4726 Clauzon, G., 1990. Restitution de l'évolution géodynamique néogène du bassin du Roussillon et de l'unité
 4727 adjacente des Corbières d'après les données écostratigraphiques et paléogéographiques. *Paléobiol.*
 4728 *Continent. (Montpellier)* 17, 125–155.
- 4729 Clauzon, G., Cravatte, J., 1985. Révision chronostratigraphique de la série marine pliocène traversée par le
 4730 sondage Canet 1 (Pyrénées-Orientales) : apport à la connaissance du Néogène du Roussillon. C. R. Acad. Sc.
 4731 Paris II 301, 1351–1354.
- 4732 Clauzon, G., Aguilar, J.P., Michaux, J., 1987. Le bassin pliocène du Roussillon (Pyrénées-Orientales, France) :
 4733 exemple d'évolution géodynamique d'une ria méditerranéenne consécutive à la crise de salinité
 4734 messinienne. C. R. Acad. Sc. Paris II 304, 585–590.
- 4735 Clauzon, G., Suc, J.P., Aguilar, J.P., Ambert, P., Capetta, H., Cravatte, J., Drivaliari, A., Domènech, R., Dubar, M.,
 4736 Leroy, S., Martinell, J., Michaux, J., Roiron, P., Rubino, J.L., Savoye, B., Vernet, J.L., 1990. Pliocene
 4737 geodynamic and climatic evolutions in the French mediterranean region, Field Guidebook. In: Agustí, J.,
 4738 Domènech, R., Julià, R., Martinell, J. (eds), Iberian Neogene basins. *Paleontol. Evol. (Sabadell)*, Spec. Publ. 2,
 4739 pp. 131–186.
- 4740 Clerc, C., Lagabrielle, Y., 2014. Thermal control on the modes of crustal thinning leading to mantle exhumation.
 4741 Insights from the Cretaceous Pyrenean hot paleomargins. *Tectonics* 33, 1340–1359.
- 4742 Clot, A., Duranthon, F., 1990. Les mammifères fossiles du Quaternaire dans les Pyrénées. Muséum d'Histoire
 4743 Naturelle de Toulouse and Accord Editions, 80 p.
- 4744 Clottes, J., 1999. La vie et l'art des Magdaléniens en Ariège. La maison des roches, Paris, 700 p.
- 4745 Cochelin, B., Lemirre, B., Denèle, Y., de Saint Blanquat, M., Lahfid, A., Duchêne, S., 2018. Structural inheritance
 4746 in the Central Pyrenees: the Variscan to Alpine tectonometamorphic evolution of the Axial Zone. *J. Geol.*
 4747 *Soc. (London)* 175, 336–351.
- 4748 Cocherie, A., Baudin, T., Guerrot, C., Autran, A., Fanning, M.C., Laumonier, B., 2005. Evidence of the Lower
 4749 Ordovician intrusion age for metagranites in the Late Proterozoic Canaveilles Group of Pyrénées and
 4750 Montagne noire (France): new U–Pb datings. *Bull. Soc. Géol. Fr.* 176, 269–282.
- 4751 Collina-Girard, J., 1976. Les alluvions fluviales des fleuves côtiers dans le Roussillon. In: de Lumley, H. (Ed.), *La*
 4752 *Préhistoire française*. CNRS Editions, Paris, t. 1, pp. 78–82.
- 4753 Collina-Girard, J., 1986. Grille descriptive et évolution typologique des industries archaïques : le modèle
 4754 catalan. *Bull. Soc. Préhist. Fr.* 83, pp. 383–403.
- 4755 Coney, P.J., Muñoz, A.J., McClay, K.R., Evenchik, C.A., 1996. Syntectonic burial and post-tectonic exhumation of
 4756 the southern Pyrenees foreland fold-thrust belt. *J. Geol. Soc. (London)* 153, 9–16.
- 4757 Conway-Jones, B. W., Roberts, G. G., Fichtner, A., Hoggard, M., 2019. Neogene epeirogeny of Iberia. *Geochem.,*
 4758 *Geophys., Geosyst.* 20, 1138–1163.

- 4759 Corbier, P., Karnay, G., Bourguine, B., Saltel, M., 2010. Gestion des eaux souterraines en région Aquitaine
4760 Reconnaissance des potentialités aquifères du Mio-Plio-Quaternaire des Landes de Gascogne et du Médoc
4761 en relation avec les SAGE. Rapport final, BRGM/RP-57813-FR. BRGM, Orléans, 187 p.
- 4762 Cordier, S., Adamson, K., Delmas, M., Calvet, M., Harmand, D., 2017. Of ice and water: Quaternary fluvial
4763 response to glacial forcing. *Quat. Sci. Rev.* 166, 57–73.
- 4764 Costa, J.M., Maestro-Maideu, E., Betzler, C., 1996. The Paleogene basin of the Eastern Pyrenees. In: Friend, P.F.,
4765 Dabrio, C.J. (eds), *Tertiary basins of Spain, the stratigraphic record of crustal kinematics*. Cambridge
4766 University Press, Cambridge, pp. 106–113.
- 4767 Costa, E., Garcés, M., López-Blanco, M., Beamud, E., Gómez-Paccard, M., Larrasoaña, J.C., 2010. Closing and
4768 continentalization of the South Pyrenean foreland Basin (NE Spain): magnetostratigraphical constraints.
4769 *Basin Res.* 22, 904–917.
- 4770 Costa, E., Garcés, M., Sáez, A., Cabrera, L., López-Blanco, M., 2011. The age of the “Grande Coupure” mammal
4771 turnover: new constraints from the Eocene–Oligocene record of the Eastern Ebro Basin (NE Spain).
4772 *Palaeogeogr. Palaeoclim. Palaeoecol.* 301, 97–107.
- 4773 Costa, E., Garcés, M., López-Blanco, M., Serra-Kiel, J., Bernaola, G., Cabrera, L., Beamud, E., 2013. The
4774 Bartonian–Priabonian marine record of the eastern South Pyrenean foreland basin (NE Spain): a new
4775 calibration of the larger foraminifers and calcareous nannofossil biozonation. *Geol. Acta* 11, 177–193.
- 4776 Costamagna, L.G., Schäfer, A., 2013. The Cixerri Fm (Middle Eocene–Early Oligocene): analysis of a “Pyrenean”
4777 continental molassic system in southern Sardinia. *J. Medit. Earth Sci., Spec. Issue*, pp. 41–44.
- 4778 Cravatte, J., Dufaure, J.F., Prim, M., Rouaix, S., 1974. Les forages du Golfe du Lion : stratigraphie,
4779 sédimentologie. *Notes et Mémoires du C.F.P.* 11, 209–274.
- 4780 Crest, Y., Delmas, M., Braucher, R., Gunnell, Y., Calvet, M., ASTER Team, 2017. Cirques have growth spurts
4781 during deglacial and interglacial periods: evidence from ¹⁰Be and ²⁶Al nuclide inventories in the central and
4782 eastern Pyrenees. *Geomorphology* 278, 60–77.
- 4783 Crochet, B., 1991. Molasses syntectoniques du versant nord des Pyrénées : la série de Palassou. *Doc. BRGM*
4784 199, 387 p.
- 4785 Crouzel, F., 1957. Le Miocène continental du bassin d'Aquitaine, *Bull. Serv. Carte Géol. de la France*. 248, LIV
4786 (1956), 264 p.
- 4787 Crusafont, M., Villalta, J.F. de, Truyols, J., 1956. Caracterización del Eoceno continental en la cuenca de Tremp y
4788 edad de la orogenesis pirenaica. *Actes du deuxième Congrès international d'études pyrénéennes, Luchon–*
4789 *Pau 1954*. 2, I, pp. 39–53.
- 4790 Crusafont, M., 1961. Sobre la probable presencia del Mioceno continental en la cuenca del Ampurdan. *Actas III*
4791 *Congreso Int. Est. Pirenaicos, Gerona, 1958*. 1, 1, pp. 57–65.
- 4792 Crusafont, M., Hartenberger, J.L., Thaler, L., 1963. Sur des nouveaux restes de mammifères du gisement Eocène
4793 supérieur de Sossis, au nord de Tremp (Lérida, Espagne). *C. R. Acad. Sci. Paris* 257, 3014–3017.
- 4794 Crusafont, M., Riba, O., Villena, J., 1966. Nota preliminar sobre un nuevo yacimiento de vertebrados
4795 aquitanienses en Santa Cília (río Formiga, provincia de Huesca), y sus consecuencias geológicas. *Not. Com.*
4796 *Inst. Geol. Min. Esp.* 83, 7–13.

- 4797 Crusafont, M., Pons, J.M., 1969. Nuevos datos sobre el Aquitaniense del norte de la provincia de Huesca. *Acta*
4798 *Geol. Hisp.* 4, 124–125.
- 4799 Crusafont, M., Golpe-Posse, J.M., 1973. Yacimientos del Eoceno Prepirenaico (nuevas localidades del
4800 Cuisiense). *Acta Geol. Hisp.* 8, 145–147.
- 4801 Cuenca, G., Aranza, B., Canudo, J.I., Fuertes, V., 1989. Los micromamíferos del Mioceno inferior de Peñalba
4802 (Huesca). Implicaciones bioestratigráficas. *Geogaceta* 6, 75–77.
- 4803 Cuenca, G., Canudo, J.I., Laplana, C., Andres, J.A., 1992. Bio y cronoestratigrafía con mamíferos en la Cuenca
4804 Terciaria del Ebro: ensayo de síntesis. *Acta Geol. Hisp.* 27 (“Homenaje a Oriol Riba Arderiu”), 127–143.
- 4805 Cuesta, M.A., Checa, L., Casanovas, M.L., 2006. Los artiodáctilos del yacimiento ludiense de Sossís (Cuenca
4806 Prepirenaica, Lleida, España). *Rev. Esp. Paleontol.* 21, 123–144.
- 4807 Curry, M.E., van der Beek, P., Huismans, R.S., Wolf, S.G., Muñoz, J.A., 2019. Evolving paleotopography and
4808 lithospheric flexure of the Pyrenean Orogen from 3D flexural modeling and basin analysis. *Earth Planet. Sci.*
4809 *Lett.* 515, 26–37.
- 4810 Daignières, M., Séguret, M., Specht, M., ECORS Team, 1994. The Azarcq–Western Pyrenees ECORS Deep
4811 Seismic Profile. In: Mascle, A. (Ed), *Hydrocarbon and petroleum geology of France*, Spec. Publ. Eur. Assoc.
4812 *Petrol. Geosci.* 4, 199–208.
- 4813 Damotte, B. (Ed.), 1998. The ECORS Pyrenean deep seismic surveys, 1985–1994. *Mém. Soc. Géol. France* 173,
4814 108 p.
- 4815 Dautria, J.M., Liotard, J.M., Bosch, D., Alard, O., 2010. 160 Ma of sporadic basaltic activity on the Languedoc
4816 volcanic line (Southern France): a peculiar case of lithosphere–asthenosphere interplay. *Lithos* 120, 202–
4817 222.
- 4818 Debals, B., 2000. Mise au point sur la chronostratigraphie des dépôts alluviaux quaternaires de la Plaine du
4819 Roussillon : exemple de la vallée de la Têt (France). *Quaternaire* 11, 31–39.
- 4820 Debroas, É.J., Azambre, B., 2012. Des brèches aux lherzolites. La mise en place des lherzolites dans les fosses du
4821 flysch albo-cénomanién de la Ballongue et d'Aulus (Zone Nord-Pyrénéenne, Ariège). *Excursion AGSO*, 9–10
4822 June 2012, Guidebook, 120 p.
- 4823 DeFelipe, I., Pedreira, D., Pulgar, J.A., van der Beek, P.A., Bernet, M., Pik, R., 2019. Unraveling the Mesozoic and
4824 Cenozoic tectonothermal evolution of the eastern Basque–Cantabrian Zone, western Pyrenees, by low-
4825 temperature thermochronology. *Tectonics* 38, 3436–3461.
- 4826 Delmas, M., Calvet, M., Gunnell, Y., 2009. Variability of Quaternary glacial erosion rates—A global perspective
4827 with special reference to the Eastern Pyrenees. *Quat. Sci. Rev.* 28, 484–498.
- 4828 Delmas, M., Gunnell, Y., Calvet, M., 2014. Environmental controls on alpine cirque size. *Geomorphology* 206,
4829 318–329.
- 4830 Delmas, M., Braucher, R., Gunnell, Y., Guillou, V., Calvet, M., Bourlès, D., 2015. Constraints on Pleistocene
4831 glaciofluvial terrace age and related soil chronosequence features from vertical ¹⁰Be profiles in the Ariège
4832 River catchment (Pyrenees, France). *Glob. Planet. Change* 132, 39–53.

- 4833 Delmas M., Calvet M., Gunnell Y., Voinchet P., Manel C., Braucher R., Tissoux H., Bahain J.J., Perrenoud C., Saos
4834 T, Aster Team, 2018. Terrestrial ¹⁰Be and Electron Spin Resonance dating of fluvial terraces quantifies
4835 Quaternary tectonic uplift gradients in the eastern Pyrenees. *Quat. Sci. Rev.*, 193, 188–211.
- 4836 Deloule É., Alexandrov P., Cheilletz A., Laumonier B., Barbey P., 2002. In-situ U–Pb zircon ages for Early
4837 Ordovician magmatism in the eastern Pyrenees, France: the Canigou orthogneisses. *Int. J. Earth Sci.*, 91,
4838 398–405.
- 4839 Demory, F., Conesa, G., Oudet, J., Mansouri, H., Münch, P., Borgomano, J., Thouveny, N., Lamarche, J., Gisquet,
4840 F., Marié, L., 2011. Magnetostratigraphy and paleoenvironments in shallow-water carbonates: the
4841 Oligocene-Miocene sediments of the northern margin of the Liguro-Provençal basin (West Marseille,
4842 southeastern France). *Bull. Soc. Géol. Fr.* 182, 37–55.
- 4843 Demoulin, A., Mather, A., Whittaker, A., 2017. Fluvial archives, a valuable record of vertical crustal
4844 deformation. *Quat. Sci. Rev.* 166, 10–37.
- 4845 Dempster, T.J., Persano, C., 2006. Low temperature thermochronology: resolving geotherm shapes or
4846 denudation histories? *Geology* 34, 73–76.
- 4847 Denizot G., 1928. Note sur la morphologie, sur l'évolution et sur l'âge des terrasses toulousaines. *Bull. Soc. Hist.*
4848 *Nat. Toulouse* 57, 346–356.
- 4849 Depéret, C., 1885. Description géologique du bassin tertiaire du Roussillon. *Ann. Sci. Géol.* 17, 1–136. Thèse,
4850 Paris. Description des vertébrés fossiles du terrain pliocène du Roussillon. *Ann. Sci. Géol.* 17, 137–268.
- 4851 Depéret, C., 1912. Sur le grès éocène de Moulas, près le Boulou (Pyrénées-Orientales). *C. R. somm. Soc. Géol.*
4852 *France*, 21–22.
- 4853 Depéret, C., 1923. Les glaciations des vallées pyrénéennes françaises et leurs relations avec les terrasses
4854 fluviales. *C. R. Acad. Sci.* 176, 1519–1524.
- 4855 Dercourt, J., Ricou, L.E., Vrielynck, B. (eds.), 1993. Atlas Tethys: palaeoenvironmental maps. Gauthier-Villars,
4856 Paris, 307 p.
- 4857 De Sitter, L.U., 1952. Pliocene uplift of Tertiary mountain chains. *Am. J. Sci.* 250, 297–307.
- 4858 De Sitter, L.U., 1954. Note préliminaire sur la géologie du Val d'Aran. *Leidse Geol. Med.* 18, 272–280.
- 4859 De Sitter L.U., 1961. La phase tectogénique pyrénéenne dans les Pyrénées méridionales. *C. R. Somm. Soc. Géol.*
4860 *Fr.* 8, 224–225.
- 4861 De Vicente, G., Cloetingh, S., Muñoz-Martin, A., Olaiz, A., Stich, D., Vegas, R., Galindo-Zaldivar, J., Fernandez-
4862 Lozano, J., 2008. Inversion of moment tensor focal mechanisms for active stresses around the
4863 microcontinent Iberia: tectonic implications. *Tectonics* 27, TC1009, doi:10.1029/2006TC002093.
- 4864 Diaz, J., Vergés, J., Chevrot, S., Antonio-Vigil, A. Ruiz, M., Sylvander, M., Gallart, J. 2018. Mapping the crustal
4865 structure beneath the eastern Pyrenees. *Tectonophysics* 744, 296–309.
- 4866 Dieni, I., Massari, F., Médus, J., 2008. Age, depositional environment and stratigraphic value of the Cuccuru 'e
4867 Flores Conglomerate: insight into the Palaeogene to Early Miocene geodynamic evolution of Sardinia. *Bull.*
4868 *Soc. Géol. Fr.* 179, 51–72.
- 4869 Donville, B., 1973a. Ages K–Ar des vulcanites du Haut Ampurdan (NE de l'Espagne). Implications
4870 stratigraphiques. *C. R. Acad. Sci. Paris* 276, 2497–2500.

- 4871 Donville, B., 1973b. Ages K–Ar des vulcanites du Bas Ampurdan. C. R. Acad. Sci. Paris 276, 3253–3256.
- 4872 Donville, B., 1973c. Ages K–Ar des roches volcaniques de la depression de La Selva (NE de l'Espagne). C. R. Acad.
4873 Sci. Paris 277, 1–4.
- 4874 Donville, B., 1973d. Géologie néogène et âge des éruptions volcaniques de la Catalogne orientale. PhD thesis,
4875 Univ. of Toulouse, 3 vols.
- 4876 Donville, B., 1976. Géologie néogène de la Catalogne orientale. Bull. BRGM 2, 177–210.
- 4877 Donzeau-Wiazemsky, M., Laumonier, B., Guitard, G., Autran, A., Llac, F., Baudin, T., Calvet, M., 2010. Carte
4878 géologique de la France, 1:50,000 scale, sheet 1096 Céret. Handbook by Laumonier, B., Calvet, M.,
4879 Donzeau-Wiazemsky, M., Barbey, P., Marignac, C., Lambert, A., Lenoble, J.L., Autran, A., Cocherie, A.,
4880 Baudin, T., Llac, F., 2015, BRGM édit., Orléans, 164 p.
- 4881 Douvillé, H., 1924. A propos du poudingue de Palassou. C. R. Somm. Soc. Géol. Fr. 15, 160–162.
- 4882 Dubos-Sallée, N., Nivière, B., Lacan, P., Hervouët, Y., 2007. A structural model for the seismicity of the Arudy
4883 (1980) epicentral area (Western Pyrenees, France). Geophys. J. Int. 171, 259–270.
- 4884 Dubreuilh, J., Capdeville, J.P., Farjanel, G., Karnay, G., Platel, J.P., Simon-Coinçon, R., 1995. Dynamique d'un
4885 comblement continental néogène et quaternaire : l'exemple du bassin d'Aquitaine. Géologie de la France 4,
4886 3–26.
- 4887 Dufrechou, G., Tiberi, C., Martin, R., Bonvalot, S., Chevrot, S., Seoane, L., 2018. Deep structure of Pyrenees
4888 range (SW Europe) imaged by joint inversion of gravity and teleseismic delay time. Geophys. J. Int. 214,
4889 282–301.
- 4890 Durand-Delga, M., Fontboté, J.M., 1980. Le cadre structural de la Méditerranée occidentale. In: Aubouin, J.,
4891 Debelmas, J., Latreille, M. (eds.), Géologie des chaînes alpines issues de la Téthys. Mém. BRGM 115, 67–85.
- 4892 Duranthon, F., 1991. Biozonation des molasses continentales oligo-miocènes de la région toulousaine par
4893 l'étude des mammifères. Apports à la connaissance du Bassin d'Aquitaine. C. R. Acad. Sc. Paris 313, 965–
4894 970.
- 4895 Duranthon, F., 1992. Les mammifères fossiles recueillis par l'Abbé Pouech. Actes du colloque J.J. Pouech,
4896 Pamiers 16–17 oct. 1992. Soc. Hist. Archéol. Pamiers Basse Ariège, pp. 49–54.
- 4897 Duranthon, F., 1993. Nouveaux gisements à rongeurs dans les molasses oligo-miocènes de la région
4898 toulousaine. Palaeovertebrata (Montpellier) 22, 113–136.
- 4899 Duranthon, F., Cahuzac, B., 1997. Eléments de corrélation entre échelles marines et continentales : les données
4900 du bassin d'Aquitaine au Miocène. In: Aguilar, J.P., Legendre, S., Michaux J. (eds.), Actes du Congrès
4901 BiochronM'97. Mém. Trav. EPHE (Montpellier) 21, pp. 591–608.
- 4902 Duvail, C., Le Strat, P., Alabouvette, B., Perrin, J. Seranne, M., 2000. Évolution géodynamique du bassin du
4903 Roussillon : analyse des profils sismiques calibrés par les sondages profonds de Elne 1 et de Canet 1.
4904 Rapport n° GTR/BRGM/1200-137, Montpellier, 23 p.
- 4905 Duvail, C., Gorini, C., Lofi, J., Le Strat, P., Clauzon, G., Dos Reis, T., 2005. Correlation between onshore and
4906 offshore Pliocene–Quaternary systems tracks below the Roussillon basin (Eastern Pyrenees, France). Mar.
4907 Petrol. Geol. 22, 747–756.

- 4908 Duval, M., Sancho, C., Calle, M., Guilarte, V., Peña-Monné, J.L., 2015. On the interest of using the multiple
4909 center approach in ESR dating of optically bleached quartz grains: some examples from the Early
4910 Pleistocene terraces of the Alcanadre River (Ebro basin, Spain). *Quat. Geochron.* 29, 58–69.
- 4911 ECORS Pyrenees Team, 1988. The ECORS deep reflection seismic survey across the Pyrenees. *Nature* 331, 508–
4912 511.
- 4913 Ellenberger, F., Gottis, M., 1967. Sur les jeux de failles pliocènes et quaternaires dans l'arrière-pays narbonnais.
4914 *Rev. Géogr. Phys. Géol. Dyn.* 9, 153–159.
- 4915 Ellenberger, F., Freytet, P., Plaziat, J.C., Bessière, G., Viillard, P., Berger, J.M., Marchal, J.P., 1987. Handbook to
4916 the Carte géologique de la France, 1:50,000 scale, sheet Capendu (1060). BRGM, Orléans, 88 p.
- 4917 Enjalbert, H., 1960. Les Pays Aquitains, le modelé et les sols. Impr. Bière, Bordeaux, 618 p.
- 4918 Escarguel, G., Marandat, B., Legendre, S., 1997. Sur l'âge numérique des faunes de mammifères du Paléogène
4919 d'Europe occidentale, en particulier celles de l'Eocène inférieur et moyen. In: Aguilar, J.P., Legendre, S.,
4920 Michaux J. (eds.), *Actes du Congrès BiochronM'97. Mém. Trav. EPHE (Montpellier)* 21, pp. 441–460.
- 4921 Espurt, N., Angrand, P., Teixell, A., Labaume, P., Ford, M., de Saint Blanquat, M., Chevrot, S., 2019. Crustal-scale
4922 balanced cross-section of the Central Pyrenean belt (Nestes–Cinca transect): highlighting the structural
4923 control of Variscan belt and Permian–Mesozoic rift systems on mountain building. *Tectonophysics* 764, 25–
4924 45.
- 4925 Etheve, N., Frizon de Lamotte, D., Mohn, G., Martos, R., Roca, E., Blanpied, C., 2016. Extensional vs
4926 contractional deformation in Ibiza (Balearic Promontory, Spain): integration in the West-Mediterranean
4927 back-arc setting. *Tectonophysics* 682, 35–55.
- 4928 Faillat, J.P., Aguilar, J.P., Calvet, M., Michaux, J., 1990. Les fissures à remplissages fossilifères néogènes du
4929 plateau de Baixas (Pyrénées orientales, France), témoins de la distension oligo-miocène. *C.R. Acad. Sci. Paris*
4930 *sér. II* 311, 205–212.
- 4931 Fernandes, R.M.S., Miranda, J.M., Meijninger, B.M.L., Bos, M.S., Noomen, R., Bastos, L., Ambrosius, B.A.C., Riva,
4932 R.E.M., 2007. Surface velocity field of the Ibero-Maghrebian segment of the Eurasia–Nubia plate boundary.
4933 *Geophys. J. Int.* 169, 315–324.
- 4934 Filleaudeau P.Y., Mouthereau F., Pik R., 2011. Thermo-tectonic evolution of the south-central Pyrenees from
4935 rifting to orogeny: insights from detrital zircon U/Pb and (U–Th)/He thermochronometry. *Basin Res.* 23, 1–
4936 17.
- 4937 Fillon, C., van der Beek, P., 2012. Post-orogenic evolution of the southern Pyrenees: constraints from inverse
4938 thermo-kinematic modelling of low-temperature thermochronology data. *Basin Res.* 23, 1–19.
- 4939 Fillon, C., Gautheron, C., van der Beek, P., 2013. Oligocene–Miocene burial and exhumation of the Southern
4940 Pyrenean foreland quantified by low-temperature thermochronology. *J. Geol. Soc. (London)* 170, 67–77.
- 4941 Fitzgerald, P.G., Muñoz, J.A., Coney, P.J., Baldwin, S.L., 1999. Asymmetric exhumation across the Pyrenean
4942 orogen: implications for the tectonic evolution of a collisional orogen. *Earth Planet. Sci. Lett.* 173, 157–170.
- 4943 Fleta, J., Vergés, J., Escuer, J., Pujadas, J., 1994. Mapa geológico de España, escala 1:50,000, Figueras (258).
4944 Memoria IGME, Madrid, 83 p.

4945 Fleta, J., Santanach, P., Goula, X., Martínez, P., Grellet, B., Masana, E., 2001. Preliminary geologic,
4946 geomorphologic and geophysical studies for the palaeoseismological analysis of the Amer fault, NE Spain.
4947 *Netherl. J. Geosci.* 80, 243–253.

4948 Ford, M., Hemmer, L., Vacherat, A., Gallagher, K., Christophoul, F., 2016. Retro-wedge foreland basin evolution
4949 along the ECORS line, eastern Pyrenees, France. *J. Geol. Soc. (London)* 173, 419–437.

4950 Ford M., Vergés J., 2020. Evolution of a salt-rich transtensional rifted margin, eastern North Pyrenees, France. *J.*
4951 *Geol. Soc. (London)*, <https://doi.org/10.1144/jgs2019-157>;

4952 Friend, P.F., Lloyd, M.J., Mcelroy, R., Turner, J., Van Gelder, A., Vincent, S.J., 1996. Evolution of the central part
4953 of the northern Ebro basin margin, as indicated by its Tertiary fluvial sedimentary infill. In: Friend, P.F.
4954 Dabrio, C.J. (eds), *Tertiary basins of Spain, the stratigraphic record of crustal kinematics*. Cambridge
4955 University Press, Cambridge, pp. 166–172.

4956 Gallart, J., Daignières, M., Banda, E., Suriñach, E., Hirn, A. 1980. The eastern Pyrenean domain: lateral variations
4957 at crust-mantle level. *Ann. Geophys.* 36, 141–158.

4958 Gallart, J., Olivera, C., Daignières, M., Hirn, A. 1982. Quelques données récentes sur la relation entre fractures
4959 crustales et séismes dans les Pyrénées orientales. *Bull. Soc. Géol. Fr.* 24, 293–298.

4960 Gallart, J., Diaz, J., Nercessian, A., Mauffret, A., Dos Reis, T., 2001. The eastern end of the Pyrenees: seismic
4961 features at the transition to the NW Mediterranean. *Geophys. Res. Lett.* 28, 2277–2280.

4962 Garcés, M., Cabrera, L., Agustí, J., Parés, J.M., 1997. Old World first appearance datum of “Hipparion” horses:
4963 late Miocene large mammal dispersal and global events. *Geology* 25, 19–22.

4964 Garcés, M., López-Blanco, M., Valero, L., Beamud, E., Muñoz, J.A., Oliva-Urcia, B., Vinyoles, A., Arbués, P.,
4965 Cabello, P., Cabrera, L., 2020. Paleogeographic and sedimentary evolution of the south-Pyrenean foreland
4966 basin. *Mar. Petrol. Geol.* 113, 104105.

4967 García-Castellanos, D., Vergés, J., Gaspar-Escribano, J., Cloetingh, S., 2003. Interplay between tectonics,
4968 climate, and fluvial transport during the Cenozoic evolution of the Ebro Basin (NE Iberia). *J. Geophys. Res.*
4969 108, 2347, doi:10.1029/2002jb002073.

4970 García-Castellanos, D., Cloetingh, S., 2012. Modeling the interaction between lithospheric and surface
4971 processes in foreland basins. In: Busby, C., Azor, A. (eds), *Tectonics of sedimentary basins: recent advances*.
4972 Blackwell, pp. 152–181.

4973 García-Castellanos, D., Larrasoaña, J.C., 2015. Quantifying the post-tectonic topographic evolution of closed
4974 basins: The Ebro basin (Northeast Iberia). *Geology* 43, 663–666.

4975 García-Ruiz, J.M., Valero-Garcés, B.L., Martí-Bono, C., González-Sampéris, P., 2003. Asynchronicity of maximum
4976 glacier advances in the central Spanish Pyrenees. *J. Quat. Sci.* 18, 61–72.

4977 García-Ruiz, J.M., Martí-Bono, C., Peña-Monné, J.L., Sancho, C., Rhodes, E., Valero, B., Gonzalez Samperiz, P.,
4978 Moreno, A., 2013. Glacial and fluvial deposits in the Aragón Valley, central western Pyrenees: chronology of
4979 the Pyrenean late Pleistocene glaciers. *Geogr. Ann., Ser. A Phys. Geogr.* 95, 15–32.

4980 García-Ruiz, J.M., Palacios, D., de Andrés, N., Valero-Garcés, B.L., López-Moreno, J., Sanjuán, Y., 2014. Holocene
4981 and ‘Little Ice Age’ glacial activity in the Marboré Cirque, Monte Perdido Massif, Central Spanish Pyrenees.
4982 *The Holocene* 24, 1439–1452.

- 4983 García Sainz, L., 1940. Las superficies de erosión que preceden a los glaciares cuaternarios del Pirineo central y
4984 sus recíprocas influencias. *Estud. Geogr.* 1, 45–73.
- 4985 García Senz, J., Ramirez, J.I., Navarro, J.J., Rodríguez, R., Castaño, R.M., Leyva, F., García, J., Ramirez del Poyo, J.,
4986 2009. Mapa geológico de España, 1:50,000, Pont de Suert, sheet no. 213, and handbook (76 p). Instituto
4987 Geológico y Minero de España.
- 4988 Gardère, P., 2002. Les Sables Fauves : dynamique sédimentaire et évolution morpho-structurale du Bassin
4989 d'Aquitaine au Miocène moyen. *Strata (Toulouse)* 40, 264 p.
- 4990 Gardère, P., 2005. La Formation des Sables Fauves : dynamique sédimentaire au Miocène moyen et évolution
4991 morpho-structurale de l'Aquitaine (SW France) durant le Néogène. *Eclog. Geol. Helv.* 97, 201–217.
- 4992 Gardère, P., Rey, J., Duranthon, F., 2002. Les « Sables Fauves », témoins de mouvements tectoniques dans le
4993 bassin d'Aquitaine au Miocène moyen. *C. R. Geoscience* 334, 987–994.
- 4994 Gardère, P., Pais J., 2007. Palynologic data from Aquitaine (SW France) Middle Miocene Sables Fauves
4995 Formation. Climatic evolution. *Ciências da Terra (Lisboa)* 15, 151–161.
- 4996 Garwin, L.G., 1985. Fission-track dating and tectonics in the Eastern Pyrenees. PhD thesis (unpubl.), Univ. of
4997 Cambridge.
- 4998 Gaspar-Escribano, J., van Wees, J.D., Ter Voorde, M., Cloetingh, S., Roca, E., Cabrera, L., Muñoz, J.A., Ziegler,
4999 P.A., 2001. Lithospheric structure of the Ebro Basin (NE Spain): constraints from 3D flexural modeling.
5000 *Geophys. J. Int.* 145, 349–367.
- 5001 Gaudant, J., 1999. Présence du genre Lates Cuvier et Valenciennes dans les grès de Moulas (Pyrénées-
5002 Orientales). *Géologie de la France* 4, 67–75.
- 5003 Gély, J.P., Sztrakos, K., 2000. L'évolution paléogéographique et géodynamique du Bassin aquitain au Paléogène
5004 : enregistrement et datation de la tectonique pyrénéenne. *Géologie de la France* 2, 31–57.
- 5005 Genna, A., Lenotre, N., Capdeville, J.P., 1997. Proposition d'un modèle d'inversion tectonique au Plio-
5006 Quaternaire dans les Corbières et le Minervois (France). Conséquences morphologiques et hydrologiques.
5007 *C. R. Acad. Paris* 325, 807–813.
- 5008 Genti, M., 2015. Impact des processus de surface sur la déformation actuelle des Pyrénées et des Alpes. PhD
5009 thesis (unpubl.), Univ. of Montpellier, 247 p.
- 5010 Gibert, J., Agustí, J., Moya, S., 1979. Bioestratigrafía de l'Emporda. *Paleontol. Evol. (Sabadell)* 9, 43–47.
- 5011 Gibert, J., Agustí, J., Moya, S., 1980. Nuevos datos sobre la bioestratigrafía del Ampurdán. *Bol. Geol. Min.*
5012 (Madrid) 41–46, 705–712.
- 5013 Gibson, M., Sinclair, H.D., Lynn, G.J., Stuart, F.M., 2007. Late- to post-orogenic exhumation of the Central
5014 Pyrenees revealed through combined thermochronological data and modelling. *Basin Res.* 19, 323–334.
- 5015 Gillot, P.Y., 1974. Chronométrie par la méthode K/Ar des laves des Causses et du Bas-Languedoc.
5016 Interprétation. MPhil. Dissertation (unpubl.), Univ. Paris-Sud, 61 p.
- 5017 Giménez, J., Surinach, E., Fleta, J. Goula, X., 1996. Recent vertical movements from high-precision leveling data
5018 in northeast Spain. *Tectonophysics* 263, 149–161.

- 5019 Glangeaud, P., 1938. Sur la découverte d'un gisement stampien à Anthracothérium dans les argiles à lignites de
5020 Nassiet (Landes). P. V. Soc. Linn. (Bordeaux) 40, 16–22.
- 5021 Golpe-Posse, J.M., 1981a. Paleobiologia dels jaciments amb vertebrats al transit Eocè-Oligocè a la Catalunya
5022 central. Bol. Inst. Catal. Hist. Nat. 48 (Sec. Geol. 3), 123–134.
- 5023 Golpe Posse, J.M., 1981b. Los Mamíferos de las cuencas de Cerdanya y Seu de Urgell y sus yacimientos;
5024 Vallesiense Medio-Superior. Bol. Geol. Min. (Madrid) 42, 91–100.
- 5025 Gómez de Soler, B., Campeny Vall-Llosera, G., Van der Made, J., Oms, O., Agustí, J., Sala, R., Blain, H.A.,
5026 Burjachs, F., Claude, J., García Catalán, S., Riba, D., Rosillo, R., 2012. A new key locality for the Pliocene
5027 vertebrate record of Europe: the Camp dels Ninots maar (NE Spain). Geol. Acta 10, 1–17.
- 5028 Gómez-Gras, D., Roigé, M., Fondevilla, V., Oms, O., Boya, S., Remacha, E., 2016. Provenance constraints on the
5029 Tremp Formation paleogeography (southern Pyrenees): Ebro Massif vs Pyrenees sources. Cretaceous Res.
5030 57, 414–427.
- 5031 Gomis Coll, E., Parés, J.M., Cabrera, L., 1997. Nuevos datos magnetoestratigráficos del tránsito Oligoceno-
5032 Mioceno en el sector SE de la Cuenca del Ebro (provincias de Lleida, Zaragoza y Huesca, NE de España). Acta
5033 Geol. Hisp. 32, 185–199 (publ. in 1999).
- 5034 Gong, Z., Langereis, C.G., Mullender, T.A.T., 2008. The rotation of Iberia during the Aptian and the opening of
5035 the Bay of Biscay. Earth Planet. Sci. Lett. 273, 80–93.
- 5036 Gorini, C., Lofi, J., Duvail, C., Dos Reis, T., Guennoc, P., Le Strat, P., Mauffret, A., 2005. The Late Messinian
5037 salinity crisis and Late Miocene tectonism: interaction and consequences on the physiography and post-rift
5038 evolution of the Gulf of Lions margin. Mar. Petrol. Geol. 22, 695–712.
- 5039 Goron, L., 1931. Un type de vallée pyrénéenne : La Barguillère (Pyrénées Ariégeoises). Rev. Géogr. Pyrén. Sud-
5040 Ouest 2, 59–94.
- 5041 Goron, L., 1937. Les unités topographiques du Pays ariégeois : Le rôle des cycles d'érosion tertiaires et des
5042 glaciations quaternaires dans leur morphologie. Rev. Géogr. Pyrén. Sud-Ouest 8, 300–334.
- 5043 Goron, L., 1941a. Les Pré-Pyrénées ariégeoises et garonnaises, essai d'étude morphogénique d'une lisière de
5044 montagne. Privat, Toulouse, 886 p.
- 5045 Goron, L., 1941b. Le rôle des glaciations quaternaires dans le modelé des vallées maîtresses des Pré-Pyrénées
5046 ariégeoises et garonnaises et leur avant-pays. Privat, Toulouse, 460 p. Abridged in: Rev. Géogr. Pyrén. Sud-
5047 Ouest 12, pp. 5–61, 147–226, 322–356, 373–430.
- 5048 Gottis, M., 1958. L'apport des travaux de la Compagnie d'Exploitation Pétrolière (CEP) dans la connaissance du
5049 bassin tertiaire du Roussillon. Bull. Soc. Géol. Fr. 6-VIII, 881–883.
- 5050 Gottis, M., Lenguin, M., Sellier, E., Tavoso, A., 1972. Hypothèses sur les causes et la chronologie des
5051 défluviations dans la gouttière de Carcassonne entre Toulouse et Narbonne. Bull. Soc. Linn. Bordeaux 6,
5052 125–132.
- 5053 Goula, X., Olivera, C., Fleta, J., Grellet, B., Lindo, R., Rivera, L.A., Cisternas, A., Carbon, D., 1999. Present and
5054 recent stress regime in the eastern part of the Pyrenees. Tectonophysics 308, 487–502.

5055 Gourinard, Y., 1971. Les moraines de la basse vallée du Carol entre Latour et Puigcerda (Pyrénées orientales
5056 franco-espagnoles). C. R. Acad. Sci. Paris D 272, 3112–3115.

5057 Granado, P., Urgeles, R., Sàbat, F., Albert-Villanueva E., Roca, E., Muñoz, J.A., Nicoletta Mazzuca, N., Gambini,
5058 R., 2016. Geodynamical framework and hydrocarbon plays of a salt giant: the NW Mediterranean Basin.
5059 Petrol. Geosci. 22, 309–321.

5060 Granger, D.E., Kirchner, J.W., Finkel, R.C., 1997. Quaternary downcutting rate of the New River, Virginia,
5061 measured from differential decay of cosmogenic ²⁶Al and ¹⁰Be in cave-deposited alluvium. *Geology* 25, 107–
5062 110.

5063 Granger, D.E., Muzikar, P., 2001. Dating sediment burial with cosmogenic nuclides: theory, techniques, and
5064 limitations. *Earth Planet. Sci. Lett.* 188, 269–281.

5065 Grool, A.R., Ford, M., Vergés, J., Huisman, R.S., Christophoul, F., Dielforder, A., 2018. Insights into the crustal-
5066 scale dynamics of a doubly vergent orogen from a quantitative analysis of its forelands: a case study of the
5067 Eastern Pyrenees. *Tectonics* 37, 450–476.

5068 Guennoc, P., Gorini, C., Mauffret, A., 2000. Histoire géologique du golfe du Lion et cartographie du rift oligo-
5069 aquitainien et de la surface messinienne. *Géologie de la France* 3, 67–97.

5070 Guitard, G., 1970. Le métamorphisme hercynien mésozonal et les gneiss œillés du massif du Canigou (Pyrénées
5071 orientales). *Mém. BRGM* 63, 353 p.

5072 Guitard, G., Geysant, J., Laumonier, B., Autran, A., Fontailles, M., Dalmayrac, M., Vidal, J.-C., Bandet, Y., 1992.
5073 Carte géologique de la France, 1:50 000 scale, sheet Prades (1095). BRGM, Orléans. Handbook by Guitard,
5074 G., Laumonier, B., Autran, A., Bandet, Y., Berger, G.-M. (1998), 198 p.

5075 Gunnell, Y., 2000. Apatite fission track thermochronology: an overview of its potential and limitations in
5076 geomorphology. *Basin Res.* 12, 115–132.

5077 Gunnell, Y., Calvet M., 2006. Comment on “Origin of the highly elevated Pyrenean peneplain”, by J. Babault et
5078 al. *Tectonics* 25, TC3003, doi:10.1029/2005TC001849.

5079 Gunnell, Y., Zeyen, H., Calvet, M., 2008. Geophysical evidence of a missing lithospheric root beneath the
5080 Eastern Pyrenees: consequences for post-orogenic uplift and associated geomorphic signatures. *Earth*
5081 *Planet. Sci. Lett.* 276, 302–313.

5082 Gunnell, Y., Calvet, M., Bricchau, S., Carter, A., Aguilar, J.P., Zeyen, H., 2009. Low long-term erosion rates in high-
5083 energy mountain belts: insights from thermo- and biochronology in the Eastern Pyrenees. *Earth Planet. Sci.*
5084 *Lett.* 278, 208–218.

5085 Harlé, E., 1893. Restes d’éléphants du sud-ouest de la France. *Bull. Soc. Hist. Nat. Toulouse*, pp. 28–34.

5086 Hartevelt, J.J.A., 1970. Geology of the Upper Segre and Valira valleys, central Pyrenees, Andorra-Spain. *Leid.*
5087 *Geol. Med.* 45, 167–236.

5088 Hernandez, M., Mercier, N., Bertran, P., Colonge, D., Lelouvier, L.A., 2012. Premiers éléments de datation des
5089 industries du Pléistocène moyen (Acheuléen–Paléolithique moyen ancien) de la région pyrénéo-garonnaise
5090 : une approche géochronologique pluri-méthodes (TL, OSL et TT-OSL) des sites de Duclos et Romentères.
5091 *Paléo* 23, 155–170.

- 5092 Hérail, G., Hubschman, J., Jalut G., 1987. Quaternary glaciation in the French Pyrenees. *Quat. Sci. Rev.* 5, 397–
5093 402.
- 5094 Hervouët, Y., 1997. Déformations alpines, inversion tectonique négative et karstogenèse : exemple de la Pierre
5095 Saint-Martin (Pyrénées-Atlantiques, France). *Bull. Soc. Géol. Fr.* 168, 663–674.
- 5096 Hez, G., Jaillet, S., Calvet, M., Delannoy, J.J., 2015. Un enregistreur exceptionnel de l'incision de la vallée de la
5097 Têt : le karst de Villefranche, Pyrénées-orientales. France. *Karstologia* 65, 9–32.
- 5098 Hilgen, F.J., Lourens, L.J., Van Dam, J.A., Beu, A.G., Boyes, A.E., Cooper, R.A., Krijgsman, W., Ogg, J.G., Piller,
5099 W.E., Wilson, D.S., 2012. The Neogene Period. In: Gradstein, F.M., Ogg, J.G., Schmitz, M.D., Ogg, G.M. (eds),
5100 The geologic time scale. Elsevier, pp. 923–978.
- 5101 Hirst, J.P.P., Nichols, G.J., 1986. Thrust tectonic controls on the Miocene distribution patterns, southern
5102 Pyrenees. In: Allen, P.A., Homewood, P. (eds), *Foreland basins*. IAS Spec. Publ. 8, pp. 247–258.
- 5103 Hogan, P.J., Burbank, D.W., 1996. Evolution of the Jaca piggyback basin and emergence of the External Sierra,
5104 southern Pyrenees. In: Friend, P.F., Dabrio, C.J. (eds), *Tertiary basins of Spain, the stratigraphic record of*
5105 *crustal kinematics*. Cambridge University Press, Cambridge, pp. 153–160.
- 5106 Hourdebaigt, M.L., Villatte, J., Crochet, B., 1986. Le poudingue de Jurançon du Sud de Pau appartient à la série
5107 syntectonique de Palassou : preuve par la découverte d'une malacofaune éocène. *C. R. Acad. Sci. Paris sér.*
5108 *II* 303, 951–955.
- 5109 Hourdebaigt, M.L., 1988. Stratigraphie et sédimentologie des molasses synorogéniques en Béarn et en Bigorre.
5110 PhD thesis (unpubl.), Univ. Paul-Sabatier, Toulouse, 240 p.
- 5111 Hubschman J., 1973. Etablissement par l'étude des faciès d'altération, d'un schéma stratigraphique du
5112 Quaternaire garonnais et ariégeois. *C. R. Acad. Sci. Paris D* 277, 753–755.
- 5113 Hubschman, J., 1975a. Morphogenèse et pédogenèse dans le piémont des Pyrénées garonnaises et ariégeoises.
5114 H. Champion, Paris, 745 p.
- 5115 Hubschman, J., 1975b. Conclusion, évolution pédo-géochimique et interprétation paléobioclimatique du
5116 piémont quaternaire garonnais. *Bull. Assoc. Fr. Étud. Quat.* 3–4, 211–216.
- 5117 Huyghe, D., Mouthereau, F., Castellort, S., Filleaudeau, P.Y., Emmanuel, L., 2009. Paleogene propagation of the
5118 southern Pyrenean thrust wedge revealed by finite strain analysis in frontal thrust sheets: Implications for
5119 mountain building. *Earth Planet. Sci. Lett.* 288, 421–433.
- 5120 Huyghe, D., Mouthereau, F., Emmanuel, L., 2012. Oxygen isotopes of marine mollusc shells record Eocene
5121 elevation change in the Pyrenees. *Earth Planet. Sci. Lett.* 345–348, 131–141.
- 5122 Huyghe D., Mouthereau F., Ségalen, L., Furió, M., 2020. Long-term dynamic topographic support during post-
5123 orogenic crustal thinning revealed by stable isotope ($\delta^{18}\text{O}$) paleo-altimetry in eastern Pyrenees. *Sci. Rep.*,
5124 doi.org/10.1038/s41598-020-58903-w.
- 5125 Icole, M., 1968. Données nouvelles sur la formation de Lannemezan. *C. R. Acad. Sci. Paris* 267, 687–689.
- 5126 Icole M., 1969. Age et nature de la formation dite « de Lannemezan ». *Rev. Géogr. Pyrén. Sud-Ouest* 40, 157–
5127 170.

- 5128 Icole, M., 1973. Géochimie des altérations dans les nappes d'alluvions du piémont occidental nord-pyrénéen.
5129 Essai de paléopédologie quaternaire. Mém. Sci. Géol. 40, Univ. Louis Pasteur, Strasbourg, 201 p.
- 5130 Jalut, G., Montserrat, J., Fontugne, M., Delibrias, G., Vilaplana, J.M., Julià, R., 1992. Glacial to interglacial
5131 vegetation changes in the northern and southern Pyrenees: deglaciation, vegetation cover and chronology.
5132 Quat. Sci. Rev. 11, 449–480.
- 5133 Jammes, S., Manatschal, G., Lavier, L., Masini, E., 2009. Tectonosedimentary evolution related to extreme
5134 crustal thinning ahead of a propagating ocean: example of the western Pyrenees. Tectonics 28, TC4012, 24
5135 p.
- 5136 Jarman, D., Calvet, M., Corominas, J., Delmas, M., Gunnell, Y., 2014. Large-scale rock slope failures in the
5137 Eastern Pyrenees: identifying a sparse but significant population in paraglacial and parafluvial contexts.
5138 Geogr. Ann. Ser. A: Phys. Geogr. 96, 357–391.
- 5139 Jolivet, M., Labaume, P., Monié, P., Brunel, M., Arnaud, N., Campani, M., 2007. Thermochronology constraints
5140 for the propagation sequence of the south Pyrenean basement thrust system (France–Spain). Tectonics 26,
5141 TC5007, doi:10. 1029 /2006 TC002080.
- 5142 Jolivet, L., Romagny, A., Gorini, C., Maillard, A., Thion, I., Couëffé, R., Ducoux, M., Séranne, M., 2020. Fast
5143 dismantling of a mountain belt by mantle flow: late-orogenic evolution of Pyrenees and Liguro-Provençal
5144 rifting. Tectonophysics 776, 228312, 15 p.
- 5145 Jones, S.J., 2004. Tectonic controls on drainage evolution and development of terminal alluvial fans, southern
5146 Pyrenees, Spain. Terra Nova 16, 121–127.
- 5147 Juez Larré, J., Andriessen, P.A.M., 2006. Tectonothermal evolution of the northeastern margin of Iberia since
5148 the break-up of Pangea to present, revealed by low-temperature fission-tracks and (U–Th)/He
5149 thermochronology, a case history of the Catalan Coastal Ranges. Earth Planet. Sci. Lett. 243, 159–180.
- 5150 Karnay, G., Dubreuilh J., 1998. Carte géologique de la France, 1:50,000 scale, sheet Lembeye (1005). BRGM,
5151 Orléans. Handbook by Kamay, G., Mauroux, B., Châteauneuf, J.J., 50 p.
- 5152 Kästle, E.D., Rosenberg, C., Boschi, L., Bellahsen, N., Meier, T., El-Sharkawy, A., 2019. Slab break-offs in the
5153 Alpine Subduction Zone. Solid Earth Discuss., 16 p., <https://doi.org/10.5194/se-2019-17>.
- 5154 Kiden, P., Törnqvist, T.E., 1998. Can river terrace flights be used to quantify Quaternary tectonic uplift rates? J.
5155 Quat. Sci. 13, 573–574.
- 5156 Kieken, M., 1973. Évolution de l'Aquitaine au cours du Tertiaire. Bull. Soc. Géol. Fr. 15, 51–60.
- 5157 Kieken, M., Burger, J.J., Thibault, C., 1975. Handbook to the Carte géologique de la France, 1:50,000 scale,
5158 sheet Saint-Vincent-de-Tyrosse (975–976). BRGM, Orléans, 46 p.
- 5159 Klein, C., 1990. L'évolution géomorphologique de l'Europe hercynienne occidentale et centrale. Aspects
5160 régionaux et essai de synthèse. CNRS Editions, Paris, 177 p.
- 5161 Kleinsmiede, W.F.J., 1960. Geology of the Valle de Aran (Central Pyrenees). Leid. Geol. Med. 25, 129–245.
- 5162 Labaume, P., Séguret, M., Seyve, C., 1985. Evolution of a turbiditic foreland basin and analogy with an
5163 accretionary prism: example of the Eocene South-Pyrenean basin. Tectonics 4, 661–685.

5164 Labaume, P., Méresse, F., Jolivet, M., Teixell, A., Lahfid, A., 2016a. Tectonothermal history of an exhumed
5165 thrust-sheet-top basin: An example from the south Pyrenean thrust belt. *Tectonics* 35, 1280–1313.

5166 Labaume, P., Meresse, P., Jolivet, M., Teixell, A., 2016b. Exhumation sequence of the basement thrust units in
5167 the west-central Pyrenees. Constraints from apatite fission track analysis. *Geogaceta* 60, 11–14.

5168 Labaume, P., Teixell, A., 2018. 3D structure of subsurface thrusts in the eastern Jaca Basin, southern Pyrenees.
5169 *Geol. Act*, 16, 477–498.

5170 Labaume, P., Teixell, A., 2020. Evolution of salt structures of the Pyrenean rift (Chaînons Béarnais, France):
5171 From hyper-extension to tectonic inversion.
5172 *Tectonophysics*, <https://doi.org/10.1016/j.tecto.2020.228451>.

5173 Lacan, P., Ortuño, M., 2012. Active tectonics of the Pyrenees: a review. *J. Iberian Geol.* 38, 9–30.

5174 Lacan, P., Nivière, B., Rousset, D., Sénéchal, P., 2012. Late Pleistocene folding above the Mail Arrouy Thrust,
5175 North-Western Pyrenees (France). *Tectonophysics* 541–543, 57–68.

5176 Lacombe, O., Jolivet, L., 2005. Structural and kinematic relationships between Corsica and the Pyrenees–
5177 Provence domain at the time of the Pyrenean orogeny. *Tectonics* 24, TC1003, doi: 10.1029/2004TC001673.

5178 Lagabrielle, Y., Labaume, P., de Saint Blanquat, M., 2010. Mantle exhumation, crustal denudation, and gravity
5179 tectonics during Cretaceous rifting in the Pyrenean realm (SW Europe): insights from the geological setting
5180 of the Iherzolite bodies. *Tectonics* 29, TC4012, doi:10.1029/2009TC002588.

5181 Lagabrielle, Y., Asti, R., Fourcade, S., Corre, B., Poujol, M., Uzel, J., Labaume, P., Clerc, C., Lafay, R., Picazo, S.,
5182 Maury, R., 2019. Mantle exhumation at magma-poor passive continental margins. Part 1. 3D architecture
5183 and metasomatic evolution of a fossile exhumed mantle domain (Urdach Iherzolite, north-western
5184 Pyrenees, France). *Bull. Soc. Géol. Fr.* 190, 8. <https://doi.org/10.1051/bsgf/2019007>

5185 Lagasquie, J.J., 1969. Le Bassin de Saint-Girons et la vallée du Baup (Pyrénées du Couserans). Etude
5186 morphologique. *Rev. Géogr. Pyrén. Sud-Ouest* 40, 267–286.

5187 Lagasquie, J.J., 1984a. Géomorphologie des granites, les massifs granitiques de la moitié orientale des Pyrénées
5188 françaises. Thèse doct. (1982), éd. Régionales du CNRS, Toulouse, 374 p.

5189 Lagasquie, J.J., 1984b. Les relations piémont-montagne en Couserans et Bas-Salat. Actes du colloque
5190 « Montagnes et piémonts » (12–15 May 1982), Hommage à F. Taillefer. *Rev. Géogr. Pyrén. Sud-Ouest*,
5191 Travaux I, pp. 239–245.

5192 Lagasquie, J.J., 1987. Signification géodynamique des formes et dépôts de piémont dans la moitié orientale des
5193 Pyrénées. *Rev. Géomorph. Dyn.* 36, 85–86.

5194 Larena, Z., Arenas, C., Baceta, J.I., Murelaga, X., Suarez-Hernando, O., 2020. Stratigraphy and sedimentology of
5195 distal-alluvial and lacustrine deposits of the western-central Ebro Basin (NE Iberia) reflecting the onset of
5196 the middle Miocene Climatic Optimum. *Geol. Acta* 18, 1–26.

5197 Larrasoña, J.C., Murelaga, X., Garcés, M., 2006. Magnetobiochronology of Lower Miocene (Ramblian)
5198 continental sediments from the Tudela Formation (western Ebro basin, Spain). *Earth Planet. Sci. Lett.* 243,
5199 409–423.

5200 Larue, J.-P., 2001. Tectonique et dynamique fluviale quaternaires : l'exemple de la basse vallée de l'Aude
5201 (France). *Quaternaire* 12, 169–178.

- 5202 Larue, J.P., 2007. Drainage pattern modifications in the Aude basin (France): tectonic and morphodynamic
5203 implications. *Proc. Geol. Assoc.* 118, 187–200.
- 5204 Larue, J.P., 2008. Effects of tectonics and lithology on long profiles of 16 rivers of the southern Central Massif
5205 border between the Aude and the Orb (France). *Geomorphology* 93, 343–367.
- 5206 Laumonier, B., 2008. Les Pyrénées pré-hercyniennes et hercyniennes. In : Canérot, J., Colin, J.-P., Platel, J.-P.,
5207 Bilotte, M. (eds), *Pyrénées d'hier et d'aujourd'hui*, Pau, 20–21 septembre 2008. Atlantica and BRGM,
5208 Biarritz–Orléans, pp. 23–35.
- 5209 Laumonier, B., Barbey, P., Denèle, Y., Olivier, P., Paquette, J.-L., 2014. Réconcilier les données stratigraphiques,
5210 radiométriques, plutoniques, volcaniques et structurales au Pennsylvanien supérieur (Stéphanien–Autunien
5211 p.p.) dans l'Est des Pyrénées hercyniennes (France, Espagne). *Rev. Géol. Pyrén.* 1, 10 pp.
5212 <http://www.geologie-despyrenees.com/>
- 5213 Laumonier, B., 2015. Les Pyrénées alpines sud-orientales (France, Espagne) : essai de synthèse. *Rev. Géol.*
5214 *Pyrén.* 2, 44 pp. <http://www.geologie-despyrenees.com/>
- 5215 Laumonier, B., Le Bayon, B., Calvet, M., 2015. Handbook to the Carte géologique de la France, 1:50.000 scale,
5216 sheet Prats-de-Mollo–La-Preste (1099). BRGM, Orléans, 189 p. Geological map by Laumonier, B. et al.
5217 (2015).
- 5218 Laumonier, B., Calvet, M., Delmas, M., Barbey, P., Lenoble, J.-L., Autran, A. (2017). Handbook to the Carte
5219 géologique de la France (1:50,000 scale, sheet Mont-Louis (1094). BRGM, Orléans, 139 p. Geological map by
5220 Autran, A., Calvet, M., Delmas, M. (2005).
- 5221 Legendre, S., Lévêque, F., 1997. Étalonnage de l'échelle biochronologique mammalienne du Paléogène
5222 d'Europe occidentale : vers une intégration à l'échelle globale. In: Aguilar, J.P., Legendre, S., Michaux J.
5223 (eds), *Actes du Congrès BiochronM'97*. *Mém. Trav. EPHE (Montpellier)* 21, pp. 461–473.
- 5224 Legendre, S., Sigé, B., Astruc, J.G., de Bonis, L., Crochet, J.-Y., Denys, C., Godinot, M., Hartenberger, J.-L., Lévêque,
5225 F., Marandat, B., Mourer-Chauviré, C., Rage, J.-C., Remy, J.A., Sudre, J., Vianey Liaud, M., 1997. The
5226 phosphorites of Quercy: 30 years of investigations, results and prospects. *Geobios* 20, 331–345.
- 5227 Legigan, P., 1979. L'élaboration de la formation du Sable des Landes, dépôt résiduel de l'environnement
5228 sédimentaire pliocène–pléistocène centre aquitain. *Mém. Inst. Géol. Bass. Aquit.*, 429 p.
- 5229 Lenôtre, N., Fourniguet, J., 1987. Mouvements verticaux actuels : comparaison des nivellements. Synthèse
5230 géologique des Pyrénées, Rapport groupe de travail Tectonique récente et actuelle, 7 p. and 2 maps, Doc.
5231 BRGM–IGME (unpubl).
- 5232 Le Pichon, X., Bonnin, J., Sibuet, J.-C., 1970. La faille nord-pyrénéenne : faille transformante liée à l'ouverture
5233 du Golfe de Gascogne. *C. R. Acad. Sci. Paris sér. D* 271, 1941–1944.
- 5234 Leroux, E., Aslanian, D., Rabineau, M., Pellen, R., Moulin, M., 2018. The late Messinian event: a worldwide
5235 tectonic revolution. *Terra Nova* 30, 207–214.
- 5236 Lewis, C.J., Vergés, J., Marzo, M., 2000. High mountains in a zone of extended crust: Insights into the Neogene-
5237 Quaternary topographic development of northeastern Iberia. *Tectonics* 19, 86–102.

- 5238 Lewis, C.J., McDonald, E.V., Sancho, C., Peña, J.L., Rhodes, E.J., 2009. Climatic implications of correlated Upper
5239 Pleistocene and fluvial deposits on the Cinca and Gállego Rivers (NE Spain) based on OSL dating and soil
5240 stratigraphy. *Glob. Planet. Change* 67, 141–152.
- 5241 Lewis, C.J., Sancho, C., McDonald, E.V., Peña-Monné, J.L., Pueyo, E.L., Rhodes, E., Calle, M., Soto, R., 2017. Post-
5242 tectonic landscape evolution in NE Iberia using staircase terraces: combined effects of uplift and climate.
5243 *Geomorphology* 292, 85–103.
- 5244 Lofi, J., Rabineau, M., Gorini, C., Berné, S., Clauzon, G., de Clarens, P., dos Reis, T., Mountain, G.S., Ryan, W.B.F.,
5245 Steckler, M.S., Fouchet, C., 2003. Plio-Quaternary prograding clinoform wedges of the western Gulf of Lion
5246 continental margin (NW Mediterranean) after the Messinian Salinity Crisis. *Mar. Geol.* 198, 289–317.
- 5247 Lofi, J., Gorini, C., Berné, S., Clauzon, G., Dos Reis, T., Ryan, W.B.F., Steckler, M.S., 2005. Erosional processes and
5248 paleo-environmental changes in the Western Gulf of Lions (SW France) during the Messinian Salinity Crisis.
5249 *Mar. Geol.* 217, 1–30.
- 5250 Londeix L., (Ed.), 2014. Stratotype Aquitanien. Muséum National d'Histoire Naturelle, Paris, 416 p.
- 5251 López-Gómez, J. (Ed.), 2019. Permian-Triassic rifting stage. In: Quesada, C., Oliveira, J.T. (eds), *The geology of*
5252 *Iberia: a geodynamic approach*, vol. 3, *The Alpine cycle*. Springer, pp. 29–112.
- 5253 López-Martínez, N., Civis, J., Casanovas, L., Daams, R. (eds), 1998. *Geología y Paleontología del Eoceno de la*
5254 *Pobla de Segur (Lleida)*. Edicions Universitat de Lleida, Lleida, 267 p.
- 5255 López-Martínez, N., 1998. Los yacimientos de mamíferos del Eoceno de la Pobla de Segur. In: López-Martínez,
5256 N., Civis, J., Casanovas, L., Daams, R. (eds), *Geología y Paleontología del Eoceno de la Pobla de Segur*
5257 *(Lleida)*, Edicions Universitat de Lleida, Lleida, pp. 9–18.
- 5258 López Ruiz, J., Rodríguez Badiola, E., 1985. La region volcanica mio-pleistocena del NE de España. *Estud. Geol.*
5259 41, 105–126.
- 5260 Losantos, M., Aragonès, E., Berástegui, X., Palau, J., Puigdefàbregas, C., 1989. Mapa geològic de Catalunya,
5261 1:250,000 scale. Institut Cartogràfic de Catalunya, Barcelona.
- 5262 Lustrino, M., Wilson, M., 2007. The circum-Mediterranean anorogenic Cenozoic igneous province. *Earth-Sci.*
5263 *Rev.* 81, 1–65.
- 5264 Luzón, A., 2005. Oligocene–Miocene alluvial sedimentation in the northern Ebro Basin, NE Spain: tectonic
5265 control and palaeogeographical evolution. *Sed. Geol.* 177, 19–39.
- 5266 Macchiavelli, C., Vergés, J., Schettino, A., Fernández, M., Turco, E., Casciello, E., Torné, M., Pierantoni, P.P.,
5267 Tunini, L., 2017. A new southern North Atlantic isochron map: insights into the drift of the Iberian Plate
5268 since the late Cretaceous. *J. Geophys. Res., Solid Earth* 122, 9603–9626.
- 5269 Macles, O., Vernant, P., Chéry, J., Camps, P., Cazes, G., Ritz, J.F., Fink, D., 2020. Determining the Plio-Quaternary
5270 uplift of the southern French Massif Central; a new insight for intraplate orogen dynamics. *Solid Earth* 11,
5271 241–258.
- 5272 Maestro-Maideu, E., Serra Roig, J., 1996. The Late Eocene–Early Oligocene deposits of the NE Ebro basin, west
5273 of the Segre River. In: Friend, P.F., Dabrio, C.J. (eds), *Tertiary basins of Spain, the stratigraphic record of*
5274 *crustal kinematics*. Cambridge University Press, Cambridge, pp. 134–143.
- 5275 Magné, J., 1978. *Études microstratigraphiques sur le Néogène de la Méditerranée nord-occidentale*. vol. 1: Les

- 5276 bassins néogènes catalans, 259 p.; vol. 2: Le Néogène marin du Languedoc méditerranéen, 435 p. Éd. CNRS,
5277 Toulouse.
- 5278 Magné, J., Baudelot, S., Crouzel, F., Gourinard, Y., Wallez, M.J., 1985. La mer du Langhien inférieur a envahi le
5279 centre du bassin d'Aquitaine : arguments biostratigraphiques et géochronologiques. C. R. Acad. Sc. Paris II
5280 300, 961–964.
- 5281 Maire, R., 1990. La haute montagne calcaire : karsts, cavités, remplissages, Quaternaire, paléoclimats.
5282 Karstologia Mém. 3, 731 p.
- 5283 Maire, R., Vanara, N., 2008. Les karsts du domaine pyrénéen, témoins des paléoenvironnements depuis le
5284 Paléozoïque (transect Zone axiale–Zone nord pyrénéenne dans les Pyrénées atlantiques). In: Canérot, J.,
5285 Colin, J.-P., Platel, J.-P., Bilotte, M. (eds), Pyrénées d'hier et d'aujourd'hui. Atlantica and BRGM, Biarritz–
5286 Orléans, pp. 109–127.
- 5287 Maldonado, A., Riba, O., Orche, E., Colombo, F., 1979. Mapa geológico de España al 1/50,000, sheet n° 255
5288 Tortosa, Memoria explicativa. IGME, Madrid, 54 p.
- 5289 Marandat, B., 1991. Mammifères de l'Ilerdien moyen (Eocène inférieur) des Corbières et du Minervois,
5290 systématique, biostratigraphie, corrélations. Palaeovertebrata (Montpellier) 20, 55–144.
- 5291 Marandat, B., Adnet, S., Marivaux, L., Martinez, A., Vianey-Liaud, M., Tabuce, R., 2012. A new mammalian
5292 fauna from the earliest Eocene (Ilerdian) of the Corbières (Southern France): palaeobiogeographical
5293 implications. Swiss J. Geosci. 105, 417–434.
- 5294 Marcet-Riba, J., Solé-Sabaris, L., 1949. Mapa geológico de España, escala 1:50,000, explicación de la hoja 334
5295 Gerona. IGME, Madrid, 140 p.
- 5296 Marcet-Riba, J., 1954. El Villafranquiense de la vertiente meridional de los Pirineos orientales en la provincia de
5297 Gerona (España). Actes du II Congrès int. Etudes pyrénéennes, Luchon–Pau. Privat, Toulouse, pp. 143–146.
- 5298 Margerie, E. de, 1946. Études Pyrénéennes. In : Critique et Géologie, contribution à l'histoire des sciences de la
5299 terre (1882–1942), vol. III, A. Colin, Paris, pp. 1157–1714.
- 5300 Martínez, A., Rivero, L., Casas, A., 1997. Integrated gravity and seismic interpretation of duplex structures and
5301 imbricate thrust systems in the southeastern Pyrenees (NE Spain). Tectonophysics 282, 303–329.
- 5302 Martínez del Olmo, W., 1996. Depositional sequences in the Gulf of Valencia Tertiary basin. In: Friend, P.F.,
5303 Dabrio, C.J. (eds), Tertiary basins of Spain, the stratigraphic record of crustal kinematics. Cambridge
5304 University Press, Cambridge, pp. 55–67.
- 5305 Martínez-Rius, A., Tudela, M., Taliada, A., Copons, R., 2013. Mapa geologic de Catalunya, escala 1:25,000, La
5306 Pobla de Lillet, 255-1-2 (71-22). Institut Geologic de Catalunya-Institut Cartografic de Catalunya.
- 5307 Martinius, A.W., 2012. Contrasting styles of siliciclastic tidal deposits in a developing thrust-sheet-top basin. the
5308 Lower Eocene of the central Pyrenees (Spain). In: Davis Jr., R.A., Dalrymple, R.W. (eds), Principles of tidal
5309 sedimentology. Springer, pp. 473–506.
- 5310 Martonne, E. de, 1910. Remarque sur la communication de M. L. Carez, « Résumé de la géologie des
5311 Pyrénées », Séance du 2 mai 1910, C. R. séances Soc. Géol. Fr., p. 425.
- 5312 Martí, J., 2004. La región volcánica de Gerona. In: Vera, J.A. (Ed.), Geología de España. SGE–IGME, Madrid, pp.
5313 672–675.

- 5314 Martí, J., Mitjavila, J., Rocá, E., Aparicio, A., 1992. Cenozoic magmatism of the Valencia trough (western
5315 Mediterranean): relationship between structural evolution and volcanism. *Tectonophysics* 203, 145–165.
- 5316 Martí Bono, C.E., Puigdefábregas, C., 1968. Estudio del Parque Nacional de Aigues Tortes y Lago de San
5317 Mauricio (Pirineos centrales): geología y morfología. *Publ. Centro Piren. Biol. Exper. (Jaca)* 2, 7–37.
- 5318 Martí Bono, C.E., García Ruiz, J.M. (eds), 1994. El glaciario surpirenaico: nuevas aportaciones. *Geoforma*,
5319 Logroño, 142 p.
- 5320 Martzluff, M., 2006. Entre Pebble Culture, bifaces et érosion, le « Tautavélien » des terrasses quaternaires en
5321 Roussillon. *Archéo* 66 (Bull. Assoc. Archéo. Pyrén. Orient.) 21, 89–112.
- 5322 Masana, E., 1994. Neotectonic features of the Catalan Coastal Ranges, Northeastern Spain. *Acta Geol. Hisp.* 29,
5323 107–121 (Publ. in 1996).
- 5324 Masana, E., Villamarín, J.A., Sánchez Cabañero, J., Plaza, J., Santanach, P., 2001a. Seismogenic faulting in an
5325 area of low seismic activity: Paleoseismicity of the El Camp fault (Northeast Spain). *Neth. J. Geosci.* 80, 229–
5326 241.
- 5327 Masana, E., Villamarín, J.A., Santanach, P., 2001b. Paleoseismic results from multiple trenching analysis along a
5328 silent fault: the El Camp fault (Tarragona, northeastern Iberian Peninsula). *Acta Geol. Hisp.* 36, 329–354.
- 5329 Mattauer, M., 1968. Les traits structuraux essentiels de la chaîne pyrénéenne. *Rev. Géogr. Phys. Géol. Dyn.* 10,
5330 3–12.
- 5331 Mattauer, M., Henry, J., 1974. Pyrenees. In: Spencer, A.M. (Ed), *Mesozoic–Cenozoic belts: data for orogenic*
5332 *studies*, Geol. Soc. London, Spec. Publ. 4, 3–21.
- 5333 Mauffret, A., Durand de Grossouvre, B., dos Reis, A.T., Gorini, C., Nercessian, A., 2001. Structural geometry in
5334 the eastern Pyrenees and western Gulf of Lion (Western Mediterranean). *J. Struct. Geol.* 23, 1701–1726.
- 5335 Maurel, O., Monié, P., Pik, R., Arnaud, N., Brunel, M., Jolivet, M., 2008. The Meso-Cenozoic thermo-tectonic
5336 evolution of the eastern Pyrenees: an $^{40}\text{Ar}/^{39}\text{Ar}$ fission track and (U–Th)/He thermochronological study of
5337 the Canigou and Mont-Louis massifs. *Int. J. Earth Sci.* 97, 565–584.
- 5338 Meigs, A.J., Vergés, J., Burbank, D.W., 1996. Ten-million-year history of a thrust sheet. *Geol. Soc. Am. Bull.* 108,
5339 1608–1625.
- 5340 Meigs, A., 1997. Sequential development of selected Pyrenean thrust faults. *J. Struct. Geol.* 19, 481–502.
- 5341 Mellere, D., Marzo, M., 1992. Los depósitos aluviales sintectónicos de la Poble de Segur: alogrupos y su
5342 significado tectonoestratigráfico. *Acta Geol. Hisp.* 27, 145–159.
- 5343 Mencos, J., Carrera, N., Muñoz, J.A., 2015. Influence of rift basin geometry on the subsequent postrift
5344 sedimentation and basin inversion: The Organyà Basin and the Bóixols thrust sheet (south central
5345 Pyrenees). *Tectonics* 34, 1452–1474.
- 5346 Menendez Amor, J., 1955. La depression ceretana Española y sus vegetales fósiles. Características
5347 fitopaleontológicas del Neogeno de la Cerdaña Española. *Mem. Real Acad. Sci. ex., fis. y nat.* 18, 345 p.
- 5348 Mensua, S., Ibañez, J., Yetano, M., 1977. Sector central de la depresión del Ebro, mapa de terrazas fluviales y
5349 glaciales (5 hojas al 1:100,000, Comentario a los mapas). Departamento de Geografía, Universidad de
5350 Zaragoza, 18 p.
- 5351 Meresse, F., 2010. Dynamique d'un prisme orogénique intracontinental : évolution thermochronologique

5352 (traces de fission sur apatite) et tectonique de la Zone Axiale et des piémonts des Pyrénées centro
5353 occidentales. PhD thesis (unpubl.), Univ. of Montpellier 2, 277 p.

5354 Metcalf, J.R., Fitzgerald, P.J., Baldwin, S.L., Muñoz, J.A., 2009. Thermochronology of a convergent orogen:
5355 Constraints on the timing of thrust faulting and subsequent exhumation of the Maladeta Pluton in the
5356 Central Pyrenean Axial Zone. *Earth Planet. Sci. Lett.* 287, 488–503.

5357 Miall A., 2016. *Fluvial depositional systems*. Springer, 316 p.

5358 Michael, N.A., Carter, A., Whittaker, A.C., Allen, P.A., 2014. Erosion rates in the source region of an ancient
5359 sediment routing system: comparison of depositional volumes with thermochronometric estimates. *J. Geol.*
5360 *Soc. (London)* 171, 401–412.

5361 Michaux, J., Lopez-Martínez, N., Beaumont, G. de, Ginsburg, L., Thomas, H., Eisenmann, V., Guérin, C., Tobien,
5362 H., Legendre, S., Sen, S., 1988. Contribution à l'étude du gisement du Miocène supérieur de Montredon
5363 (Hérault). *Les grands mammifères. Palaeovertebrata (Montpellier), Mém. Extraordinaire*, 192 p.

5364 Millán, H., den Bezemer, T., Vergés, J., Zoetemeijer, R., Cloetingh, S., Marzo, M., Muñoz, J.A., Puigdefábregas,
5365 C., Roca, E., Cirés, J., 1995. Present-day and middle Lutetian flexural modeling in the eastern Pyrenees and
5366 Ebro basin. *Mar. Petrol. Geol.* 12, 917–928.

5367 Miller, K.G., Mountain, G.S., Wright, J.D., Browning, J.V., 2011. A 180-million-year record of sea level and ice
5368 volume variations from continental margin and deep-sea isotopic records. *Oceanography* 24, 40–53.

5369 Molliex, S., Rabineau, M., Leroux, E., Boulès, D.L., Authemayou, C., Aslanian, D., Chauvet, F., Civeta, F., Jouët,
5370 G., 2016. Multi-approach quantification of denudation rates in the Gulf of Lion source-to-sink system (SE
5371 France). *Earth Planet. Sci. Lett.* 444, 101–115.

5372 Molnar P., England P., 1990. Late Cenozoic uplift of mountain ranges and global climate change: chicken or
5373 egg? *Nature* 346, 29–34.

5374 Molnar, P., 2004. Late cenozoic increase in accumulation rates of terrestrial sediment: How might climate
5375 change have affected erosion rates? *Ann. Rev. Earth Planet. Sci.*, 32, 67–89.

5376 Monaco, A., Thommeret, J., Y., 1972. L'âge des dépôts quaternaires sur le plateau continental du Roussillon
5377 (golfe du Lion). *C. R. Acad. Sci. Paris D* 274, 2280–2283.

5378 Monod, B., Regard, V., Carcone, J., Wyns, R., Christophoul, F., 2016. Postorogenic planar palaeosurfaces of the
5379 central Pyrenees: Weathering and neotectonic records. *C. R. Géoscience* 348, 184–193.

5380 Montgomery, D.R., 1994. Valley incision and the uplift of mountain peaks. *J. Geophys. Res.* 99, 13,913–13,921.

5381 Morris, R.G., Sinclair, H.D., Yelland, A.J., 1998. Exhumation of the Pyrenean orogen: implications for sediment
5382 discharge. *Basin Res.* 10, 69–85.

5383 Mouchéné, M., van der Beek, P., Carretier, S., Mouthereau, F., 2017a. Autogenic versus allogenic controls on
5384 the evolution of a coupled fluvial megafan–mountainous catchment system: numerical modelling and
5385 comparison with the Lannemezan megafan system (northern Pyrenees, France). *Earth Surf. Dyn.* 5, 125–
5386 143.

- 5387 Mouchené, M., van der Beek, P., Mouthereau, F., Carcaillet, J., 2017b. Controls on quaternary incision of the
5388 northern Pyrenean foreland: chronological and geomorphological constraints from the Lannemezan
5389 megafan, SW France. *Geomorphology* 281, 78–93.
- 5390 Mouline, M.P., 1967. Etude des poudingues dits de Puylaurens, leurs conditions de mise en place, les
5391 conséquences paléoclimatiques de ces phénomènes. *Actes Soc. Linn. Bordeaux* 104 B, 3–15.
- 5392 Mouline, M.P., 1978. Les épandages conglomératiques de l'Eocène inférieur à l'Oligocène dans le Castrais et
5393 l'Albigeois : l'importance de l'orographie et ses conséquences climatiques dans une des principales
5394 manifestations de la rhexistasie paléopyrénéenne d'origine tectonique. *Bull. Soc. Géol. Fr.* 20, 215–219.
- 5395 Mouline, M.P., 1989. Sédimentation continentale en zone cratonique. Le Castrais et l'Albigeois au Tertiaire.
5396 PhD thesis (unpubl.), Univ. Bordeaux Montaigne, 878 p.
- 5397 Mouline, M.P., Birot, P., Paquereau, M., 1969. Le rebord NE de la Montagne Noire dans la région de Revel.
5398 Livret guide excursion A6, Pyrénées orientales et centrales, Roussillon, Languedoc occidental. VIIIe Congrès
5399 INQUA, Paris, pp. 106–109.
- 5400 Mourre, V., Colonge, D., 2007. Et si l'Acheuléen méridional n'était pas là où on l'attendait ? In: Evin, J. (Ed.), Un
5401 siècle de construction du discours scientifique en Préhistoire, Avignon 21–25 sept. 2004. Congrès du
5402 Centenaire de la Société Française de Préhistoire, vol. 3, pp. 68–78.
- 5403 Mouthereau, F., Filleaudeau, P.Y., Vacherat, A., Pik, R., Lacombe, O., Fellin, M.G., Castelltort, S., Christophoul, F.,
5404 Masini, E., 2014. Placing limits to shortening evolution in the Pyrenees: role of margin architecture and
5405 implications for the Iberia/Europe convergence. *Tectonics* 33, 2283–2314.
- 5406 Muñoz, J.A., 1992. Evolution of a continental collision belt: ECORS-Pyrenees crustal balanced cross-section. In:
5407 McClay, K.R. (Ed.), *Thrust tectonics*. Chapman and Hall, New York, pp. 235–246.
- 5408 Muñoz, J.A., 2002. The Pyrenees. In: Gibbons, W., Moreno, T. (eds), *The Geology of Spain*. Geol. Soc., London,
5409 370–385.
- 5410 Muñoz, J.A., 2019. Alpine Orogeny: Deformation and Structure in the Northern Iberian Margin (Pyrenees
5411 s.l.). In: Quesada, C., Oliveira, J.T. (eds.), *The geology of Iberia: a geodynamic approach*, vol. 3: The Alpine
5412 cycle. Springer Nature, 433–451.
- 5413 Muñoz, J.A., Martínez, A., Vergés, J., 1986. Thrust sequences in the Eastern Spanish Pyrenees. *J. Struct. Geol.* 8,
5414 399–405.
- 5415 Muñoz, J.A., Carrera, N., Mencos, J., Beamud, E., Perea, H., Arbués, P., Rivas, G., Bausà, J., García, J.M., Solà, J.,
5416 Montaner, J., Rivas, G., Serra, L., Picart, J., Caus, E., Boix, C., Villalonga, R., Martínez, R., Rosell, J., 2010.
5417 Mapa geològic de Catalunya, Aramunt 252-2-2 (66-22), 1:25,000. Institut Geològic de Catalunya-Institut
5418 Cartogràfic de Catalunya, Generalitat de Catalunya.
- 5419 Muñoz, J.A., Beamud, E., Fernández, O., Arbués, P., Dinarès-Turell, J., Poblet, J., 2013. The Ainsa fold and thrust
5420 oblique zone of the central Pyrenees: Kinematics of a curved contractional system from palaeomagnetic and
5421 structural data. *Tectonics* 32, 1142–1175.
- 5422 Muñoz, J.A., Mencos, J., Roca, E., Carrera, N., Gratacós, O., Ferrer, O., Fernández, O., 2018. The structure of the
5423 South-Central-Pyrenean fold and thrust belt as constrained by subsurface data. *Geol. Acta* 16, 439–460.

- 5424 Muratet B., Cavelier C., 1992. Caractère séquentiel discontinu des molasses oligocènes à la bordure orientale
5425 du Bassin aquitain ; signification des conglomérats bordiers (Tarn, Tarn et Garonne, Sud-Ouest de la
5426 France). *Géologie de la France*, 1, 3–14.
- 5427 Muratet B., Duranthon F., Lange-Badré B., Riveline J., 1992. Discontinuité d'origine eustatique dans les
5428 molasses oligocènes de l'Est du Bassin Aquitain (SW France). Apport de la biochronologie. *C. R. Acad. Sci.*
5429 *Paris sér. II* 315, 1113–1118.
- 5430 Murelaga X., Pérez-Rivarés F.J., Vázquez-Urbez M., Zuluaga M.C., 2008. Nuevos datos bioestratigráficos y
5431 paleoecológicos del Mioceno medio-superior (Aragoniense) del área de Tarazona de Aragón (Cuenca del
5432 Ebro, provincia de Zaragoza, España). *Ameghiniana*, Buenos-Aires, 45, 393–406.
- 5433 Murru, M., Farrara, C., da Pelo, S., Ibba, A., 2003. The Palaeogene–Middle Eocene deposits of Sardinia (Italy)
5434 and their palaeoclimatic significance. *C. R. Geoscience* 335, 227–238.
- 5435 Murru, M., Ferrara, C., Matteucci, R., da Pelo, S., Vacc,a A., 2007. I depositi continentali ferruginosi del
5436 Maastrichtiano sommitale–Paleocene della Sardegna meridionale (Italia). *Geol. Romana* 40, 175–186.
- 5437 Nercessian, A., Mauffret, A., dos Reis, A.T., Vidal, R., Gallart, J., Diaz, J., 2001. Deep reflection seismic images of
5438 the crustal thinning in the eastern Pyrenees and western Gulf of Lion. *J. Geodyn.* 31, 211–225.
- 5439 Nguyen, H.N., Vernant, P., Mazzotti, S., Khazaradze, G., Asensio, E., 2016. 3D GPS velocity field and its
5440 implications on the present-day postorogenic deformation of the Western Alps and Pyrenees. *Solid Earth* 7,
5441 1349–1363
- 5442 Nichols, G.J., 2005. Tertiary alluvial fans at the northern margin of the Ebro Basin. In: Harvey, A.M., Mather,
5443 A.E., Stokes, M. (eds), *Alluvial fans: geomorphology, sedimentology, dynamics*. Geological Society, London,
5444 *Spec. Publ.* 251, pp. 187–206.
- 5445 Nichols, G.J., 2018. High-resolution estimates of rates of depositional processes from an alluvial fan succession
5446 in the Miocene of the Ebro Basin, northern Spain. In: Ventra, D., Clarke, L.E. (eds), *Geology and*
5447 *geomorphology of alluvial and fluvial fans: terrestrial and planetary perspectives*. Geological Society,
5448 London, *Spec. Publ.* 440, pp. 159–173.
- 5449 Nijman, W., 1989. Thrust sheet rotation? The South Pyrenean Tertiary basin configuration reconsidered.
5450 *Geodin. Acta* 3, 17–42.
- 5451 Nijman, W., 1998. Cyclicity and basin axis shift in a piggyback basin: towards modelling of the Eocene Tresp-
5452 Ager Basin, South Pyrenees, Spain. In: Mascle A., Puigdefabregas C., Luterbacher H.P., Fernández M. (eds)
5453 *Cenozoic foreland basins of Western Europe*. Geological Society, London, *Spec. Publ.* 134, pp. 135–162.
- 5454 Nivière, B., Lacan, P., Regard, V., Delmas, M., Calvet, M., Huyghe, D., Roddaz, B., 2016. Evolution of the late
5455 Pleistocene Aspe river (western Pyrenees, France). Signature of climatic events and active tectonics. *C. R.*
5456 *Geoscience* 348, 203–212.
- 5457 Nocquet, J.M., Calais, E., 2003. The crustal velocity field in Western Europe from permanent GPS array
5458 solutions, 1996–2001. *Geophys. J. Int.* 154, 72–88.
- 5459 Nocquet, J.M., Calais, E., 2004. Geodetic measurements of crustal deformation in the western Mediterranean
5460 and Europe. *Pure Appl. Geophys.* 161, 661–681.
- 5461 Nussbaum, F., 1930. Morphologische studien in den östlichen Pyrenäen. *Z. Ges. Erdkunde* (Berlin), 200–210.

- 5462 Nussbaum, F., 1931. Sur les surfaces d'aplanissement d'âge tertiaire dans les Pyrénées-Orientales et leurs
5463 transformations pendant l'époque quaternaire. C. R. Congrès Int. Géogr., Paris, pp. 529–534.
- 5464 Nussbaum, F., 1943. Orographische und morphologische untersuchungen in den östlichen Pyrenäen. Jahr.
5465 Geogr. Ges. Bern 35, 1–148 (publ. in 1945).
- 5466 Odlum, M.L., Stockli, D.F., Capaldi, T.N., Thomson, K.D., Clark, J., Puigdefabregas, C., Fildani, A., 2019. Tectonic
5467 and sediment provenance evolution of the South Eastern Pyrenean foreland basins during rift margin
5468 inversion and orogenic uplift. *Tectonophysics* 765, 226–248.
- 5469 Oele, E., Sluiter, J., Pannekoek, A.J., 1963. Tertiary and Quaternary sedimentation in the Conflent. An
5470 intramontane rift valley in the Eastern Pyrenees. *Leid. Geol. Med.* 28, 297–319.
- 5471 Oliva-Urcia, B., 2018. Thirty years (1988–2018) of advances in the knowledge of the structural evolution of the
5472 south-central Pyrenees during the Cenozoic collision, a summary. *Rev. Soc. Geol. Esp.* 31, 51–68.
- 5473 Oliva-Urcia, B., Beamud, E., Garcés, M., Arenas, C., Soto, R., Pueyo, E.L., Pardo, G., 2016. New
5474 magnetostratigraphic dating of the Palaeogene syntectonic sediments of the west-central Pyrenees:
5475 tectonostratigraphic implications. In: Pueyo, E.L., Cifelli, F., Sussman, A.J., Oliva-Urcia, B. (eds),
5476 Palaeomagnetism in fold and thrust belts: new perspectives. Geological Society, London, Spec. Publ. 45, pp.
5477 107–128.
- 5478 Oliva-Urcia, B., Beamud, E., Arenas, C., Pueyo, E.L., Garcés, M., Soto, R., Valero, L., Pérez-Rivarés, F.J., 2019.
5479 Dating the northern deposits of the Ebro foreland basin; implications for the kinematics of the SW Pyrenean
5480 front. *Tectonophysics* 765, 11–34.
- 5481 Ortiz, A., Guillocheau, F., Lasseur, E., Briais, J., Robin, C., Serrano, O., Fillon, C., 2020. Sediment routing system
5482 and sink preservation during the post-orogenic evolution of a retro-foreland basin: the case example of the
5483 North Pyrenean (Aquitaine, Bay of Biscay) basins. *Mar. Petrol. Geol.* 112, 104085.
- 5484 Ortuño, M., Queralt, P., Martí, A., Ledo, J., Masana, E., Perea, H., Santanach, P., 2008. The North Maladeta Fault
5485 (Spanish Central Pyrenees) as the Vielha 1923 earthquake seismic source: recent activity revealed by
5486 geomorphological and geophysical research. *Tectonophysics* 453, 246–262.
- 5487 Ortuño, M., Martí, A., Martin-Closas, C., Jimenez-Moreno, G., Martinetto, E., Santanach, P., 2013.
5488 Palaeoenvironments of the Late Miocene Pruëdo Basin: implications for the uplift of the Central Pyrenees. *J.*
5489 *Geol. Soc. (London)* 170, 79–92.
- 5490 Ortuño, M., Guinau, M., Calvet, J., Furdada, G., Bordonau, J., Ruiz, A., Camafort, M., 2017. Potential of airborne
5491 LiDAR data analysis to detect subtle landforms of slope failure: Portainé, Central Pyrenees. *Geomorphology*
5492 295, 364–382.
- 5493 Ortuño, M., Viaplana-Muzas, M., 2018. Active fault control in the distribution of elevated low relief topography
5494 in the Central-Western Pyrenees. *Geol. Acta* 16, 499–518.
- 5495 Oudet, J., Münch, P., Borgomano, J., Quillevère, F., Melinte-Dobrinescu, M.C., Demory, F., Viseur, S., Cornée,
5496 J.J., 2010. Land and sea study of the northeastern Golfe du Lion rifted margin: the Oligocene–Miocene of
5497 southern Provence (Nerthe area, SE France). *Bull. Soc. Géol. Fr.* 181, 591–607.
- 5498 Oudet, J., Münch, P., Verati, C., Ferrandini, M., Melinte-Dobrinescu, M., Gattacceca, J., Cornée, J.J., Oggiano, C.,
5499 Quillevère, F., Borgomano, J., Ferrandini, J., 2010. Integrated chronostratigraphy of an intra-arc basin:

- 5500 ⁴⁰Ar/³⁹Ar datings, micropalaeontology and magnetostratigraphy of the early Miocene Castelsardo basin
5501 (northern Sardinia, Italy). *Palaeogeogr. Palaeoclim. Palaeoecol.* 295, 293–306.
- 5502 Palassou, P.B., 1781. *Essai sur la minéralogie des Monts-Pyrénées*. Didot-A. Jombert, Esprit éditions, reprint La
5503 Découvrance, 2007, 367 p.
- 5504 Palassou, P.B., 1815. *Mémoire pour servir à l’histoire naturelle des Pyrénées et des pays adjacents*. Imprimerie
5505 de Vignancour, Pau, 485 p.
- 5506 Palassou, P.B., 1819. *Suite des mémoires pour servir à l’histoire naturelle des Pyrénées et des pays adjacents*.
5507 Imprimerie de Vignancour, Pau, 428 p.
- 5508 Palassou, P.B., 1823. *Nouveau mémoire pour servir à l’histoire naturelle des Pyrénées et des pays adjacents*.
5509 Imprimerie de Vignancour, Pau, 192 p.
- 5510 Panzer, W., 1926. *Talentwicklung und Eiszeitklima in nord-östlichen Spanien*. *Abh. Senckenb. Naturforsch. Ges.*
5511 (Frankfurt) 39, 141–182.
- 5512 Panzer, W., 1933. *Die Entwicklung der Täler Kataloniens*. *Géologie des Pays Catalans*, III, 21, Barcelona.
- 5513 Pannekoek, A.J., 1935. *Évolution du bassin de la Têt dans les Pyrénées-Orientales pendant le Néogène : étude*
5514 *de morphotectonique*. Univ. of Utrecht, 72 p.
- 5515 Pardé, M., 1941. *La formidable crue d’octobre 1940 dans les Pyrénées-Orientales*. *Rev. Géogr. Pyrén. Sud-*
5516 *Ouest* 12, 237–279.
- 5517 Parize, O., Mulder, T., Cahuzac, B., Fiet, N., Londeix, L., Rubino, J.L., 2008. *Sedimentology and sequence*
5518 *stratigraphy of Aquitanian and Burdigalian stratotypes in the Bordeaux area (southwestern France)*. *C. R.*
5519 *Geoscience* 340, 390–399.
- 5520 Parsons, A.J., Michael, N.A., Whittaker, A.C., Duller, R.A., Allen, P.A., 2012. *Grain-size trends reveal the late*
5521 *orogenic tectonic and erosional history of the south–central Pyrenees, Spain*. *Journal of the Geological*
5522 *Society*, London, 169, 111–114.
- 5523 Pasumot, F., 1797. *Voyages physiques dans les Pyrénées en 1788 et 1789, Histoire naturelle d’une partie de ces*
5524 *montagnes*. Le Clère, Paris, 420 p.
- 5525 Patin, J., 1967. *L’évolution morphologique du plateau de Lannemezan*. *Rev. Géogr. Pyrén. Sud-Ouest* 38, 325–
5526 337.
- 5527 Payros, A., Tosquella, J., Bernaola, G., Dinarès-Turell, J., Orue-Etxebarria, X., Pujalte, V., 2009. *Filling the North*
5528 *European Early/Middle Eocene (Ypresian/Lutetian) boundary gap: insights from the Pyrenean continental to*
5529 *deep-marine record*. *Palaeogeogr. Palaeoclim. Palaeoecol.* 280, 313–332.
- 5530 Pedreira, D., Pulgar, J.A., Gallart, J., Diaz, J., 2003. *Seismic evidence of Alpine crustal thickening and wedging*
5531 *from the western Pyrenees to the Cantabrian Mountains (north Iberia)*. *J. Geophys. Res.* 108, 2204,
5532 doi.org/10.1029/2001JB001667
- 5533 Pedreira, D., Pulgar, J.A., Gallart, J., Torné, M., 2007. *Three-dimensional gravity and magnetic modeling of*
5534 *crustal indentation and wedging in the western Pyrenees-Cantabrian Mountains*. *J. Geophys. Res.* 112,
5535 B12405, doi.org/10.1029/2007JB005021.
- 5536 Pedreira, D., Afonso, J.C., Pulgar, J.A., Gallastegui, J., Carballo, A., Fernández, M., García-Castellanos, D.,
5537 Jiménez-Munt, I., Semprich, J., 2015. *Geophysical petrological modeling of the lithosphere beneath the*

- 5538 Cantabrian Mountains and North-Iberian margin: geodynamic implications. *Lithos* 230, 46–68.
- 5539 Peña, J.L., 1984. La conca de Tremp y sierras prepirenaicas comprendidas entre los ríos Segre y Noguera
5540 Ribagorzana, estudio geomorphológico. Instituto de Estudios Ilerdenses, SCIC, 2 vols, 373 p.
- 5541 Peña, J.L., Sancho, C., 1988. Correlación y evolución cuaternaria del sistema fluvial Segre-Cinca en su curso bajo
5542 (Provincias de Lerida y Huesca). *Cuat. Geomorfol.* 2, 77–83.
- 5543 Peña, J.L., Turu, V., Calvet, M., 2011. Les terrasses fluvials del Segre i afluent principals: descripció
5544 d'afloraments i assaig de correlació. In: Turu, V., Constante, A. (eds), *El Cuaternario en España y areas*
5545 *afines, avances en 2011. XIII Reunión Nacional de Cuaternario, Andorra, 4–7 July. Asociación Española para*
5546 *el Estudio del Cuaternario (AEQUA)*, pp. 51–55.
- 5547 Penck, A., 1883. *Die Eiszeit in den Pyrenäen. Mitteilungen Ver. für Erdkunde, Leipzig*, pp. 163–231.
- 5548 Penck, A., 1894. *Studien über das Klima Spaniens während der jüngeren Tertiärperiode und diluvialperiode. Z*
5549 *Ges. Erdkunde (Berlin)* 29, 109–141.
- 5550 Pérez-Rivarés, F.J., Garcés, M., Arenas, C., Pardo, G., 2002. Magnetocronología de la sucesión miocena de la
5551 Sierra de Alcubierre (sector central de la Cuenca del Ebro). *Rev. Soc. Geol. Esp.* 15, 217–231.
- 5552 Pérez-Rivarés, F.J., Garcés, M., Arenas, C., Pardo, G., 2004. Magnetostratigraphy of the Miocene continental
5553 deposits of the Montes de Castejón (central Ebro basin, Spain): geochronological and paleoenvironmental
5554 implications. *Geol. Acta* 2, 221–234.
- 5555 Pérez-Rivarés, F.J., Arenas, C., Pardo, G., Garcés, M., 2018. Temporal aspects of genetic stratigraphic units in
5556 continental sedimentary basins: examples from the Ebro basin, Spain. *Earth-Sci. Rev.* 178, 136–153.
- 5557 Perrouty, S., Moussirou, B., Martinod, J., Bonvalot, S., Carretier, S., Gabalda, G., Monod, B., Hérail, G., Regard,
5558 V., Remy, D., 2015. Geometry of two glacial valleys in the northern Pyrenees estimated using gravity data.
5559 *C. R. Geoscience* 347, 13–23.
- 5560 Peybernès, B., Fondécave-Wallez, M.-J., Combes, J.-P., Eichène, P., 2001. Mise en évidence d'un sillon marin à
5561 brèches paléocènes dans les Pyrénées centrales (Zone interne métamorphique et Zone nord-pyrénéenne).
5562 *C. R. Acad. Sci. Paris* 332, 379–386.
- 5563 Peybernès, B., Fondécave-Wallez, M.-J., Combes, J.-P., Séranne, M., 2007. Remplissages marins successifs,
5564 paléocènes et éocènes, de paléokarsts polyphasés dans les calcaires crétacés des nappes de l'Empordà
5565 (Pyrénées catalanes, Espagne) : relations tectonique-karstification. *Bull. Soc. Géol. Fr.* 178, 15–24.
- 5566 Peybernès, B., Melinte-Dobrinescu, M.C., Fondécave-Wallez, M.-J., 2014. Découverte de nannofossiles calcaires
5567 paléocènes dans les brèches marines remplissant les paléokarsts du synclinal d'Amélie-les-Bains (couverture
5568 de la Haute-Chaîne Primaire, Pyrénées Orientales, France). *Rev. Paléobio (Geneva)* 33, 455–462.
- 5569 Philip, H., Bousquet, J.C., Escuer, J., Fleta, J., Goula, X., Grellet, B., 1992. Présence de failles inverses d'âge
5570 quaternaire dans l'est des Pyrénées : implications sismotectoniques. *C. R. Acad. Sci. Paris sér. II* 314,
5571 1239–1245.
- 5572 Philip, H. (Ed.), 2018. *Tectonique récente et actuelle — Synthèse géophysique et géologique des Pyrénées —*
5573 *Volume 3 : Cycle alpin : phénomènes alpins. AGSO and BRGM, Pau–Orléans*, pp. 361–404.
- 5574 Plaziat, J.C., 1981. Late Cretaceous to late Eocene paleogeographic evolution of southwest Europe.
5575 *Palaeogeogr. Palaeoclim. Palaeoecol.* 36, 263–320.

- 5576 Plaziat, J.C., 1984. Stratigraphie et évolution paléogéographique du domaine pyrénéen de la fin du Crétacé
5577 (phase maastrichtienne) à la fin de l'Éocène (phase pyrénéenne). Thèse doct. État, Univ. Paris-Sud, 1362 p.
- 5578 Potter, P.E., Szatmari, P., 2009. Global Miocene tectonics and the modern world. *Earth-Sci. Rev.* 96, 279–295.
- 5579 Pouech, J.J., 1873. Note au sujet des restes d'un éléphant fossile découvert à Pamiers (Ariège). *C.R. Somm. Bull.*
5580 *Soc. Géol. Fr.*, 8–14.
- 5581 Pous, J., Julià, R., Sole Sagrañes, L., 1986. Cerdanya basin geometry and its implication on the Neogene
5582 evolution of the eastern Pyrenees. *Tectonophysics* 129, 355–365.
- 5583 Pous, J., Solé Sagrañes, L., Badiella, P., 1990. Estudio geoelectrico de la depresión de La Selva (Girona). *Acta*
5584 *Geol. Hisp.* 25, 261–269.
- 5585 Pous, J., Ledo, J., Marcuello, A., Daignières, M., 1995a. Electrical resistivity model of the crust and upper mantle
5586 from a magnetotelluric survey through the central Pyrenees. *Geophys. J. Int.* 121, 750–762.
- 5587 Pous, J., Muñoz, J.A., Ledo, J.J., Liesa, M., 1995b. Partial melting of subducted continental lower crust in the
5588 Pyrenees. *J. Geol. Soc. (London)* 152, 217–220.
- 5589 Puigdefàbregas, C., 1975. La sedimentación molásica en la cuenca de Jaca. *Monografias del Instituto de*
5590 *Estudios Pirenaicos. Pirineos (Jaca)* 104, 188 p.
- 5591 Puigdefàbregas, C., Soler, M., 1973. Estructura de las Sierras Exteriores Pirenaicas en el corte del río Gállego
5592 (prov. de Huesca). *Pirineos (Jaca)* 109, 5–15.
- 5593 Puigdefàbregas, C., Souquet, P., 1986. Tecto-sedimentary cycles and depositional sequences of the Mesozoic
5594 and Tertiary from the Pyrenees. *Tectonophysics* 129, 173–203.
- 5595 Pujadas, C., Casas, J.M., Muñoz, J.A., Sabat, F., 1989. Thrust tectonics and Paleogene syntectonic sedimentation
5596 in the Empordà area, Southeastern Pyrenees. *Geodin. Acta* 3, 195–206.
- 5597 Pujalte, V., Baceta, J.I., Schmitz, B., Orue-Etxebarria, X., Payros, A., Bernaola, G., Apellaniz, E., Caballero, F.,
5598 Robador, A., Serra-Kiel, J., Tosquella, J., 2009. Redefinition of the Ilerdian Stage (early Eocene). *Geol. Acta* 7,
5599 177–194.
- 5600 Pujos-Lamy, A., 1984. Foraminifères benthiques et bathymétrie : le Cénozoïque du Golfe de Gascogne.
5601 *Palaeogeogr. Palaeoclim. Palaeoecol.* 48, 39–60.
- 5602 Quirantes, J., Riba, O., 1973. Materiales pirenaicos depositados en la Depresión terciaria del Ebro. *Actes du VI*
5603 *Congrès international d'Etudes pyrénéennes, Bagnères-de-Bigorre, 1971. Pirineos (Jaca)* 107, 13–24.
- 5604 Rahl, J.M., Haines, S.H., van der Pluijm, B.A., 2011. Links between orogenic wedge deformation and erosional
5605 exhumation: Evidence from illite age analysis of fault rock and detrital thermochronology of syn-tectonic
5606 conglomerates in the Spanish Pyrenees. *Earth Planet. Sci. Lett.* 307, 180–190.
- 5607 Ramond de Carbonnières, L.F.E., 1789. *Voyages et observations faites dans les Pyrénées ; pour servir de suite à*
5608 *des observations sur les Alpes, insérées dans une traduction des Lettres de W. Coxe sur la Suisse.* Belin,
5609 Paris, 452 p.
- 5610 Razin, P., 1989. Évolution tectono-sédimentaire alpine des Pyrénées basques à l'Ouest de la transformante de
5611 Pamplona (Province du Labourd). Unpubl. PhD thesis, Univ. of Bordeaux 3, 464 p.

- 5612 Rehault, J.P., Boillot, G., Mauffret, A., 1984. The western Mediterranean basin geological evolution. *Mar. Geol.*
5613 55, 447–477.
- 5614 Reille, J.L., 1967. Subdivisions stratigraphiques et phases de plissement dans le Paléogène continental sud-
5615 pyrénéen (region de Barbastro, province de Huesca). *C. R. Acad. Sci. Paris Sér. D* 265, 852–854.
- 5616 Reille, J.L., 1971. Les relations entre tectogenèse et sédimentation sur le versant sud des Pyrénées centrales
5617 d'après l'étude des formations tertiaires essentiellement continentales. Thèse de Doct. Etat, Univ. of
5618 Montpellier, 330 p.
- 5619 Renaud, S., Michaux, J., Schmidt, D.N., Aguilar, J.P., Mein, P., Auffray, J.C., 2005. Morphological evolution,
5620 ecological diversification and climate change in rodents. *Proc. Roy. Soc. B* 272, 609–617.
- 5621 Rey, J., Duranthon, F., Gardère, P., Gourinard, Y., Magné, J., Feinberg, H., Muratet, B., 1997. Découverte d'un
5622 encaissement entre dépôts de sables fauves dans la région de Sos (Miocène centre-aquitain). *Géologie de la*
5623 *France* 2, 23–29.
- 5624 Riba, O., 1973. Las discordancias syntectónicas del Alto Cardener (Prepirineo catalán), ensayo de
5625 interpretación. *Acta Geol. Hisp* 8, 90–99.
- 5626 Riba, O., 1976. Syntectonic unconformities of the Alto Cardener, Spanish Pyrenees: A genetic interpretation:
5627 *Sed. Geol.* 15, 213–233.
- 5628 Richard, M., 1948. Contribution à l'étude du bassin d'Aquitaine. Les gisements de mammifères tertiaires. *Mém.*
5629 *Soc. Géol. France* 52, 380 p.
- 5630 Rigo, A., Cushing, M., 1999. Effets topographiques sur les comparaisons de profils de nivellement : cas français
5631 de Saint-Paul-de-Fenouillet (Pyrénées-Orientales) et d'Arudy (Pyrénées-Atlantiques). *C. R. Acad. Sci. Paris*
5632 329, 697–704.
- 5633 Rigo, A., Vernant, P., Feigl, K.L., Goula, X., Khazaradze, G., Talaya, J., Morel, L., Nicolas, J., Baize, S., Chery, J.,
5634 Sylvander, M., 2015. Present-day deformation of the Pyrenees revealed by GPS surveying and earthquake
5635 focal mechanisms until 2011. *Geophys. J. Int.* 201, 947–964.
- 5636 Roca, E., 1996a. The Neogene Cerdanya and Seu d'Urgell intramontane basins (eastern Pyrenees). In: Friend,
5637 P.F., Dabrio, C.J. (eds), *Tertiary basins of Spain, the stratigraphic record of crustal kinematics*. Cambridge
5638 University Press, Cambridge, pp. 114–118.
- 5639 Roca, E., 1996b. La evolución geodinámica de la Cuenca Catalano-Balear y áreas adyacentes desde el
5640 Mesozoico hasta la actualidad. *Acta Geol. Hisp.* 29, 3–25.
- 5641 Roca, E., Sans, M., Cabrera, L., Marzo, M., 1999. Oligocene to Middle Miocene evolution of the central Catalan
5642 margin (northwestern Mediterranean). *Tectonophysics* 315, 209–233.
- 5643 Rodríguez-Vidal, J., 1986. Geomorfología de las sierras exteriores oscenses y su piedemonte. PhD thesis (1983),
5644 Univ. de Zaragoza, Instit. Estud. Alto Aragoneses, CSIC, 172 p.
- 5645 Roigé, M., Gómez-Gras, D., Remacha, E., Daza, R., Boya, S., 2016. Tectonic control on sediment sources in the
5646 Jaca basin (Middle and Upper Eocene of the South-Central Pyrenees). *C. R. Geoscience* 348, 236–245.
- 5647 Roigé, M., Gómez-Gras, D., Remacha, E., Boya, S., Viaplana-Muzas, M., Teixell, A., 2017. Recycling an uplifted
5648 early foreland basin fill: An example from the Jaca basin (Southern Pyrenees, Spain). *Sed. Geol.* 360, 1–21.
- 5649 Roigé, M., Gómez-Gras, D., Stockli, D.F., Teixell, A., Boya, S., Remacha, E., 2019. Detrital zircon U–Pb insights

- 5650 into the timing and provenance of the South Pyrenean Jaca Basin. *J. Geol. Soc. (London)* 176, 1182–1190.
- 5651 Rosell, J., Riba, O., 1966. Nota sobre la disposicion sedimentaria de los conglomerados de La Poble de Segur.
- 5652 *Pirineos (Jaca)* 81–82, 61–74.
- 5653 Rosell Sanuy, J., 1967. Estudio geológico del sector del Prepirineo comprendido entre los ríos Segre y Noguera
- 5654 Ribagorzana. *Pirineos (Jaca)* 21, pp. 9–214.
- 5655 Rosell, J., Linares, R., Llompart, C., 2001. El «Garumniense» prepirenaico. *Rev. Soc. Geol. Esp.* 14, 47–56.
- 5656 Rosenbaum, G., Lister, G.S., Duboz, C., 2002. Relative motions of Africa, Iberia and Europe during Alpine
- 5657 orogeny. *Tectonophysics* 359, 117–129.
- 5658 Rosset, C., 1964. Les formations du bassin oligocène de Sigean–Portel et leur chronologie. *C. R. Somm. Soc.*
- 5659 *Géol. Fr.*, 415–417.
- 5660 Rougier, G., Ford, M., Christophoul, F., Bader, A.G., 2016. Stratigraphic and tectonic studies in the central
- 5661 Aquitaine Basin, northern Pyrenees: Constraints on the subsidence and deformation history of a retro-
- 5662 foreland basin. *C. R. Geoscience* 348, 224–235.
- 5663 Roure, F., Choukroune, P., 1998. Contribution of the ECORS seismic data to the Pyrenean geology: crustal
- 5664 architecture and geodynamic evolution of the Pyrenees. In: Damotte B., The ECORS Pyrenean deep seismic
- 5665 surveys, 1985–1994. *Mém. Soc. Géol. Fr.* 173, 37–52.
- 5666 Sancho, C., Calle M., Peña-Monné, J.L., Duval, M., Oliva-Urcia, B., Pueyo, E.L., Benito, G., Moreno, A., 2016.
- 5667 Dating the earliest Pleistocene alluvial terrace of the Alcanadre River (Ebro Basin, NE Spain): insights into
- 5668 the landscape evolution and involved processes. *Quatern. Int.* 407, 86–95.
- 5669 Sanjuan, J., Martín-Closas, C., Serra-Kiel, J., Gallardo, H., 2012. Stratigraphy and biostratigraphy (charophytes)
- 5670 of the marine-terrestrial transition in the Upper Eocene of the NE Ebro Basin (Catalonia, Spain). *Geol. Acta*
- 5671 10, 19–31.
- 5672 Sartégou, A., Bourlès, D.L., Blard, P.H., Braucher, R., Tibari, B., Zimmermann, L., Leanni, L., Aumaître, G.,
- 5673 Keddadouche, K., 2018. Deciphering landscape evolution with karstic networks: a Pyrenean case study.
- 5674 *Quat. Geochron.* 43, 12–29.
- 5675 Saspiturry, N., Razin, P., Baudin, T., Serrano, O., Issautier, B., Lasseur, E., Allanic, C., Thinon, I., Leleu, S., 2019.
- 5676 Symmetry vs asymmetry of a hyper-thinned rift: Example of the Mauléon Basin (Western Pyrenees, France).
- 5677 *Mar. Petrol. Geol.* 104, 86–105.
- 5678 Saula, E., Picart, J., Mató, E., Llenas, M., Losantos, M., Berástegui, X., Agustí, J., 1994. Evolución geodinámica de
- 5679 la fosa del Emporda y las Sierras Transversales. *Acta Geol. Hisp.* 29, 55–75.
- 5680 Sauvage, J., 1969. Etude sporo-pollinique des formations miocènes d’Orignac (Pyrénées centrales françaises).
- 5681 *Doc. Lab. Géol. Fac. Sci. Lyon* 31, 1–19.
- 5682 Schettino, A., Turco, E., 2011. Tectonic history of the western Tethys since Late Triassic. *Geol. Soc. Am. Bull.*
- 5683 123, 89–105.
- 5684 Schoeffler J., 1969. L’âge des molasses de Pau à Peyrehorade. *Bull. Soc. Géol. Fr.* 7, 28–34.
- 5685 Schoeffler, J., 1971. Étude structurale des terrains molassiques du piémont nord des Pyrénées de Peyrehorade
- 5686 à Carcassonne. Thèse Doct. Etat (unpubl.), Univ. of Bordeaux 1, 323 p.

- 5687 Schoeffler, J., 1973. Étude structurale des terrains molassiques du piémont nord des Pyrénées de Peyrehorade
5688 à Carcassonne. *Rev. Inst. Fr. Pétrole* 28, 515–549 and 639–665.
- 5689 Séguret, M., 1972. Étude tectonique des nappes et séries décollées de la partie centrale du versant sud des
5690 Pyrénées. Caractère synsédimentaire, rôle de la compression et de la gravité. *Publ. USTELA, Montpellier,*
5691 *Sér. Géol. Struct.* 2, 162 p.
- 5692 Sen, S., 1990. Hipparion datum and its chronologic evidence in the Mediterranean area. In: Lindsay, E.H.,
5693 Fahlbusch, V., Mein, P. (eds), *European Neogene mammal chronology*. Plenum Press, New York, pp. 495–
5694 505.
- 5695 Séranne, M., 1999. The Gulf of Lion continental margin (NW Mediterranean) revisited by IBS: an overview. In:
5696 Durand, B., Jolivet, L., Horvath, F., Séranne, M. (eds), *The Mediterranean basins: Tertiary extension within*
5697 *the Alpine orogen*. Geological Society, London, *Spec. Publ.* 156, pp. 15–36.
- 5698 Sère, V., 1993. Analyse cinématique et évolution thermotectonique des mylonites de la faille de la Têt (versant
5699 nord du Canigou, Pyrénées-Orientales). *MPhil Dissertation (unpubl.)*, Univ. of Montpellier 2, 51 p.
- 5700 Sermet, J., 1950. Réflexions sur la morphologie de la Zone Axiale des Pyrénées. *Pirineos (Jaca)* 6, 323–404.
- 5701 Serra-Kiel, J., Mato, E., Saula, E., Travé, A., Ferrandez-Cañadell, C., Busquets, P., Samsó, J.M., Tosquella, J.,
5702 Barnolas, A., Alvarez-Perez, G., Franquès, J., Romero, J., 2003. An inventory of the marine and transitional
5703 Middle/Upper Eocene deposits of the Southeastern Pyrenean Foreland Basin (NE Spain). *Geol. Acta* 1, 201–
5704 229.
- 5705 Serrano, O., Guillocheau, F., Leroy, E., 2001. Évolution du bassin compressif Nord-Pyrénéen au Paléogène
5706 (bassin de l'Adour) : contraintes stratigraphiques. *C. R. Acad. Sci. Paris* 332, 37–44.
- 5707 Serrano E., Agudo C., 2004. Glaciares rocosos y deglaciación en la alta montaña de los Pirineos aragoneses
5708 (España). *Boletín Real Sociedad Española de Historia Natural (Sección Geología)* 99, 159–172.
- 5709 Serrano, E., Agudo, C., Delaloye, R., Gonzalez-Trueba, J.J., 2001. Permafrost distribution in the Posets massif,
5710 central Pyrenees. *Norsk Geogr. Tidsskr.* 55, 245–252.
- 5711 Serrat, D., Bordonau, J., Bru, J., Furdada, G., Gomez, A., Marti, J., Marti, M., Salvador, F., Ventura, J., Vilaplana,
5712 J.M., 1994. Síntesis cartográfica del glaciarismo surpirenaico oriental. In: Martí Bono, C.E., García Ruiz, J.M.
5713 (eds), *El glaciarismo surpirenaico: nuevas aportaciones*. Geoforma, Logroño, pp. 9–15.
- 5714 Sigé, B., 1997. Les mammifères insectivores des nouvelles collections de Sosis et sites associés (Éocène
5715 supérieur, Espagne). *Geobios* 30, 91–113.
- 5716 Sinclair, H.D., Gibson, M., Naylor, M., Morris, R.G., 2005. Asymmetric growth of the Pyrenees revealed through
5717 measurement and modelling of orogenic fluxes. *Am. J. Sci.* 305, 369–406.
- 5718 Sinclair, H.D., Gibson, M., Lynn, G., Stuart, F., 2009. The evidence for a Pyrenean resurrection: a response to
5719 Babault et al. (2008). *Basin Res.* 21, 143–145.
- 5720 Sitzia, L., 2014. Chronostratigraphie et distribution spatiale des dépôts éoliens quaternaires du bassin Aquitain.
5721 PhD thesis, Univ. of Bordeaux I, 341 p.
- 5722 Sitzia, L., Bertran, P., Bahain, J.J., Bateman, M.D., Hernandez, M., Garon, H., de Lafontaine, G., Mercier, N.,
5723 Leroyer, C., Queffélec, A., Voinchet, P., 2015. The Quaternary coversands of southwest France. *Quat. Sci.*
5724 *Rev.* 124, 84–105.

- 5725 Solé Sabaris, L., 1951. Los Pirineos, el medio y el hombre. Editorial Martin, Barcelona, 624 p.
- 5726 Soler, D., Teixell, A., García-Sansegundo, J., 1998. Amortissement latéral du chevauchement de Gavarnie et sa
5727 relation avec les unités sud-pyrénéennes. C. R. Acad. Sci. Paris 327, 699–704.
- 5728 Sorre, M., 1913. Les Pyrénées méditerranéennes, étude de géographie biologique. Thèse, A. Colin, Paris, 508 p.
- 5729 Sorriaux, P., Delmas, M., Calvet, M., Gunnell, Y., Durand, N., Pons-Branchu, E., 2016-2018. Relations entre karst
5730 et glaciers depuis 450 ka dans les grottes de Niaux-Lombrives-Sabart (Pyrénées ariégeoises). Nouvelles
5731 datations U/Th dans la grotte de Niaux. *Karstologia* 67, 3–16.
- 5732 Soto, R., Larrasoaña, J.C., Beamud, E., Garcés, M., 2016. Early–Middle Miocene subtle compressional
5733 deformation in the Ebro foreland basin (northern Spain); insights from magnetic fabrics. C. R. Geoscience
5734 348, 213–223.
- 5735 Souquet, P., Peybernès, B., Bilotte, M., Debroas, E.J., 1977. La chaîne alpine des Pyrénées. *Géol. Alpine* 53, 193–
5736 201.
- 5737 Souquet, P., Rey, J., Peybernès, B., Cavallé, A., Ternet, Y., 1977. Carte géologique de la France, 1:50,000 scale,
5738 sheet Le Mas-d'Azil (1056), BRGM, Orléans. Handbook by Souquet, P., Rey, J., Peybernès, B., Bilotte, M.,
5739 Cosson, J., Cavallé, A., Roche, J.H., Bambier, A., 39 p.
- 5740 Souquet, P., Debroas, E.J., 1980. Tectorogenèse et évolution des bassins de sédimentation dans le cycle alpin
5741 des Pyrénées. I : Autran A., Dercourt J. (eds), Évolutions géologiques de la France, Mém. BRGM. 107, 213–
5742 233.
- 5743 Souquet, P., Debroas, É.J., Boirie, J.M., Pons, P., Fixari, G., Roux, J.C., Dol, J., Thieuloy, J.P., Bonnemaison, M.,
5744 Manivit, H., Peybernès, B., 1985. Le Groupe du Flysch noir (Albo-Cénomanién) dans les Pyrénées. *Bull. Cent.*
5745 *Rech. Explor. Prod. Elf-Aquitaine* 9, 183–252.
- 5746 Souriau, A., Granet, M., 1995. A tomographic study of the lithosphere beneath the Pyrenees from local and
5747 teleseismic data. *J. Geophys. Res.* 100, 18,117–18,134.
- 5748 Souriau, A., Pauchet, H., 1998. A new synthesis of the Pyrenean seismicity and its tectonic implications.
5749 *Tectonophysics*, 290, 221–224.
- 5750 Souriau, A., Chevrot, S., Olivera, C., 2008. A new tomographic image of the Pyrenean lithosphere from
5751 teleseismic data. *Tectonophysics* 460, 206–214.
- 5752 Stange, K.M., van Balen, R.T., Vandenberghe, J., Peña, J.L., Sancho, C., 2013a. External controls on Quaternary
5753 fluvial incision and terrace formation at the Segre River, southern Pyrenees. *Tectonophysics* 602, 316–331.
- 5754 Stange, K.M., van Balen, R., Carcaillet, J., Vandenberghe, J., 2013b. Terrace staircase development in the
5755 Southern Pyrenees foreland: inferences from ¹⁰Be terrace exposure ages at the Segre River, *Glob. Planet.*
5756 *Change* 101, 97–112.
- 5757 Stange, K.M., van Balen, R.T., Kasse, C., Vandenberghe, J., Carcaillet, J., 2014. Linking morphology across the
5758 glaciofluvial interface: a 10Be supported chronology of glacier advances and terrace formation in the
5759 Garonne River, northern Pyrenees, France. *Geomorphology* 207, 71–95.
- 5760 Stange, K.M., Van Balen, T., Garcia-Castellanos, D., Cloetingh, S., 2016. Numerical modelling of Quaternary
5761 terrace staircase formation in the Ebro foreland basin, southern Pyrenees, NE Iberia. *Basin Res.* 28, 124–
5762 146.

- 5763 Stange, K.M., Midtkandal, I., Nystuen, J.P., Kuss, H.J., Spiegel, C., 2018. Direct response of small non-glaciated
5764 headwater catchments to Late Quaternary climate change: The Valle de la Fueva, southern Pyrenees.
5765 *Geomorphology* 318, 187–202.
- 5766 Stehlin, H.G., 1910. Die Säugetiere des schweizerischen Eocaens. *Mém. Soc. Paléont. Suisse* 36, 838–1164.
- 5767 Suc, J.P., Fauquette, S., 2012. The use of pollen floras as a tool to estimate palaeoaltitude of mountains: The
5768 eastern Pyrenees in the Late Neogene, a case study. *Palaeogeogr. Palaeoclim. Palaeoecol.* 321–322, 41–54.
- 5769 Sudre, J., de Bonis, L., Brunet, M., Crochet, J.Y., Duranthon, F., Godinot, M., Hartenberger, J.L., Jehenne, Y.,
5770 Legendre, S., Marandat, B., Remy, J.A., Ringeade, M., Sigé, B., Vianey-Liaud, M., 1992. La biochronologie
5771 mammalienne du Paléogène au Nord et au Sud des Pyrénées : état de la question. *C. R. Acad. Sci. Paris sér.*
5772 *II* 314, 631–636.
- 5773 Sztrakos, K., Gély, J.P., Blondeau, A., Müller, C., 1998. L'Éocène du bassin sud-aquitain : lithostratigraphie,
5774 biostratigraphie et analyse séquentielle. *Géologie de la France* 4, 57–105.
- 5775 Sztrakos, K., Steurbaut, E., 2017. Révision lithostratigraphique et biostratigraphique de l'Oligocène d'Aquitaine
5776 occidentale (France). *Geodiversitas (Paris)* 39, 741–781.
- 5777 Taillefer, F., 1951. Le piémont des Pyrénées françaises, contribution à l'étude des reliefs de piémont. Privat,
5778 Toulouse, 383 p.
- 5779 Taillefer, F., 1957. Le glacière pyrénéen : versant nord et versant sud. *Rev. Géogr. Pyrén. Sud-Ouest* 28, 221–
5780 244.
- 5781 Taillefer, F., 1967. Extent of Pleistocene glaciation in the Pyrenees. In: Wright, H.E., Osborne, W.H. (eds), *Arctic
5782 and Alpine environments*. Indiana University Press, Bloomington, pp. 255–266.
- 5783 Taillefer, F., 1969. Les glaciations des Pyrénées. Actes du VIII^e Congrès international de l'INQUA, supplément au
5784 *Bulletin de l'Association Française pour l'Etude du Quaternaire*, Paris, pp. 19–32.
- 5785 Taillefer, F., 1982. Les conditions locales de la glaciation pyrénéenne. *Pirineos (Jaca)* 116, 5–12.
- 5786 Tassy, P., 1990. "The Proboscidean datum event": how many proboscideans and how many datum events. In:
5787 Lindsay E.H. et al. (eds), *European Neogene mammal chronology*. Plenum Press, New York, p. 237–252.
- 5788 Tavani, S., Bertok, C., Granado, P., Piana, F., Salas, R., Vigna, B., Muñoz, J.A., 2018. The Iberia–Eurasia plate
5789 boundary east of the Pyrenees. *Earth-Sci. Rev.* 187, 314–337.
- 5790 Teixell, A., 1990. Alpine thrusts at the western termination of the Pyrenean Axial zone. *Bull. Soc. Géol. Fr.* 8,
5791 241–249.
- 5792 Teixell, A., 1998. Crustal structure and orogenic material budget in the west-central Pyrenees. *Tectonics* 17,
5793 395–406.
- 5794 Teixell, A., García-Sansegundo, J., 1995. Estructura del sector central de la Cuenca de Jaca (Pirineos
5795 meridionales). *Rev. Soc. Geol. Esp.* 8, 215–228.
- 5796 Teixell, A., Muñoz, J.A., 2000. Evolución tectonosedimentaria del Pirineo meridional durante el Terciario: una
5797 síntesis basada en la transversal del río Noguera Ribagorçana. *Rev. Soc. Geol. Esp.* 13, 251–264.
- 5798 Teixell, A., Ayarza, P., Zeyen, H., Fernández, M., Arboleya, M.L., 2005. Effects of mantle upwelling in a
5799 compressional setting: the Atlas Mountains of Morocco. *Terra Nova* 17, 456–461.

- 5800 Teixell, A., Zamorano Cáceres, M., Ramírez Merino, J., Navarro Juli, J.J., Rodríguez Santisteban, R. Castaño,
5801 R.M., Leyva, F., Ramírez del Pozo, J., Aguilar, P., Robador Moreno, A., 2016. Mapa Geológico de España,
5802 escala 1:50,000, Graus (n° 250), Memoria 71 p., serie Magna, IGME.
- 5803 Teixell, A., Labaume, P., Lagabrielle, Y., 2016. The crustal evolution of the west-central Pyrenees revisited:
5804 Inferences from a new kinematic scenario. *C. R. Geoscience* 348, 257–267.
- 5805 Teixell, A., Labaume, P., Ayarza, P., Espurt, N., de Saint Blanquat, M., Lagabrielle, Y., 2018. Crustal structure and
5806 evolution of the Pyrenean–Cantabrian belt: A review and new interpretations from recent concepts and
5807 data. *Tectonophysics* 724–725, 146–170.
- 5808 Ternois, S., Odlum, M., Ford, M., Pik, R., Stockli, D., Tibari, B., Vacherat, A., Bernard, V., 2019.
5809 Thermochronological evidence of early orogenesis, eastern Pyrenees, France. *Tectonics* 38, 1308–1336.
- 5810 Thiry, M., 2000. Palaeoclimatic interprétation of clay minerals in marine deposits: an outlook from the
5811 continental origin. *Earth-Sci. Rev.* 49, 201–221.
- 5812 Thomson, K.D., Stockli, D.F., Clark, J.D., Puigdefabregas, C., Fildani, A., 2017. Detrital zircon (U–Th)/(He–Pb)
5813 double-dating constraints on provenance and foreland basin evolution of the Ainsa Basin, south-central
5814 Pyrenees, Spain. *Tectonics* 36, 1352–1375.
- 5815 Tosquella, J., Samsó, J.M., 1996. Bioestratigrafía y litoestratigrafía del Paleoceno superior-Eoceno inferior del
5816 sector oriental de la cuenca surpirenaica. *Acta Geol. Hisp.* 31, 3–21.
- 5817 Tricart, J., Hirsch, A.R., Griesbach, J.C., 1966. La géomorphologie du bassin du Touch (Haute-Garonne), ses
5818 implications pédologiques et hydrologiques. *Rev. Géogr. Pyrén. Sud-Ouest* 37, 5–46.
- 5819 Tugend, J., Manatschal, G., Kuszniir, N.J., Masini, E., Mohn, G., Thion, I., 2014. Formation and deformation of
5820 hyperextended rift systems: insights from rift domain mapping in the Bay of Biscay–Pyrenees. *Tectonics* 33,
5821 1239–1276.
- 5822 Turner, J.P., 1990. Structural and stratigraphic evolution of the West Jaca thrust-top basin, Spanish Pyrenees. *J.*
5823 *Geol. Soc. (London)* 147, 177–184.
- 5824 Turu, V., Boulton, G.S., Ros, X., Peña, J.L., Martí, C., Bordonau, J., Serrano-Cañadas, E., Sancho-Marcén, C.,
5825 Constante-Orrios, A., Pous, J., Gonzalez-Trueba, J.J., Palomar, J., Herrero, R., Garcia-Ruiz, J.M., 2007.
5826 Structure des grands bassins glaciaires dans le nord de la péninsule ibérique : comparaison entre les vallées
5827 d'Andorre (Pyrénées orientales), du Gállego (Pyrénées centrales) et du Trueba (Chaîne cantabrique).
5828 *Quaternaire* 18, 309–325.
- 5829 Turu V., 2011. Los complejos morrenicos terminales del Valira (Andorra–Alt Urgell). *Resúmenes XIII Reunion*
5830 *Nacional de Cuaternario, Andorra 2011, Simposio de glaciario, guía de campo*, 1–8.
- 5831 Turu, V., Vidal Romani, J.R., Fernández Mosquera, D., 2011. Dataciones con isótopos cosmogénicos (¹⁰Be): el
5832 "LGM" (Last Glacial Maximum) y the "Last Termination" en los valles del Gran Valira y la Valira del Nord
5833 (Principado de Andorra, Pirineos orientales). *Resúmenes XIII Reunion Nacional de Cuaternario, Andorra*
5834 *2011, Simposio de glaciario*, pp. 19–23.
- 5835 Turu, V., Calvet, M., Bordonau, J., Gunnell, Y., Delmas, M., Vilaplana, J.M., Jalut, G., 2017. Did Pyrenean glaciers
5836 dance to the beat of global climatic events? Evidence from the Würmian sequence stratigraphy of an ice-
5837 dammed palaeolake depocentre in Andorra. In: Hughes, P.D., Woodward, J.C. (eds), *Quaternary glaciation*

5838 in the Mediterranean mountains. Geological Society, London, Spec. Publ. 433, pp. 111–136.

5839 Urgeles, R., Camerlenghi, A., Garcia-Castellanos, D., de Mol, B., Garcés, M., Vergés, J., Haslam, I., Hardman, M.,
5840 2011. New constraints on the Messinian sealevel drawdown from 3D seismic data of the Ebro Margin,
5841 western Mediterranean. *Basin Res.* 23, 123–145.

5842 Uzel, J., Nivière, B., Lagabrielle, Y., 2020. Fluvial incisions in the North-Western Pyrenees (Aspe Valley):
5843 dissection of a former planation surface and some tectonic implications. *Terra Nova* 32, 11–22.

5844 Vacca, A., Farrara, C., Matteucci, R., Murru, M., 2012. Ferruginous paleosols around the Cretaceous–Paleocene
5845 boundary in central-southern Sardinia (Italy) and their potential as pedostratigraphic markers. *Quatern. Int.*
5846 265, 179–190.

5847 Vacher, P., Souriau, A., 2001. A 3D-model of the Pyrenean deep structure based on gravity modelling, seismic
5848 images and petrological constraints. *Geophys. J. Int.* 145, 460–470.

5849 Vacherat, A., Mouthereau, F., Pik, R., Bernet, M., Gautheron, C., Masini, E., Le Pourhiet, L., Tibari, B., Lahfid, A.,
5850 2014. Thermal imprint of rift-related processes in orogens as recorded in the Pyrenees. *Earth Planet. Sci.*
5851 *Lett.* 408, 296–306.

5852 Vacherat, A., Mouthereau, F., Pik, R., Bellahsen, N., Gautheron, C., Bernet, M., Daudet, M., Balansa, J., Tibari,
5853 B., Pinna Jamme, R., Rada, J., 2016. Rift-to-collision transition recorded by tectono-thermal evolution of the
5854 northern Pyrenees. *Tectonics* 35, 907–933.

5855 Vacherat, A., Mouthereau, F., Pik, R., Huyghe, D., Paquette, J.L., Christophoul, F., Loget, N., Tibari, B., 2017. Rift-
5856 to-collision sediment routing in the Pyrenees: A synthesis from sedimentological, geochronological and
5857 kinematic constraints. *Earth-Sci. Rev.* 172, 43–74.

5858 Valero, L., Garcés, M., Cabrera, L., Costa, E., Sáez, L., 2014. 20 Myr of eccentricity-paced lacustrine cycles in the
5859 Cenozoic Ebro Basin. *Earth Planet. Sci. Lett.* 408, 183–193.

5860 Vanara, N., Maire, R., Lacroix, J., 1997. La surface carbonatée du massif des Arbailles (Pyrénées Atlantiques) :
5861 un exemple de paléoréseau hydrographique néogène déconnecté par la surrection. *Bull. Soc. Géol. Fr.* 168,
5862 255–265.

5863 Vanara, N., 2000. Le Karst des Arbailles. *Karstologia Mém.* 3, 320 p.

5864 Vandenberghe, N., Hilgen, F.J., Speijer, R.P., Ogg, J.G., Gradstein, F.M., Hammer, O., 2012. The Paleogene
5865 period. In: Gradstein, F.M., Ogg, J.G., Schmitz, M.D., Ogg, G.M. (eds), *The geologic time scale*. Elsevier, pp.
5866 855–921.

5867 Vanderhaeghe, O., Grabkowiak, A., 2014. Tectonic accretion and recycling of the continental lithosphere during
5868 the Alpine orogeny along the Pyrenees. *Bull. Soc. Géol. Fr.* 185, 143–155.

5869 Van der Made, J., Mazo, A.V., 2003. Proboscidean dispersals from Africa towards Western Europe. In: Reumer,
5870 J.W.F., de Vos, J., Mol, D. (eds), *Advances in Mammoth research (Proceedings of the Second International*
5871 *Mammoth Conference, Rotterdam, May 16–20 1999)*. *DEINSEA* 9, 437–452.

5872 Van der Meer, D.G., van Hinsbergen, D.J.J., Spakman, W., 2018. Atlas of the underworld: slab remnants in the
5873 mantle, their sinking history, and new outlook on mantle viscosity. *Tectonophysics* 723, 309–448.

- 5874 Van Hinsbergen, D.J.J., Torsvik, T.H., Schmid, S.M., Mañenco, L.C., Maffione, M., Vissers, R.L.M., Gürer, D.,
5875 Spakman, W., 2019. Orogenic architecture of the Mediterranean region and kinematic reconstruction of its
5876 tectonic evolution since the Triassic. *Gond. Res.* 81, 79–229.
- 5877 Vázquez-Urbez, M., Arenas, C., Pardo, G., Pérez-Rivarés, J., 2013. The effect of drainage reorganization and
5878 climate on the sedimentologic evolution of intermontane lake systems: the final fill stage of the Tertiary
5879 Ebro Basin (Spain). *J. Sed. Res.* 83, 562–590.
- 5880 Ventra, D., Clarke, L.E., 2018. Geology and geomorphology of alluvial and fluvial fans: current progress and
5881 research perspectives. In: Ventra, D., Clarke, L.E. (eds), *Geology and geomorphology of alluvial and fluvial*
5882 *fans: terrestrial and planetary perspectives*. Geological Society, London, Spec. Publ. 440, pp. 1–21.
- 5883 Vergés, J., Martínez, A., 1988. Corte compensado del Pirineo oriental: Geometría de las cuencas de antepaís y
5884 edades de emplazamiento de los mantos de corrimiento. *Acta Geol. Hisp.* 23, 95–105.
- 5885 Vergés, J., Muñoz, J.A., 1990. Thrust sequences in the southern central Pyrenees. *Bull. Soc. Géol. Fr.* 8, 265–
5886 271.
- 5887 Vergés, J., Martínez-Rius, A., Domingo, F., Muñoz, J.A., Losantos, M., Gisbert, J., Fleta, J., 1994. Mapa geológico
5888 de España, 1:50 000 scale, sheet 225, La Pobla de Lillet. IGME, Madrid. Handbook by Vergés, J., Martínez-
5889 Rius, A., Fleta, J., Pujadas, J., Tosquella, J., Samsó, J.M., Sanz, J., Barberà, M., Berástegui, X.
- 5890 Vergés, J., Millán, H., Roca, E., Muñoz, J.A., Marzo, M., Cirés, J., den Bezemer, T., Zoetemeijer, R., Cloetingh, S.,
5891 1995. Eastern Pyrenees and related foreland basins: pre-, syn- and post-collisional crustal scale cross-
5892 sections. *Mar. Petrol. Geol.* 12, 893–915.
- 5893 Vergés, J., Burbank, D.W., 1996. Eocene–Oligocene thrusting and basin configuration in the eastern and central
5894 Pyrenees (Spain). In: Friend, P.F., Dabrio, C.J. (eds), *Tertiary basins of Spain, the stratigraphic record of*
5895 *crustal kinematics*. Cambridge University Press, Cambridge, pp. 120–133.
- 5896 Vergés, J., Marzo, M., Santaularia, T., Serra-Kiel, J., Burbank, D.W., Muñoz, J.A., Giménez-Montsant, J., 1998.
5897 Quantified vertical motions and tectonic evolution of the SE Pyrenean foreland basin. In: Mascle, A.,
5898 Puigdefabregas, C., Luterbacher, H.R., Fernandez, M. (eds), *Cenozoic foreland basins of Western Europe*.
5899 Geological Society, London, Spec. Publ. 134, pp. 107–134.
- 5900 Vergés, J., Fernández, M., Martínez, A., 2002. The Pyrenean orogen: pre-, syn-, and post-collisional evolution.
5901 In: Rosenbaum, G., Lister, G.S. (eds), *Reconstruction of the evolution of the Alpine–Himalayan Orogen*. *J.*
5902 *Virtual Explorer* 8, 55–74.
- 5903 Vergés, M., Fernández, M., 2006. Ranges and basins in the Iberian Peninsula: their contribution to the present
5904 topography. In: Gee, D.G., Stephenson, R.A. (eds), *European lithosphere dynamics*. Geological Society,
5905 London, Memoir 32, pp. 223–234.
- 5906 Vernant, P., 2018. Apports du karst du Cotiella aux débats scientifiques sur l'érosion dans les Pyrénées, *Revista*
5907 *Cotiella, ACEC, Plan 6*, 37–47.
- 5908 Viers, G., 1960. Le relief des Pyrénées occidentales et leur piémont. *Pays Basque français et Barétous*. Privat,
5909 Toulouse, 604 p.

- 5910 Viers, G., 1961. La tectonique post-pliocène sur le littoral atlantique entre Biarritz et Hendaye. Actes VI°
5911 congrès INQUA, Varsovie, vol. 1, pp. 539–544.
- 5912 Villalta, J.F. de, Crusafont, M., 1943. Los vertebrados del Mioceno continental de la Cuenca del Vallés-Penedés.
5913 Bol. Inst. Geol. Min. Esp. 59, 147–336.
- 5914 Villalta, J.F. de, Palli, L., 1973. Presencia del Mioceno continental bajo et cauce del rio Onyar en Gerona. Acta
5915 Geol. Hisp. 8, 109–110.
- 5916 Villena, J., Gonzalez, A., Muñoz, A., Pardo, G., Perez, A., 1992. Síntesis estratigráfica del Terciario del borde Sur
5917 de la Cuenca del Ebro: unidades genéticas. Acta Geol. Hisp. 27 (Homenaje a Oriol Riba Arderiu), 225–245.
- 5918 Vincent, S.J., Elliott, T., 1996. Long-lived fluvial palaeovalleys sited on structural lineaments in the Tertiary of
5919 the Spanish Pyrenees. In: Friend, P.F., Dabrio, C.J. (eds), Tertiary basins of Spain, the stratigraphic record of
5920 crustal kinematics. Cambridge University Press, Cambridge, pp. 161–165.
- 5921 Vincent, S.J., 2001. The Sis palaeovalley: a record of proximal fluvial sedimentation and drainage basin
5922 development in response to Pyrenean mountain building. *Sedimentology* 48, 1235–1276.
- 5923 Vinyoles, A., López-Blanco, M., Garcés, M., Arbués, P., Valero, L., Beamud, E., Oliva-Urcia, B., Cabello, P., 2020.
5924 10 Myr evolution of sedimentation rates in a deep marine to non-marine foreland basin system: tectonic
5925 and sedimentary controls (Eocene, Tremp–Jaca Basin, Southern Pyrenees, NE Spain). *Basin Res.* 00, 1–31,
5926 [https://doi: 10.1111/bre.12481](https://doi.org/10.1111/bre.12481).
- 5927 Viret, J., 1938. Sur l'âge des argiles ligniteuses de Nassiet près Amou (Landes). *C. R. Acad. Sci. Paris* 207, 500–
5928 501.
- 5929 Vissers, R.L.M., Meijer, P.T., 2012a. Mesozoic rotation of Iberia: subduction in the Pyrenees? *Earth-Sci. Rev.*
5930 110, 93–110.
- 5931 Vissers, R.L.M., Meijer, P.T., 2012b. Iberian plate kinematics and Alpine collision in the Pyrenees. *Earth-Sci. Rev.*
5932 114, 61–83.
- 5933 Vissers, R.L.M., van Hinsbergen, D.J.J., van der Meer, D.G., Spakman, W., 2016. Cretaceous slab break-off in the
5934 Pyrenees: Iberian plate kinematics in paleomagnetic and mantle reference frames. *Gond. Res.* 34, 49–59.
- 5935 Wang, Y., Chevrot, S., Monteiller, V., Komatitsch, D., Mouthereau, F., Manatschal, G., Sylvander, M., Diaz, J.,
5936 Ruiz, M., Grimaud, F., Benahmed, S., Pauchet, H., Martin, R., 2016. The deep roots of the western Pyrenees
5937 revealed by full waveform inversion of teleseismic P waves. *Geology* 44, 475–478.
- 5938 Wehr, H., Chevrot, S., Courrioux, G., Guillen, A., 2018. A three-dimensional model of the Pyrenees and their
5939 foreland basins from geological and gravity data. *Tectonophysics* 734–735, 16–32.
- 5940 Whitchurch, A.L., Carter, A., Sinclair, H.D., Duller, R.A., Whittaker, A.C., Allen, P.A., 2011. Sediment routing
5941 system evolution within a diachronously uplifting orogen: insights from detrital zircon thermochronological
5942 analyses from the South-Central Pyrenees. *Am. J. Sci.* 311, 442–482.
- 5943 Wiazemsky, M., Calvet, M., Laumonier, B., Guitard, G., Autran, A., Llac, F., Baudin, T., 2010. Carte géologique de
5944 la France, 1:50,000 scale, sheet Céret (1096). BRGM, Orléans. Handbook by Laumonier, B., Calvet, M.,
5945 Wiazemsky, M., Barbey, P., Marignac, C., Lambert, J., Lenoble, J.L. (2015), 164 p.
- 5946 Willett, S.D., Brandon, M.T., 2002. On steady states in mountain belts. *Geology* 30, 175–178.
- 5947 Winnock, E., Fried, E., Kieken, M., 1973. Les caractéristiques des sillons aquitains. *Bull. Soc. Géol. Fr.* 15, 51–60.

- 5948 Yelland, A., 1990. Fission track thermotectonics in the Pyrenean orogen. *Nuclear Tracks and Radiation*
5949 *Measurements*, 17, 293–299.
- 5950 Yelland, A., 1991. Thermo-tectonics of the Pyrenees and Provence from fission-track studies, PhD thesis
5951 (unpubl.), Univ. of London.
- 5952 Yuste, A., Luzón, A., Bauluz, B., 2004. Provenance of Oligocene–Miocene alluvial and fluvial fans of northern
5953 Ebro Basin (NE Spain): an XRD, petrographic and SEM study. *Sed. Geol.* 172, 251–268.
- 5954 Zandvliet, J., 1960. The geology of the upper Salat and Pallaresa valleys, Central Pyrenees, France/Spain. *Leid.*
5955 *Geol. Med.* 25, 1–127.
- 5956 Zeck, H.P., 1999. Alpine plate kinematics in the Western Mediterranean: a westward directed subduction
5957 regime followed by slab roll-back and slab detachment. In: Durand, F., Jolivet, L., Horvath, M., Séranne, M.
5958 (eds), *The Mediterranean basins: Tertiary extension within the Alpine orogen*. Geological Society, London,
5959 *Spec. Publ.* 156, pp. 109–120.

5960

5961 **Figure captions**

5962

5963 **Fig. 1. Simplified geological map of the Pyrenees.** 1: Paleogene reverse faults and thrusts.
5964 2a: Neogene normal faults. 2b: probable Neogene faults. 2c: other faults. 3: Hercynian
5965 basement, folded Paleozoic sequences, metasedimentary and granitoid rocks (basement
5966 outcrops in the Axial Zone, North-Pyrenean and Sub-Pyrenean zones, Catalan Range, and
5967 Massif Central). 4: folded Mesozoic and Cenozoic cover rocks; Paleogene conglomerate
5968 beds. 5: Neogene sedimentary rocks. 6: Neogene and Quaternary volcanic rocks. Relief base
5969 map: SRTM digital elevation model (3 arcsec).

5970

5971 **Fig. 2. Structural subdivisions of the Pyrenean crustal wedge.** A: classic tectonostratigraphic
5972 zoning. Note that all the contacts between zones are tectonic, except partly in the southeast.
5973 B: map of tectonic units and their associated thrusts, classified according to their direction of
5974 travel (northwards in the European Pyrenees, southwards in the Iberian Pyrenees) and, for
5975 the Iberian domain, the home area of the major thrust units. In red and yellow: upper units
5976 rooted to the north of the Axial Zone and NPF (southern NPZ or Chaînons béarnais,
5977 Noguères unit, and part of the SPZ). In green: intermediate units with their home areas in
5978 the Axial Zone and involving both Axial Zone rocks (Hercynian basement) and the SPZ (cover
5979 rocks). In blue: lower units rooted beneath the Axial Zone and with outcrops either within
5980 the Axial Zone (Hercynian basement) or the SPZ (cover rocks). White arrows indicate the

5981 southward displacement of the Cotiella–Organyà–upper-Pedraforca Cretaceous unit relative
5982 to its pre-orogenic home area situated above the northern part of the Axial Zone; and more
5983 generally the sense of displacement of the SPCU–Pedraforca units. After Laumonier (2015,
5984 modified).

5985 **Fig. 3. Tectonostratigraphic cross-sections through the eastern and central Pyrenees.** A:
5986 structural units encountered along the ECORS-Pyrenees profile, after Muñoz (1992). Note
5987 the prevalence of steeply dipping discontinuities in the northern and central part of the Axial
5988 Zone, and the southward tilt of similar structures in its southern part. These southward dips
5989 have given the Nogueres units their classic impression of a ‘false syncline’ (Séguret, 1972). B,
5990 C: two alternative interpretations of the Axial Zone along the ECORS-Pyrenees profile: the
5991 ‘standard’ model according to Muñoz (1992) in B, and according to Laumonier (2015) in C,
5992 respectively. Muñoz (1992) considered that the Axial Zone was a huge anticlinal stack
5993 involving a major thrust, the Nogueres–Gavarnie Thrust, implying substantial depths of
5994 crustal denudation of the basement (up to 20 km). According to Laumonier’s (2015)
5995 alternative model, an overspanning Supra-Axial Thrust, rooted north of the Axial Zone (i.e.,
5996 beneath the NPZ), transported the central SPZ (i.e., the SPCU) and the Nogueres units
5997 southward. There is no major antiformal hump except along the marginal flexure, and the
5998 magnitude of uplift of the Axial Zone basement core is less than in the ‘standard’ model. This
5999 alternative view is supported by a number of field constraints, including the preservation of
6000 residual, unmetamorphosed Triassic cover deposits at Pruëdo (red star; see location in Fig.
6001 2), which suggests comparatively much smaller depths of denudation than implied by the
6002 thickness of the Nogueres (Gavarnie) nappe in Fig. 3B. D: schematic structural cross-section
6003 through the eastern Pyrenees (after Laumonier, 2015, modified and updated). The domain
6004 affected by Cretaceous metamorphism (i.e., the IMZ on the European side) is a very early
6005 (latest Cretaceous) nappe. It was incorporated into the overspanning Supra-Axial Thrust
6006 which propagated southward over the future Axial Zone. This IMZ represents the inverted
6007 core of the mid-Cretaceous rift and its pop-up-style ejection.

6008 **Fig. 4. Geophysical imaging of the deep lithospheric structure of the Pyrenees.** A: location
6009 of geophysical swath profiles (lines 1 to 4) and seismic profiles (lines A to E). Relief base map:
6010 Copernicus EU-DEM v1.1. B: lithospheric cross-sections obtained from simultaneous best fits
6011 between free-air gravity, geoid, thermal, and topographic data (after Gunnell et al., 2008,

6012 modified); note lithospheric taper in the east (shallowing of lithosphere–asthenosphere
6013 boundary), along profiles 3 and 4. Profile 4 extends to the Massif Central and reveals the
6014 well-documented thinned lithosphere and shallow lithosphere–asthenosphere boundary
6015 explaining the volcanic activity and dynamic uplift in that region. C: map of the lithosphere–
6016 asthenosphere boundary interpolated from profiles 1 to 4 (after Gunnell et al., 2009,
6017 modified). D: crustal-scale cross-sections through the Pyrenees (data from Chevrot et al.,
6018 2018); note the thinner crust along profiles D and E, immediately east of the ECORS-
6019 Pyrenees profile (C).

6020

6021 **Fig. 5. Parallel tectono-sedimentary evolutions of the European retro-wedge and Aquitaine**

6022 **Basin, and Iberian pro-wedge and Ebro Basin.** These scaled diagrams are

6023 chronostratigraphic (indicate the age of sedimentary formations) and tectonostratigraphic

6024 (show the contents of tectonic units delimited by major thrusts). Horizontal scale is

6025 unspecified because the N–S widths of the tectonic domains narrowed progressively over

6026 time. The chronology of thrust activity (continuous or episodic) and apparent fission-track

6027 rock exhumation age ranges for a number of massifs are also indicated. The international

6028 stratigraphic scale includes the ELMA biozones. Three synthetic transects spanning the

6029 Pyrenees from foreland to retro-foreland include an eastern one from the Montagne Noire

6030 to NE Catalonia; a central one from Ariège to eastern Aragón; and a western one from Béarn

6031 to western Aragón through the western termination of the Axial Zone.

6032 Key to symbols, colours and ornaments. 1: marine sequences; 2: deltaic and base-level

6033 floodplain sequences; 3: continental sequences; 4a: proximal conglomerates; 4b: other

6034 coarse-textured debris-fan formations; 5: clay with decalcified pebbles; 6: sand- and clay-

6035 textured, carbonate-rich fluvial molasse; 7: other sand- and clay-textured molasse

6036 occurrences; 8: sand- and clay-textured deltaic facies; 9: other marine sandstones; 10: shelf

6037 limestone, and lacustrine or palustrine limestone; 11a: epipelagic carbonates; 11b: outer-

6038 shelf marls; 12: slope and abyssal flysch and turbidites; 13: marine or continental evaporites

6039 (gypsum, salt); 14a: main mammalian fossil site; 14b: stratigraphic type section; 15: main

6040 lithostratigraphic units; 16a: transverse drainage systems; 16b: strike-parallel drainage

6041 systems; 17a: apatite fission-track (AFT) age range; 17b: zircon fission-track (ZFT) age range;

6042 18: main thrusts (a) and/or faults (b). In red: main tectonic structures, thrusts, and thrust

6043 soles. AFT and ZFT apparent cooling ages after Yelland (1991), Maurel (2003), Maurel et al.

6044 (2002, 2008), Gunnell et al. (2009), Rushlow et al. (2013), Vacherat et al. (2016), Fitzgerald et
6045 al. (1999), Sinclair et al. (2005), Jolivet et al. (2007), Bosch et al. (2016), DeFelipe et al.
6046 (2019).

6047

6048 **Fig. 6. Map of elevated erosion surfaces and other diagnostic landforms in the Pyrenees,**
6049 **with correlated sedimentary deposits.** The map is based on a systematic map and field
6050 survey of each individual topographic unit. 1: range-top surface S (late Oligocene to
6051 Aquitanian). 2: range-flank pediment P1 (middle Miocene); in the western Pyrenees S and P1
6052 are indistinguishable. 3: base-level connections for P1; 3a: Langhian–Serravallian coastal
6053 deposits; 3b; Serravallian and Tortonian lacustrine limestones. 4: elevated massifs of the
6054 western Axial Zone never bevelled by S or P1. 5: late Neogene local pediments P2 and P3,
6055 also represented as karstic poljes when in limestone outcrops. 6: deposits relating to the
6056 generation of P2 or P3; 6a: Mediterranean Pliocene sediments, Lannemezan Formation
6057 (ancient range-front fluvial megafans), calcrete-capped upper wash pediments of the Ebro
6058 Basin; 6b: isolated vestiges of siliciclastic lag gravels capping P2; 6c: upper slope breccia
6059 deposits of the Cinca watershed (Merli Fm.). 7: main palaeovalleys associated with P1 (7a),
6060 with P2 (7b), and of middle Pleistocene age (7c).

6061

6062 **Fig. 7. Diagnostic erosion surfaces of the Pyrenees: Axial Zone and northern retro-wedge.**

6063 A. middle Miocene pediment in the eastern Corbières, cross-cutting folded
6064 Aptian/Barremian limestone beds (Urgonian facies). Note how the erosional surface grades
6065 to the top of the marine Miocene sequence of the Serre du Scorpion (consists of a Langhian
6066 littoral facies at its base and terminates with offlapping lacustrine limestones). Leucate
6067 lagoon and modern Mediterranean coastline in the background. B. Shore platform cut in the
6068 Urgonian limestone at the base of the marine Miocene outcrop and displaying fossil
6069 *Gastrochaenolites* (Serre du Scorpion). C. Summit surface at Roc Paradet (Corbières). Here
6070 the Pyrenean Frontal Thrust and the entire North-Pyrenean limestone sequence (visible in
6071 the walls of the Galamus canyon) have been cross-cut by this erosional surface. D.
6072 Panoramic view of the Fenouillèdes and the Agly massif; surface S cuts across all the
6073 geological structures of the North-Pyrenean Zone, and has been tilted from the Madrès
6074 massif (where S lies at 2400 m) to the Mediterranean. Miocene surface P1 extends at lower
6075 elevations, and in this area takes the form of anomalously wide, flat-floored valleys. On the

6076 far horizon: late Neogene horsts of the Canigou and Albères. E. Erosion surfaces of the Carlit
6077 massif (eastern Pyrenees). Miocene pediment P1, here unscathed by glaciation, forms an
6078 extensive topographic bench in granite and gneiss sloping SSE (2350–2000 m); the Carlit
6079 massif rises as a residual mass capped by summit surface S (inset F), itself bearing an isolated
6080 monadnock (Pic Péric) and cutting across Cambrian schist and hornfels. G. Vestiges of
6081 pediment P1 below the more elevated surface S in the Aston massif (Ariège), all cut in
6082 gneiss. H. Vast sweep of pediment P1 at the Plateau de Beille, Aston massif (also shown in
6083 G). Note residual topographic masses rising above P1 in the Carlit and Hospitalet massifs.
6084

6085 **Fig. 8. Diagnostic erosion surfaces of the Pyrenees: southern pro-wedge and western**
6086 **massifs.** A. Summit surface, S, in the Port de Comte massif (eastern South-Pyrenean Zone).
6087 The land surface cuts across folds in the Upper Cretaceous and Eocene limestone beds as
6088 well as upturned breccia units attributed to the Priabonian–Oligocene boundary. Note the
6089 low-angle fault-drag deformation of the Oligocene conglomerate beds (Berga
6090 conglomerates) beneath the Vallfogona Thrust (i.e., the SPFT). Partial pediments (generation
6091 P2) have cut benches into the conglomerate sequence along the mountain front. B. Erosion
6092 surfaces at the Montsec thrust (SPCU). Summit surface, S (tilted), on the Montsec thrust-
6093 front ridgetop and on the Serra de Sant Mamet; pediment P1 cuts across deformed
6094 Oligocene conglomerate beds and the north-dipping Upper Cretaceous units at the eastern
6095 termination of the Montsec. C. Summit surface S cutting across Upper Cretaceous limestone
6096 beds in the Montsec massif. D. The Montsec rising as a residual inselberg above pediment P1
6097 at the Col de Comiols. E. Summit surface at the Sierra de Sevil (eastern Sierra de Guara, i.e.,
6098 Sierras Exteriores), cutting across the Balcez anticline (thick Eocene limestone) with beds
6099 vertically upturned at its western limb). Unconformable early Miocene conglomerate beds
6100 supplied by the eroding relief have partially buried the south-facing mountain flank and are
6101 overlain by finer molasse deposits (Sariñena Fm.). This upward-fining sequence is consistent
6102 with the upland topography having attained gentle gradients towards the end of the local
6103 denudation history, thereby supplying finer debris. Note identical gradient between the
6104 slope of the erosion surface and the dip of the clastic beds. F. Erosion surface in the central
6105 Sierra de Guara. Note the numerous monadnocks rising above it; the surface (as in E) grades
6106 to the Sariñena clastic sequence at the southern mountain front and bevels the northward-
6107 dipping sandstone beds of the Campodarbe Fm. on the northern mountain flank. G. the N–S

6108 Turbon anticline. The limestone structure and its subvertical limbs are completely bevelled
6109 by the ridgetop erosion surface. H. Summit surface in the Basque Pyrenees. The Okabé
6110 plateau cuts across the Hercynian basement rocks of the Iraty massif as well as its
6111 Cretaceous and Eocene envelopes. I. The Arres d'Anie: an erosion surface cutting across the
6112 folded and faulted Canyon Limestone. Note its pyramidal monadnocks.

6113

6114 **Fig. 9. Cross-cutting relations between low-gradient topography, geological structure, and**
6115 **the unconformable syn-orogenic Paleogene conglomerate sequences of the south-central**

6116 **Pyrenees.** The proximal facies of these conglomerate deposits, which consists of massive
6117 boulder beds, is incompatible with the scenario of an overfilled basin onlapping northward
6118 onto a low-gradient erosion surface in its final stages of completion and itself supplying
6119 those boulder beds. Rather than a low-relief, low-energy hinterland, such deposits
6120 document steep, high-energy, and perhaps tectonically active orogenic relief upstream. A:
6121 Col de Perves (outcrops around Tossal Gros, Antist allogroup); these are >> 1-m-sized
6122 boulders of granite and Devonian source-rocks; in the background, the Axial Zone is entirely
6123 devoid of documented summit erosion surfaces. Elevations in metres. B: western summit
6124 zone of Boumort (outcrops around Planell Ras, Pallaresa allogroup), displaying metre-sized
6125 boulders of grey limestone, red Devonian limestone ('calcaire griotte', in foreground), and
6126 Triassic sandstone; in the background: cupola of Cenomanian–Turonian limestone cut by the
6127 vestige of an erosion surface. C: from Boumort, view to the NE, showing tectonic
6128 deformations in the Cogomera alluvial conglomerate sequence and the summit erosion
6129 surface cross-cutting the massive Urgonian limestone of Serra de Prada. D: Planell Ras
6130 outcrop, close-up of a boulder of Triassic conglomerate (height: 1.6 m). E: Serrat Negre–
6131 Catllaras outcrop, here showing the terminal Priabonian conglomerates containing
6132 megaboulders of granite (long axis: 3 m). The Paleogene conglomerates in the area
6133 everywhere are tectonically deformed and cross-cut by the low-gradient erosion surface. F:
6134 view from Boumort to the west towards the outcrops of La Pobla de Segur; note tectonic
6135 deformation of the entire series, terminal Antist allogroup included; to the SW, also note the
6136 vestiges of low-gradient erosion surfaces at the top Serra de Sis, Turbon (see also Fig. 8G), St
6137 Gervas–Mt. d'Adons, and Serra de Comillini–Plan del Mont (elevations in metres); to the
6138 NW, elevated massifs of the Axial Zone (Aneto) and its cover rocks (Monte Perdido), neither
6139 bearing clearly definable erosion surfaces. G, H: geological cross-sections through the

6140 Boumort massif, showing that the conglomerate deposits have buried a palaeolandscape of
6141 high relief and that the land surface cross-cuts these underlying structures as well as the
6142 deformed conglomerate sequences. Section G cuts across the eastern extremity of Boumort;
6143 section H cuts through the summit area, where residual conglomerate beds still occur;
6144 position of the conglomerate sequence before erosion also schematically represented (cross-
6145 sections from Peña, 1983, redrawn, augmented and modified in the light of more recent
6146 data concerning the dip of the conglomerate beds as measured in the field and/or depicted
6147 on the detailed geological map (sheet: Aramunt) authored by Muñoz et al., 2010.

6148

6149 **Fig. 10. Low-temperature thermochronology in relation to range-top or range-flank**
6150 **erosion surfaces in the Pyrenees.** A: AFT and AHe age–elevation plot (data from Gunnell et
6151 al., 2009). Abbreviated massif names: CMPC–Campcardos; CAN–Canigou; POMA–Pla de
6152 Pomarola; GUIL–Pla Guillem; CAR–Carlit; MAD–Madres; DONZ–Donnezan; BAS–Bassiès; AS-
6153 Aston; LLES–Tossa Plana de Llès; LPCH–Col de la Perche; MTBA–Massif de Montalba; AGLY–
6154 Massif de l'Agly. AFT ages produced by Yelland (1991) and Maurel et al. (2008) (marked Y
6155 and M, respectively) are given to show good agreement between independent workers. B:
6156 plot of mean fission-track length vs. topographic elevation. C: cooling paths obtained by
6157 forward thermal modelling of the AFT and AHe data. The best-fitting cooling trajectories
6158 pooled and scaled in this way highlight the residence times of individual samples at near-
6159 surface conditions since 35–25 Ma irrespective of their current elevations (after Gunnell et
6160 al., 2009, modified). D: cooling paths for the Aneto massif (after Gibson et al., 2007,
6161 modified); note similarities with cooling paths obtained in the eastern Pyrenees.

6162

6163 **Fig. 11. Conceptual scenarios for explaining the observed distribution of range-top erosion**
6164 **surfaces in the Pyrenees.** Scenarios A and C are the two end-member situations detailed in
6165 the text. Scenario B is a variant of A. In A, the range-top surface (peneplain S) occurs
6166 throughout the range. The population of pediment surfaces (P) were generated during the
6167 middle Miocene except in the Basque Pyrenees, where P and S are indistinguishable. In B,
6168 the altitudinal offset between S and P only exists in the east, and is a response to changes in
6169 base level caused by Mediterranean rifting; further west, the two surfaces merge but
6170 erosion has obliterated them in the central Pyrenees because of more intense crustal uplift
6171 in this segment of the orogen. In C, the altitudinal offset between S and P is again a response

6172 to Mediterranean rifting. The elevation offset disappears further west, where the surfaces
6173 only occur as summit bevels across the outer fold and thrust belts. The distinction with
6174 scenario B is that, in scenario C, the high massifs of the Axial Zone in the central Pyrenees
6175 never were bevelled by the range-top 'peneplain'.

6176

6177 **Fig. 12. Neotectonic record in the Pyrenees and foreland areas.** 1: outcrops of Hercynian
6178 basement; 2: Pliocene continental and marine deposits; 3: early Pleistocene alluvial deposits,
6179 uppermost terraces; 4: middle and late Pleistocene and Holocene alluvial terraces; 5:
6180 Pleistocene glaciers; 6: late Miocene to late Pleistocene volcanic rocks; 7: continental shelf
6181 isobaths; 8a: main faults and thrusts of Hercynian and Pyrenean age; 8b: blind or probable
6182 faults and thrusts of Hercynian and Pyrenean age; 9a: main fold axis in the outer fold belts;
6183 9b: Neogene normal fault. 10: neotectonic deformations affecting Pliocene deposits; 10a:
6184 reverse fault, 10b: normal fault; 10c: strike-slip fault; 10d: faulted karstic landform of deposit
6185 (unspecified). 11: neotectonic deformations affecting Pleistocene deposits; 11a: reverse
6186 fault, fold; 11b: normal fault; 11c: strike-slip fault; 11d: faulted karstic landform of deposit
6187 (unspecified); 11e: fault (unspecified). Places names of recorded deformation indices (some
6188 are logged under a single number given their close proximity); 1: Escandorgue, 2: Le Rièges;
6189 3: Bize-Minervois; 4: Saint Chipoli–Dourgne; 5: Fabrezan; 6: Caramany–Le Mas; 7: Millas,
6190 Néfiach, Ille-sur-Têt; 8: Perpignan–Serrat d'en Vaquer; 9: Trouillas, Fourques; 10: Sorède,
6191 Laroque des Albères, Villelongue; 11: St Climent Sesebes; 12: Pontos, Fluvia; 13: Pedrinya,
6192 Incarcàl; 14: Serinya; 15: Tortella, Rajolins, Burro; 16: Camp de Tarragona; 17: Baix Ebre; 18:
6193 Villefranche karst (ND de Vie, Faubourg); 19: Estavar; 20: Osséja; 21: Martinet; 22: La Seu
6194 d'Urgell–Montferrer; 23: Balaguer NE–Rio Sio; 24: Balaguer NW; 25: Alfarras; 26: Canelles;
6195 27: Isaba; 28: Pierre-St-Martin karst; 29: Arbailles karst; 30: Lurbe–Asasp; 31: Capbis; 32:
6196 Arcizac; 33: Bastenne-Gaujac, Heugas; 34: Horsarieux; 35: Meilhan; 36: Côte Basque,
6197 Arcangue-Castagnet. After Philip (2018), Baize et al. (2002), Goula et al. (1999), Lacan and
6198 Ortuño (2012), and other references provided in the text. For the Plio-Pleistocene fluvial
6199 deposits, data sources: 1:1,000,000 scale geological map of France (BRGM), 1:400,000 map
6200 of Quaternary deposits of the Pyrenees (Barrère et al., 2009), 1:50,000 scale geological maps
6201 of Spain (IGME), with additional data from Mensua et al. (1977). Glacial extent after Calvet
6202 (2004) and Calvet et al. (2011).

6203

6204 **Fig. 13. Seismic activity in the Pyrenees.** A: historical earthquakes since the Middle Ages. B:
6205 instrumentally measured seismicity since 1997 (source: Réseau de Surveillance Sismique des
6206 Pyrénées, Observatoire Midi-Pyrénées, Toulouse).

6207
6208 **Fig. 14. Aspects of the Pyrenean partial pediments (generation P2), suggesting a late**
6209 **Neogene lull in rates of base-level change.** A. Erosional piedmont of the Basque Country,
6210 here looking west from Isturitz. P2 cuts across Cretaceous flysch, massive and vertically
6211 upturned Malm to Aptian/Barremian limestone, and the Hercynian core of schist in the
6212 Ursuya–Baigura massifs. In foreground: Pleistocene polje of Isturitz. In background: residual
6213 inselbergs rising above P2. B. Erosional piedmont of the Basque Country, here looking east
6214 from Isturitz. P2 cuts across Cretaceous flysch; vestiges of an older surface at higher
6215 elevation caps the foothills situated below the snowline (Ostabat–Ainharp). On the far
6216 horizon, and extending in topographic continuity from P2: top of the de Lannemezan Fm.,
6217 here preserved as strips of the Ossau and Ger megafans. C. Erosional piedmont P2 in the
6218 central Pyrenees of the Ariège, here seen from the village of Carla-Bayle. The erosion surface
6219 cuts across the Sub-Pyrenean folds of the Plantaurel–Mas d’Azil (Petite Pyrénées: Paleocene
6220 and Lower Eocene limestones), the NPT, the Cretaceous flysch of the Camarade Basin, and
6221 massive limestones of the North-Pyrenean Zone at the foot of the Arize massif. P2 displays a
6222 residual hill in flysch at Cabanères, and grades westward along the strike of the mountain
6223 front to the top of the residual Salat megafan (Lannemezan Fm.). Vestiges of this alluvial
6224 deposit cap the Miocene molasse outcrop in the foreground. D. Well-preserved example of
6225 pediment P2 at the Col de La Perche, between the Cerdagne and Conflent intermontane
6226 half-grabens (eastern Pyrenees). The erosion surface cuts across the basement rocks of the
6227 Axial Zone as well as across upturned Upper Miocene beds of the Cerdagne Basin fill
6228 sequence. P2 is deeply incised on the east side of La Perche by the Têt knickzone near Mont-
6229 Louis. In the background, note surfaces S and P1 present in massifs on either side of the
6230 Cerdagne Basin. E. P2 pediment in the Port de Comte massif (eastern South-Pyrenean Zone).
6231 The Pla de Riard is the top of a clastic accumulation considered here to be an Iberian
6232 equivalent of the Lannemezan Fm. F. Palaeovalley P2 at the Col du Puymorens (eastern Axial
6233 Zone), with palaeodrainage probably directed towards the Querol and Cerdagne but later
6234 captured by the Ariège River and thus diverted northward. G. Palaeovalley P2 at Pla de Beret

6235 (central Pyrenees), at the source of the Noguera Pallaresa. The upper catchment was
6236 captured and diverted by the Garonne.

6237

6238 **Plate I. Palaeogeography of the Pyrenees and its surrounding regions from the early**

6239 **Paleocene (65–60 Ma) to the Quaternary.** These ten maps crafted from a geomorphological

6240 perspective indicate the relative distribution of eroding land areas (specifying their high,

6241 moderate or low relief) and of three main depositional domains: (i) continental (fluvial,

6242 lacustrine), and (ii) carbonate- or clastic-dominated marine in (iia) a shallow shelf

6243 environment or (iib) a deeper palaeobathymetric setting (lower shelf, continental slope,

6244 trough). Boundary fluctuations between these domains were caused by tectonic and/or

6245 eustatic drivers but are too numerous to all be illustrated on these highly synthetic maps.

6246 For the Pyrenean mountain belt, Ebro and Aquitaine basins, and Basque and Cantabrian

6247 regions, the maps are based on the detailed (but partly outdated) maps of the “Synthèse

6248 géologique et géophysique des Pyrénées” atlas, volume 2, produced in 1997 but only

6249 published in 2018 (see Barnolas et al., 2018). Like their excellent antecedents produced by

6250 Plaziat (1981), those atlas maps displayed the modern-day geology; whereas the maps here

6251 take account of Alpine tectonic movements and crustal shortening. They are thus

6252 retrotectonic as well as palaeogeographic, and conform to the tectonic model advocated in

6253 this study for the nappe stack on the south side of the range (see Figs. 2, 3). Other work used

6254 to reconstruct the Pyrenean mountain belt include Andeweg (2002), Barnolas et al. (2019),

6255 Garcés et al. (2020), Ortiz et al. (2020), and the many additional references cited in the text.

6256 Kinematics of the main crustal blocs (i.e., Aquitaine–Massif Central; Bay of Biscay;

6257 Cantabrian–Pyrenean Range; Ebro Basin; Catalan Coastal Ranges, or Catalanides; Iberian

6258 Range and central Iberia) were calibrated on the works of Roca et al. (2011), Vissers and

6259 Meijer (2012b), Tugend et al. (2014), and Nirrengarten et al. (2018). For the eastern area

6260 (Tethyan, then Mediterranean: Languedoc; Provence; Sardinia; Balearic Islands), the

6261 reconstructions are underpinned by Dercourt et al. (1993), Séranne (1999), Murru et al.

6262 (2003, 2007), Lacombe and Jolivet (2005), Dieni et al. (2008), Cherchi et al. (2008), Leleu et

6263 al. (2009), Bache et al. (2009, 2010), Barca and Costamagna (2010), Oudet et al. (2010a,

6264 2010b), Costamagna and Schäfer (2013), Bestani et al. (2016), Etheve et al. (2016, 2018), and

6265 van Hinsbergen et al. (2020). For reasons of visual clarity, tectonic lineaments (thrusts,

6266 normal faults) have generally not been depicted, but the regional tectonic stress field has
6267 been indicated with arrows.

6268 **A. 65–60 Ma, early Paleocene (Danian–Selandian).** Sardinia is placed here according to the
6269 preferred model of Advokaat et al. (2014). The Danian–Selandian marine turbiditic trough
6270 model associated with karst development (see Peybernès et al., 2001, 2014) was not
6271 favoured here (see Canérot, 2006). Grey stars ('Ferruginous deposits', termed
6272 'Sidérolithique' in the Massif Central) locate occurrences of tropical laterites (age: late
6273 Maastrichtian to early Paleocene; e.g., Thiry, 2000; Vacca et al., 2012). Extent of late
6274 Cretaceous deposits in the Proto-Pyrenees has been portrayed schematically; the eastern
6275 boundary of this domain corresponds to a hypothetical (intracontinental) transform fault
6276 generated during earlier Mesozoic kinematics. Areas above sea-level other than the Proto-
6277 Pyrenees are evolving in unspecified ways (but resulting in an early Paleocene erosion
6278 surface in the Massif Central — previously named 'surface éogène': Baulig, 1928, or 'surface
6279 éotertiaire': Klein, 1990).

6280 **B. 56–53, Ma early Ypresian (Ilerdian).** The tectonically active domain (Ancestral Pyrenees)
6281 corresponds to the current eastern NPZ (some nummulites of probable Ypresian age have
6282 been reworked and included in Pliocene beds at Néfiach, between Prades and Perpignan, at
6283 the boundary between Axial Zone and NPZ; Astre, 1937). At the time, most of the
6284 northeastern AZ was located south of the rising Ancestral Pyrenees and drowned by the
6285 Ypresian transgression.

6286 **C. 45 Ma, middle Lutetian.** The Ancestral Pyrenees have grown south- and westward, and
6287 the pro- and retro-foreland basins have narrowed; magnitudes of N–S crustal shortening
6288 reach ca. 50 km in the central Pyrenees; Sardinia has begun to rotate counterclockwise. The
6289 South-Pyrenean Basin is still open to the Atlantic. An elevated mountain range (Ancestral
6290 Pyrenees) is supplying conglomerate sequences to both forelands, north and south (Palassou
6291 and Bellmunt–Campanue formations, respectively).

6292 **D. 38–36 Ma, Bartonian–Priabonian transition.** This period was a tectonic paroxysm in
6293 Languedoc and Provence ('Bartonian event') and involved the collision of Sardinia and
6294 Provence (ca. 40 km of total shortening since the latest Cretaceous). Between Iberia and
6295 Europe, shortening had exceeded ~100 km by the late Eocene. In the Pyrenees, the peak of
6296 uplift and denudation recorded by thermochronology begins around 37 Ma and coincides

6297 with the formation of the basement nappe stack in the Axial Zone. By this time, the deep
6298 South-Pyrenean Basin (and its Hecho canyon) has nearly overfilled.

6299 **E. 30–28 Ma, late Rupelian.** The Pyrenees are now continuous with the Cantabrian Range
6300 and form a narrow mountain belt, still feeding thick conglomerate sequences to the
6301 piedmonts. The Ebro Basin has been internally drained since ~36 Ma. The peak of uplift and
6302 denudation continues until ~30 Ma and then abates considerably. In the east, convergence
6303 ceases abruptly and gives way to an extensional regime in Provence, Languedoc, Sardinia,
6304 and even the Catalanides.

6305 **F. 25–24 Ma, Chattian.** The Pyrenees form two contrasting domains: (i) continuing
6306 convergence in the west and centre drives southward fold propagation out into the Iberian
6307 foreland; thick syntectonic conglomerate beds continue to accumulate in the Ebro Basin, but
6308 not in the Aquitaine. The northeastern Catalan Range is still undergoing compressive
6309 tectonics, and piggyback basins are generated in the area corresponding to the future
6310 Valencia Trough. In contrast, (ii) the NE part of the Pyrenees undergoes crustal extension;
6311 this promotes the formation of a partial peneplain (surface S). Sea level rises across the Gulf
6312 of Lion in Chattian time and advances westward during Aquitanian time. In Aquitanian time,
6313 the sea-level highstand briefly reached as far as Agen from the west.

6314 **G. 20–18 Ma, early Burdigalian.** The previously established E–W tectonic divide is
6315 maintained. Convergence in the west is nonetheless declining, and the last synorogenic
6316 conglomerates (Huesca Fm.) are deposited. Footwall uplifts in the Mediterranean
6317 extensional domain generate high mountain topography in the eastern Pyrenees and
6318 Catalanides, with very coarse clastic output as a result in the Roussillon, Conflent, and Vallès
6319 basins. Southward drift and rotation of the Corsica–Sardinia bloc generates the deep Liguro-
6320 Provençal Basin. The Valencia Basin had already switched to an extensional regime in
6321 Aquitanian time.

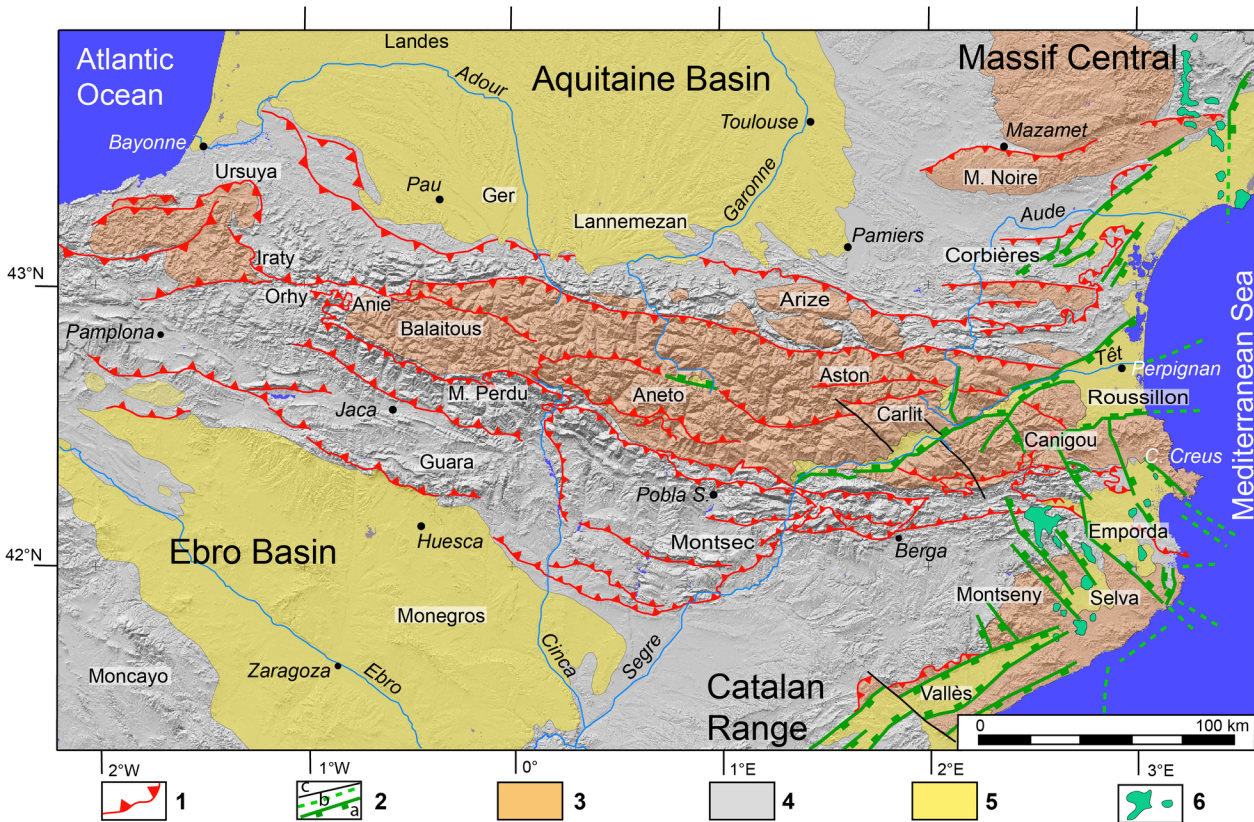
6322 **H. 14–12 Ma, middle Miocene.** This is a period of crustal relaxation. All tectonic convergence
6323 in the Pyrenees has ceased (except perhaps in the west between the Sierra de la Demanda
6324 and the Cantabrian Range), and the Corsica–Sardinia bloc has approximately reached its
6325 current position. A widespread partial erosion surface, P1, while preserving often large
6326 residual ridges and ranges, has cut pediment bench systems throughout the Iberian Range,
6327 Pyrenees, Massif Central and Provence. The central and western parts of the Axial Zone,
6328 however, were unaffected by P1; as a result, these areas constitute the last upstanding

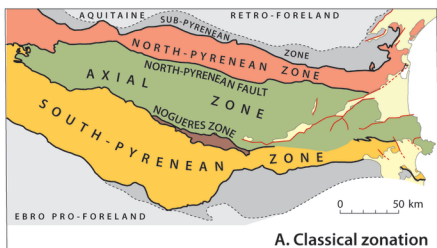
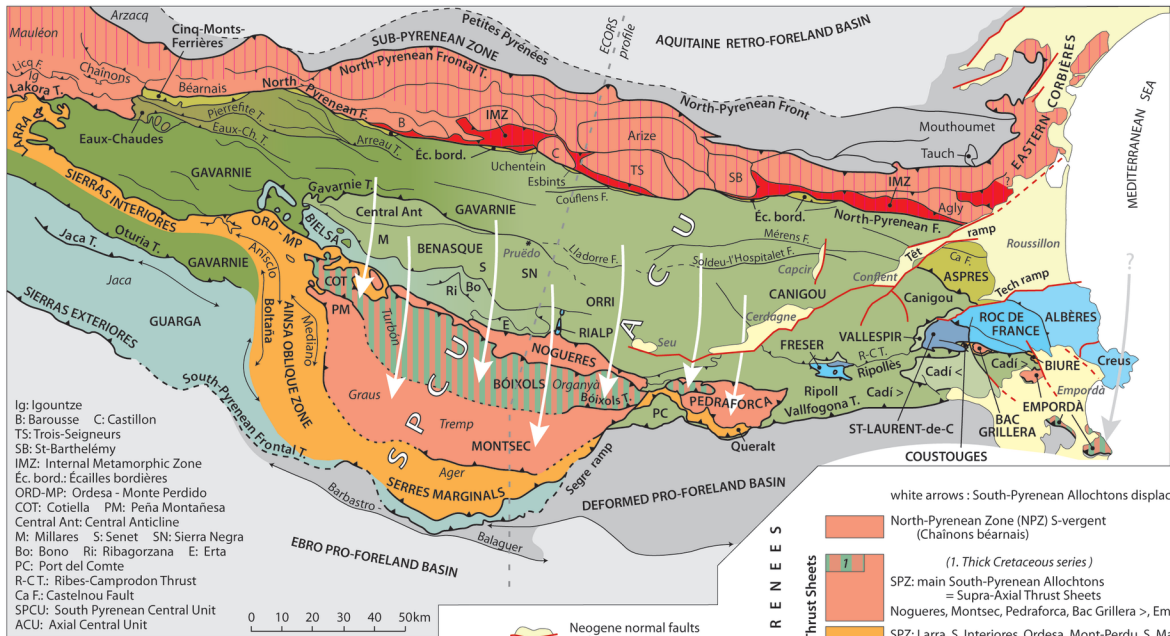
6329 vestiges of the Ancestral Pyrenees. Marine incursions are advancing over the Aquitaine, Gulf
6330 of Lion and Provence. Continental sedimentation is dominated by lacustrine limestones and
6331 is relatively starved of clastic inputs.

6332 **I. 10–6 Ma, late Miocene.** Progressive, regional uplift, reaching maxima over the Pyrenees
6333 but also affecting the Massif Central and the entire Iberian peninsula, is associated with
6334 intraplate volcanism from the Massif Central to northern Catalonia. The youngest (10 Ma)
6335 lacustrine carbonate beds recorded occur in the Ebro Basin and in Languedoc. Extensional
6336 grabens and horsts are forming across the Western Mediterranean and deep into the central
6337 Pyrenean Axial Zone. The Ebro Basin is reconnected to marine base levels and undergoing
6338 fluvial incision, all of this prior to the construction of the Lannemezan retro-foreland
6339 megafan in Aquitaine. Marine shorelines are receding in the Aquitaine Basin and the
6340 Mediterranean.

6341 **J. 5–2 Ma, Pliocene.** This map captures the region immediately after the late Messinian
6342 Salinity Crisis (5.6–5.46 Ma), which generated thick evaporite deposits in the deeper
6343 bathymetric levels of the Mediterranean and deeply incising canyons around the edges.
6344 Regional uplift continues, interrupted by brief pauses (e.g., formation of generation P2 of
6345 local pediments during the late Pliocene); volcanic activity intensifies. The Ebro Basin is
6346 undergoing deep dissection but the Lannemezan Formation continues to aggrade along the
6347 North-Pyrenean mountain front. This geomorphological asymmetry of the Pyrenees
6348 promotes drainage capture of north-flowing rivers by their south-flowing counterparts.
6349 Coarse-textured clastic input to eastern coastal basins intensifies, generating thick
6350 siliciclastic depositional wedges offshore.

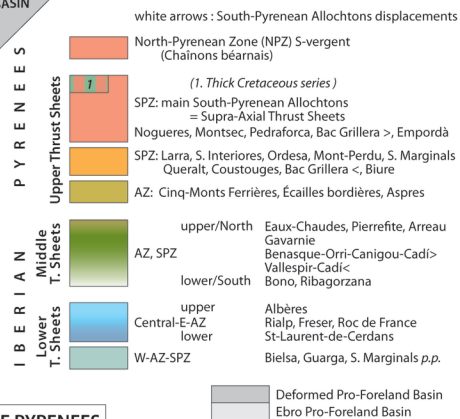
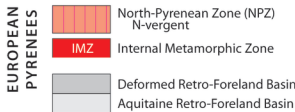
6351 **K. 2–0 Ma, Quaternary.** As testified by widespread staircases of Quaternary alluvial terraces,
6352 mountain uplift continues in the Pyrenees and throughout the region. Volcanism is still very
6353 active from the Massif Central to Catalonia. Valley incision is also ubiquitous, except in the
6354 Landes area, which became an erg during cold and dry glacial stages. Most of the coarse
6355 clastic depocentres are very thick and now situated offshore. An icefield develops over the
6356 more humid massifs (Atlantic influence), and glacial–interglacial oscillations control the
6357 alluvial terrace aggradation/incision regime. Drainage captures occur in the piedmont zones
6358 rather than in the mountain-range headwaters, mostly benefiting the Mediterranean base
6359 level (e.g., Aude River catchment).

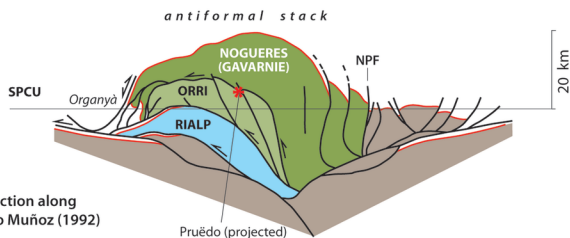
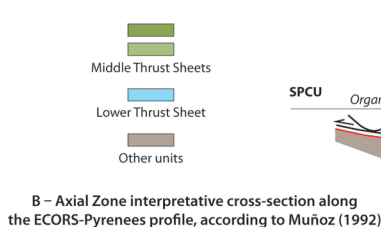
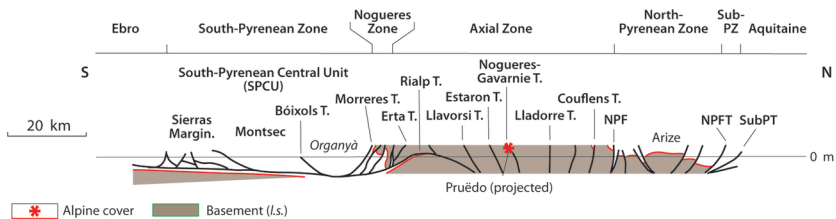




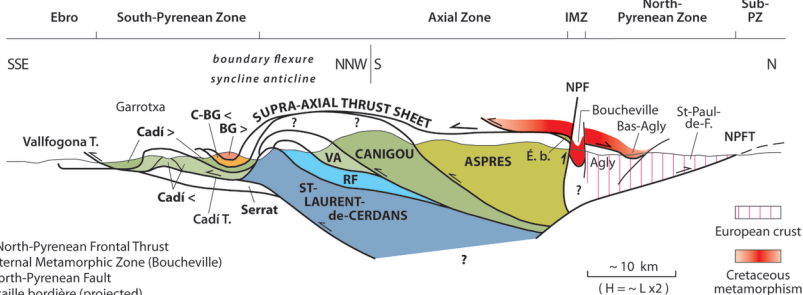
STRUCTURAL MAP OF THE ALPINE PYRENEES

B. Alpine tectonic units and thrusts



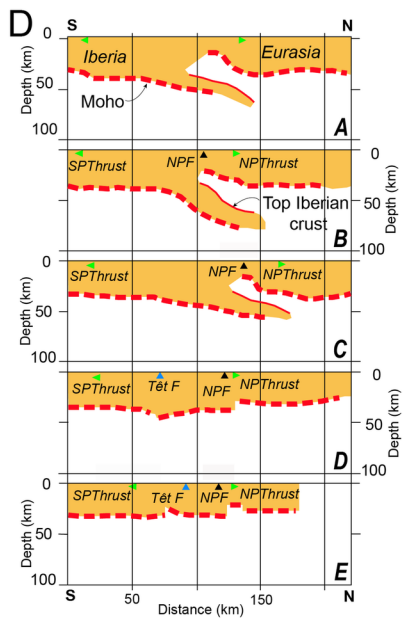
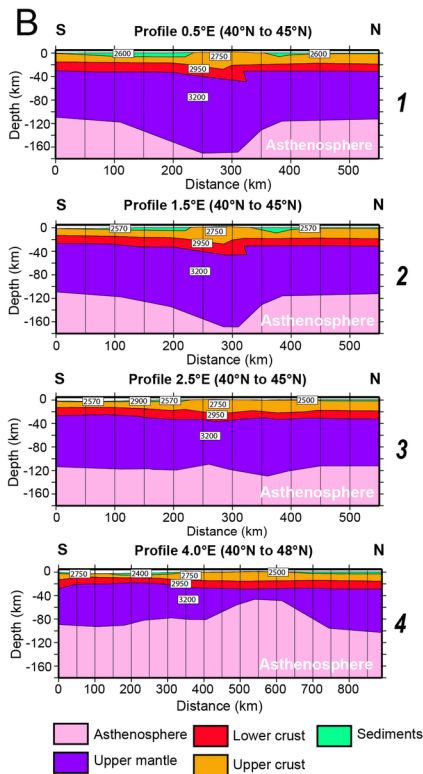
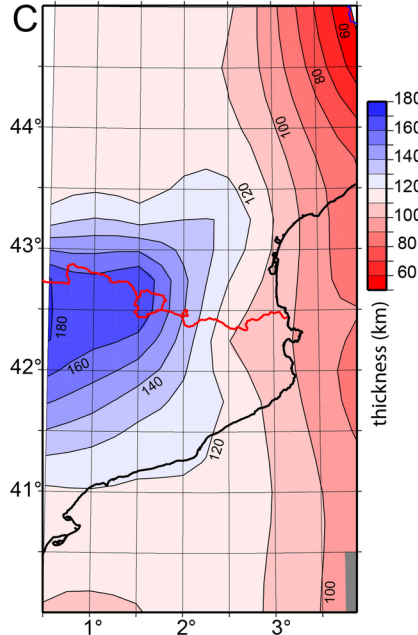
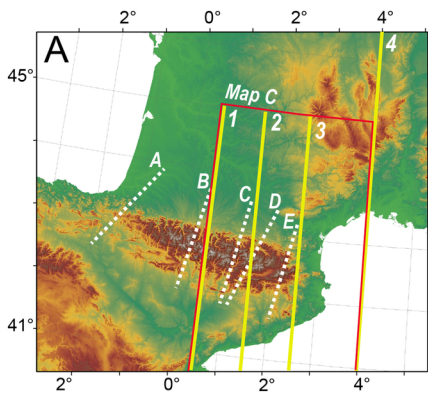


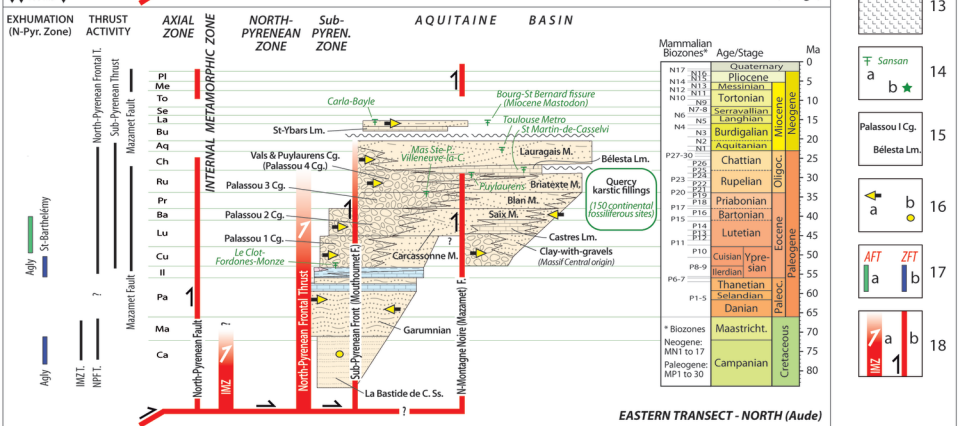
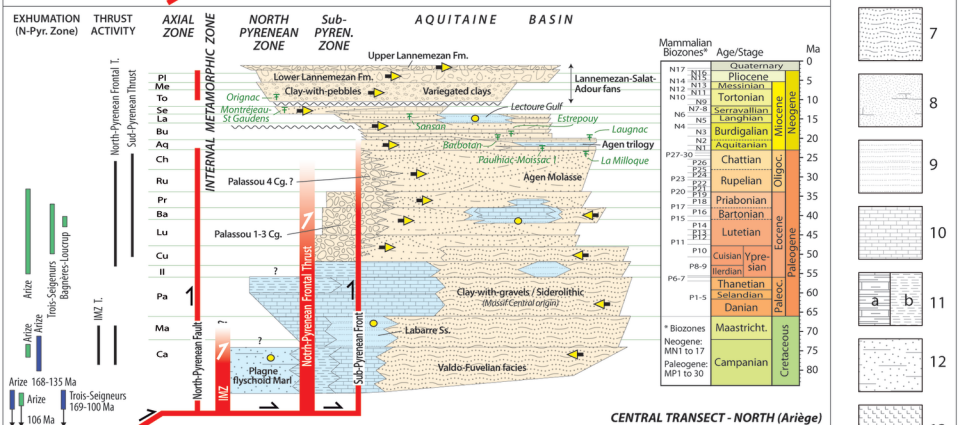
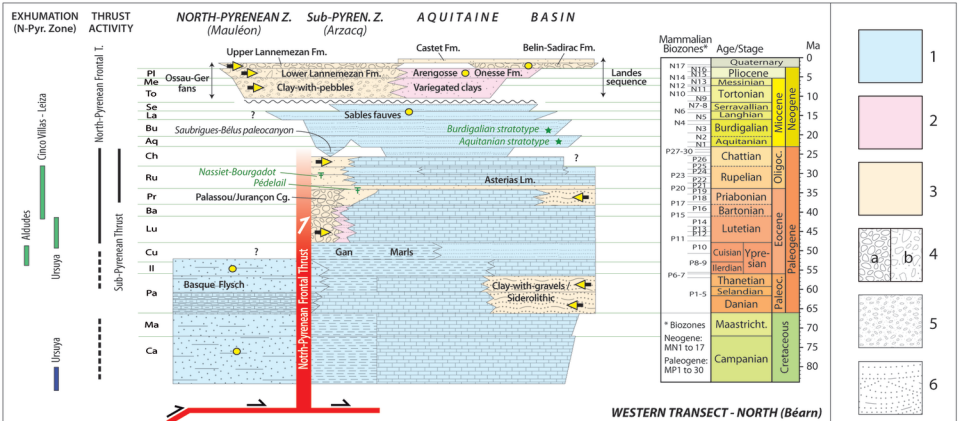
ACU: Axial Central Unit (Gavarnie + Orri)
 SPCU: South-Pyrenean Central Unit
 NPF: North-Pyrenean Fault

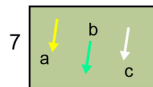
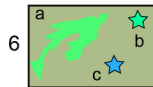
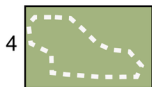
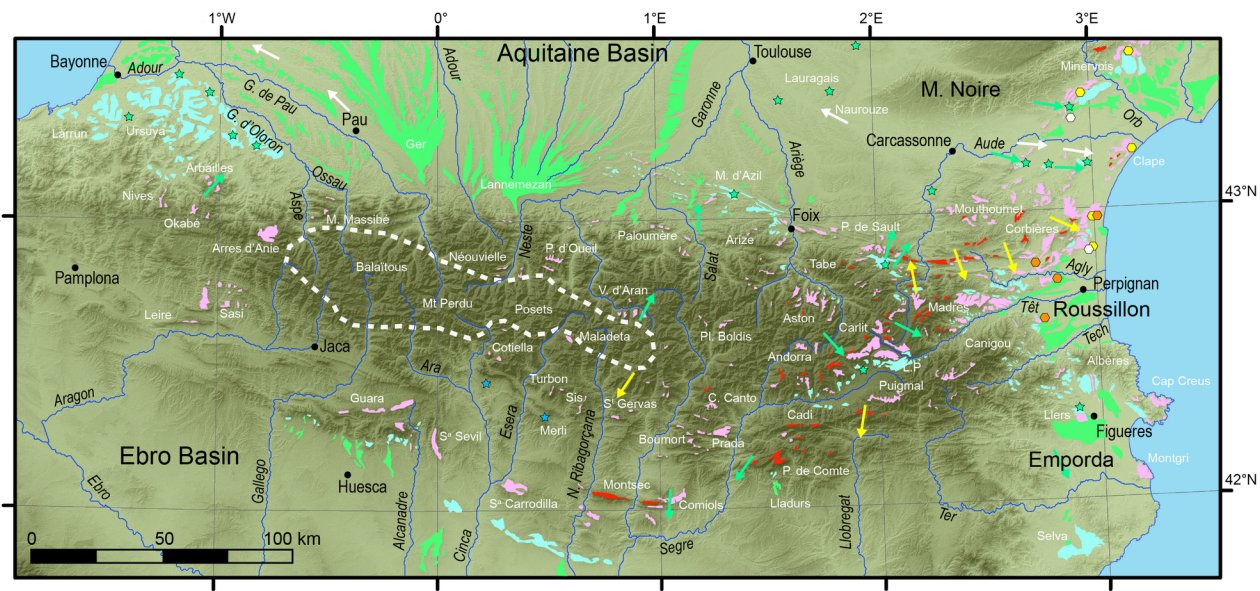


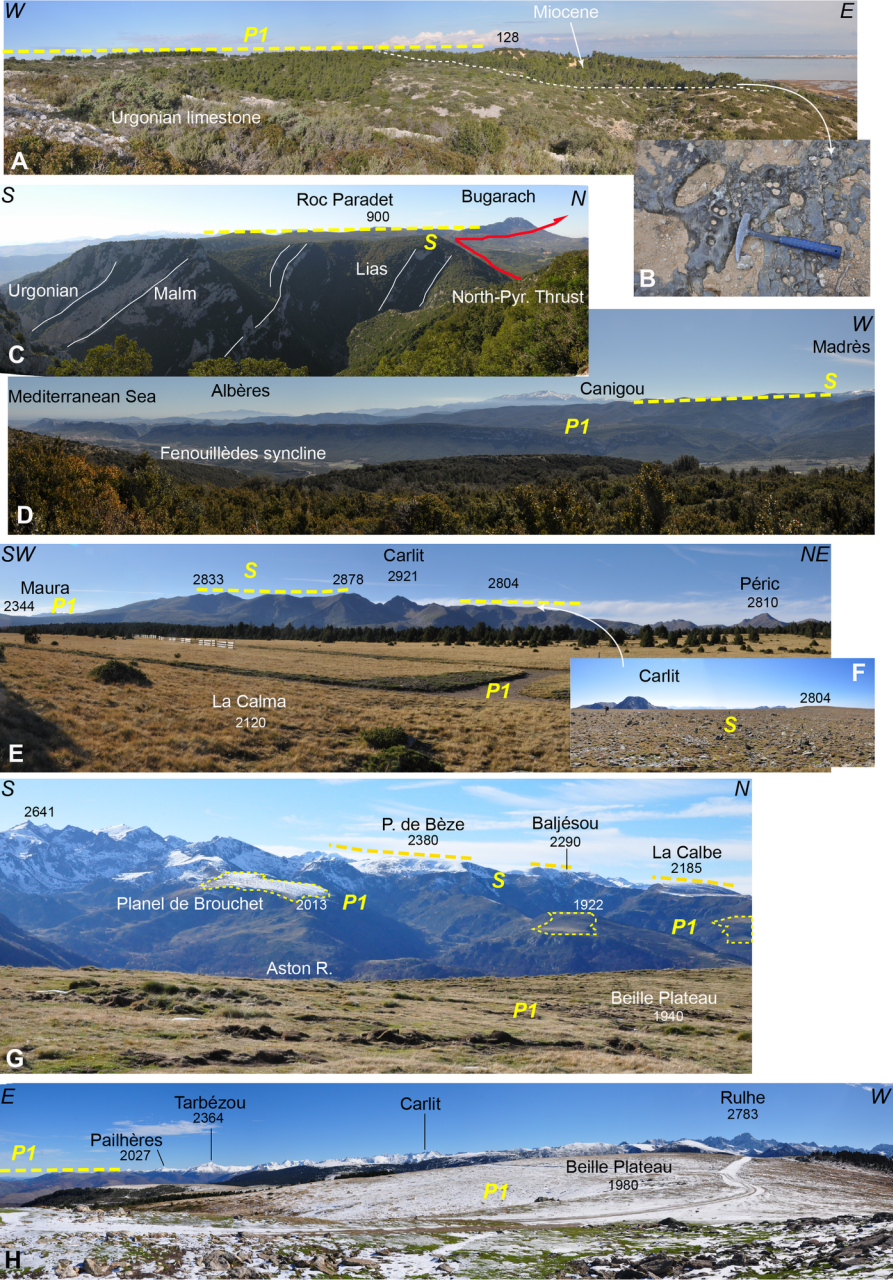
NPFT: North-Pyrenean Frontal Thrust
 IMZ: Internal Metamorphic Zone (Boucheville)
 NPF: North-Pyrenean Fault
 É. b.: Ecaille bordière (projected)
 VA: Vallespir
 RF: Roc de France
 BG >: Upper Bac Grillera
 C-BG <: Coustouges - Lower Bac Grillera

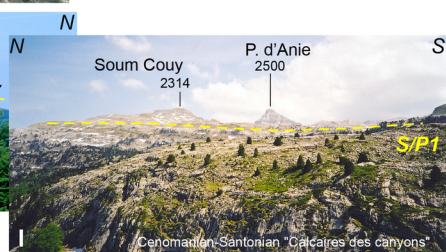
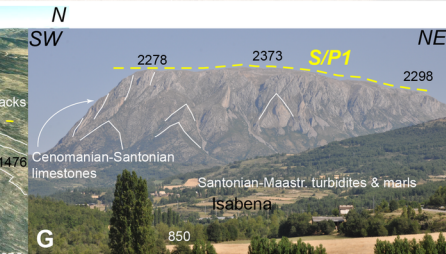
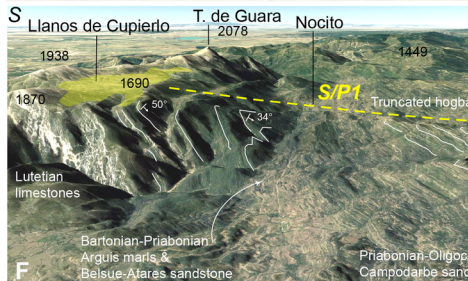
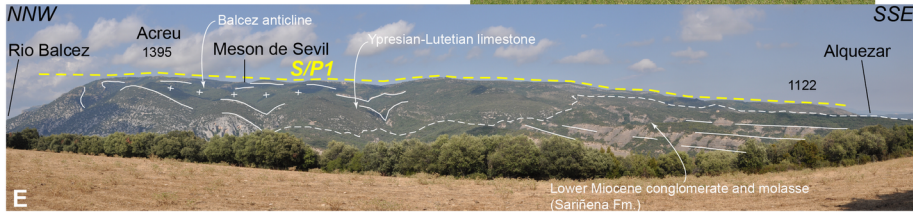
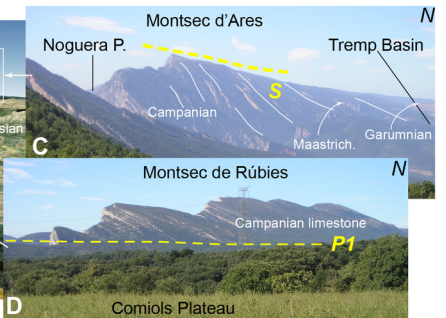
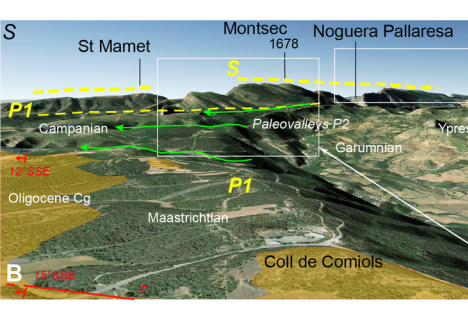
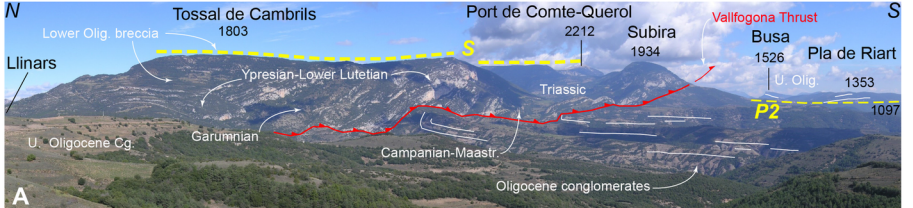
STRUCTURAL CROSS-SECTIONS OF THE CENTRAL AND EASTERN PYRENEES

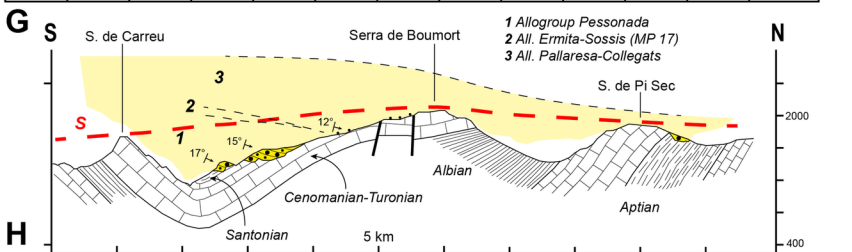
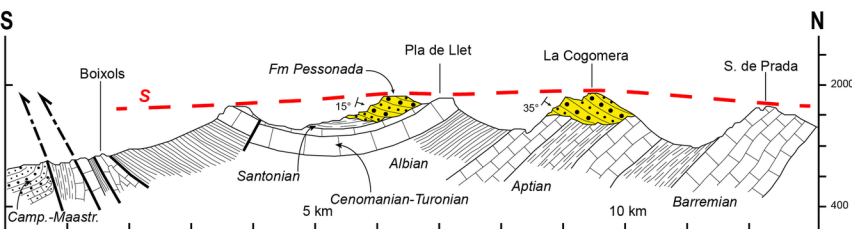
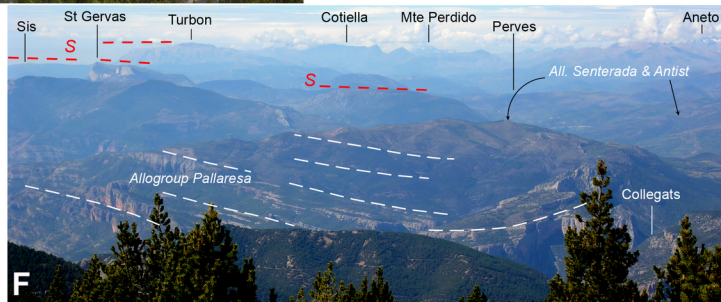
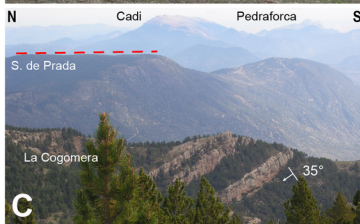
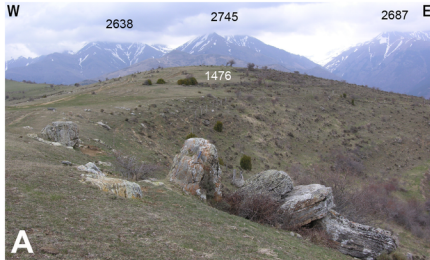


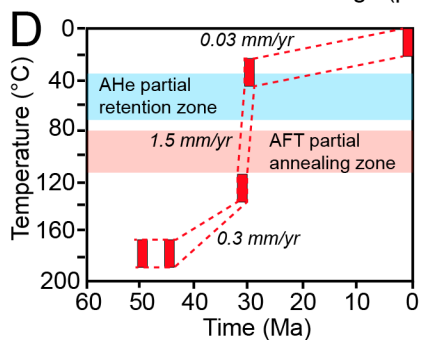
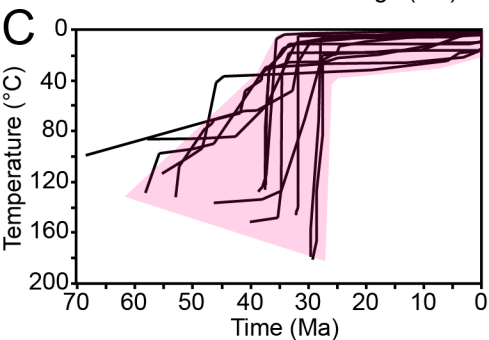
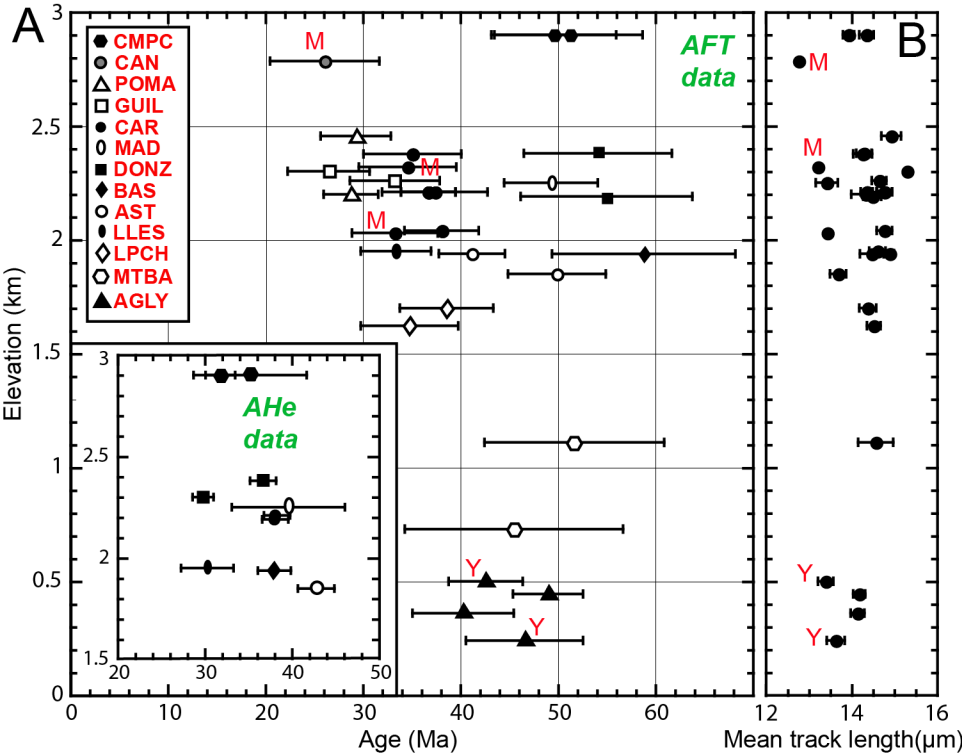












Topographic state at completion of P1 (Pyrenees ca. 12–10 Ma)

Late convergence until ~20–18 Ma

High uplift rates, lithospheric and crustal roots still uneroded

Extension after 28–25 Ma

Discontinuous uplift, lithospheric and crustal roots eroded

Current topographic state (Pyrenees after 10 Ma)

Uplift since 10 Ma

Lithospheric and crustal roots still uneroded, but heated

Uplift and faulting since 10 Ma

Transpression, nonequilibrium, lithospheric and crustal roots eroded

